INFORMATION TO USERS

This manuscript has been reproduced from the microfilm master. UMI films the text directly from the original or copy submitted. Thus, some thesis and dissertation copies are in typewriter face, while others may be from any type of computer printer.

The quality of this reproduction is dependent upon the quality of the copy submitted. Broken or indistinct print, colored or poor quality illustrations and photographs, print bleedthrough, substandard margins, and improper alignment can adversely affect reproduction.

In the unlikely event that the author did not send UMI a complete manuscript and there are missing pages, these will be noted. Also, if unauthorized copyright material had to be removed, a note will indicate the deletion.

Oversize materials (e.g., maps, drawings, charts) are reproduced by sectioning the original, beginning at the upper left-hand corner and continuing from left to right in equal sections with small overlaps.

Photographs included in the original manuscript have been reproduced xerographically in this copy. Higher quality 6" x 9" black and white photographic prints are available for any photographs or illustrations appearing in this copy for an additional charge. Contact UMI directly to order.

Bell & Howell Information and Learning
300 North Zeeb Road, Ann Arbor, MI 48106-1346 USA

UMI®
800-521-0600

WAKE CLOSURE CONDITIONS IN PLUG NOZZLE FLOWFIELDS

by

Derek Edward Lang

A dissertation submitted in partial fulfillment of the requirements for the degree of

Doctor of Philosophy

University of Washington

1999

Program Authorized to Offer Degree: Department of Aeronautics and Astronautics

UMI Number: 9952856

Bell & Howell Information and Learning Company
300 North Zeeb Road
P.O. Box 1346
Ann Arbor, MI 48106-1346

In presenting this dissertation in partial fulfillment of the requirements for the Doctoral degree at the University of Washington, I agree that the Library shall make its copies freely available for inspection. I further agree that extensive copying of the dissertation is allowable only for scholarly purposes, consistent with "fair use" as prescribed in the U.S. Copyright Law. Requests for copying or reproduction of this dissertation may be referred to UMI Dissertation Services, 300 North Zeeb Road, P.O. Box 1346, Ann Arbor, MI 48106-1346, to whom the author has granted "the right to reproduce and sell (a) copies of the manuscript in microform and/or (b) printed copies of the manuscript made from microform."

Signature Derek Lam

Date 12/15/99

University of Washington
Graduate School

This is to certify that I have examined this copy of a doctoral dissertation by

Derek E Lang

and have found that it is complete and satisfactory in all respects,
and that any and all revisions required by the final
examining committee have been made.

Chair of Supervisory Committee:

Arthur T. Mattick

Reading Committee:

David A. Russell

John J. Bertin

Reiner Decher

Date: 12/16/99

University of Washington

Abstract

Wake Closure Conditions in Plug Nozzle Flowfields

Derek Edward Lang

Chairperson of the Supervisory Committee:
Professor Arthur T. Mattick
Department of Aeronautics and Astronautics

The aerospike, or plug, nozzle is being proposed for future space launch vehicle applications. The design of the nozzle involves complex wake structures that directly affect engine performance. In particular, the closed or open wake condition of the flow determines the dependence of the base pressure on the ambient environment, and therefore affects overall thrust. An experimental, numerical, and analytical investigation characterized the transition of the wake between closed and open conditions in order to determine the physical mechanism leading to wake closure. A common feature between different modes of wake closure was the presence of a shock structure that forced changes to the wake critical point. Wake closure is defined as the limiting condition at which external pressure gradients change the properties and location of the critical point. Changes to critical point directly influence the nozzle base pressure due to the critical point's uniqueness property. Supersonic wake methods can determine wake closure trends for mission optimization. Increased wake closure nozzle pressure ratios and closed wake pressures can be achieved through design Mach Number, nozzle size, length and ramp shape.

TABLE OF CONTENTS

Page

LIST OF FIGURES

Number Page

LIST OF TABLES

LIST OF SYMBOLS

Alphanumeric Symbols	
a	Speed of Sound, m/s
a(x)	Tani's Shape Factor
A, B, C, D	Design of Experiment Factor Codes
Ae	Area at Nozzle Exit (m^2)
AGARD	Advisory Group for Aerospace Research and Development
At	Area at Nozzle Throat (m^2)
C	Velocity Parameter, as defined by Equation (3)
C_D	Drag Coefficient
CFD	Computational Fluid Dynamics
C_F	Coefficient of Thrust or Thrust Efficiency
D	Lees-Reeves Critical Point Denominator, as defined by Equations (18)
DAS	Data Acquisition System
DOE	Design of Experiment
DSL	Dividing Streamline
f	Lees-Reeves parameter, as defined by Equation (11)
F	Thrust
g	Gravitational Acceleration (m/s^2)
G_s	Mass Flow Rate Parameter, as defined by Equation (3)
H	Shape Factor, as defined by Equation (9)
H	Lees-Reeves parameter, as defined by Equation (10)
H	Static Enthalpy, J/kg.K
Isp	Specific Impulse (seconds)
J	Shape Factor, as defined by Equation (9)
K	Kelvin
Kg	Kilograms
Km	Kilometers

Alphanumeric Symbols

KPa	Kilopascals
L	Length of plug nozzle (m)
L_{max}	Length of a fully expanded aerospike nozzle (m)
LED	Light Emitting Diode
LU-SGS	Lower/Upper-Symmetric Gauss Seidell
M	Meters
M	Mach Number
M	Reference Mach Number $(\gamma-1)/2M^2$, or mass (kg)
m-dot	Mass Flow Rate, (kg/s)
N	Newtons
N_1, N_2, N_3	Lees-Reeves Critical Point Numerators, as defined by Equations (15-17)
NASA	National Aeronautics and Space Administration
NPR	Nozzle Pressure Ratio (thruster total pressure to ambient static pressure)
p	Static Pressure (psia or N/m^2)
P_{tot}	Total pressure (psia or N/m^2)
Pr	Prandtl Number
Psia	pounds-force per square inch
R	Shape Factor, as defined by Equation (9)
Re	Reynolds Number
RSM	Response Surface Methodology
RSP	Rear Stagnation Point
t	Time (seconds)
T	Temperature (Kelvin)
u	Velocity (m/s)
U	Stewartson Incompressible velocity (m/s)
x	Axial Distance from Base or Axial Distance from Throat to a Station Along the Ramp Surface (m)

Alphanumeric Symbols

X	Stewartson Incompressible Axial Distance from Base, as defined by Equation (4)
x_{ji}, x_{ui}	Design of Experiment Matrix Elements
y	Transverse Distance from Axis, m, or altitude (km)
$\bar{y}$, $\hat{y}$	Average and Predicted Response, respectively
Y	Stewartson Incompressible Transverse Distance from Axis, as defined by Equation (4)
Z	Shape Factor, as defined by Equation (9)

Greek Letters

φ	Velocity ratio, as defined by Equation (3)
η	Blasius scale length, position parameter
ψ	Pitch Angle (degrees)
Δ	Average Effect
Θ	Flow inclination angle, degrees
β	Integration variable
δ	Boundary Layer Thickness or Outer Edge Height, m
δ^*	Displacement Thickness, as defined by Equation (8)
γ	Ratio of Specific Heats
μ	Absolute Viscosity ($N.s/m^2$)
θ	Momentum Thickness, as defined by Equation (8)
ρ	Density, kg/m^3
τ	Shear Stress, N/m^2
ω	Vorticity, 1/second

Subscripts

∞	Freestream
$-\infty$	Far Downstream of the Nozzle
amb	Ambient
base	Base
cl	Centerline
DSL	Along Dividing Streamline
e	Shear Flow Outer Edge
exit	At Exit Plane of Nozzle
i	Transformed Incompressible Value
inf	Freestream
j	External Jet Streamline
opt	Optimum
RSP	Rear Stagnation Point
s	Distance Along Surface
t1, t2	Total in initial jet and total in flowfield, respectively
tot	Total
u=0	Along Stagnation Streamline
wall	At wall or along axis

Acknowledgements

My Doctor of Philosophy endeavor began a little over five years ago with a leap of faith to step away from a promising career in industry to fulfill a life-long dream. This journey led me across the ocean to Europe, to the mountain tops of Colorado, and to the rainy weather of Washington. Along the way, many colleagues and friends have supported my pursuit of this dream.

I wish to express gratitude to my supervisory committee for this research. Drs. Tom Mattick, David Russell, Reiner Decher and John Bertin were invaluable for their expertise and advisement on the direction and progress of this research. Mr. Dennis Peterson and Mr. Dzung Tran of the Aeronautics and Aerospace Department machine shop in providing guidance and assistance in the design and fabrication of the test facility and nozzle models. Mr. James Beck, Boeing North American, was a significant source of industry expertise and made it possible to navigate through the intricacies of plug nozzle design and operation.

My parents, sister, and grandmother were a constant source of encouragement and made all of this possible. To my girlfriend, Ellen, I express my deepest gratitude for her patience and love. Thanks to my roommate, Winthrop, for his extensive computer and video resources. And, thanks to God for strength, endurance, wisdom, and hope.

Dedication

To my loving parents, Ed and Arlene Lang, who have devoted their lives to building a nurturing family.

Chapter 1
INTRODUCTION

The plug nozzle, or truncated aerospike nozzle, is a proposed alternative to the bell nozzle traditionally used on space launch vehicles. One advantage of this nozzle is its higher performance under "open wake" conditions. The aft end of the nozzle is a blunt base that creates a wake flow, and the resulting base pressure base contributes positively or negatively to thrust. The amount of thrust produced depends on the gas pressure pushing against the base, which is a function of nozzle geometry and the exhaust jet flow. At low thrust chamber pressure (or exhaust jet total pressure)-to-ambient pressure ratios (Nozzle Pressure Ratio - NPR), the base pressure depends on ambient environment pressure and this condition is referred to as an "open wake." The base pressure is independent of ambient environment at high NPR – a condition called "closed wake." The transition between these two conditions is the point of wake closure. This research characterizes the fluid dynamic mechanisms leading to wake closure using experimental and computational methods.

1.1 Background

Plug nozzle research was primarily conducted from the 1950's to the 1970's as part of the United States early space launch program. The application of this alternative design, however, involved complex aerodynamics that affected its performance and the decision to bypass this alternative in favor of more traditional designs cut short the research in this area before it moved beyond developmental testing. Interest has returned to plug nozzles for recent Single-Stage-to-Orbit (SSTO) launch vehicles, such as the National Aeronautics and Space Administration (NASA) X-33 shown in Figure 1.1, which demand higher performance rocket engines.

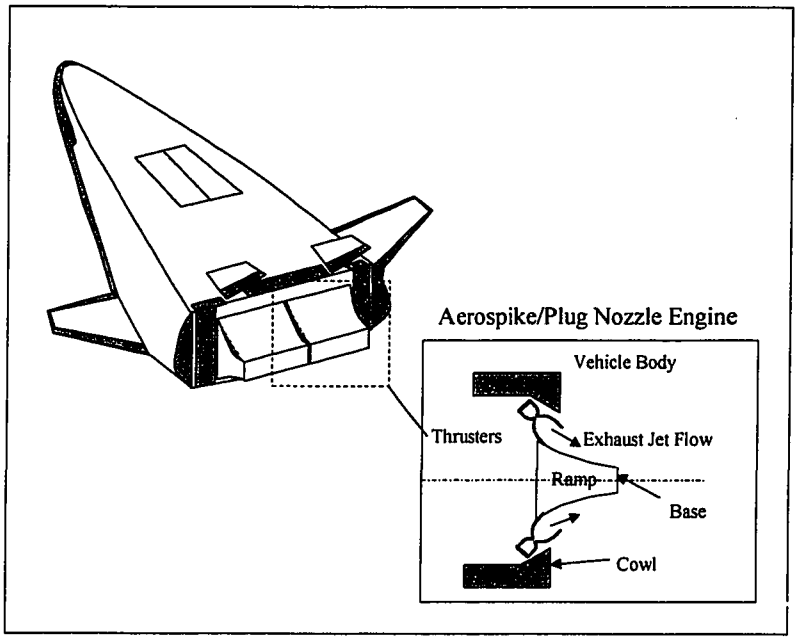

Figure 1.1: NASA X-33 and Linear Aerospike/Plug Nozzle Engine

The plug nozzle promises improved engine performance, size reductions, and weight savings. However the associated integrated system weight, cost and technical complexities raise questions as to the overall effectiveness of the engine. Since open wake performance is a primary benefit of the plug nozzle, the issue of wake closure is directly relevant to assessing the nozzle's potential benefits and limitations in improving overall launch vehicle capability.

1.1.1 Plug Nozzle Design

A brief description of bell and aerospike nozzles provides a context for understanding plug nozzle aerodynamics. The "bell nozzle" refers to the shape of the diverging section of the De Laval nozzle used on rocket engines. Propellants are combusted in a combustion chamber and then expelled through the converging-diverging nozzle shown in Figure 1.2. Moving at subsonic speed upstream of the nozzle throat, the flow accelerates in the converging passageway. As it passes through the throat, the flow reaches a critical point, i.e., it chokes, and then accelerates supersonically out the diverging section.

The expansion of the flow as it moves through the diverging section changes the flow's static pressure, temperature, and Mach Number according to gas dynamics relations. The optimum shape of the diverging section is designed so that the pressure in the exit plane at the end of the nozzle matches the outside pressure and the flow is directed parallel to the nozzle longitudinal axis.

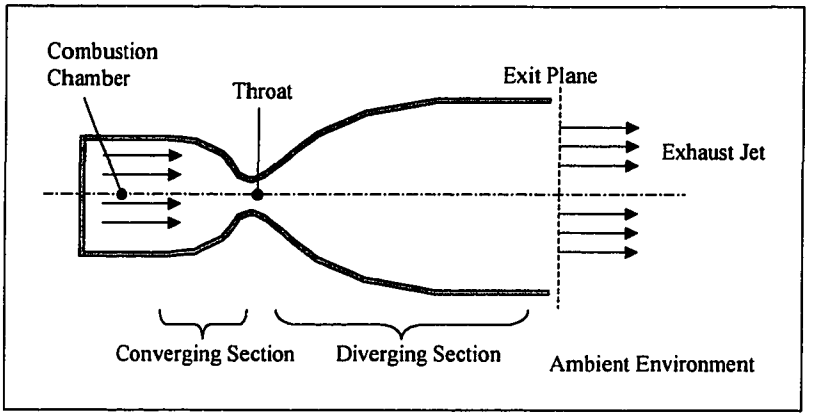

Figure 1.2: Bell Nozzle Configurations

In an aerospike nozzle, small thrusters expel supersonic gas onto a contoured ramp shown in Figure 1.3. The external boundary of the jet is determined by the ambient conditions, while the ramp surface governs the flow expansion. The ramp can be contoured for isentropic expansion or planar (conical for axisymmetric nozzles), i.e., a straight line between the thruster exit and ramp corner. The ramp shape turns the supersonic flow through a series of Prandtl-Meyer expansions, thereby increasing the flow Mach Number and expanding the gas until the end of the contour is achieved. The specification of a design Mach Number and exit cross-sectional area determines the angle and position of the thrusters and the ramp contour so that the gas flows parallel to longitudinal axis by the time it reaches the exit plane of the nozzle.

Generally, a full-length aerospike is not practical when considering the thermal and structural loads of during launch conditions. However, it was found that the aerospike could be truncated (thus becoming a "plug nozzle"), without

significantly impacting the nozzle aerodynamics (1). The wake that forms at the base of the plug turns the flow similar to a solid boundary, and retains much of the aerodynamic advantage without the same structural and thermal disadvantages. Thus, the aerospike and plug nozzle terminology is generally interchangeable when comparisons are made to the bell nozzle.

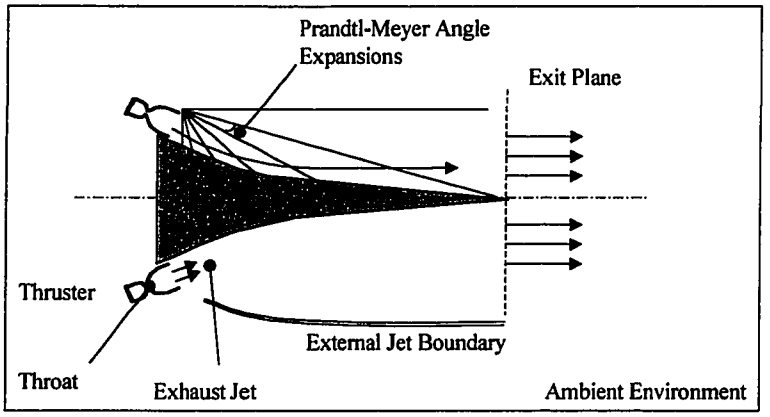

Figure 1-3: Aerospike Contour Design

1.1.2 Plug Nozzle Performance

The key difference in the aerospike or plug nozzle operation compared to the bell nozzle is its altitude adaptation. Figure 1.4 shows a comparison of the flow expansions at different altitudes during the rocket ascent to space. The conventional bell nozzle has a design altitude where the gas flow expands until the pressure at the exit matches the ambient pressure. At lower altitudes (or lower NPR), the ambient pressure is higher than the exit pressure, which is fixed by the nozzle geometry, and is considered "overexpanded." At higher altitudes, the exit pressure is higher than the ambient pressure and the flow expands outward once it leaves the nozzle exit plane. In comparison, the expansion occurring in the aerospike nozzle varies so that the pressure in the flow matches that of the ambient environment.

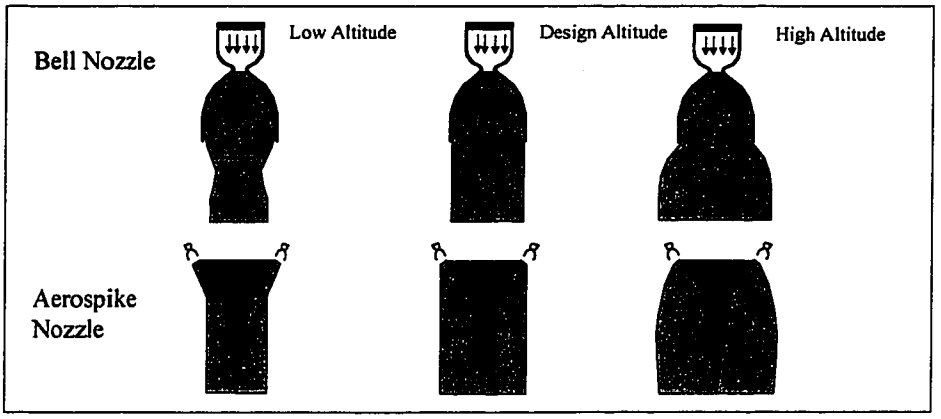

Figure 1.4: Bell versus Plug Nozzle Expansion Characteristics

At low altitudes when a bell nozzle is overexpanded, the adverse pressure gradient causes boundary layer separates from the wall. The actual thrust and thrust coefficient under separated conditions is higher than if the flow remained attached as the NPR continues to decrease. However, under these conditions, a portion of the nozzle (which translates to size and weight) is underutilized, thereby reducing the "overall" system efficiency. In the case of the aerospike nozzle at NPR lower than design conditions, the flow is pressed all along the ramp surface. A series of alternating compression and expansion waves are generated within this narrowed flow that reduce the peak pressure gradients and the potential for boundary layer separation (Figure 1.5).

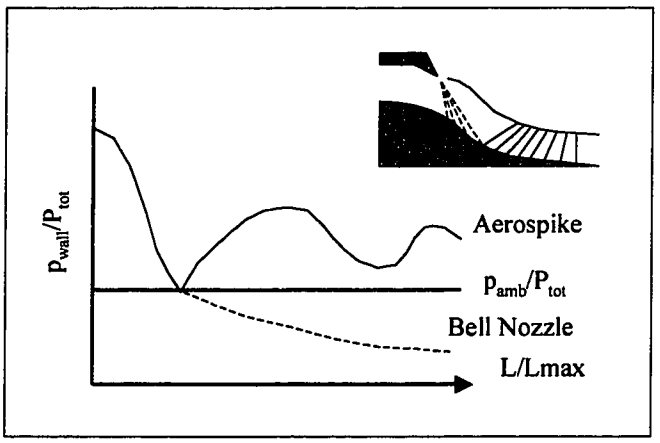

Figure 1.5: Wall Pressure Along Aerospike Nozzle (2)

Since the nozzle thrust is directly related to the expansion of the gases, the bell nozzle with its fixed geometry reaches its optimum thrust efficiency at the design altitude. In closed wake conditions, the aerospike nozzle is also limited by its design expansion geometry. However, under open wake conditions, the aerospike nozzle continually matches the ambient pressure and follows the optimum expansion curve shown in Figure 1.6.

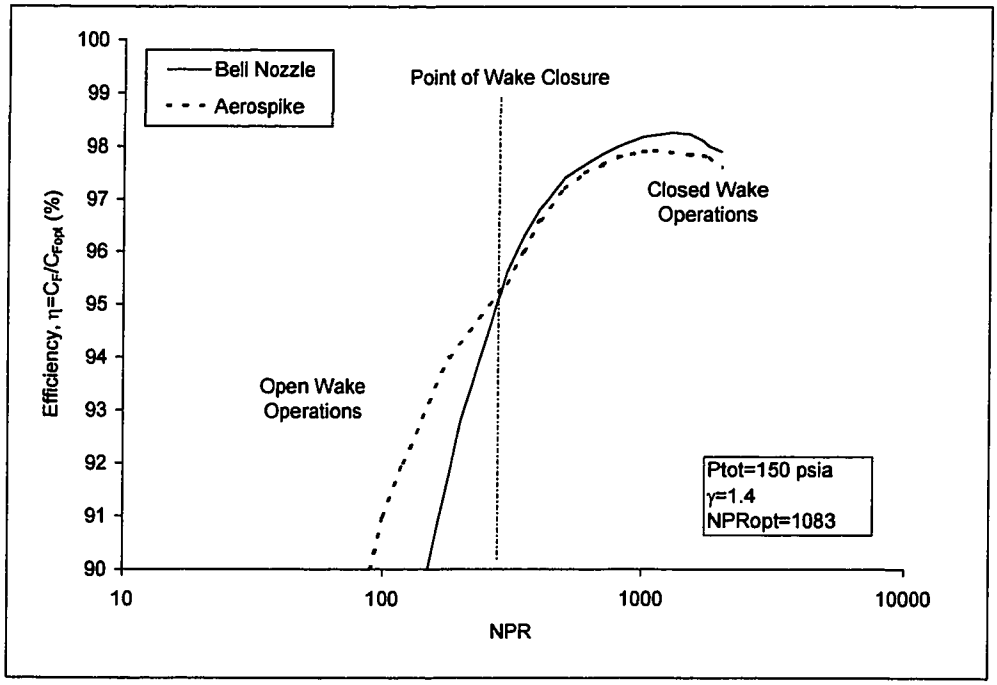

Figure 1.6: Comparison of Bell and Plug Nozzle Performance (2)

1.1.3 Wake Closure

While the inviscid exhaust jet flow over the aerospike and plug nozzle ramps are generally the same, the addition of a base area on the plug nozzle does alter the flow aft of the body by creating a wake. A component of the plug nozzle's thrust is the force of the pressure against the base of the plug. The prediction of base pressure represents a long-standing fluid dynamics problem that has yet to be fully understood. In traditional wakes, the base pressure is a function of the pressure in the freestream flow. Due to the "wake closure" phenomenon, the

base pressure in plug nozzles is a function of the pressure in the exhaust jet and/or the ambient freestream.

A general illustration of the two conditions is shown in Figure 1.7. In the open wake condition, the base pressure is roughly equivalent to the ambient pressure. As the NPR increases (such as when the altitude increases), and the jets converge to form a "closed" wake, and the base region is isolated from the ambient environment, making base pressure independent of ambient pressure.

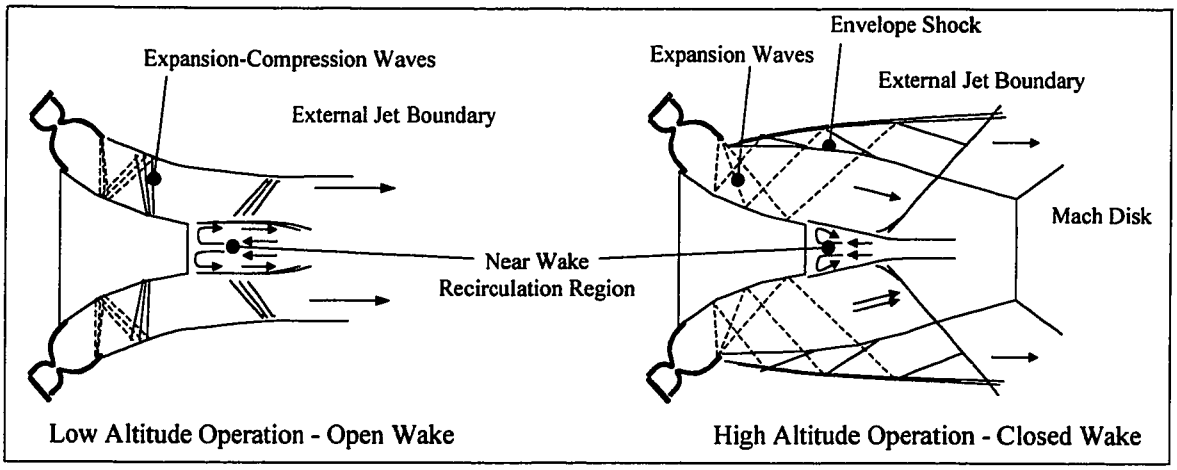

Figure 1.7: Open and Closed Wake Condition in Plug Nozzles

An example of the base pressure changes with NPR is shown in Figure 1.8. In Region 1, the wake is open and the base pressure is nearly the identical to ambient pressure and varies linearly. The wake is closed in Region 3 where base pressure is independent of ambient pressure. A transition region occurs in Region 2 where the base pressure is not equal to, but still a function of, ambient pressure. A jump in the transition and represents the pressure as the envelope impinges on the near-wake region.

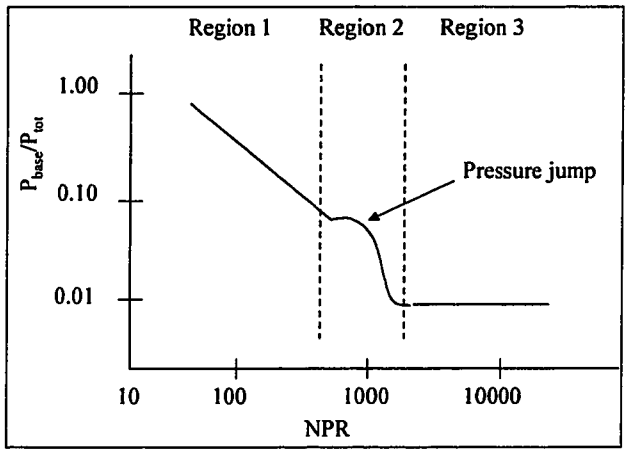

Figure 1.8: Typical Base Pressure Variation

The present definition of wake closure thus far has been whether or not the base pressure is dependent on ambient pressure. This "definition" might be considered an "engineering definition" in that its principal use is to provide a criterion in thrust performance analyses. Researchers have described two sets of conditions associated with wake closure for different plug nozzles (not necessarily mutually exclusive) and have a general understanding of the mechanisms involved. But because wake closure has only been addressed at this global level, the prediction of wake closure is primarily empirical. The interrelated factors, such as ramp geometry, jet angle and position, slipstream effects, etc., have made wake closure prediction a configuration and/or situation-dependent problem. For example, some researchers have analyzed contoured ramps and have linked the position of the envelope shock to wake closure for this configuration; whereas others have tied wake closure to the occurrence of flow separation from the ramp surface in some planar ramps.

1.1.4 Design Implications of Wake Closure

Wake closure affects the plug nozzle operations and can improve vehicle capability. From a design perspective, prediction of wake closure affects the analysis of vehicle performance. During the ascent phase of the NASA X-33, as

an example, wake closure is expected to occur between 25,000 and 30,000 ft. Thus, the wake is closed for the major portion of flight and precise determination of wake closure is not necessary for initial performance analyses. These performance analyses relied on traditional wake methods to compute closed wake base pressures. Once the base pressure equaled the ambient pressure, the wake was considered open and the base pressure was set equal to ambient pressure. In another method, wake closure was predicted to occur based on the same criteria used for predicting boundary layer separation overexpanded bell-nozzles (e.g., separation occurs when $p_{exit,design}$ is approximately $0.4p_{amb}$).

The inability to accurately predict engine performance throughout the duration of the launch will have significant impacts on the launch vehicle capability and its operation. Uncertainties in the thrust, or specific impulse (a measure of engine efficiency), computations must be incorporated into design margins that reduce the advertised payload-to-orbit lift capacity. Figure 1.9 illustrates the impact of such uncertainties on a single-stage-to-orbit rocket.

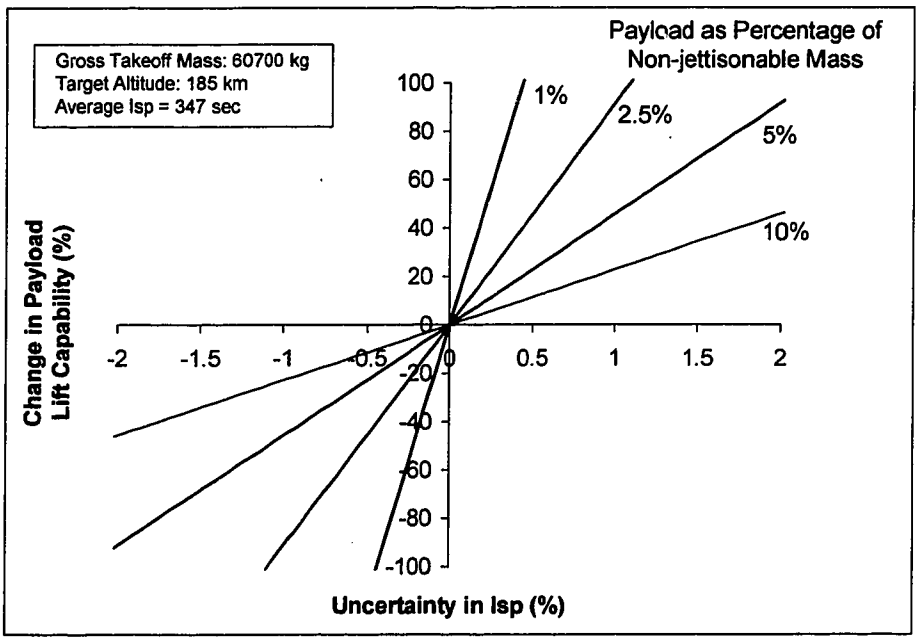

Figure 1.9: Effect of Rocket Performance Uncertainty on Payload Design

If the payload constitutes 10% of the non-jettisonable mass of the launch vehicle (i.e., the mass of the vehicle that is retained for the duration of flight), a 1% uncertainty in the specific impulse results in a 20% reduction in the predicted launch vehicle payload capacity. Seconds of specific impulse determine whether or not the vehicle will reach orbit with its payload.

For reusable launch vehicles that return from orbit and maneuver at low altitudes, the problem of predicting when the plug nozzle wake is open or closed complicates the definition of its flight envelope. The throttling of the engines from full-thrust to engine-off conditions will affect the wake condition, and thus impact both the launch vehicle lift as well as control authority during landing.

1.2 Research Objective

While extensive research has been conducted on plug nozzles, the research has been driven by technology demonstration and flight hardware programs and thus has primarily addressed the plug nozzle flow at an engineering level (3). Since open wake conditions constitute a small portion of the launch ascent, wake closure has not been a significant design. Moreover, many analytical concepts and tools used to investigate supersonic wake flows were still in their infancy during the peak plug nozzle research activity (i.e., 1960's). As a result, a detailed understanding of the flow physics and mechanics of how wake closure occurs remains an issue. These issues must be addressed for further development and optimization of the plug nozzle as an operational engine.

In broad terms, the objectives of this research are 1) to characterize in more detail the changes occurring in the wake as it transitions between closed and open conditions, and 2) based on this characterization, explain the mechanism(s) leading to wake closure. This research provides greater insight of the flow dynamics and a more physical understanding to the existing engineering definition of wake closure. Further, the characterization of the

near-wake flow dynamics also provides insight into extent, or limits, to which traditional wake research results are applicable to plug nozzle flows. The problem is broken down into the following areas:

- Characterization of the plug nozzle flowfield structure in open and closed wakes and the conditions under which they occur,
- Characterization of changes in plug nozzle wake structure,
- Relationship of these changes to base pressure and wake closure,
- Development of a physical model for wake closure, and
- Assessment of the implications of wake closure on design

Table 1.1 explains the specific technical contributions of this dissertation. Much of the data development was driven by hardware and technology demonstration. While significant knowledge already exists to characterize plug nozzle flows, additional basic research was required to explain the wake flow. The dissertation provides deeper insights into those areas already addressed by existing research and develops new understandings of plug nozzle flows.

Table 1.1: Dissertation Technical Contributions

		New Contributions	
Objective	Existing Knowledge	Developed Deeper Knowledge	Developed New Knowledge
Characterization of Wake Closure Conditions	• Envelope shock and compression waves cause wake closure • Correlation between wall separation and wake closure	• More complete characterization of wake closure transition • Classification of wake closure modes	• Compilation of data and analysis specifically addressing wake closure • Characterization of downstream flow structures for wall-separation mode
Explanation of Wake Structure and Wake Closure Mechanism	• Use of supersonic wake models for closed wake base pressure prediction	• Evaluation of traditional wake analyses for plug nozzle wakes	• Comparison of plug nozzle and supersonic wake structures • Linkage between wake closure and analytical wake concepts
Wake Closure Implications to Design Process	• Dependence of wake closure on plug length	• Analysis of design factor effects on wake closure	• Assessment of how wake closure may be designed into performance improvement

The results of this research provide benefits to plug nozzle development as well as a broader understanding of wake dynamics. At a programmatic level, the key benefits include:

- Improved accuracy for performance analyses for design of launch vehicle payload-to-orbit capability
- Better understanding of the near-wake dynamics interactions necessary to improve of base pressure prediction
- Improvement of off-design data for performance analyses of low altitude operations and throttling capability

1.3 General Approach

This research combines theoretical, experimental, and numerical efforts to characterize and analyze the wake closure mechanisms. The organization of the research to accomplish the tasks defined above is shown in Figure 1-10.

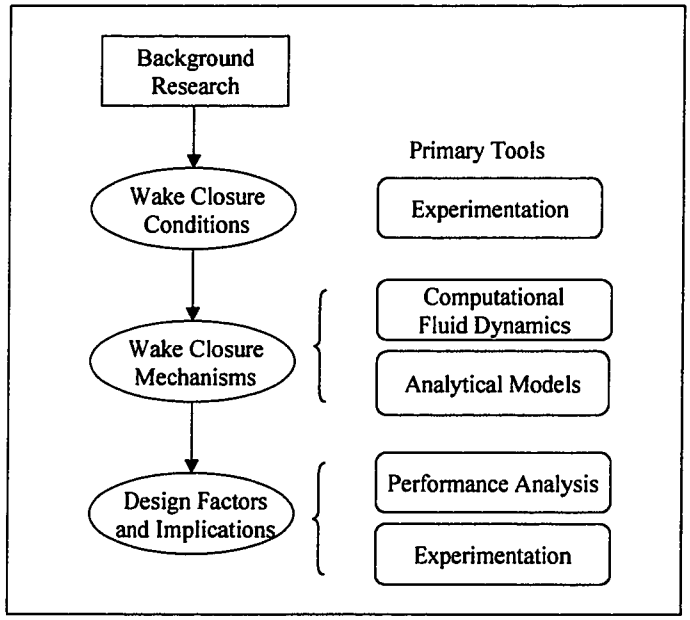

Figure 1.10: Research Tasks and Structure

Background Research. The research began with a survey of available literature to develop an overall understanding of plug nozzles and plug nozzle flowfields. Specific emphasis was placed on existing theoretical models for wakes and base pressure predictions. Based on these models, several methods were identified for analyzing the near-wake of the plug nozzle and the effects of wake closure.

Wake Closure Conditions. The characterization of plug nozzle flowfields in open and closed wake conditions was conducted experimentally. A test facility was designed and fabricated specifically for these tests. Experiments provided a reference for analysis, identified the wake closure modes and conditions, and allowed development of qualitative correlations between flowfield changes and wake closure. The major measurements included base pressure, sidewall centerline pressure, and Pitot pressure measurements and Schlieren photography.

Wake Closure Mechanisms. Numerical simulations of the plug nozzle flow, using Computational Fluid Dynamics (CFD), were conducted to provide detailed information on the internal flowfield. These simulations provided detailed flowfield information for the wake in open and closed conditions. Concepts and metrics from theoretical wake analyses were then used to relate the physical flowfield changes to the wake closure mechanisms.

Design Factors Analysis. Wake closure has been a phenomenon that is predicted and then incorporated into performance analyses. Although recognized to improve engine performance, no effort has been made to assess whether or how wake closure can be manipulated for performance improvement. The ability to incorporate wake closure into the design process has been hindered by the empirical nature of the criteria and limited understanding of the wake closure mechanisms. This last analyzes the effect of different design factors using the Design of Experiment (DOE) methodology and then examines how these effects can contribute to improved performance.

Chapter 2
PLUG NOZZLE FLOW THEORY

This chapter provides the theoretical background for the analysis of the wake closure in plug nozzles. The first part of the chapter is a brief summary of the plug nozzle's research evolution. The remaining sections are descriptions of the plug nozzle flowfield, the flow conditions linked to wake closure, and trends in wake closure resulting from changes in nozzle geometry and test conditions. Since the research analyzes the plug nozzle wake, an explanation of the traditional supersonic wake structure is provided and the wake analysis methods and flow separation theories used to examine plug nozzle wakes are described.

2.1 Plug Nozzle Research Overview

Much of the research on plug nozzles was sponsored under contract to the U.S. Government from 1956 through the 1970's and is summarized by Bollard (3). General Electric conducted some of the early studies (3), but Rocketdyne (4, 5) continued the bulk of this research under contract to NASA and the U.S. Air Force. Although much of the data and experience from these research efforts was classified with limited distribution outside of the U.S. Government, it is apparent that significant strides were accomplished in building and testing components for the aerospike/plug nozzle. This research developed a large resource of test data on base pressure and engine performance for a wide range of hardware configurations and components, propellant mixtures, and test conditions. Most of the effort focused on the testing of hardware, but there were theoretical and semi-empirical processes in which to validate the designs.

The open literature published by NASA and academia generally focused on two areas: thrust performance experiments or closed wake base pressure analyses. Investigations at the NASA laboratories consisted primarily of wind tunnel testing on full-length aerospike nozzles of different configurations using load cells or strain gauges to measure thrust (6, 7, 8). Theoretical performance analyses were based on Method of Characteristics for the inviscid jet flow and Korst models for base pressure (9, 10, 11). The research conducted at academic institutions such as Cornell University and Notre Dame University complemented the industry efforts by studying more detailed flow characteristics such as the wake (12, 13, 14, 15).

As engine designs for lunar launch vehicles and the Space Shuttle focused on the proven bell nozzle, funding and research was cut for the aerospike nozzle. It was not until the late 1980's with a resurgent interest in SSTO launch vehicles that aerospike nozzles were reexamined as a means for providing additional performance. NASA's X-33 program reintroduced funding in the United States for aerospike development. NASA (2) conducted some recent computational analyses on the plug nozzle. Much of the funding however has been directed to Boeing North American (i.e., Rocketdyne) for the development of flight hardware for the X-33 with the assumption that enough data was collected from prior research to build an engine that support a test vehicle. The technical details of engine design have yet to be published. Testing of the engine will not occur until later. In Europe and Japan, researchers have gone back to the basic fluid analyses to build the knowledge base to apply aerospike engines to their own launch vehicle initiatives (16, 17, 18).

2.2 Wake Closure Development

The key features of the plug nozzle flow during closed wake conditions are depicted in Figure 2.1. The jet is exhausted onto the nozzle ramp and expands into the ambient environment. The expansion waves reflect from the solid

surface and continue as expansion waves. But once they intersect with the free jet boundary, they reflect again as compression waves and coalesce into an envelope shock. As the flow turns around the ramp lip, the flow again expands through expansion waves and then separates from the ramp surface. A shear layer is created with a recirculation region aft of the base.

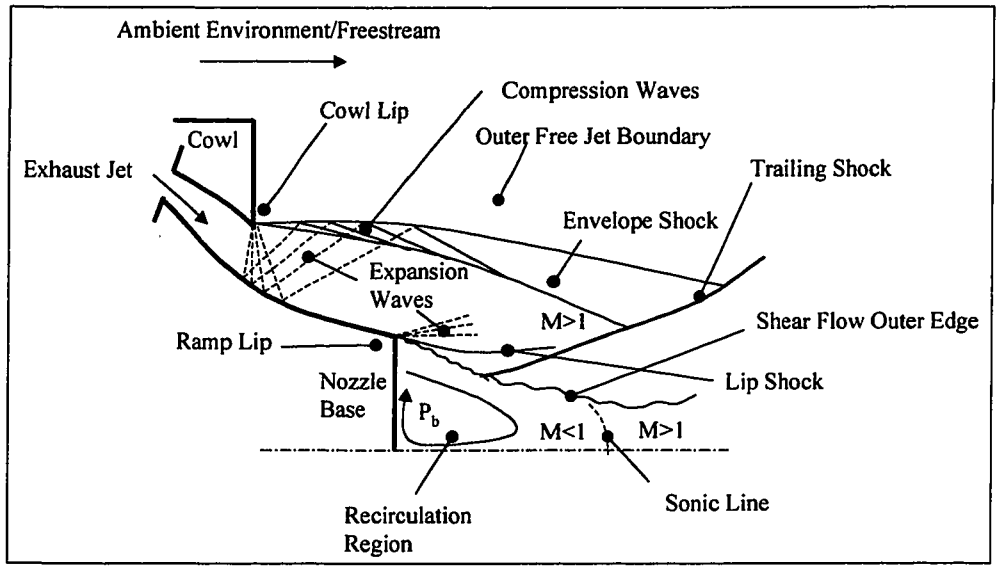

Figure 2.1: Plug Nozzle Flow Structure

While most researchers have recognized the occurrence of wake closure, little quantitative data exists in the open literature to identify the NPR at which wake closure occurs. Table 2.1 lists the experimental and CFD data from which wake closure could be determined. Wake closure data was extracted from base pressure data by researchers at Rocketdyne (3, 4) and Tomita, et. al., (18) for their specific geometries over a set range of conditions. Sule and Mueller (14) specifically addressed the affect of plug nozzle length on the point of closure. The point of wake closure in the data by Rommel, et. al., (16) was extrapolated from computational data.

Table 2.1: Selected Wake Closure Data

Ramp Shape	γ	Area Ratio, (A_e/A_t)	Length	NPR	Reference
Contour	1.654	148	10%*	2000	4
Contour	**	25	20%*	210	5
Contour	**	25	20%*	165	5
Contour	**	25	20%*	175	5
Conical (10°)	1.4	1.555	0.2184-0.4802	5-7	14
Conical (10°)	1.4	1.688	0.1449-0.3785	5-10	14
Conical (40°)	1.2	55	0.53	255	16
Contour	1.4	6.5	0.20	30	18
Contour	1.4	6.5	0.10	30	18

* Length as a percentage of an equivalent 15° cone
** Hydrogen Peroxide Propellant

From the literature summarized in Section 2.1, plug nozzle wakes undergo two types of changes with varying NPR (not necessarily mutually exclusive). The first set of changes shown in Figure 2.2 has been associated with research on contoured plug nozzles. At low NPR, the outer free jet boundary lies close to the ramp surface. The compression waves emanating from the boundary compress the flow along the ramp, but also enter the near-wake region. The ability for the external environment to affect the base pressure through these compression waves constitutes an open wake condition.

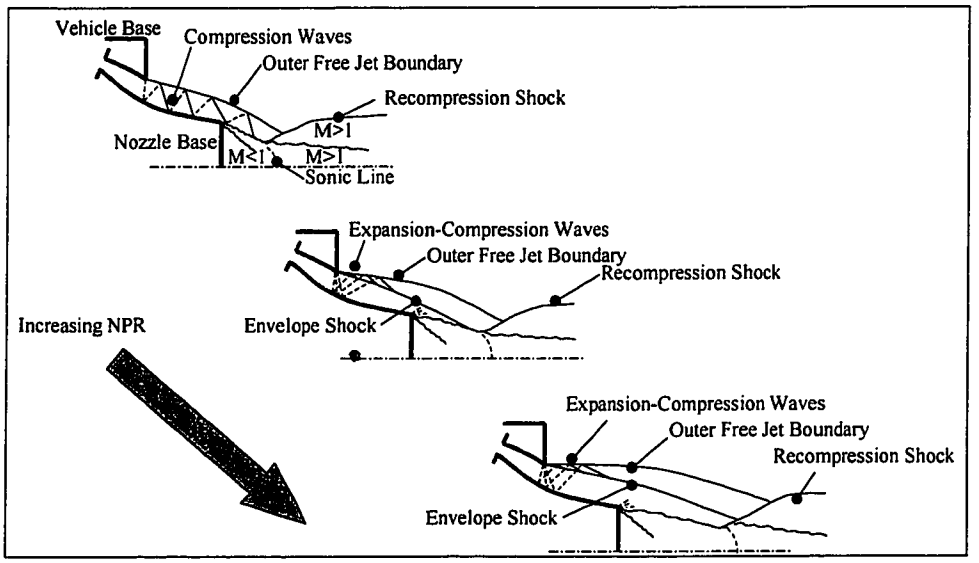

Figure 2.2: Envelope Shock Mode of Wake Closure

As the NPR increases, the compression waves coalesce into an envelope shock. Initially this envelope shock impinges the ramp surface, but then the point of impingement moves downstream along the ramp surface with higher NPR. Eventually, the envelope shock no longer impinges the ramp surface, and at even higher NPR, impinges the near wake far enough downstream that the compression waves no longer affect the base pressure.

The second set of changes leading to wake closure is not as well documented but is linked to the separation of the exhaust jet flow from the ramp surface. During its conical nozzle tests, Rocketdyne researchers (4) found that flow separation occurred at a certain NPR. The flow separation was attributed to the need to satisfy the downstream wake recompression conditions, and predicted the point of separation from its base pressure analyses. The open literature did not elaborate further (probably assuming the reader could access the classified base pressure analysis), and no linkage was made to wake closure.

Based on their review of Rocketdyne literature, Fick and Schmucker (19) concluded that flow separation occurred in plug nozzles and was responsible for the plug nozzle altitude compensation, contrary to previous claims. In order to compute the plug nozzle performance, they demarcated the point of wake closure based on empirical relations used to predict separation in overexpanded bell nozzles (20). Reassessment by Rocketdyne researchers (21) of the past experimental data confirmed their earlier conclusions that flow separation did not occur on the contoured nozzles, and surmised that Fick and Schmucker's (19) flow separation interpretation may have been based on limited information about the experimental apparatus.

Based on their own experiments, Tomita, et. al. (18), described three types of flow patterns for a conical nozzle as a function of NPR. At low NPR, a small separation region existed on the ramp surface (linked to the impingement of the envelope shock on the ramp). The flow reattached to the surface once the

pressure was recovered downstream of the expansion/recompression typical of impinging shock/boundary layer separation-reattachment. The flow separation line moved toward the plug tip at an intermediate NPR, and the flow failed to reattach to the ramp surface. At high NPR, the separation line moved to the plug tip. Separation on contoured nozzles did occur, but only at low NPR. The transition between the flow patterns at intermediate and high NPR occurred rapidly, and wake closure occurred during this transition. The flow also separated on contoured nozzles, but only very low NPR (18). Rommel, et. al. (16), comparisons of the German Aerospace Research Establishment (DLR) experiments to CFD simulations also confirm flow separation on conical nozzles.

Figure 2.3 was constructed from descriptions by Tomita, et. al, (18), and depicts the changes in flow over the ramp with NPR as it undergoes wake closure through the wall separation mode. The flow structure downstream of the ramp not as well documented and must be characterized further. (Note: supplementary flow features not described by Tomita, et. al., were added based on the author's experiments for completeness).

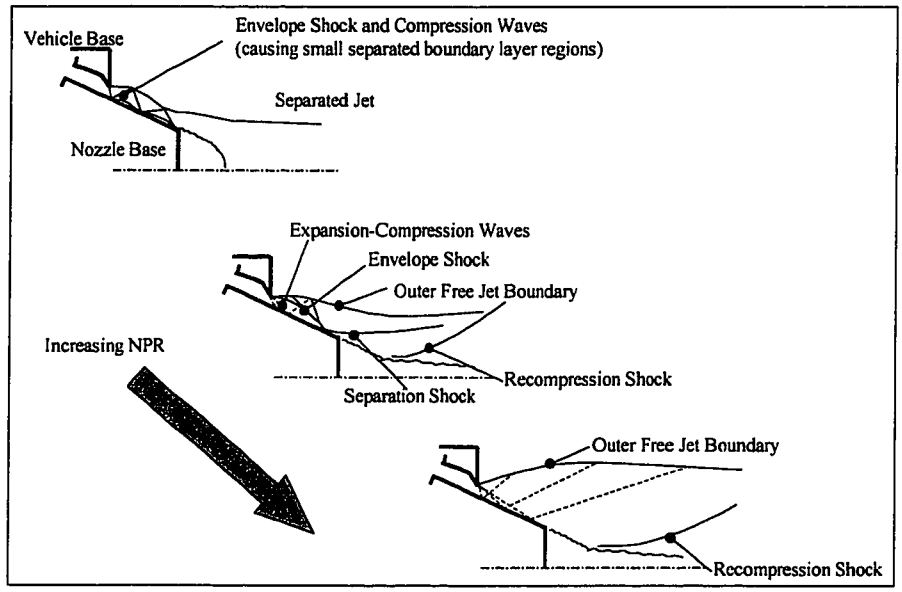

Figure 2.3: Wall Separation Mode of Wake Closure

Based on the observation that wake closure occurs during the above sets of conditions, some qualitative assessments have addressed the effect of various factors on the NPR of wake closure. These factors include jet flow conditions, thruster configuration, freestream conditions, and ramp geometry:

Exhaust Jet Conditions. The total pressure of the jet usually works in conjunction with other factors to determine when wake closure occurs. Generally the point of wake closure is depicted on graphs of base pressure-to-total pressure ratio versus NPR. The order of magnitude differences in the NPR of wake closure for the Rocketdyne experiments compared to the other data may be a result of the working gas (due to different specific heat ratios, γ) and the high temperatures from combustion. The Mach Number and Reynolds Number of the jet prior to separation from the ramp generally affect the entrainment rate in supersonic wakes and thus the base pressure. However, it is unclear whether the factors would simply cause an offset base pressure, or if it would also affect the point of wake closure. The jet angle and position determine the flow Mach Number and define the initial shape of the envelope shock in the flow. In addition, the cowl or distance between the jet and freestream creates another base flow region just above the thruster. The pressure in this region will affect the expansion of the flow as well as the envelope shock shape.

Freestream Conditions. The ambient pressure of the freestream determines the expansion of the flow for a given ramp geometry. Ambient pressure relative to total jet pressure is a metric for depicting the changes in base pressure and thus identifying the point of wake closure. Rocketdyne researchers (5) conducted several experiments to examine the effect of the freestream Mach Number. This "slipstream" effect on wake closure is due to the interaction of the freestream with the recirculation region aft of the cowl. Depending on the pressure and Mach Number of the freestream, the recirculation region can extend far downstream, thus affecting the envelope shock shape.

Ramp Configuration. Based on the available literature, Fick and Schmucker (17) found the ramp configuration to have two counteracting effects on base pressure affecting wake closure. For a shorter plug, the pressure level of the core flow at the plug exit increases, leading to a wake closure at lower NPR. The plug exit wall pressure equals ambient pressure at a lower altitude. On the other hand, the total base area increases, leading to a bigger volume to be secluded by the core flow flowfield, which tends to become more difficult to close, thus leading to a wake closure at higher NPR (12, 13 – as referenced in 17). Sule and Mueller (14) conducted tests of several conical plug lengths for two design Mach Numbers. Their experimental results showed that for these configurations, the NPR at which wake closure occurred increased with ramp length and design Mach Number.

Base Bleed. Base bleed is the expulsion of gas from the base of the plug. Base bleed can be used as a means of cooling the hot base surface. This base bleed increases thrust due to the added mass being expelled from the vehicle, but it also reduces engine specific impulse because of its lower energy flow. The expelled gas changes the mass flow, velocity and enthalpy profiles of the flow within the wake. Cursory review of the Rocketdyne data (4) suggests that the point of wake closure occurs at higher NPR with increased base bleed.

2.3 Plug Nozzle Flowfield and Analysis

The plug nozzle flowfield consists of an inviscid flow emanating from the thrusters and a viscous flow region aft of the plug base. Wake closure has been linked to changes in the inviscid flow structure, such as the position of the envelope shock or the presence of flow separation from the ramp surface. The inviscid flow has been extensively researched, and though requiring significant effort to analyze, is generally well understood. Though not a focus of this dissertation, the inviscid flowfield is briefly reviewed to provide context for

interpretation of the experimental results and highlight some of the key structures that occur in the flow that affect wake closure.

To develop a more detailed physical interpretation of wake closure, it is necessary investigate the how changes in the external flowfield affect the internal structure of the viscous base flow. In the past, traditional supersonic wake methods have been applied to the analysis of the plug nozzle base flow at in closed wake conditions. These methods serve as a departure point for investigating wake closure and the transition from closed to open conditions. The methods are reviewed in the following sections, and the major concepts applicable to plug nozzle flows are identified.

2.3.1 Inviscid Flowfield

Though more sophisticated CFD tools are now available, the typical approach used to analyze the inviscid flowfield has been the Method of Characteristics. The standard approach illustrated in Figure 2.4 begins with the computation of characteristics from points or cells (depending on the method used) at the exit plane of the thruster. Subsequent characteristics are then determined throughout the jet flow along the ramp surface. The jet differs from internal flows in that the outer boundary is defined by a pressure distribution from the ambient environment rather than a solid surface. The contoured ramp shapes are designed so that at design conditions, the initial expansion characteristic lines intersect the ramp surface, but do not reflect back into the flow due to the slope of the surface. The planar ramps will always reflect the expansion waves since the angle of the surface is not matched to the in-coming characteristic line angles. At lower NPR, both types of ramp shapes will involve a system of intersecting compression and expansion waves until the NPR is so low that the exhaust jet does not expand at the exit plane.

Initial applications of Method of Characteristics matched the free jet boundary to the ambient conditions. More accurate representations of the flow included the envelope shock that arises when the characteristic lines reflected from the free jet boundary coincide. To facilitate locating the envelope shock, University of Notre Dame researchers (14) applied the Hartree technique by defining the points of interest and then iterating on the upstream characteristics to determine the local flow conditions. This approach is particularly appropriate at lower NPR conditions when the envelope shock plays an important part of the inviscid flow dynamics. Physically, the envelope shock arises due to the over-expansion of the inviscid flow as it exits the thruster and turns the corner of the thruster (or cowl) lip. The shock turns the flow back to match the ambient conditions. Since the envelope shock is the intersection of the reflected compression waves from the free jet boundary, the flow between the envelope shock and free jet boundary is governed by the conditions at the free jet boundary, or ambient environment. Depending on the location of the envelope shock, these compression waves may impinge on the near wake region and thus affect base pressure. This is the basis for the envelope shock mode of wake closure.

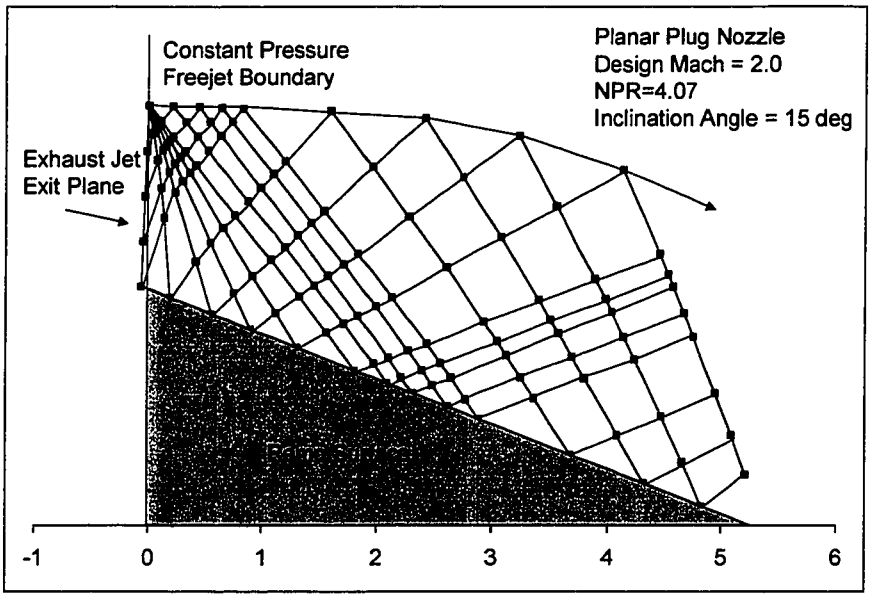

Figure 2.4: Inviscid Jet Characteristics on Planar Ramp

The boundary layer flow along the nozzle ramp under adverse (or positive) pressure gradient is subject to separation from the surface. Under isentropic expansion conditions, the flow along the ramp undergoes continual expansion (i.e., negative pressure gradient) and thus avoids separation. But as the NPR decreases, the flow no longer undergoes isentropic expansion. At some point, the NPR decreases to a level where the exhaust jet is pushed against the ramp surface. For planar ramps, the resulting pressure gradient leads to flow separation. The contoured ramps are less susceptible to this flow separation because of the lower average pressure gradient associated with the surface slope. Schmucker (22) summarized several methods for predicting flow separation in liquid propellant rocket nozzles. The prediction of flow separation is generally a complex fluid dynamics problem. Present prediction methods are based on the effects of pressure gradient, Mach Number, displacement and momentum thickness, and empirically derived separation constants. As described by Tomita, et. al. (18), regions of flow separation along the ramp may also occur due to the impingement of the envelope shock on the surface. Flow separation leads to inviscid-viscous interactions by which the inviscid flow characteristics may change. The wake structure may also be significantly affected if the flow does not reattach to the surface prior to the ramp corner.

For standard supersonic wake flows, Hama (23) found that the flow around the afterbody corner may not separate precisely at the corner. Instead, the flow may "over-expand," and the boundary layer separates on the base plane. The over-expansion decreases the flow pressure below the base pressure, so the lip shock develops to bring the flow back to equilibrium conditions. The lip shock distorts the velocity profile of the mixing layer, and has an unknown influence on near wake. Though having decreasing effect downstream, the lip shock also causes an increase in pressure in the inviscid flow along the near wake, which would also increase base. Hama found that laminar boundary layer flows just prior to the afterbody corner were more susceptible to having this lip shock, whereas the lip shock may not exist with turbulent boundary layers.

2.3.2 Near Wake Flow

Figure 2.5 illustrates the common features that are considered in theoretical models to affect base pressure. A boundary layer of finite thickness develops on the body and separates near the body corner. The flow undergoes an expansion as it turns the corner toward the axis, and a sharp drop in static pressure. The separated flow creates a mixing layer between the freestream and dead-air region. The separating streamline defines the outer boundary of the mixing layer interfacing with the freestream flow. As the flow approaches the axis, compression waves develop and causing the flow to turn in parallel to the axis. At a certain point, the flow reaches a "reattachment" point (or rear stagnation point, RSP) where the shear flows from both sides of the afterbody merge into one flow. The outer edge of the shear layer reaches a minimum (or wake neck) aft of the reattachment point prior to growing again.

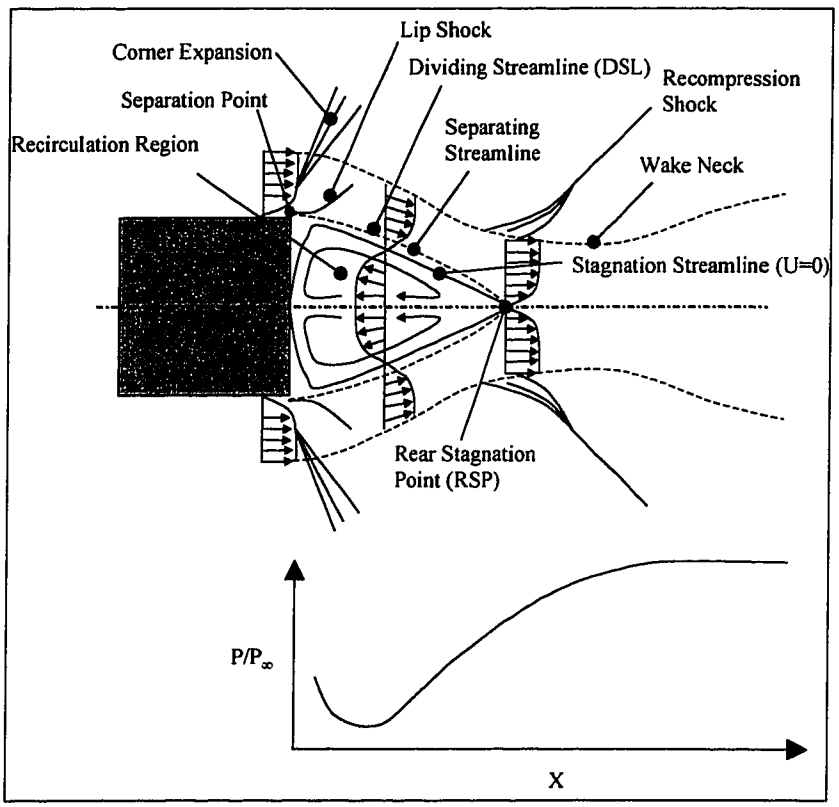

Figure 2.5: Near-Wake Structure

The dividing streamline (DSL) is the inner boundary of the original boundary layer and is drawn from separation to the reattachment point. The high-energy flow in the mixing layer passes through the recompression region and flows downstream eventually recovering the freestream pressure, while the low-energy flow is turned back toward the body. The stagnation streamline separates fluid that continues downstream from that which recirculates in the dead-air region. When no mass is injected from the base (i.e., base bleed), the stagnation streamline and the dividing streamline are the same. The lip shock extends from separation point and causes a recompression of the flow to match conditions at the separating streamline. A constant-pressure mixing region exists just after separation as a jet velocity profile transitions from the pre-separated boundary layer to a mixing region wake profile with backflow.

The analysis of the internal wake structure and base pressure remains a significant research problem. In mathematical terms, the recirculation region is governed by the full Navier-Stokes equations, which are elliptical in nature, and the free interaction boundary condition of the viscous flow also introduces elliptic features into the problem (24). These types of equations allow perturbations anywhere in the flow can be communicated throughout the region (as opposed to, for example, hyperbolic equations found in inviscid supersonic flow where perturbations can only propagate downstream).

Dutton, et. al., (25) identified several factors that make prediction of the wake structure and base pressure difficult. In supersonic flow, the shear layer of the separated flow is compressible, thereby affecting the rate of mixing between the inviscid external flow and the viscous wake. Initially, the shear layer is under constant pressure conditions and then transitions to adverse pressure gradient conditions due to the recompression process. The corner expansion is also influenced by the turbulent structure of the boundary layer at separation from the afterbody, which then affects the shear layer and mixing process. Moreover, the streamline curvature of the viscous flow causes transverse pressure

gradients, and in general, the wake may contain non-uniform, non-isoenergetic flow regions. As a result, researchers have developed a range of empirical relations, analytical methods, and computational fluid dynamics (CFD) techniques, all seeking to improve the ability to predict base pressure and analyze wake flows.

Empirical Relations. Because the problem is so complex, many designers utilize simple empirical relations to predict base pressure. These relations are similar in form to the example shown in equation (1) below by Lamb-Oberkampf (26) and highlight the major parameters that influence base pressure.

$$\frac{p_{base}}{p_\infty} = \left(1 + \frac{2}{\gamma - 1} M_e^{-2}\right)^3 \left[M_e^2 \, \mathrm{Re}_s^{-1/2}\right]^{0.6} \qquad \text{(laminar)} \qquad (1)$$

$$\frac{p_{base}}{p_\infty} = 0.01 + 1.03\left\{1 - \left[1 - \left(1 + \frac{\gamma - 1}{2} M_e^2\right)^{-1}\right]^{1/2}\right\} \qquad \text{(turbulent)}$$

Fick and Schmucker (17) compare several different empirical relations specific to plug nozzles with closed wakes. Most of the empirical relations used for plug nozzles, such as Equation (2), are based on cylindrical configurations in supersonic flow. These relations produce results within a few percent to an order of magnitude difference from the measured base pressures.

$$\frac{p_{base}}{p_\infty} = M_e \left(\frac{2}{\gamma + 1}\right)^{\frac{\gamma}{\gamma - 1}} \left[0.05 + \frac{0.967}{1 + \frac{(\gamma - 1)}{2} M_e^2}\right] \qquad (2)$$

These relations illustrate the importance to base pressure of edge Mach Number prior to separation. Base pressure is generally a fraction of freestream pressure and decreases with increasing Mach Number. Laminar wakes are also

dependent on Reynolds Number prior to separation, whereas turbulent wakes are Reynolds Number independent.

Theoretical Models. The theoretical approaches for modeling the wake are generally divided into two categories: Multi-component methods and Inviscid-Viscous Interaction (IVI) methods. Berger (27), Delery and Lacau (28), and Ohrenberger, et. al. (29) provide extensive surveys of the analytical methods developed within these classes of analysis. Some of the better known investigators in this field are identified in Figure 2.6. The Chapman-Korst models introduced an approach that divides the flow into components or flow regions. Each region is treated independently and then patched together for the overall solution. The IVI methods based on Crocco-Lees incorporate the interaction between the external inviscid flow and viscous shear flow as a continuous process leading to recompression and reattachment. Subsequent research in both approaches has focused on improving criteria or refining model details. Though based on finite difference methods, Baum and Dennison are listed in this figure for the contribution of their results to the IVI methods.

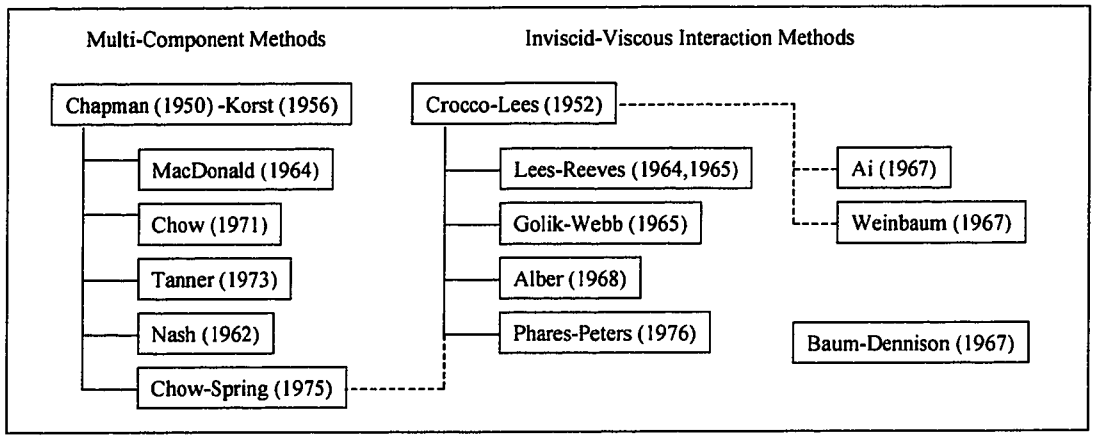

Figure 2.6: Theoretical Base Pressure Methods (30-44)

Multi-Component Methods. The flow regions and structures used by the Multi-Component methods are shown in Figure 2.7. These methods assume that the expansion and compression processes occur over finite lengths and therefore

the flow regions can be separated into several components (i.e., oncoming freestream, expansion, recompression, and far downstream). The conditions of each region are then matched at the junction between them.

The basic tenet of the Multi-Component method is that flow above the DSL passes through the recompression process downstream, whereas flow below the DSL recirculates back into the wake. The recirculated mass flow then determines the base pressure from continuity relations.

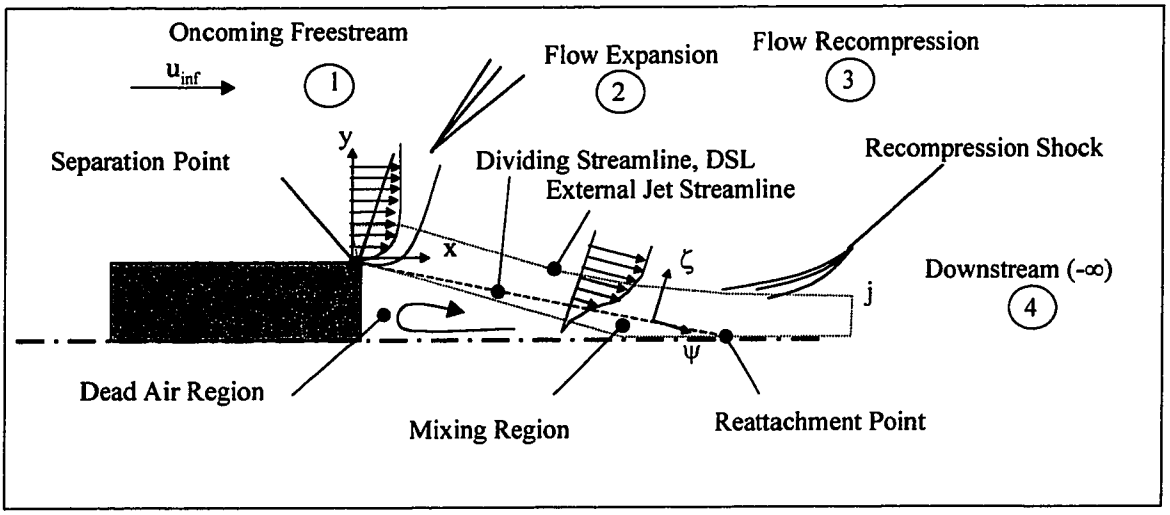

Figure 2.7: Multi-Component Model of Wake Flow

The original formulation by Korst (30) determines the location of the DSL from the continuity equation. The continuity equation (3) is an integral relation between the mass flow streamline, s, the DSL, and the external jet streamline, j. A velocity profile, φ, and shear layer spreading parameter, σ, are assumed.

$$\int_{\eta s}^{\eta DSL} \frac{\varphi d\eta}{1-C^2\varphi^2} + \frac{\sigma G_s}{x\rho u(1-C^2)} = -\int_{-\infty}^{\eta DSL} \frac{\varphi^2 d\eta}{1-C^2\varphi^2} \quad \text{and} \quad \int_{\eta j}^{\eta DSL} \frac{\varphi d\eta}{1-C^2\varphi^2} = \int_{-\infty}^{\eta DSL} \frac{\varphi^2 d\eta}{1-C^2\varphi^2} \quad (3)$$

where $\varphi = \frac{1}{2}[1 + erf(\eta - \eta_b)] + \frac{1}{\sqrt{\pi}} \int_{\eta_p}^{\eta} \varphi\left(\frac{\eta - \beta}{\eta_p}\right) e^{-\beta^2} d\beta$, mixing layer velocity profile

$G_s = \int_{yj}^{yDSL} \rho u dy$, mass flow between the j and DSL streamlines

$C = \left[1 + \frac{2}{(\gamma - 1)M^2}\right]^{-1/2}$, a dimensionless velocity parameter

$\eta_P = \frac{1}{2\sqrt{\frac{1}{2\sigma^2} \int_0^{\psi} \psi f(\psi) d\psi}}$ and $\eta = \zeta \eta_P$, are position parameters

β = an integration constant

For a given set of initial conditions, Equation (3) is solved by iteration for an assumed C. The solution is computed iteratively until it meets a "reattachment criterion" which defines the requirement for flow to pass completely through the recompression process or is turned back. The examples of reattachment criterion shown in Table 2.2 relate the flow ahead of the recompression shock to conditions downstream of recompression.

Table 2.2: Multi-Component Method Reattachment Criteria

Korst (30, 28)	$P_{tot,u=0} = p_{-\infty}$
Nash (34)	$N = \frac{p_c - p_{base}}{p_\infty - p_{base}}$, where N is found empirically
MacDonald (33)	$H_{-\infty,c} = 1.63 - 0.0775\left(\log_{10} \frac{\mu_\infty \theta_{-\infty}}{\mu_{-\infty} \theta_\infty}\right)$, where H is the shape factor, c means compressible, θ is the momentum thickness

Later refinements of the Multi-component Method by Chow (32) and Chow and Spring (35) utilize an integral momentum boundary layer relation similar to that used in the IVI method. The governing equations contain a singularity that

replaces the reattachment criterion, and the solution is solved iteratively using a downstream marching procedure until it passes through the singularity.

As an additional note, Korst uses the terminology "open" and "closed" wakes to determine the value of G_s necessary to compute a unique solution. In a closed wake, G_s is simply zero (i.e., the wake is a closed mass flow rate system). The open wake exists when G_s is not zero as in the case of base bleed existed or backflow from the high pressure region behind the recompression zone pressure. The primary usage of this terminology is to determine the need for an additional equation for the mass flow rate. It is not clear that this terminology is directly applicable to the plug nozzle terms.

IVI Methods. The IVI method illustrated in Figure 2.8 treats the wake as a separated-reattaching boundary layer. The wake is initiated at the separation from the afterbody with an outer edge at a negative inclination. The subsequent velocity profiles have both forward and backflow (or recirculation) components. The boundary layer equations are solved as the wake develops and passes downstream. The initial conditions and boundary layer assumptions lead to a physically real solution only if the boundary layer flow parameters develop such that the solution passes through a "critical point," which determines a unique, closed-form solution to the base pressure problem.

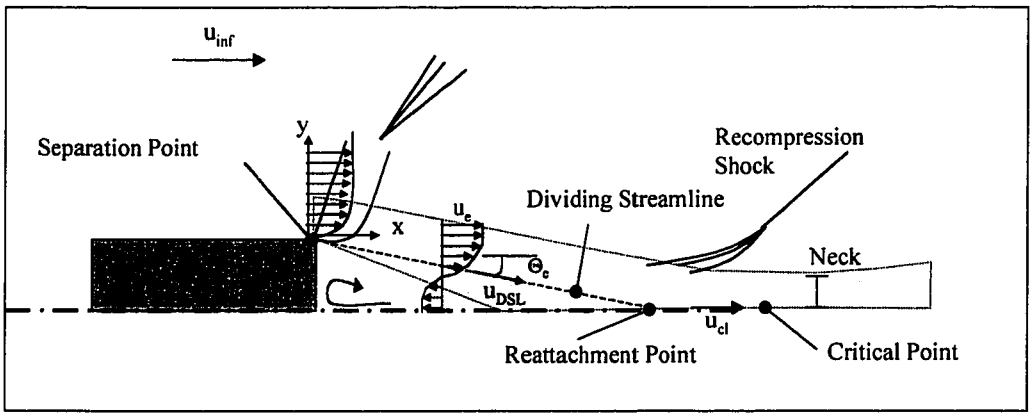

Figure 2.8: IVI Model of Wake Flow

Lees and Reeves (36, 37) method illustrates the IVI Method formulation and process. Using the Stewartson transformation, Lees and Reeves change the compressible boundary layer equations into incompressible form. The equations of motion are derived in the form shown below:

Stewartson Transformation:

$$dX = \frac{a_e}{a_\infty}\frac{p_e}{p_\infty}dx, \qquad dY = \frac{a_e}{a_\infty}\frac{\rho_e}{\rho_\infty}dy, \qquad U = \frac{a_\infty}{a_e}u \tag{4}$$

Continuity:

$$\left(H + \frac{1+m_e}{m_e}\right)\frac{d\delta_i^*}{dX} + \delta_i^*\frac{dH}{dX} + f\frac{\delta_i^*}{M_e}\frac{dM_e}{dX} = \frac{h}{\mathrm{Re}_{\delta_i^*}} \tag{5}$$

Momentum:

$$H\frac{d\delta_i^*}{dX} + \delta_i^*\frac{dH}{dX} + (2H+1)\frac{\delta_i^*}{M_e}\frac{dM_e}{dX} = 0 \tag{6}$$

First Moment of Momentum (Mechanical Energy)

$$J\frac{d\delta_i^*}{dX} + \delta_i^*\frac{dJ}{dH}\frac{dH}{dX} + 3J\frac{\delta_i^*}{M_e}\frac{dM_e}{dX} = \frac{R}{\mathrm{Re}_{\delta_i^*}} \tag{7}$$

where

$$\delta_i^* = \int_0^{\delta_i}\left(1-\frac{U}{U_e}\right)dY, \quad \theta_i = \int_0^{\delta_i}\frac{U}{U_e}\left(1-\frac{U}{U_e}\right)dY, \quad \theta_i^* = \int_0^{\delta_i}\frac{U}{U_e}\left(1-\frac{U^2}{U_e^2}\right)dY \tag{8}$$

$$H = \frac{\theta_i}{\delta_i^*}, \quad J = \frac{\theta_i^*}{\delta_i^*}, \quad R = \frac{2\delta_i^*}{U_e^2}\int_0^{\delta_i}\left(\frac{\partial U}{\partial Y}\right)^2 dY, \quad Z = \frac{1}{\delta_i^*}\int_0^{\delta_i}\left(\frac{U}{U_e}\right)dY \tag{9}$$

$$m_e = \frac{\gamma - 1}{2} M_e^2, \qquad \mathrm{Re}_{\delta_i^*} = \frac{a_\infty M_e \delta_i^*}{\upsilon_\infty}$$

$$h = \mathrm{Re}_{\delta_i^*} \frac{1 + m_e}{m_e (1 + m_\infty)} \tan\Theta \text{ (and } \Theta \text{ = angle of incidence)}, \tag{10}$$

$$f = \left(\frac{3\gamma - 1}{\gamma - 1}\right) + \left(2 + \frac{\gamma + 1}{\gamma - 1} \frac{m_e}{1 + m_e}\right) H + \frac{M_e^2 - 1}{m_e (1 + m_e)} Z \tag{11}$$

Equations 5, 6, and 7 govern the viscous flow development of the wake from afterbody separation to the far downstream flow. To determine the flow characteristics at each axial location, these equations are solved as a system of linear differential equations, simplified by Cramer's Rule:

$$\frac{\delta_i^*}{M_e} \frac{dM_e}{dX} = \frac{1}{\mathrm{Re}_{\delta_i^*}} \frac{N_1}{D}, \tag{12}$$

$$\delta_i^* \frac{dH}{dX} = \frac{1}{\mathrm{Re}_{\delta_i^*}} \frac{N_2}{D} \tag{13}$$

$$\frac{d\delta_i^*}{dX} = \frac{1}{\mathrm{Re}_{\delta_i^*}} \frac{N_3}{D} \tag{14}$$

where

$$N_1 = \left(J - H \frac{dJ}{dH}\right) h + HR - R\left(H + \frac{1 + m_e}{m_e}\right) \tag{15}$$

$$N_2 = J(H - 1)h - HRf + (2H + 1)R\left(H + \frac{1 + m_e}{m_e}\right) \tag{16}$$

$$N_3 = (2J + 1)\frac{dJ}{dH} h + Rf - (2H + 1)R \tag{17}$$

$$D=\left(J-H\frac{dJ}{dH}\right)f+(H-1)J+\left[(2H+1)\frac{dJ}{dH}-3J\right]\left(H+\frac{1+m_e}{m_e}\right) \qquad (18)$$

Reynolds Number and Mach Number influence the wake development through the f and h terms. The remaining terms H, J, R, and Z are functions of the local velocity profile in the viscous flow and are simply shape factors. For adiabatic, compressible shear flow, the velocity profiles are locally "self-similar." Reeves and Lees (38) used a single parameter, i.e., Tani's a(x), to represent a given velocity profile and defined it as the ratio of edge velocity to velocity along the dividing streamline in separated flow or the centerline for reattached flow. The shape factors, H, J, R, and Z could then be approximated from the following polynomial relations:

Table 2.3: Polynomial Approximations for Shape Factors

Upstream of RSP	Downstream of RSP
$a(x)=\frac{u_{DSL}}{u_e}, 0.54<a<0$	$a(x)=\frac{u_{cl}}{u_e}, 0<a<0.75$
$H=0.2482-0.4351a-0.0366a^2$	$H=0.2482+0.880a-0.1585a^2$
$J=0.376-0.528a$	$J=0.376+1.177a+0.427a^2$
$R=1.26+2.280a+30.4a^5$	$R=0.020+2.39(a-0.72)^2$
$Z=1.034-1.38a$	$Z=1.034+2.932a+12.65a^4$

To compute the pressure distribution along the wake, the initial conditions are specified and Equations (4)-(6) are integrated downstream. The form of Equations (4)-(6) includes a singularity at D=0. In order for the solution integrate through the singularity, the numerators must vanish simultaneously, thereby making the singularity a critical point with saddle point behavior.

There is a unique distribution of a(x), M_e, and δ^* for a given geometry and conditions that will allow the solution to pass through the critical point, as illustrated in Figure 2.9. The problem is solved by trial and error method until

solution passes through the critical point. The distribution joining the flow separation from the afterbody to the beginning of this mixing region solution is computed through a similar process.

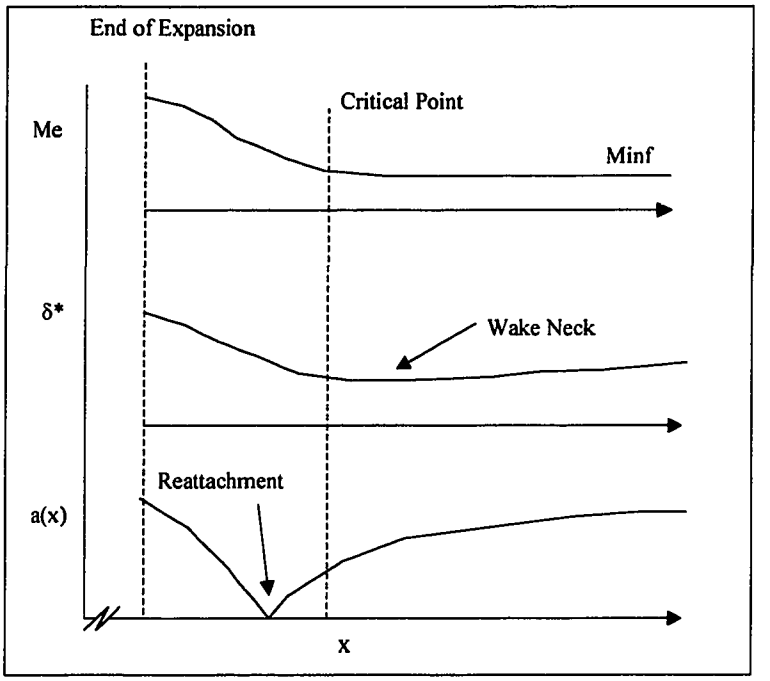

Figure 2.9: Example Parameter Distributions Leading to Wake Solution

Crocco and Lees (36) and later Lees and Reeves (37) examine the critical point and the physical implications of sub- and supercritical flow for wake flows and separating/reattaching boundary layers. The critical point of the wake is viewed similar to that of a subsonic/supersonic nozzle. In order for the flow to pass through this critical point, the flow must be subcritical prior to reaching the critical point and supercritical thereafter. Subcritical refers to flow that is subsonic in the mean; whereas supercritical flow is supersonic in the mean. Subcritical flow can be influenced by upstream propagation; while supercritical flow can not. Since the critical point is the last point that downstream perturbations can be propagated forward, the existence of the critical point isolates the near wake from downstream influences and uniquely determines

the wake properties as a function of the distribution of flow characteristics ahead of the critical point.

Several researchers have since scrutinized the IVI method and its results. Webb, et. al., (39) found that wake flows below a certain Reynolds Number and at low supersonic Mach numbers did not appear to have critical points. Ai (45) found that the existence of a critical point does not necessarily lead to a unique solution. Weinbaum (46) also questioned applicability the mathematical development of IVI to the problem conditions, i.e., the use of parabolic boundary layer equations that inherently eliminate upstream influences. He suggested the Crocco-Lees critical point was a mathematical construct, and the interpretation of the critical point as the parameter that defines a unique solution to the closed wake problem was an a posteriori conclusion. Weinbaum re-derived the wake flow governing equations based on an analogy to a 2-D viscous throat that avoided some of the previous mathematical problems of the IVI Method. The results could be correlated to those found by the IVI Methods, thus reconfirming efficacy of the IVI principles even with their mathematical limitations.

Numerical Analysis. The third tool for analyzing wake flows is numerical simulation, or CFD. Some very early numerical efforts, such as those of Baum and Dennison (44), used finite difference methods to analyze distributions of specific parameters in the flow. As computational capabilities have improved, CFD methods can solve the entire flowfield for a variety of complex flows and geometries. The implementation of CFD typically begins with the generation of a grid (or mesh) of nodal points in the flowfield, around the body of interest. At each point, the conservation equations of motion (i.e., continuity, momentum, and energy) through finite-difference or finite-volume techniques are applied. The form of the equations and the specific solver schemes are selected based on the particular flow physics and computational efficiencies. The CFD code is run iteratively until a solution is converged upon, i.e., the residual or computational

error falls below a given threshold. More detailed descriptions of this process are available in most CFD texts.

For wake flows, the key flow physics to be modeled is the mixing between the external inviscid flow and the viscous recirculation region. Some analysis has been conducted on laminar wakes, but more focus has been placed on turbulent wake problems, since they are more prevalent in application. In laminar flow, mixing is a diffusion process. CFD models this diffusion process by means of a temperature-dependent viscosity of the fluid. Mixing in turbulent flow involves the diffusion process and a transport mechanism associated with turbulent eddies or vorticies. The modeling of turbulence is an ongoing fluid dynamics challenge. Models, such as Baldwin-Lomax for boundary layer flows or k-w and k-ε models for free shear flows, simulate turbulent transport by using approximations of quantities like the transport of turbulent energy, k, and the turbulence energy dissipation rate, ε. The flow is then solved using the Reynolds-averaged Navier-Stokes form of the conservation equations. More recent efforts to incorporated Large Eddy Simulation or Direct Numerical Simulation techniques have been directed at understanding stability characteristics and large-scale turbulent structures rather than the overall effect on base pressure (25). Therefore, to date most CFD models are based on Reynolds-averaged Navier Stokes equations.

Putnam and Bissinger (47) summarized an Advisory Group for Aerospace Research and Development (AGARD) comparison of theoretical and computational methods. They found that CFD results were accurate for predicting pressure distributions along the afterbody up to the point of separation, but lagged behind the others in accurate base pressure prediction. Petrie and Walker's (48) comparison of Thin-Layer Navier-Stokes (with algebraic turbulence model) and Full Navier-Stokes (with k-w and k-ε turbulence models) CFD results to experimental data determined that CFD could qualitatively capture the basic flow characteristics. But they all had difficulty accurately

predicting base pressure magnitude and radial variations, recirculation region size, and Mach disk location and size. The major issue in resolving the wake structure has been the modeling of turbulence. However, the continued difficulties in wake analysis even with turbulence modeling improvements suggest that other factors may contribute to this problem, including grid resolution, accuracy of the numerical solver, and treatment of boundary conditions (25).

2.3.3 Assessment of Wake Analysis Tools

Past efforts to compute plug nozzle base pressure have relied on Korst-type models for closed wakes. The recent efforts to analyze and build plug nozzles now have the benefit of more sophisticated tools. To the extent that analytical models have been used, the more developed Multi-component and IVI Methods have been successful for analyzing plug nozzles in closed wake conditions and flows without base bleed. The Multi-component methods simpler and more successful for analyzing complex geometries and conditions. However, the IVI methods are more accurate when they can be applied successfully. One of the issues in applying these supersonic wake methods to plug nozzle flow is the extent of their validity as the plug nozzle operating range changes the external flow (e.g., the non-uniformity of the flow) from that found in traditional supersonic wakes. Part of this research will identify some of these differences.

Many current plug nozzle research efforts are exploiting the use of powerful CFD tools. But, as discussed earlier, CFD is still limited in its modeling capabilities and therefore analytical methods may for the time being provide more accurate and useful results. Figures 2.10a and b is a comparison of some analytical models to CFD and empirical data for laminar and turbulent wakes. The theoretical papers on laminar wakes tended to only predict base pressure for specific test cases, whereas later papers on turbulent wakes provided base pressure curves. The laminar pressures are strongly dependent on Reynolds

Number, as shown by the barred empirical data and empirical relation by Lamb and Oberkampf (26). Petrie and Walker's (48) comparison of k-w and k-ε models illustrated a base pressure over-prediction of 50% and 35%, respectively, versus the 10-20% differences resulting from Multi-component Methods. Tucker and Shyy (49) focused specifically on the effect of finite difference schemes and k-ε turbulence modeling on CFD results and found an under-prediction of base pressure up to 30%.

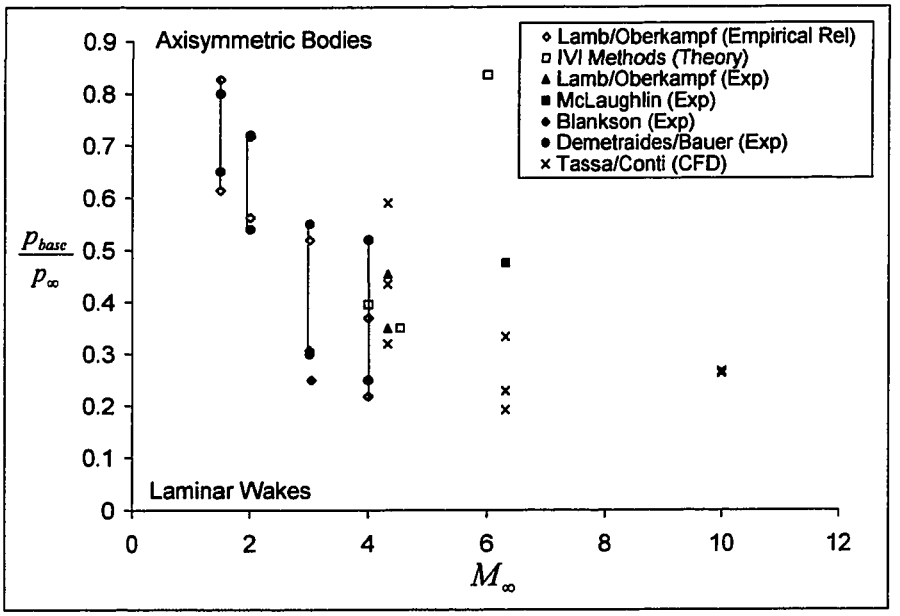

Figure 2.10a: Comparison of Laminar Base Pressure Predictions (26, 32, 50-53)

No single method best predicts base pressure satisfactorily. For the purposes of this study, experimental, analytical, and numerical methods are used to characterize the plug nozzle wake. The empirical data provided physical realism to the problem, whereas the numerical solutions provided detailed flowfield information. The analytical methods were used in conjunction with the CFD to synthesize the flowfield data into an understanding of the physical mechanisms causing wake closure.

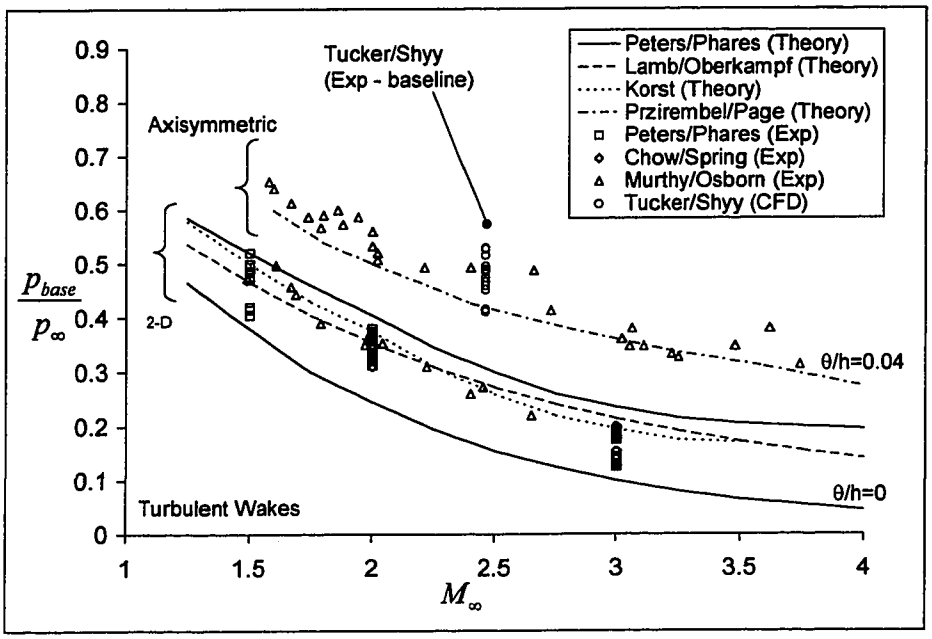

Figure 2.10b: Comparison of Turbulent Base Pressure Predictions (26, 30, 35, 41, 49, 55)

The plug nozzle wakes examined during this study were generally transitional or turbulent. The Multi-component and IVI Methods were developed or later adapted to analyze both laminar and turbulent flows. As in boundary layer theory, the effect of turbulence in a time-averaged sense was a change in velocity profile. For the Multi-component Methods, this effect was incorporated by using varying σ in Equation (3). This empirical jet spreading parameter models the rate at which the shear layer spreads out.

Alber (56) reformulated the IVI Method momentum integral equations by replacing the dissipation terms by an eddy viscosity term. As a result, the mixing mechanisms were modified by the incorporation of turbulence, but the fundamental equations of motion and resulting focus on the reattachment criterion or critical point remained the same. Thus, the analytical models and concepts used in this research were applicable to both laminar and turbulent plug nozzles. The CFD solutions were computed using a laminar model. Since the objective of this research was to explain the physical mechanisms

associated with wake closure, the qualitative trends provided by the CFD solution were sufficient and avoided the complexities and uncertainties incurred by turbulence modeling, much less the effect of these factors on wake closure.

2.3.4 Key Points for Plug Nozzle Application

The base pressure for a plug nozzle in closed wake conditions has typically been computed analytically using supersonic wake methods. However, the plug nozzle flowfield differs from the supersonic wake, so part of the present research determines the extent to which the applicability of these methods is valid for the plug nozzle flow in closed and open wake conditions.

A wake is the velocity defect in the flow behind a body. Due to viscous forces, all bodies immersed in a flow generally have wakes. The supersonic wake methods are applied to those flows where the freestream Mach Number is greater than unity. The cross-section velocity profiles are subject to the boundary conditions:

$$f(0) = f''(0) = 0 \text{ and } f'(\infty) = 1$$

$$\text{where } f'(\eta) = \frac{u}{u_e}$$

The plug nozzle and supersonic wake flows are different, e.g., $f'(\infty) \neq 1$ for the plug nozzle. In order to apply the analytical supersonic wake methods to the plug nozzle analysis, it is necessary to ensure that the flowfield is sufficiently similar to a supersonic wake. As part of the experimental flowfield characterization, the plug nozzle is examined to ascertain that the main supersonic wake-type features exist and a determination is made of the extent to which the supersonic wake methods can therefore be applied. These features include:

- Corner expansion leading to flow convergence toward the axis,
- Recompression shock that turns the flow parallel to the axis,
- Reattachment of the converging shear flows that results in a single downstream viscous flow, and
- Recirculation region aft of the base.

Such a flow is governed by the same equations of motion as the supersonic wake flow, so several conclusions can be made about the flow characteristics. The flow expansion around the afterbody corner must be matched by the flow recompression to reattach the flow and recover freestream conditions. The wake can be uniquely defined by a recompression criterion. This criterion determines the flow that continues downstream from flow that recirculates. Because of inviscid-viscous interaction, the external flow characteristics relate directly (e.g., integral momentum equation) to the changes in velocity profile and displacement thickness. The analogous recompression criterion for the IVI Method was derived by Crocco and Lees (36) as a "critical point." A unique distribution of the flow parameters from the separation point to the wake downstream that passes through the critical point. Thus, the critical point also defines a unique base pressure. Using Lees and Reeves (38) derivation of this critical point, this unique flow parameter distribution can be described by Me, a(x) (or H), and δ^*.

Chapter 3
FLOWFIELD CHARACTERIZATION

An extensive database exists for plug nozzle flowfields. However, the data and characterization of the flow structures has generally been configuration specific, and has not focused specifically on wake closure. As a result, there are different interpretations of the wake closure mechanisms and some of the detailed characterizations of the flowfield that could resolve potential discrepancies are incomplete. The purpose of this research was to provide a more complete characterization of the plug nozzle flowfield and specifically the wake flow to analyze wake closure.

The first part of this research consists of experiments on a range of plug nozzle configurations. These experiments provide a common data set for analysis and provided additional characterization of the flowfields where previous data was lacking. The data are then used to determine the conditions and modes under which wake closure occurs. Some specific issues examined include:

- More precise identification of the point of wake closure for the envelope shock mode,
- More complete the description of flow development and wake closure for the flow separation mode,
- Determination of whether the open wake condition retains a wake structure,
- Determination of whether the downstream flow recovers supersonic speeds in open wake conditions, and
- Identification of flow structures common to both modes.

This chapter describes the test facility and experimental approaches used to characterize the plug nozzle flowfield. The investigation results are a characterization of the plug nozzle flowfield in the context of wake closure.

3.1 Investigation Approach

The test facility and nozzle models were designed and fabricated specifically for this research. After characterization of the test facility operational conditions and calibration, the next task was to conduct experimental tests to characterize and analyze the plug nozzle flowfield. A reference flow for a single design Mach Number plug nozzle was used initially to demonstrate the basic flow features and wake closure phenomenon. A range of nozzle geometries and sizes were then tested to determine the wake closure conditions and modes.

3.1.1 Test Facility and Model Configurations

The test facility consists of a wind tunnel system, plug nozzles, and measurement instrumentation. A brief description of these components is presented below. Detailed facility and nozzle design descriptions, operating characteristics, instrumentation specifications, and uncertainty analysis are described in Appendix A.

Wind Tunnel System. The wind tunnel in Figure 3.1 consists of a gas storage ballast tube, flow control system, settling chamber, test section and dump tank. All tests were conducted using air as the working fluid. The NPR is set by upstream flow regulation of the total pressure and the initial ambient pressure of the test section. The facility is operated at total pressures of 35-120 psia (0.69-8.3 bars) and total temperature of 288K, while the test section and dump tank is evacuated to as low as 0.05 bars prior to a test. The pressure increase in the tank during a run is relatively small over a typical 1-3 second run duration. Examples of the pressure histories for the various plug nozzle flows

are provided in Appendix A. This duration is sufficient for the flow to be established and to capture the change of the wake from closed to open conditions using schlieren photography and pressure measurements. Total and ambient pressures are monitored to determine the instantaneous NPR. Tests are conducted for a specified NPR with a constant total pressure or over a range of NPR by allowing total pressure to decrease from its initial maximum. Depending on the nozzle design Mach Number, the operating unit Reynolds Number ranges from 7.00 x10^6 to 2.57 x 10^7/m.

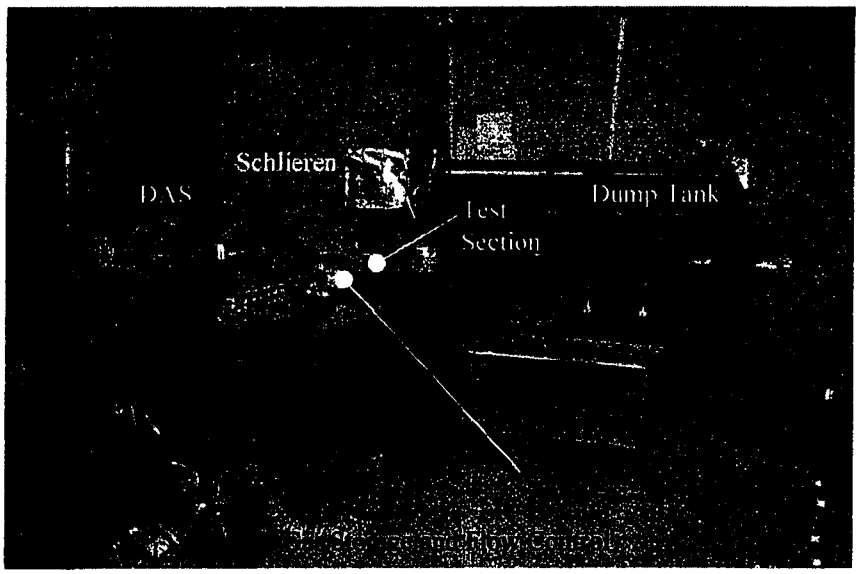

Figure 3.1: Plug Nozzle Research Test Facility

Plug Nozzles. The plug nozzle ramps and cowls used for the experimental analysis are shown in Figure 3.2. Each nozzle is designated by a 4-group code to indicate the shape (contoured or planar), design Mach Number (e.g., 20 represents M=2.0), jet height (e.g., 10 represents 1.0 inches), and truncation length (e.g., 25 represents 25%).

The contoured ramps are designed using Angelino's (57) method for specific Mach Numbers and jet heights. The truncation of the plug nozzle is determined as a percentage of the desired length divided by the isentropic aerospike length

(e.g., L/Lmax=0.25=25%), and the tip of the cowl determines the design jet height. The planar ramp throat height, lip height and truncation length are based on the contoured ramp design. But the ramp shape is defined as a straight line between the throat and lip.

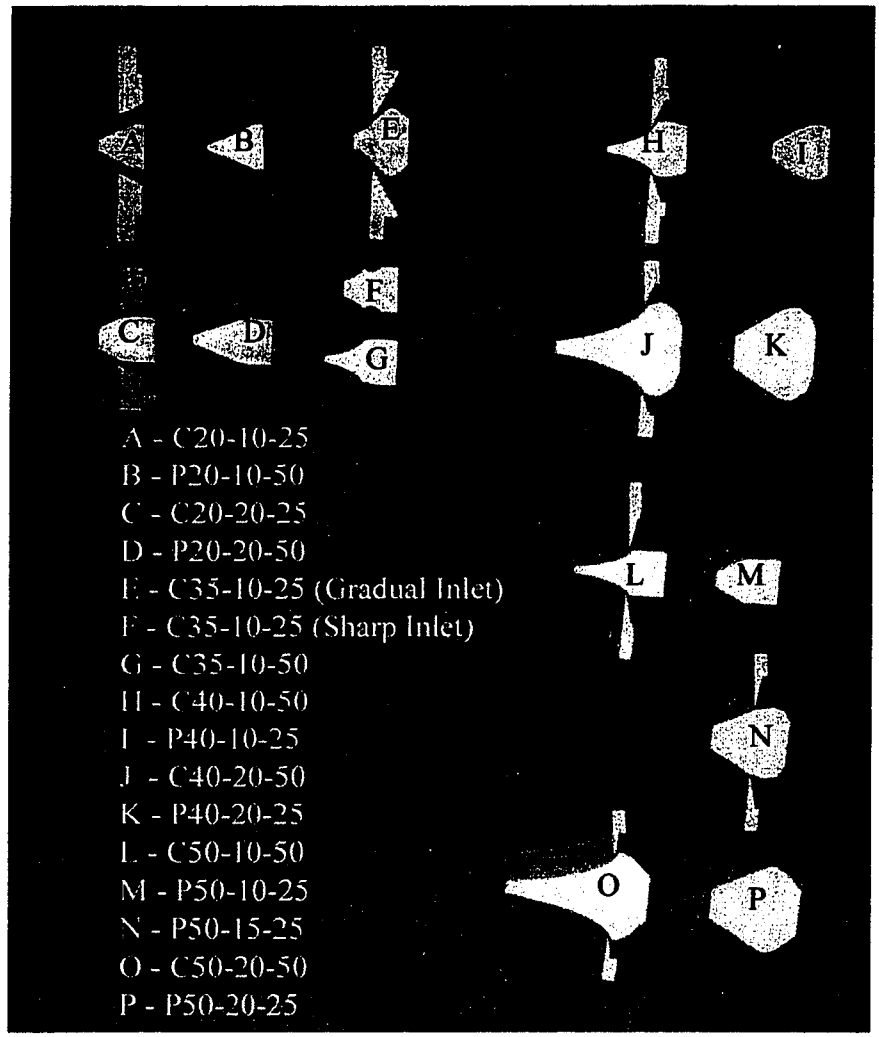

Figure 3.2: Plug Nozzle Models

Measurement Instrumentation. The measurement instrumentation collect pressure data and record changes in flow structures. Pressures are measured using electronic pressure transducers. A National Instruments PC-based Data Acquisition System (DAS) collects data from 13 channels (3 temperature and 10

pressure) every 50-60 milliseconds as well as initiates a schlieren time counter. Pressures are measured in various locations along the test facility and on the cowl for total and ambient pressures. Five ports are located on the nozzle base for base pressure readings. An interchangeable test section side panel can be used to measure centerline pressures from the sidewall or to mount a pitot rake for flowfield measurements. A measurement uncertainty analysis is presented in Appendix A. The typical uncertainty for measured NPR is ±0.87 (or 3.1%) and ±0.001 (or 3.1%) for p_{base}/P_{tot} and p_{cl}/P_{tot}.

Alternatively, a glass or Plexiglas panel is installed for schlieren pictures. The single pass, halogen lamp schlieren system illuminates shocks and shear layers in the flow. A Charge-Coupled Device (CCD) video camera records the resulting images. A Light Emitting Diode (LED) counter mounted on the schlieren image screen is used to relate time records from the pressure data to the flow changes. The typical uncertainty of correlated values with the schlieren images is ±4.534 (or 15.9%) for measured NPR and ±0.773 (or 26.4%) for measured Mach Number.

3.1.2 Reference Flow Experiments

A reference flow is used to demonstrate the basic flow characteristics of the plug nozzle. Comparisons are then made between the reference flow and other nozzle geometries and conditions to assess the impact of the changes to wake closure.

Table 3.1 summarizes the tests conducted on this reference flow, the measurements taken, and test objectives. Changes to the overall flow structure are identified using schlieren photography. In order to determine whether the wake was open or closed, the schlieren pictures are correlated to base pressure measurements using the LED counter and DAS time records. The axial

pressure distribution downstream of the ramp base is measured from pressure taps along the sidewall panel.

Table 3.1: Baseline Flow Experiments Summary

Test Objectives	Nozzle Geometry	Measurements
Demonstration of key flow features	C35-10-25	Schlieren
Characterization of flow changes with NPR	C35-10-25	Base Pressure
Wake closure and base pressure correlations to flow changes	C35-10-25	Schlieren and Base Pressure
Axial characterization of the wake	C35-10-25	Sidewall Pressure
Characterization of flow changes with longer nozzle	C35-10-50	Schlieren
Wake closure and base pressure with longer nozzle	C35-10-50	Schlieren and Base Pressure

The C35-10-25 nozzle serves as the reference configuration for these experiments. This nozzle produces the envelope shock mode of wake closure. Though better understood than the wall separation mode, key data are still required to analyze the envelope shock mode. It is important to verify that the movement of the envelope shock coincides with the changes in base pressure. Moreover, it is necessary to determine whether the primary supersonic wake features are present during the transition to open wake conditions, so that the supersonic wake analyses can be applied later. The downstream flow is examined to determine the appropriate modeling boundary conditions and whether downstream influences can propagate disturbances to the base region. Tests are conducted on the longer C35-10-50 nozzle to provide additional information on the envelope shock mode of wake closure.

3.1.3 Wake Closure Conditions Experiments

A series of tests isolate the conditions under which wake closure occur via the envelope shock versus the wall separation mode. Once the nozzle geometries

and conditions that resulted in the wall separation mode are identified, a more detailed description of the flow changes for this mode is developed. Emphasis is placed on understanding those changes occurring downstream of the ramp base not as well documented in past research.

The test objectives, configurations and measurements for these tests are listed Table 3.2. To facilitate the comparisons, the tests and their results are categorized by the design Mach Number of the nozzle.

Table 3.2: Wake Closure Conditions Experiments Summary

Test Objectives	Nozzle Geometry	Measurements
Characterization of low Mach Number nozzle flow	C20-10-25 C20-20-25 P20-10-50 P20-20-50	Schlieren
Base pressure changes and correlation to low Mach Number Nozzle flow changes	C20-10-25 C20-20-25 P20-10-50 P20-20-50	Base Pressure
Characterization of high Mach Number nozzle flow	P40-10-25 P40-20-25 C40-10-50 C40-20-50 P50-10-25 P50-15-25 P50-20-25 C50-20-50	Schlieren
Base pressure changes and correlation to high Mach Number nozzle flow changes	P40-10-25 P40-20-25 C40-10-50 C40-20-50	Base Pressure

The ramp shape, nozzle design Mach Number, jet height (or nozzle size), and truncation length are varied to determine the conditions and the modes under which each configuration passed through the point of wake closure. The ramp configurations tested are selected through a Taguchi matrix for use in the design factors analysis in Chapter 5. Chapter 5 examines quantitative trends that determine the effect of the design factors on wake closure.

3.2 Reference Flow Experiment Results

The analysis of experimental results include the identification of reference flow features, characterization of flow changes, wake closure and base pressure correlation, axial characterization of the wake, characterization of flow changes with a longer nozzle, and wake closure-base pressure correlations.

3.2.1 Reference Flow Features

Figure 3.3 shows the key flow features for the baseline nozzle in closed wake conditions. The primary features used to characterize the changes in the flowfield as the wake passes through the point of wake closure include: the free jet boundary, envelope shock, recirculation region, lip shock, shear layer, recompression shock, and far wake shear layer aft of recompression.

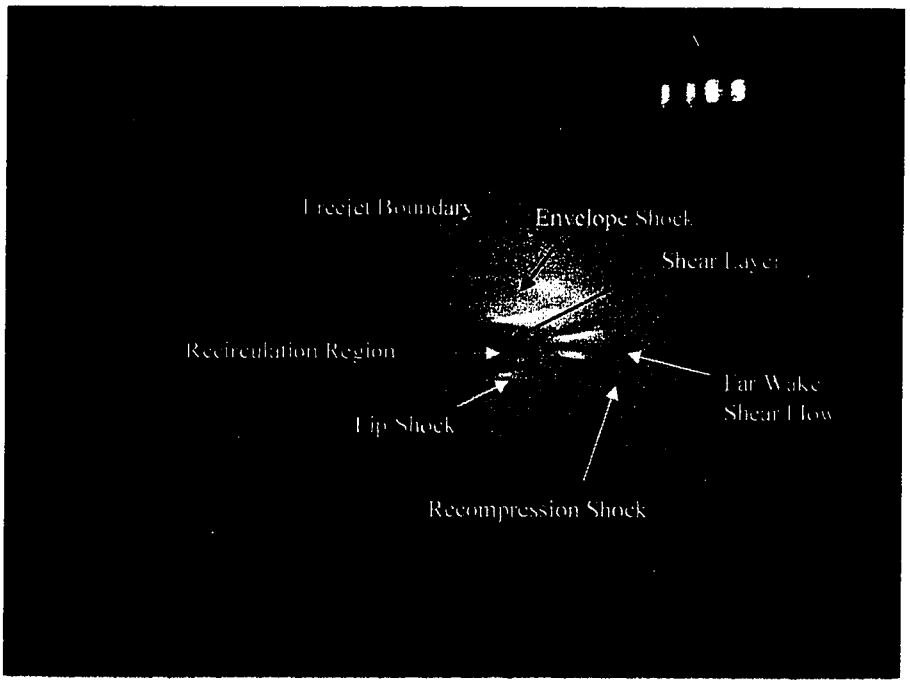

Figure 3.3: Experimental Plug Nozzle Flow Features

3.2.2 Characterization of Flow Changes

The changes in flow for the C35-10-25 nozzle as pressure ratio varies from high to low NPR are shown in Figure 3.4. At the start of the run (a), the flow is in the near design pressure ratio conditions, and the gradients are very sharp and distinct. The closed wake flow structures are easily identified. The wake reattachment point is located approximately 1.25 ramp lip heights from the base, which is similar to that found in supersonic wakes. The point does not move appreciably through the duration of the test. Some flow separation from the ramp wall appeared to exist during these conditions as indicated by the flow gradient coming from the ramp. This was likely due to the non-isentropic expansion, since the nozzle shape did not account for the boundary layer displacement and was computed using a finite number of expansion steps.

At an overexpanded NPR (a), only the free jet boundary can be seen at the outer regions of the flow. The envelope shock appears almost instantaneously once a certain NPR is reached (b) and the point where the envelope shock impinges on the wake moves upstream with decreasing NPR. The free jet boundary moves closer to the nozzle axis, and the flow features downstream of reattachment point become more diffuse. The far wake shear flow appears slightly larger beginning at the same axial distance as intersection of the envelope and recompression shocks. Once the envelope shock reaches the reattachment region (c), the wake reattachment features (i.e., the shear layer convergence and recompression shock) are less distinguishable. The near wake region grows slightly, but the far wake shear flow downstream of the reattachment point appears to shorten. As the envelope shock reaches the ramp lip (d), the recompression shock is cut off by the outer free jet boundary and the lip shock disappears. The shape of the recompression shock begins to look more like a normal shock (e). The envelope shock is incorporated into the series of expansion-compression waves as the pressure ratio decreases further (f), until only free jet boundary is visible at the outer edge of the flow. The

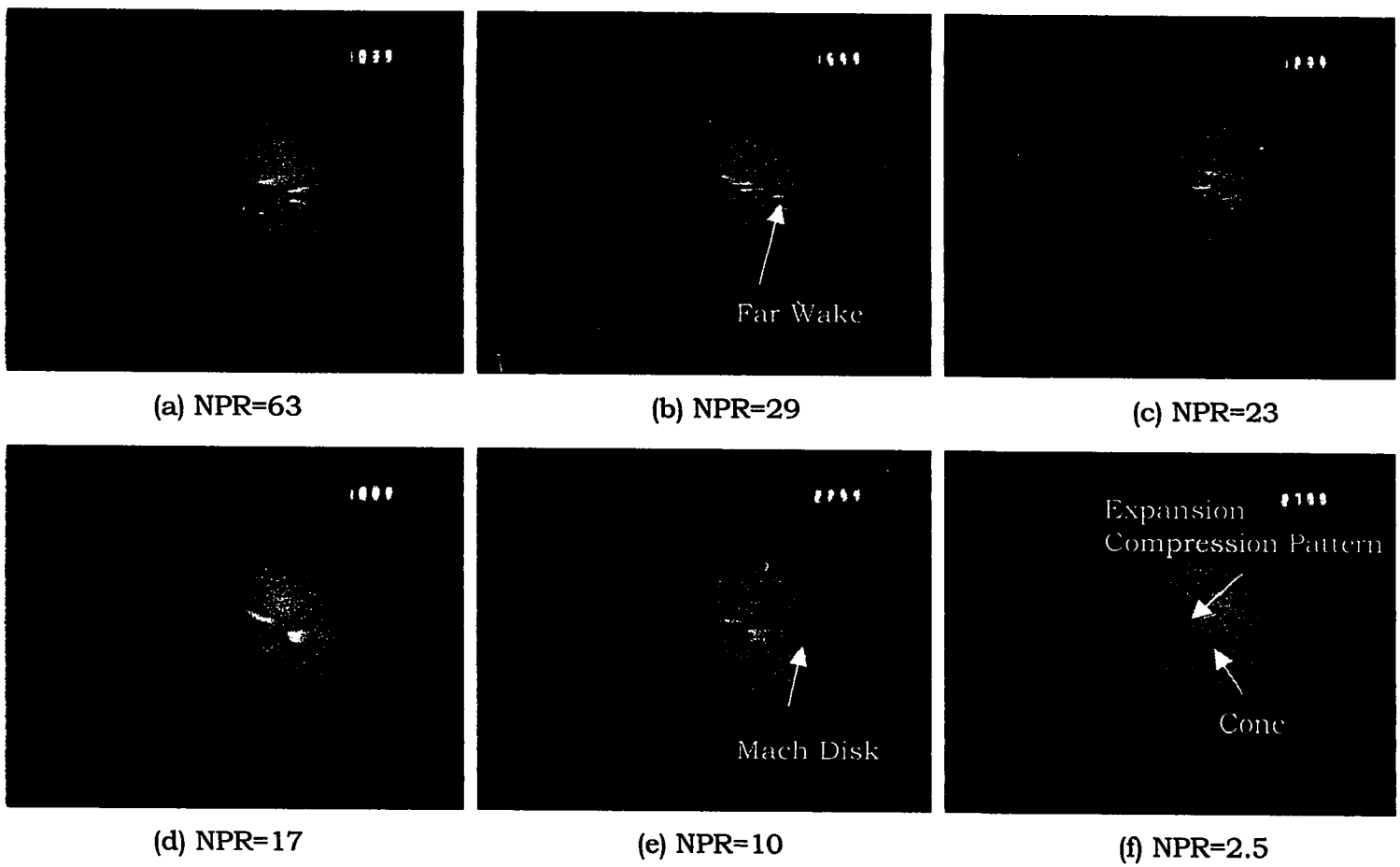

(a) NPR=63 (b) NPR=29 (c) NPR=23

(d) NPR=17 (e) NPR=10 (f) NPR=2.5

Figure 3.4: C35-10-25 Flow Development

recompression shock vanishes. The shear layers at lower NPR form a cone shape in the base region, and expansion-compression waves run along the outer edges of the shear layer. The flow at this point may be of such low energy that the wake is subsonic.

3.2.3 Wake Closure and Base Pressure Correlation

The base pressure variations during the flow development are shown as a function of p_{base}/P_{tot} versus NPR in Figure 3.5. This figure presents base pressure for several runs. The data was categorized by total pressure, and the plot of the data indicates that total pressure does not have an effect on the base pressure variation over the range of total pressures tested. The plateau at p_{base}/p_{amb} =0.036 represents the closed wake condition. The base pressure plot follows two "paths" as NPR decreases. The first departs from the closed wake base pressure at NPR=29, while the other occurs at NPR=18. In both cases, the envelope shock just reaches the reattachment region for their respective runs, which confirms the explanation of the envelope shock closure mode given in Section 2.2. At NPR=10, the envelope shock reaches the ramp lip. The two paths unite below NPR=10. The divergence of the two paths from the Pbase=Pamb line indicates that the closed wake does not change immediately to a "fully open" wake (i.e., $p_{base}=p_{amb}$). This transition region is typically found in the work of other researchers (4,5,14).

It is more difficult to determine the extent to which the plug flow retained the primary supersonic wake features during open wake conditions. While the envelope shock impinges the near wake region between reattachment and the ramp lip, the wake retains the recompression shock and the converging shear layers. The reason for the truncation of the recompression shock by the outer free jet boundary is not clear. In particular at NPR=10, the recompression shock is significantly altered. On the other hand, the presence of a downstream Mach disk Figure 3.4/frame (e) indicates that the flow does recover supersonic

speeds, thus inhibiting the downstream conditions from affecting the base region.

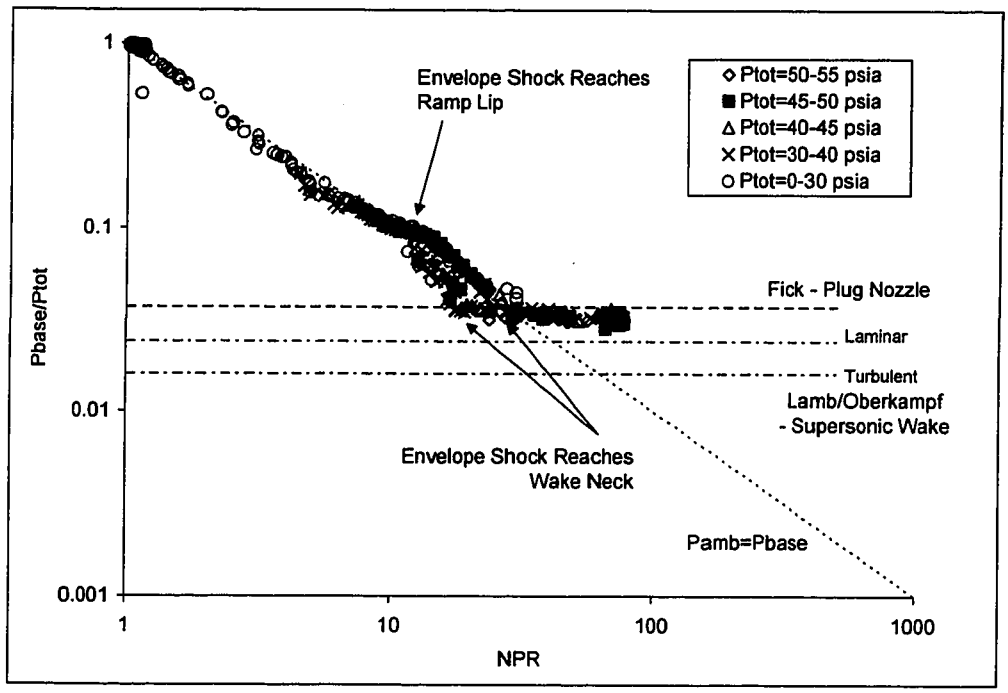

Figure 3.5: C35-10-25 Base Pressure Profile Relative to Jet Total Pressure

The base pressures from Equation (2) by Fick and Schmucker for plug nozzles and Equations (1) by Lamb and Oberkampf for laminar and turbulent supersonic wakes are shown in the above figure for comparison. From Angelino's Method (57), the Mach Number of the isentropically expanded gas is approximately M=2.5 at the end of the ramp. The Reynolds Number for the supersonic wake base pressure was approximated using the length of the plug (rather than the surface length). The measured closed wake base pressure compares well with the Fick and Schmucker prediction. The predicted supersonic wake base pressures are lower than both of these, which is consistent with the CFD analyses conducted later. Note that in this case, the laminar flow base pressure prediction is higher than the turbulent prediction due to the Reynolds Number.

Figure 3.6 redisplays the base pressure variations normalized to the ambient pressure. The base pressure depicted in this way emphasizes the relationship to ambient pressure during open wake conditions. The two different paths in the transition region can also be seen in Figure 3.5, but are accentuated here. Initially, it was believed that the difference was associated with a hysteresis phenomenon similar to that found by Tomita, et. al. (18).

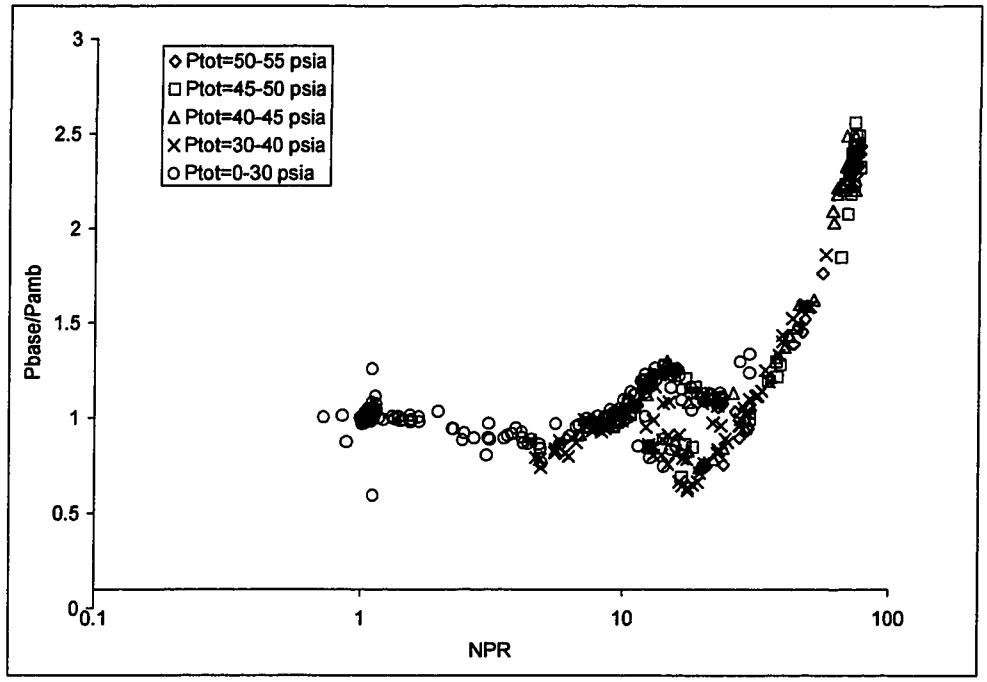

Figure 3.6: C35-10-25 Base Pressure Profile Relative to Ambient Pressure

A breakdown of the data based on the increasing or decreasing jet total pressure relative to ambient pressure shows that the increasing total pressure data is skewed toward the upper curve, but several runs with decreasing total pressure also follow this higher base pressure path. Data by Tomita, et. al., show the decreasing total pressure to have a higher base pressure curve than the increasing total pressure.

3.2.4 Axial Characterization of Wake

The centerline pressure distribution is used to characterize changes in the flow along the wake axis. The centerline pressures for the C35-10-25 nozzle as measured from the sidewall are shown in Figure 3.7. The general trends are comparable to other experimental data. The closed wake pressure distributions depicted by NPR=69 and 78 tend toward a maximum and then decrease toward far downstream freestream level. As the wake opens for NPR=16 and 23, the base pressure begins to diverge from the closed wake curve.

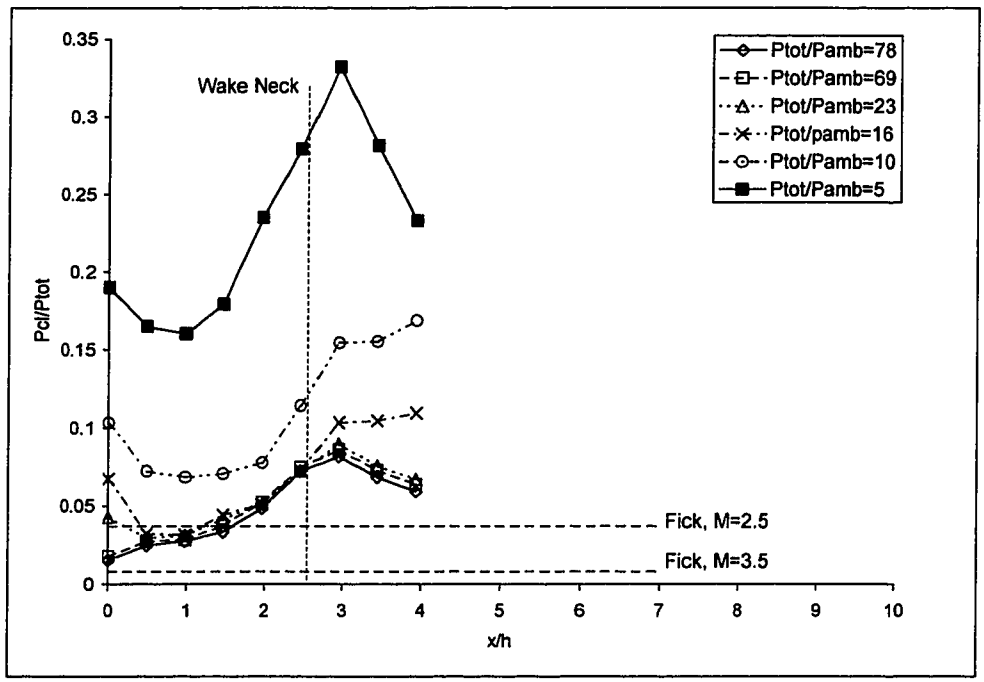

Figure 3.7: C35-10-25 Sidewall Centerline Pressures

Of interest was the fact that the pressures diverged from the closed wake curve at the base and downstream, instead of the point of divergence moving only from the downstream forward. The nature of this change suggests that the downstream conditions are not simply causing an upstream propagation of disturbances. This is emphasized by the NPR=23 curve in which the base pressure increases, but the rest of the pressure distributions lie on the closed

wake curve. This may indicate that the entire wake structure is changed once the downstream conditions move to a certain forward position. Eventually the entire pressure distribution lifts off of the closed wake curve. The open wake pressure distributions downstream of reattachment also attain a plateau rather than a maximum. This is consistent with previous research data (4). The maximum found in the NPR=5 curve may be linked to the downstream Mach Disk, which causes a total pressure loss and reduced static pressure.

The measured closed wake base pressures for this set of tests were actually lower than the previous tests. The closed wake base pressures predicted by Equation (2) is depicted in the figure above for comparison purposes. The two base pressure predictions span the range of Mach Numbers that can be found in the jet just prior to separation from the ramp depending on the height above the surface. The measured base pressure thus falls within the band defined by predicted base pressures for these two Mach Numbers.

3.2.5 Flow Features for Longer Nozzles

The effect of plug nozzle truncation can be seen by comparison of the C35-10-25 and C35-10-50 nozzle. The change in plug truncation has two effects on the nozzle geometry and thus on the flow characteristics. First, the ramp is lengthened, thereby increasing the amount of expansion that the jet undergoes. The higher Mach Number flow at the end of the ramp is generally recognized to reduce base pressure. Secondly, the ramp lip height is shorter, thus reducing the recirculation region size. Observations from previous research noted that the effects of this latter change were not clear, nor was it clear the implications of second order effects, such as changes to the lip shock. Thus, the comparison of these two nozzles provides additional insights to these issues.

Figure 3.8 shows that the two flows have qualitatively similar structures. Some additional flow features are better depicted by this set of schlieren pictures,

such as the diamond shock patterns aft of the wake reattachment point. The diamond patterns result from the reflection of the recompression shock from the free jet boundary (d). The key difference from the shorter nozzle is that the reattachment structure in the wake is retained well after the envelope shock reached the ramp surface (e). The flow along the ramp displays the expected expansion-compression wave pattern that occurs above the ramp surface as well as the outer edge of the shear layer. The existence of this distinct reattachment region for all NPR indicates that the flow along the ramp is maintained, or recovers sufficiently, to maintain the primary supersonic wake features.

The distinctive gradient at the wake reattachment point becomes more diffuse when the envelope shock reaches the ramp lip (c). As the shock moves up the ramp, this gradient regains its distinctive appearance (d). Similar to the C35-10-25 nozzle, the far wake shear flow is slightly wider as the envelope shock moves forward (e). The far wake remains visible until the diamond shock pattern moves closer to the reattachment region. The effect of the shocks in eliminating the far wake shear flow structures may also be the reason for the shortened far wake shear flow in the C35-10-25.

3.2.6 Wake Closure and Base Pressure for Longer Nozzles

The effect of longer plug length on base pressure is depicted in Figure 3.9 by comparing the base pressure data for C35-10-50 test to a single C35-10-25 run. Both nozzles have fully closed wakes for pressure ratios above NPR=29. The longer nozzle however results in a lower closed wake base pressure due to the higher Mach Number flow at the end of the ramp. The C35-10-50 nozzle is completely open at approximately NPR=6. This NPR is slightly lower than the C35-10-25 nozzle.

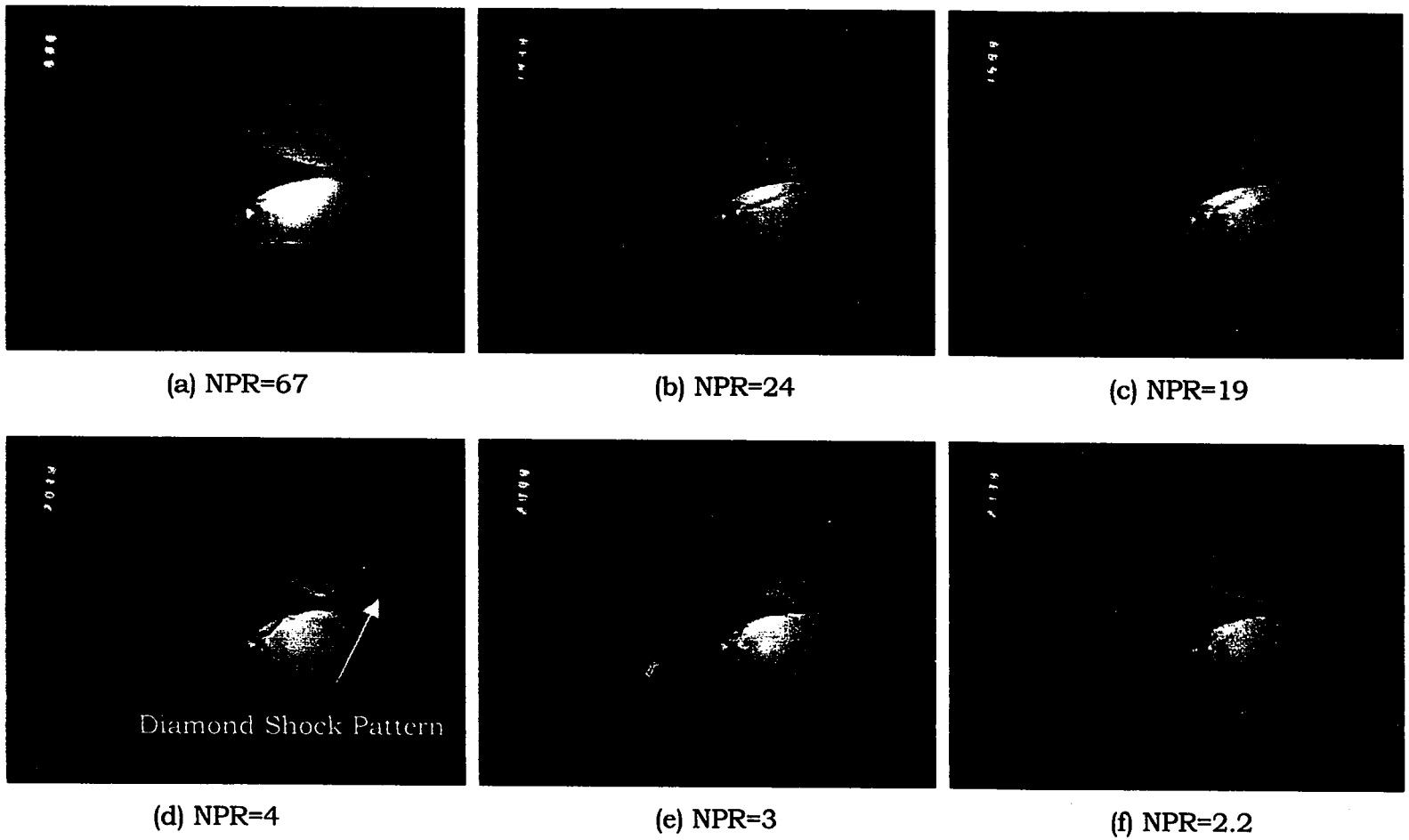

(a) NPR=67 (b) NPR=24 (c) NPR=19

(d) NPR=4 (e) NPR=3 (f) NPR=2.2

Figure 3.8: C35-10-50 Flow Development

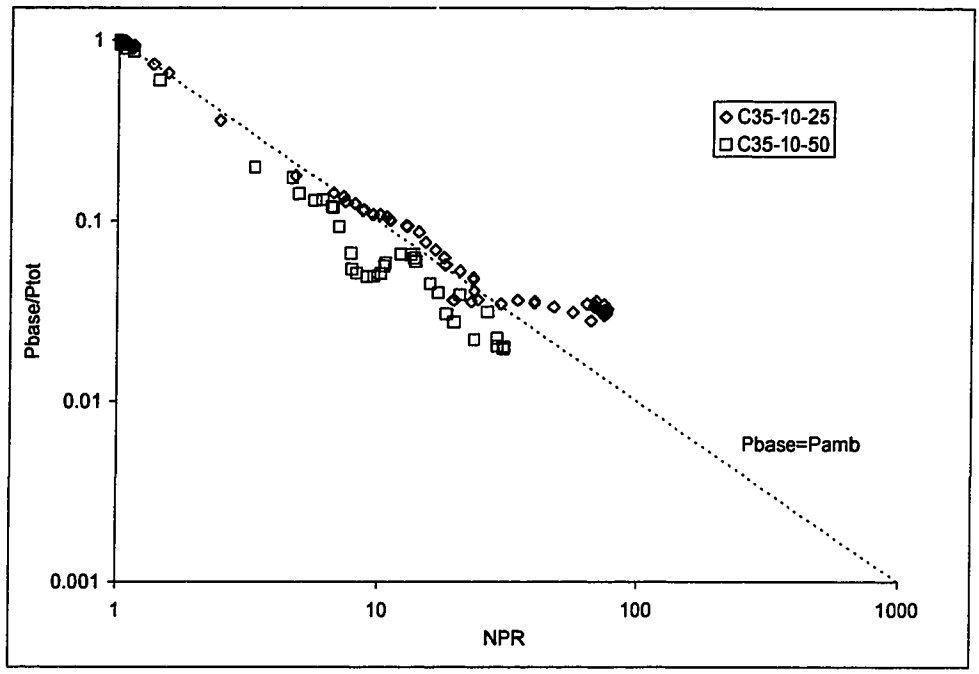

Figure 3.9: Effect of Length on Base Pressure

The other notable difference between the two configurations is the non-monotonic base pressure variation for the C35-10-50 nozzle in the transition region. Sule and Mueller (14) attribute a similar "jump" in base pressure to the impingement of the envelope shock on the near wake. This jump was not as apparent in the C35-10-25 nozzle. Since the wake structure is retained well into the NPR range where the envelope shock impinges the ramp surface for the longer plug nozzle, the near wake may be more subject to the expansion-recompression process than for the shorter plug nozzle.

3.3 Wake Closure Conditions Results

Using the Mach 3.5 nozzles as a reference point, a set of experiments examined the effects of nozzle configurations on wake closure. As discussed previously, the two primary areas of interest were to characterize in more detail the wall separation mode of wake closure and to examine the conditions under which wake closure occurred for both modes. Of particular interest was to identify

any common trends between the envelope shock and wall separation modes of wake closure.

The results of the wake closure conditions experiments are presented below. The results include the characterization of low Mach Number nozzle flow changes, wake closure and base pressure for low Mach Number nozzles, characterization of high Mach Number nozzle flow changes, and wake closure and base pressure for high Mach Number nozzles.

3.3.1 Low Mach Number Nozzle Flow Attributes

The flow development for the C20-10-25, C20-20-25, P20-10-50, and P20-20-50 nozzles were compared with that of the C35-10-25 to assess the effect of ramp size and shape at low Mach Numbers. The change in design Mach Number affects the throat inlet angle, throat size and contour shape. The flow changes for all of the low Mach Number configurations followed the envelope shock mode of wake closure. Examples of the flow development are illustrated by Figures 3.10a and b.

The larger throat size provided easier visualization of the jet flow structures. The shape of the recompression shock remains relatively constant in both figures (a-c), but the diamond shock pattern moves forward toward the reattachment region and coalesces into a normal shock (d). As this normal shock continues to move forward, the recompression shock disappears and a shock train forms along the ramp surface, extending along the outer edge of the wake shear layer (e). The near wake size increases when the envelope shock passes through the reattachment region. The far wake shear flow shortens as the downstream normal shock moves forward. The wake structure begins to diffuse as soon as the envelope shock reaches the ramp lip.

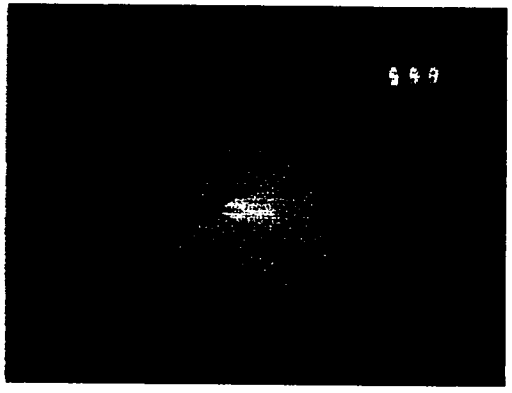

(a) NPR=6.1

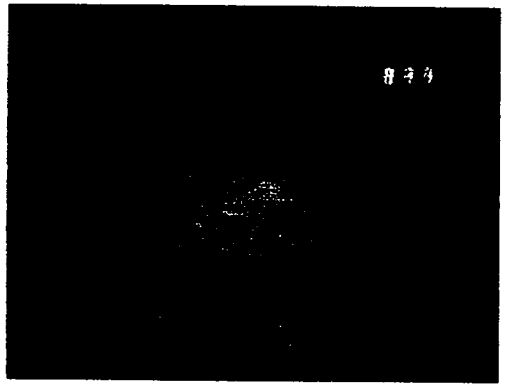

(b) NPR=4.9

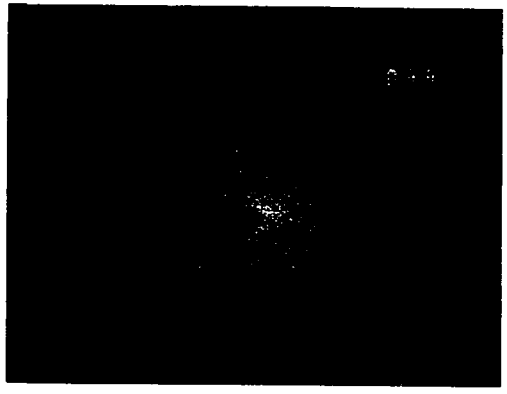

(c) NPR=4.1

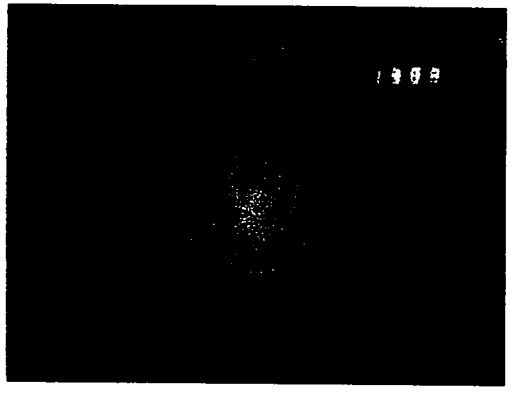

(d) NPR=2.6

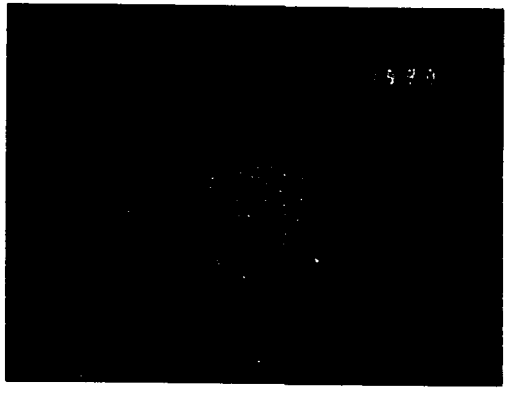

(e) NPR=2.2

Figure 3.10a: C20-10-25 Flow Development

(a) NPR=25.6

(b) NPR=8.8

(c) NPR=6.1

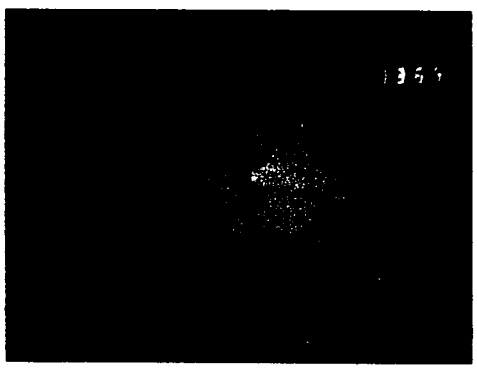

(d) NPR=3.8

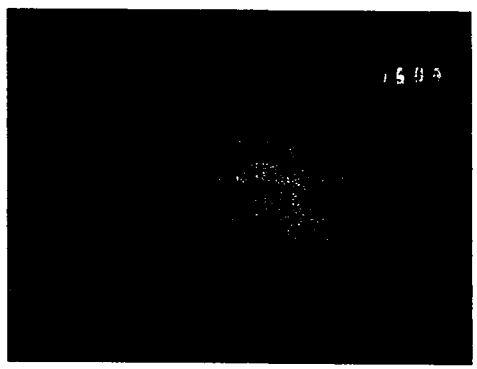

(e) NPR=3.0

Figure 3.10b: P20-10-50 Flow Development

3.3.2 Low Mach Number Nozzle Wake Closure and Base Pressure

The corresponding base pressure profiles for the Mach 2.0 nozzles are shown in Figure 3.11. The base pressures are generally the same for all of the Mach 2.0 nozzles. The wake closure NPR for the lower Mach Number nozzles is lower than the Mach 3.5 nozzles. The closed wake base pressures are higher than those found in the Mach 3.5 nozzle tests. This higher pressure results from the lower Mach Number flow at the end of the ramp prior to separation.

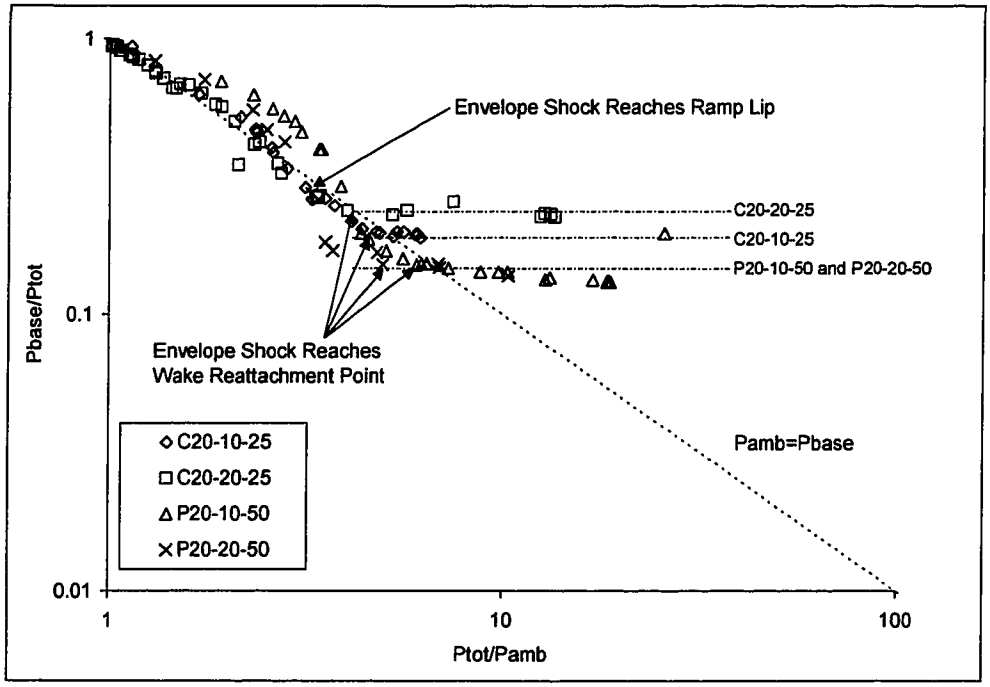

Figure 3.11: Mach 2.0 Nozzle Base Pressure Profiles

In the C35-10-25 and C35-10-50 comparisons, it was concluded that the longer plug lengths led to lower base pressures due to the amount of gas expansion prior to flow separation from the ramp lip. However, it must also be recognized that the change in truncation length affects the base height as well as the separation Mach Number. Although slight, the lower base pressure of the C20-10-25 nozzle when compared to the C20-20-25 nozzle may be attributed to the base height. Alternatively, the larger nozzle size increases the Reynolds

Number at separation due to the lengthened ramp. The increased Reynolds Number increases base pressure. These effects should be examined in follow-on research efforts.

The transition region for these nozzles was less distinctive than in the M=3.5 cases. As a result, it was difficult to determine the point at which the wakes were fully open. However, both the contoured and planar nozzles had base pressures higher than ambient pressure in the range of pressure ratios after the envelope shock reached the ramp lip. The higher base pressures were more pronounced for the planar nozzles due to the stronger shocks on the ramp and outer edge shear layer.

3.3.3 High Mach Number Nozzle Flow Attributes

Tests were conducted on Mach 4.0 and 5.0 nozzles to represent the higher Mach Number flows. The contoured nozzles had similar flow development as the other contoured nozzles at lower Mach Numbers. However, the flow features for planar shapes, as depicted in Figure 3.12, resembled those described by Tomita, et. al. (18), which were driven by the separation of flow from the ramp surface. At high NPR (a), the flow appears similar to the overexpanded flows of the Mach 2.0 and 3.5 nozzles. As the NPR decreases (b), a normal shock appears between the recompression shock and the jet outer boundary edge and moves forward toward the wake reattachment region. In some tests, a faint gradient was visible at high NPR (b) and was assumed to be the envelope shock. This structure moved toward the wake with decreased NPR, but the normal shock generally reached the reattachment region before this envelope shock. At this point (c), the recompression shock and the already faintly envelope shock vanished.

(a) NPR=75

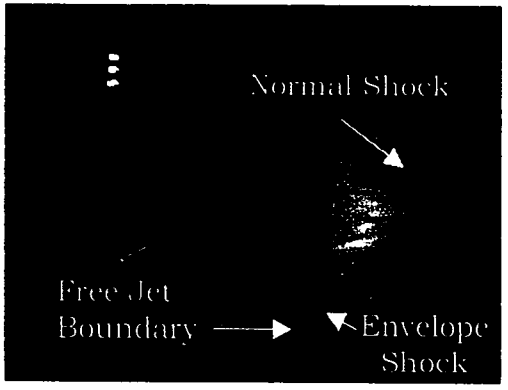

(b) NPR=64

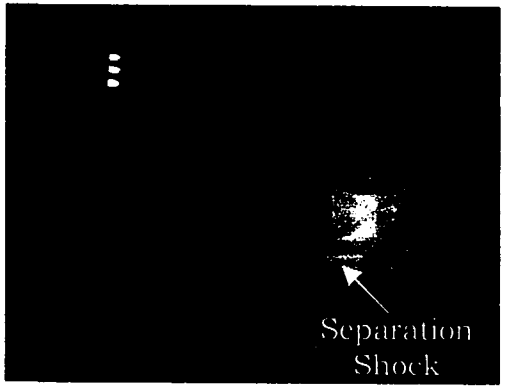

(c) NPR=55

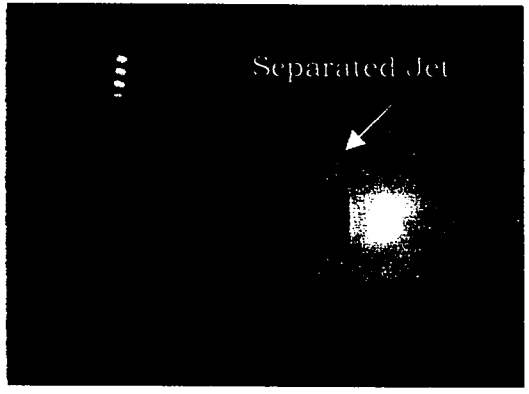

(d) NPR=22

(e) NPR=13

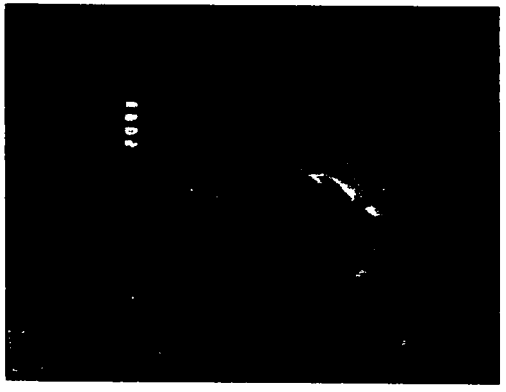

(f) NPR=7.6

Figure 3.14: P40-20-25 Flow Development

The normal shock impinges the reattachment region at NPR=60 (b-c). The lip shock becomes a separation shock that moves forward along the ramp surface with decreased NPR. At approximately NPR=22 (d), the flow exists as two separated jets, and the wake structure is broken down and nearly disappears. The flow reattaches to the ramp surface in (e), and then becomes a series of separated-reattaching flow structures with a conical shear layer flow in (f).

Operating at the highest NPR available for the test facility, it was not possible to push the separation shock to the ramp lip of the planar Mach 5.0 nozzles. The combination of the incident throat angle associated with the high Mach Number and the planar shape led to pressure gradients strong enough to separate the flow. Since the wall separation shock was also a primary feature in the P40-10-25, P50-10-25, P50-15-25, and P50-20-25 nozzles, jet height (or nozzle size) was not a significant factor dictating whether wall separation occurs.

3.3.4 High Mach Number Nozzle Wake Closure and Base Pressure

The composite base pressures for several C40-10-50 tests in Figure 3.13 have a lower closed wake base pressure than the Mach 3.5 nozzles. Similar to the C35-10-50 nozzle, there is a jump in the transition region associated with the impingement of the envelope shock on the wake.

The base pressure data for the larger C40-20-50 nozzle was significantly scattered in the transition region. To identify the cause of this variance, the data is categorized into two groups based on whether the total pressure during the test is 1) increasing (i.e., during tunnel start up) or 2) decreasing (i.e., the remainder of the test). Based on this breakdown, Figure 3.14 shows that the base pressure during tunnel startup is higher than that measured during the decreasing total pressure. This result indicates that the transition region may be subject to hysteresis. Tomita, et. al. (18) also reported hysteresis in their data. However, they found that the base pressure measurements taken when

decreasing total pressure were higher than those taken when increasing total pressure.

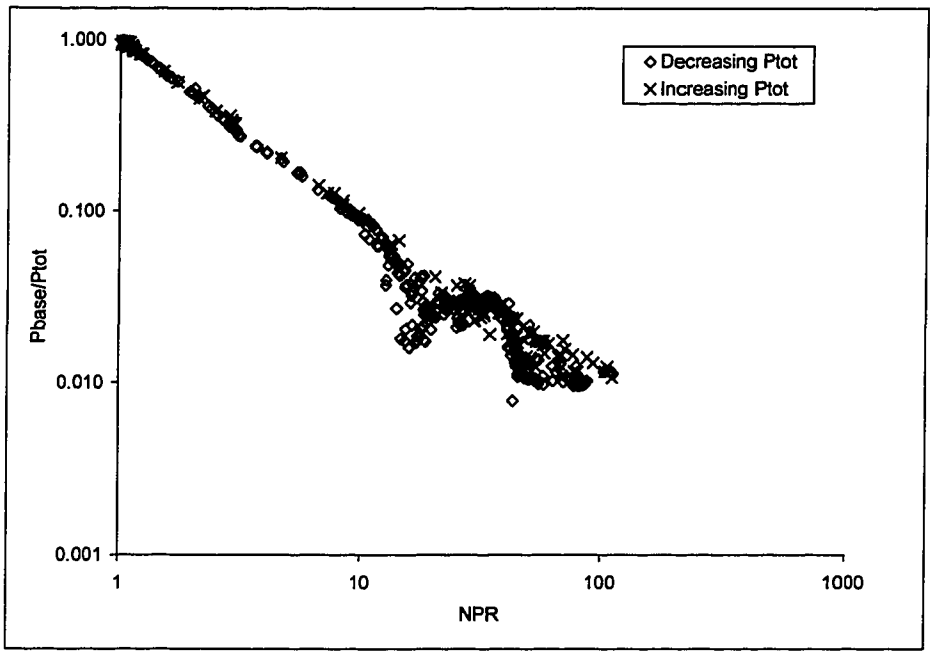

Figure 3.13: Composite C40-10-50 Nozzle Base Pressures

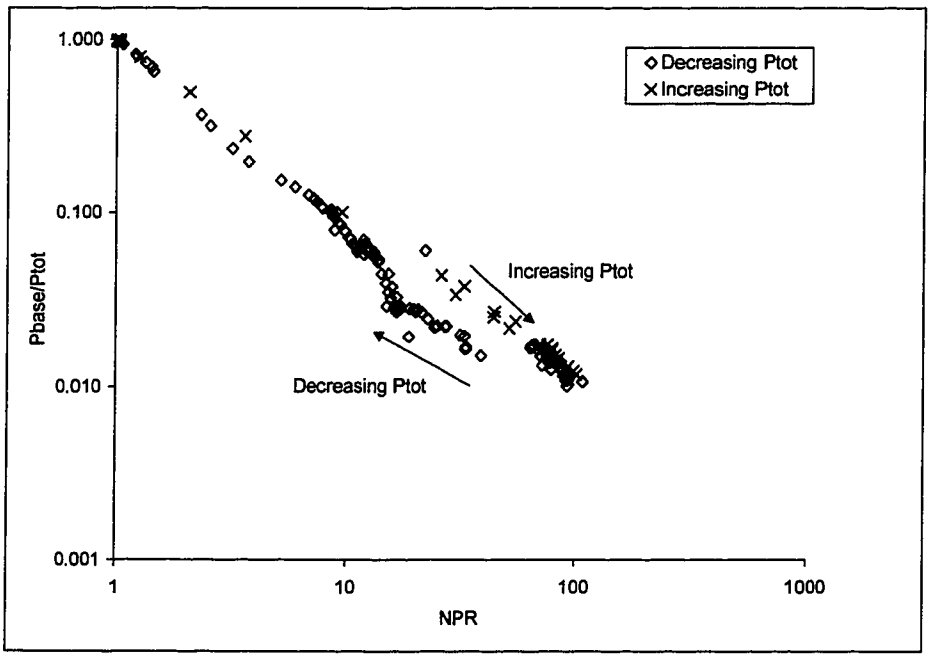

Figure 3.14: Composite C40-20-50 Nozzle Base Pressures

In the planar ramp cases of Figure 3.15, the open wake NPR correlated with the condition where the wall separation shock first appears in the schlieren pictures. It is also noted that the primary supersonic wake features are present until this wall separation shock is about mid-length along the ramp.

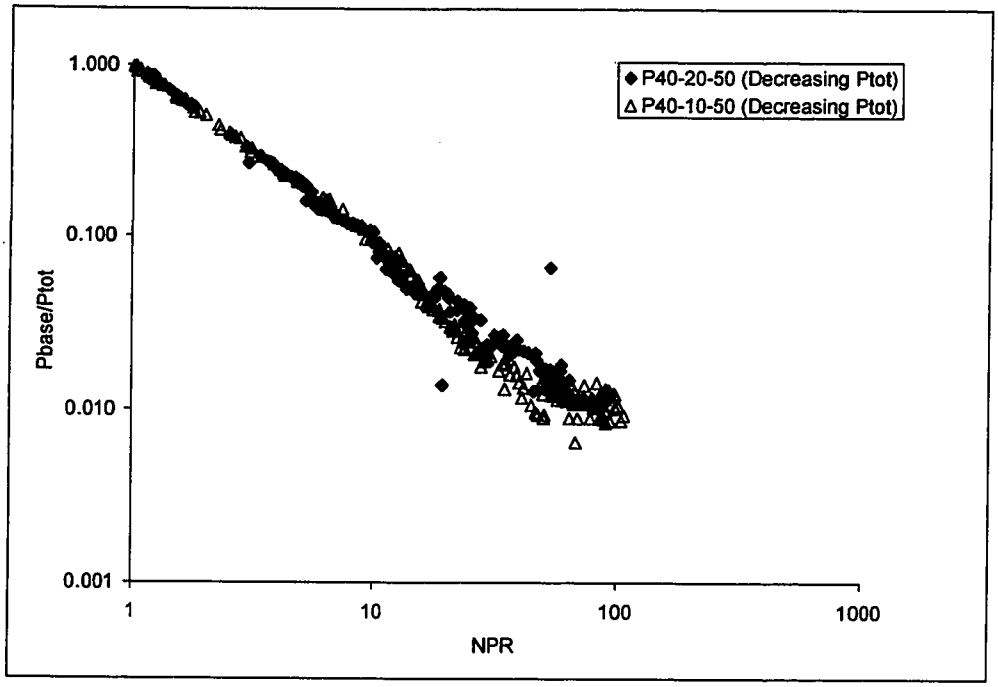

Figure 3.15: Composite P40-10-25 and P40-20-25 Nozzle Base Pressures

There was no appreciable difference in the closed wake p_{base}/P_{tot} for the M=4.0 contoured and planar nozzles. Both planar nozzles experience the hysteresis found in the C40-20-50 tests. The wake closure NPR did occur at a much lower NPR than the contoured nozzle of the same jet height. The correlation between jet height and wake closure NPR was not found for the lower M=2.0 nozzle tests. However, the difference in wake closure modes may account for this new correlation.

3.4 Summary

The purpose of these tests was to characterize the changes in flow structure for the wake in closed, transitional, and open conditions. The wake development for most of the nozzles had a dominant envelope shock. For these flows, wake closure is linked to the movement of the envelope shock to a location just aft of the reattachment region.

In high Mach Number planar nozzles, it is unclear whether an envelope shock exists. Nevertheless, the dominant feature in the flow development is the downstream normal shock that moves forward toward the reattachment region. As it reaches the reattachment region, flow along the ramp separated from the surface, and the wake changes from closed to open conditions. Therefore, the common feature in both modes of wake closure is the presence of a shock that passes through the wake reattachment region. The mode by which wake closure occurs is dependent on a combination of Mach Number and ramp shape.

The primary supersonic wake features exist for closed wake conditions and open wake conditions (near the wake closure NPR). For these conditions, the flow downstream of the reattachment region recovers supersonic speeds until the downstream normal shock or diamond shock structure is reached. In addition, the changes to the centerline distribution imply that an upstream propagation of ambient conditions does not occur or is not a significant factor relating base and ambient pressures.

Chapter 4
WAKE CLOSURE ANALYSIS

The experimental effort provides a physical understanding of the global changes to the plug nozzle flowfield in open and closed wake conditions. Based on this understanding, a detailed investigation focuses on the internal changes occurring specifically in the wake and how these changes lead to wake closure. Some of the key issues addressed include:

- Relation between the changes in the velocity and pressure profiles within the viscous wake and base pressure,
- Identification of flow parameter trends associated with wake closure,
- Determination of whether traditional analytical wake methods can be used to analyze open and closed wakes, and
- Explanation of wake closure using traditional analytical wake concepts.

This chapter describes the numerical tools and the approach used to characterize the details of the wake's internal structure. The subsequent investigation results include an evaluation of wake closure on the plug nozzle wake and analysis of the mechanism(s) leading to wake closure.

4.1 Investigation Approach

The analysis of the wake closure mechanism consists of two parts. In the first part, the changes in the flowfield are characterized as a function of NPR. Changes in the axial distributions of key wake properties are used to determine the means by which the inviscid flow influence base pressure and give preliminary insights to the wake closure mechanism. In the second part,

analytical wake concepts are applied to the CFD solution. The key parameters from the analytical wake methods are used to explain how wake closure occurs.

For the purposes of this analysis, the computations are conducted assuming for a laminar flow. In general, the shear layer transitions rapidly to turbulent mixing shortly after separation from the ramp, so the CFD results are not expected to accurately predict the absolute magnitude of the flow properties. While the CFD code offers the option to model turbulence, the impact on the wake analysis of the model type, technique, and implementation is uncertain. The trends given by the laminar models are sufficient, since the emphasis of this effort is to analyze wake closure rather than a turbulence modeling analysis. The effect of turbulence is briefly examined in the wake closure mechanism analysis.

The analysis of wake changes and determination of the wake closure mechanism is conducted on a contoured ramp that undergoes the envelope shock mode of wake closure. The resulting explanation of wake closure mechanism is examined further to determine whether it is also consistent with the flow changes found in the wall separation mode of wake closure and used to explain both modes.

4.1.1 Computational Tools

The analysis of the wake and wake closure mechanism is conducted using CFD and analytical methods. The CFD code is INCA: Version 2.0, by Amtec Engineering Inc. INCA is a 3-dimensional multiblock upwind implicit Navier-Stokes code. It solves the compressible or incompressible Reynolds-averaged Navier-Stokes equations. The field equations are solved using a Lower/Upper-Symmetric Gauss Seidell (LU-SGS) implicit finite-volume method. The inviscid terms are approximated using flux-vector or flux-difference splitting in combination with upwind biased or total variation diminishing (TVD)

differencing. The diffusion terms are evaluated using standard central differences.

The CFD techniques and analytical methods are numerical models of the flow, but have the advantage of providing detailed profiles and distributions of flow properties throughout the flowfield. They also avoid any non-ideal flow issues associated with the wind tunnel operation or hardware fabrication.

The reader is referred to the INCA Users Guide (58) for explanation of the terms and assumptions. The principal equations of motion solved by INCA are given below:

$$\frac{\partial}{\partial t}\iiint_{Vol} U dV + \iint_{S} \vec{P}\cdot\vec{n}\, dS = \iiint_{Vol} N dV$$

$$\text{where } \vec{P} = F_1\vec{i} + F_2\vec{j} + F_3\vec{k}$$

$$U = \begin{bmatrix} \rho_1 \\ \vdots \\ \rho_s \\ \vdots \\ \rho_{NS} \\ \rho u_1 \\ \rho u_2 \\ \rho u_3 \\ E \\ \rho e_{ve} \end{bmatrix}; \quad F_i = \begin{bmatrix} \rho\, u_i + \rho_1 v_{1i}^d \\ \vdots \\ \rho_s u_{i1} + \rho_s v_{si}^d \\ \vdots \\ \rho_{NS} u_i + \rho_{NS} v_{NSi}^d \\ \rho_{NS} u_i + p\delta_{1i} + \tau_{1i} \\ \rho_{NS} u_i + p\delta_{2i} + \tau \\ \rho_{NS} u_i + p\delta_{3i} + \tau \\ (E+p)u_i + u_j\tau_{ij} + q_i + \sum_s \rho_s v_{si}^d h_s \\ \rho e_{ve} u_i + q_{ve_i} + \sum_x \rho_s v_{si}^e e_{ve_s} \end{bmatrix}; \quad N = \begin{bmatrix} w_1 \\ \vdots \\ w_x \\ \vdots \\ w_{NS} \\ 0 \\ 0 \\ 0 \\ 0 \\ w_{ve} \end{bmatrix}$$

$$E = \rho\left(e + \frac{1}{2}u_j u_j\right) = \rho H - p$$

$$\tau_{ij} = -(\mu + \mu_t)\left[\left(\frac{\partial u_i}{\partial x_j} + \frac{\partial u_j}{\partial x_i}\right) - \frac{2}{3}\delta_{ij}\frac{\partial u_k}{\partial x_k}\right]$$

$$q_i = -(k_l + k_t)\frac{\partial T}{\partial x_i}$$

$$q_{ve_i} = -(k_{ve} + k_t)\frac{\partial T_{ve}}{\partial x_i}$$

$$\rho_x v_{si}^d = -\rho D_s \frac{\partial X_s}{\partial x_i}$$

INCA offers the option to use Steger-Warming or Harten-Yee flux functions. The Harten-Yee flux function is written as a central difference flux plus a dissipation term. By setting the dissipation term to zero, the equation gives Roe's first-order approximate Riemann solver. Since the key data sought was the viscous wake region, Roe's flux-difference splitting was selected for the wake analyses. INCA uses laminar flows or allows the option to use several turbulence models, including Baldwin-Lomax algebraic model, the Baldwin-Barth one-equation model, and the two-equation k-ε model.

The meshes used to model the geometries required are generated with Amtec's GRIDALL software. GRIDALL is a three-dimensional multiblock, structured (I,J,K) grid generator to support INCA and creates meshes that are visualized with Amtec's TECPLOT graphical visualization program. The user specifies top level definitions for points, lines and zones, and GRIDALL creates the desired meshes using algebraic and elliptic grid generation techniques. Although INCA has the option to implement grid adaptation techniques during the run, the grids were left unrefined to facilitate post-processing in grid convergence analyses and application of analytical wake methods.

Once a CFD solution is obtained, the desired wake analysis parameters for assessing changes are computed as a function of NPR and used to examine the

wake closure mechanism. Specifically, a Visual Basic post-processing code extracts the desired CFD data, generates a new grid and solution set, locates key wake surfaces, and then computes the IVI Method wake parameters.

The numerical analysis verification is conducted in two parts. Since INCA is a commercial off-the-shelf code, the first part of the verification process ensures that the input parameters are selected correctly and that the grid sizes are designed adequately. To address these issues, INCA was run for a standard sharp leading edge flat plate in supersonic flow and an afterbody with supersonic flow. In each case, the Mach isolines, velocity and pressure profiles, and streamwise pressure distributions are examined to evaluate the qualitative accuracy of the solution and grid convergence. The results are presented in Appendix B. The uncertainty level of the CFD solutions is represented by the percent difference between CFD and empirical base pressures. An uncertainty level of 48-72% is computed for the supersonic wake flow, but higher accuracy is expected for the plug nozzle due to the better grid convergence.

The second part of the verification process focuses on validation of the post-processor. Although the CFD results provide data throughout the flowfield, there are certain limitations in the incorporation of these data into analytical computations. These results consist of discrete point data based on finite-difference approximations. In contrast, the analytical methods solution utilize smooth, continuous functions and make assumptions about the flow, such as the asymptotic nature of the velocity profile or the development of the flow from a separated jet to a mixing viscous flow. Thus, the verification process (Appendix C) determines that the CFD results can be incorporated into an analytical method as well as determining of the limitations of this approach.

4.1.2 Wake Closure Effects

The C35-10-25 nozzle is modeled to isolate the point of wake closure and examine the flow changes with NPR. An 8-zone mesh represents the C35-10-25 nozzle (Figure 4.1). The specific sizes and dimensions of the grid and grid convergence results are presented in Appendix B. The analysis of wake closure focus on Zones 7 and 8, each of which is sized 129x81, 129 horizontal and 81 vertical, nodal points. The exhaust jet inlet is an M=1.10 flow with P_{tot}=35 psia (2.413 bars) and T_{tot}=288K, injected at angle of -58.53 degrees from horizontal.

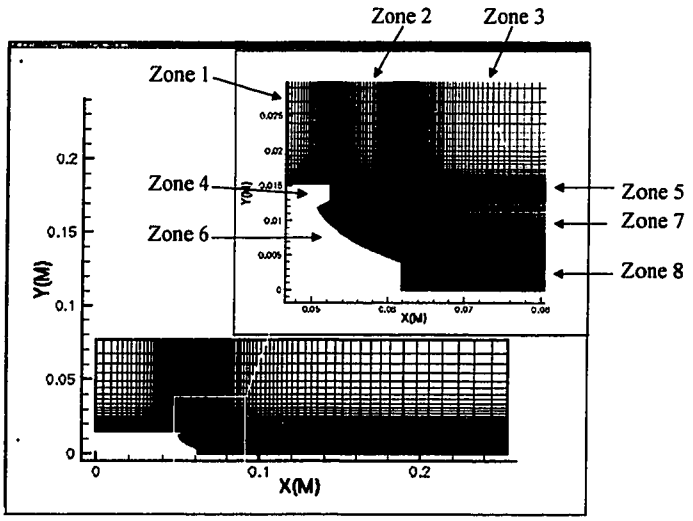

Figure 4.1: C35-10-25 Plug Nozzle Grid

The initial attempts to model the enclosed experimental test section were unsuccessful in obtaining a solution consistent with the user-defined outlet boundary conditions. Modifications to the boundary conditions bypass this problem. An external M=1.25 flow is added just above the cowl, and the solid surface boundary conditions are defined as free-slip wall conditions. The top and downstream (i.e., j-plus and i-plus) boundaries are defined as supersonic outlet conditions. (Note: this configuration more closely represents a nozzle in flight). No-slip conditions are imposed on the ramp surfaces. The only remaining issue is whether any of the downstream conditions are modeled

correctly as supersonic outlets. The experimental results confirm that these boundary conditions are supersonic as long as the supersonic wake features exist for the plug nozzle flow.

CFD runs are conducted for the range of pressure ratios shown in Table 4.1. Each run is iterated until the residual is reduced by six orders of magnitude. INCA offers the capability to use restart files to initialize the solution. Therefore, the output solution of the design condition (i.e., NPR=76) is used as the initial condition for the shear flow regions of the other case in order to improve the convergence of the solution. Zones containing freestream flow are initialized with a uniform flow at the desired ambient condition.

Table 4.1: M=3.5 Plug Nozzle CFD Test Conditions

Test Case	NPR	P_{amb} (bars)
1 (design)	76	0.03614
2	25	0.09653
3	20	0.12066
4	18.5	0.13045
5	17.5	0.13790
6	16	0.15082
7	15	0.16088
8	12.5	0.19306
9	10	0.24132
10	5	0.48265
11	2.1	1.15836

The changes in wake flow as a function of NPR are examined in four areas. First, the flowfield Mach isolines, velocity, and pressure profiles provide a qualitative overview of the flow changes with wake closure. These data indicate the position of the envelope shock, viscous wake shape and size, reattachment location and recompression characteristics. Second, the changes occurring in the base region are correlated using base pressure trends to the closed or open wake condition of the flow. Third, an analysis of the separation point region provides a comparison of the flow behavior at separation and the subsequent corner expansion. Finally, the variations in centerline pressure, velocity, and

velocity shape parameters are examined to characterize structural changes in the wake and provide preliminary indications of how wake closure occurs.

4.1.3 Wake Closure Mechanism

The second phase of the analysis focuses specifically on the mechanism by which wake closure occurs and explains the change between open and closed wakes in the context of overall flow parameters. From the Multi-Component and IVI methods described in Chapter 2, a reattachment criteria or wake critical point is required to compute a unique closed-form solution. The experimental data from Chapter 3 indicate that the primary supersonic wake flow features exist for the plug nozzle in both open and closed wake conditions, and suggest that a wake critical point should exist. Using Lees-Reeves method, the CFD data is used to confirm the existence a critical point for the open and closed wake conditions, and thus whether traditional wake analysis methods are applicable.

Changes in base pressure due to wake closure should be reflected by changes in the critical point parameters. Therefore, the flow properties used to determine the critical point (i.e., the edge Mach Number, the velocity shape parameter, a(x), and displacement thickness) are examined in detail. Wake closure is described in terms of the changes in these parameters. The critical point is further examined using Weinbaum's 2-D viscous throat interpretation to provide alternative explanation of the wake closure mechanism.

The wall separation mode of wake closure is also reexamined to determine whether the physical interpretation of wake closure is equally applicable. The effects of turbulence are briefly examined. The explanation of wake closure is then compared with overall flowfield changes and wake closure interpretations by other researchers to assure consistency.

4.2 Wake Closure Effects on Internal Flow Structure

The first step in understanding changes in the wake structure is a comparison to supersonic wake to identify the similarities and differences that should be considered in applying supersonic wake methods to the plug nozzle analysis. The results are discussed in more detail in Appendix D. The C35-10-25 plug nozzle at design operating conditions most comparable to the M=2.5 supersonic wake flow due to the similar conditions of the boundary layer flows prior to separation from the afterbody. The inviscid flowfield of the plug nozzle is non-uniform, and varies from M=2.5 to M=3.5. The difference in the external flowfield leads to a faster wake flow development in the plug nozzle and shorter RSP distance. The recompression process for the plug nozzle however occurs further downstream and with sharper a gradient than the supersonic wake when normalized to the respective RSP distance. While there are some relatively small differences in parameter profiles inside the viscous wake, the overall effect is negligible on base pressure. A critical point exists for the plug nozzle flow, and is located upstream of the supersonic wake. As a result, it is concluded that the analytical wake methods are applicable, at least under closed wake conditions.

4.2.1 Overview of Wake Changes

The next step is to characterize the changes occurring in the internal wake structure as NPR decreases from closed to open wake conditions. The series of Mach isoline pictures for the C35-10-25 nozzle in Figure 4.2 illustrates the transition of the wake from closed to open conditions. The jet total pressure is held constant, and the ambient pressure was specified to give the desired NPR. Qualitatively, the results of the CFD runs show the same trends in flow structures as those found experimentally in Figure 3.4 (note that the picture shows Mach isolines versus the density gradients depicted by Schlieren photography). The primary difference between the CFD and experimental data

is the expansion fan at the top corner of the cowl that occurs in the CFD due to the supersonic freestream. As the NPR decreases (a-e), the exhaust jet boundary moves closer to the ramp surface, and the point where the envelope shock impinges on the near wake region moves forward. Eventually (f), the envelope shock reaches the ramp lip and the wake structure is no longer intact. Closer examination of the flow near the ramp corner also shows that the flow has separated from the surface under this low NPR condition.

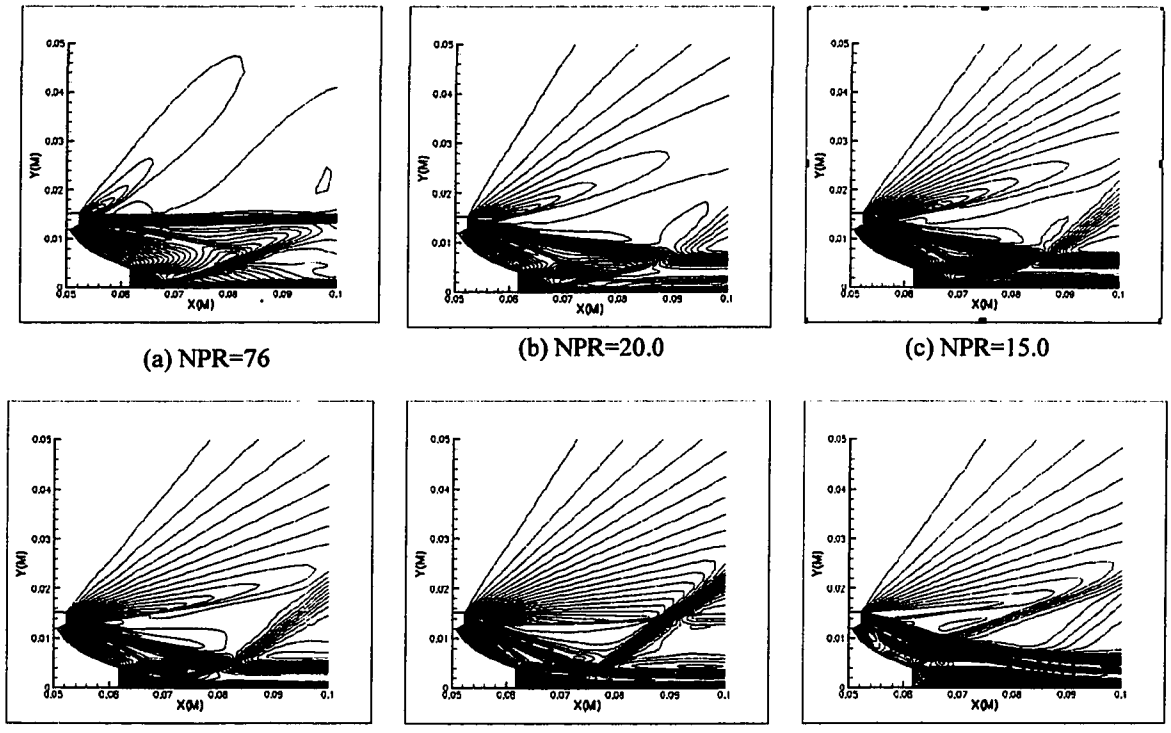

(a) NPR=76 (b) NPR=20.0 (c) NPR=15.0

(d) NPR=10.0 (e) NPR=5.0 (f) NPR=2.1

Figure 4.2: Wake Closure Development for Contoured Nozzle

An interesting feature was the presence of the envelope shock at design conditions (a), which results from the compression of the flow prior to reaching the outer jet boundary. Based on the existing literature, the envelope shock only occurs at this condition when there is internal expansion prior to the thruster exit. The thruster exit is modeled in the CFD simulation as a uniform M=1.1 flow. At this Mach Number, the negligible internal expansion is assumed

negligible. The presence the envelope shock suggests that overexpansion is occurs for flight hardware under all conditions. Additional CFD tests at higher pressure ratios are needed to confirm this hypothesis.

Figure 4.3 depicts the velocity, pressure and total pressure profiles, respectively, for representative open and closed wake conditions. The closed wake transitions from the separated jet velocity profiles to mixing layer profiles more rapidly than the open wake and consequently reaches a reattachment point earlier. The open wake has a greater velocity defect far downstream.

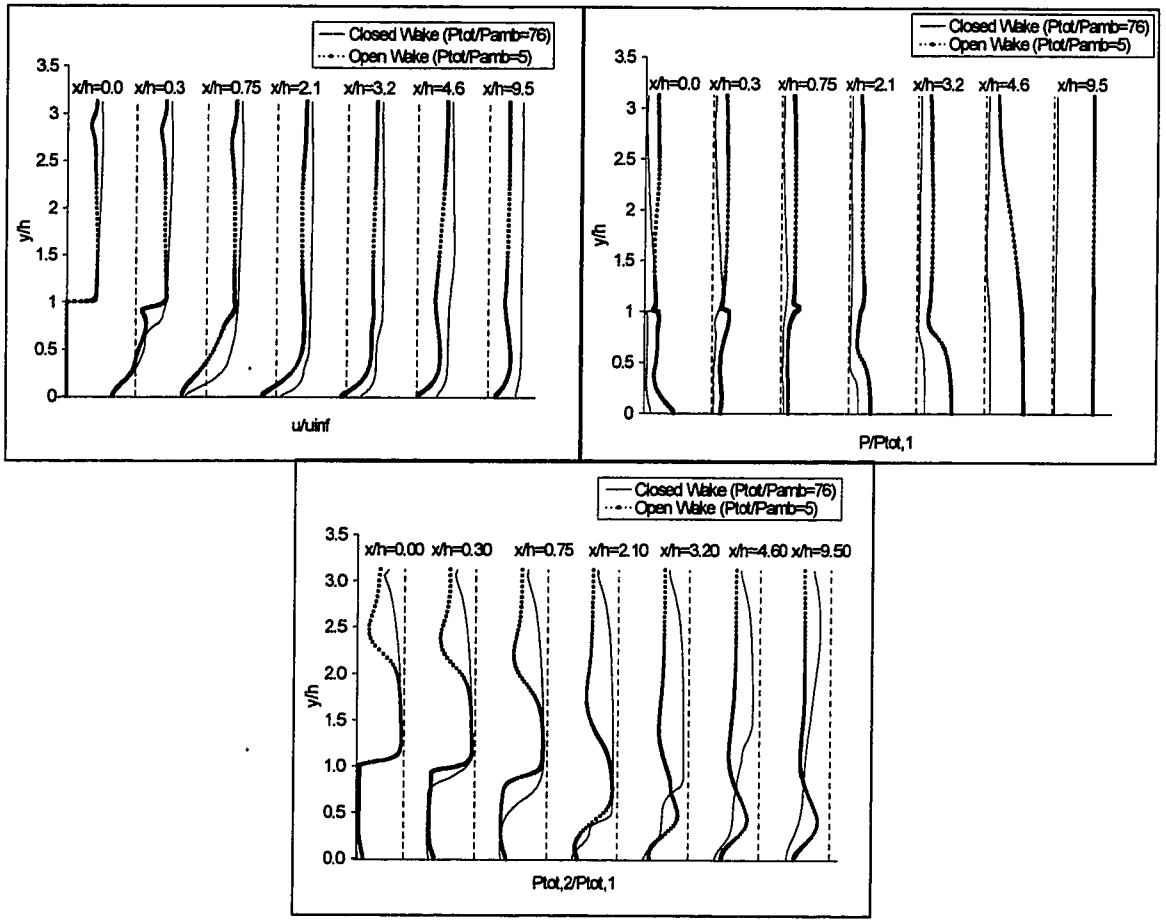

Figure 4.3: Open and Closed Wake Profile Comparisons

The higher open wake static pressure profiles in the inviscid flow represent the lower Mach Number flow after passing through the envelope shock and the recompression shock further downstream. A shock emanating from the ramp corner in the open wake condition causes a jump in pressure at y/h=1. The higher pressure inviscid flow of the open wake condition result in higher pressures in the viscous wake. Although the open wake pressure profiles are proportionately higher in the wake region, the region near the base exhibits a significantly larger difference between the open and closed wake pressures. The mechanical energy (or total pressure) of the wake develops from the shear layer as the flow proceeds toward the reattachment point and then recirculates back to the base. The last frame of Figure 4.3 shows only a slightly higher total pressure within the recirculation region for the open wake. The base at y/h=0 is a stagnation point, so the static pressure equals the total pressure. Thus, the higher base pressure for the open wake reflects a lower total pressure loss or greater entrainment of the jet flow into the recirculation region. This greater entrainment results in a greater velocity defect as shown in the downstream velocity profiles.

4.2.2 Base Region Changes

The CFD base pressure results are compared to experimental measurements at the same total pressure. Though not exactly the same condition (since the experiment had no external flow), the comparison provides some sense of the data quality. The experimental data and CFD solution compare relatively well in Figure 4.4. The closed wake base pressures are nearly identical. This suggests that the velocity of the external environment is not as critical as matching pressure conditions when the wake is closed.

The CFD prediction of wake closure is close to the left path of the experimental data. However, once the wake is open, the experimental data lies closer to the $p_{amb}=p_{base}$ line, whereas the CFD solution remains below the line. Since the

base pressure is dependent on the ambient environment for open wake conditions, the gap between the experimental and CFD data may be a direct representation of the differences in external environments. Additional CFD simulations with no external flow would clarify this further.

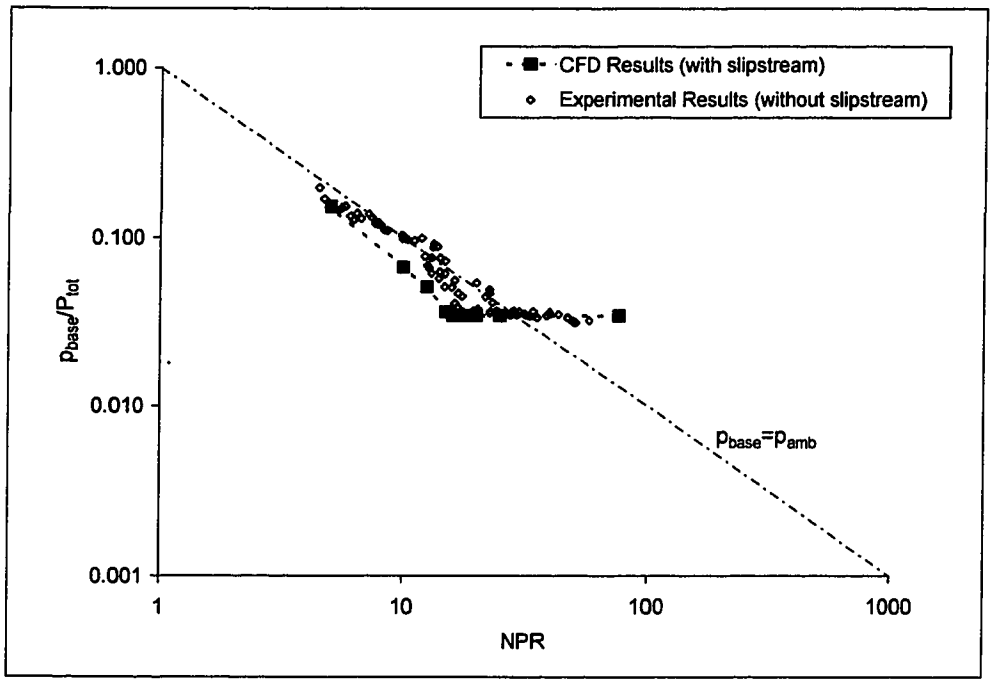

Figure 4.4: C35-10-25 Composite Base Pressures

Based on an empirical survey by Pallone, et. al. (59), it earlier was assumed that the wake would be turbulent. The resolution of the Schlieren pictures in Chapter 3 was insufficient to determine the state of the far wake, but the shear layers were assumed to undergo transition almost immediately from laminar to turbulent mixing in the near wake. The correlation between the experimental and CFD base pressure data in Figure 4.4 suggests that the near wake may be laminar. Alternatively, the boundary layer may have been thick enough at these Reynolds Numbers to cause the laminar and turbulent base pressures to be similar.

The efficacy of using CFD for this problem given the numerical assumptions and limitations built into the model is demonstrated by the open and closed wake behavior exhibited by the base pressure data in Figure 4.4. The precise wake closure NPR is difficult to determine from the CFD results. The base pressure at NPR=15 is slightly different from those at higher NPR and assumed to be the beginning of the wake closure transition. The CFD wake closure NPR is in the same vicinity as the experimental results.

The position of the envelope shock as denoted by the CFD Mach isolines differs slightly from the experimental schlieren pictures for similar NPR. A correlation between the Mach isolines in Figure 4.2 to the base pressures in Figure 4.4 indicates that the wake closure NPR occurs prior to the envelope shock reaching the root of the recompression shock. This transition was also seen in experimentally (though not as precisely) and is consistent with the theory that wake closure is tied to the isolation of the wake from the inviscid flow compression waves between the outer jet boundary and the envelope shock. Thus, wake closure occurred at this NPR rather than a NPR when the envelope shock intersects the root of the recompression shock. It appears that even though the inviscid flow compression waves are "absorbed" by the recompression shock, their effects still pass through the shock into the portion of the wake aft of the recompression shock root and the reattachment point (upstream of wake critical point).

4.2.3 Separation Point Changes

An enlarged view of the Mach isolines in the area around the ramp lip (Figure 4.5) shows some immediate consequences to the flowfield due to the decreased NPR and transition from closed to open wake conditions. In the closed wake, the flow over the ramp is continuously expanding so that the Mach Number increases away from the ramp surface to a value of about M=3.6. However, the envelope shock in the open wake bounds the expansion of the flow to about

M=2.5 and then the flow decreases in Mach Number as it passes through the envelope shock and the free jet boundary.

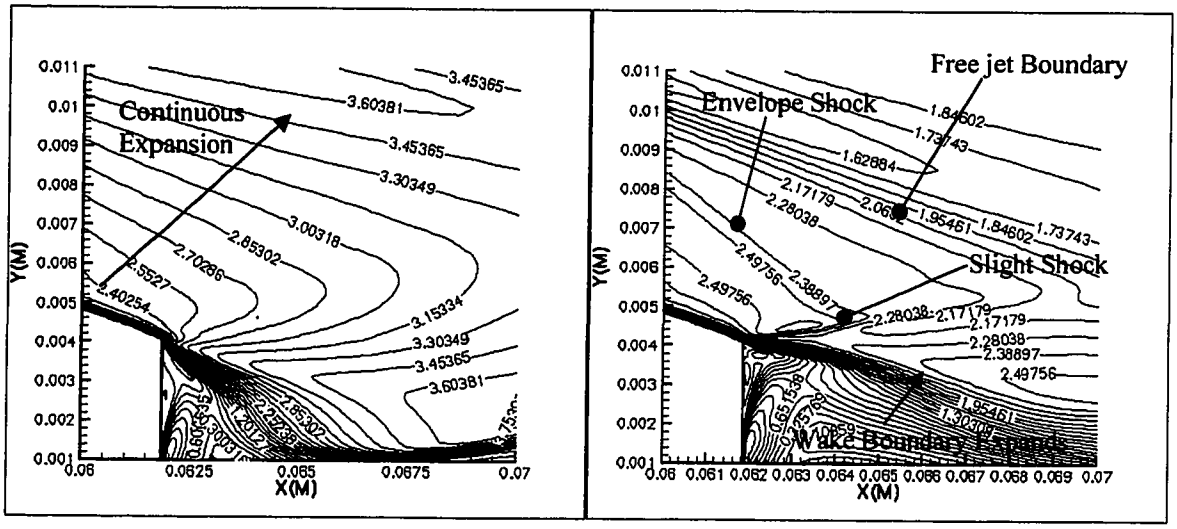

NPR=76 (Closed Wake) NPR=5 (Open Wake)

Figure 4.5: Corner Expansion in Closed and Open Wake Conditions

There are two effects on the flow as it turns the corner. First, the flow passes through a lip shock that reduces the flow Mach Number prior to expanding. Secondly, the flow undergoes less of an expansion process as it passes around the ramp corner. This latter effect illustrates the interaction between the inviscid and viscous flows. At the end of the expansion fan, the shear layer outer boundary lies much further away from the axis in the open wake condition than closed wake. (Note: this phenomenon was also seen experimentally by the enlargement of the near-wake region as the wake opened.) The expansion itself represents the difference in pressure between the flow prior to and after the expansion. Thus, the limited expansion is as much an indicator of the increased pressure in the base region as it is a cause of this pressure rise.

Although the envelope shock inhibits the expansion process as it moves closer to the ramp, this effect could not be discerned from the edge Mach Number

prior to separation alone. The envelope shock clearly affects the inviscid flow (Figure 4.6). The envelope shock causes the sharp Mach Number decrease as the shock moves closer to the ramp with decreased NPR. The boundary layer edge at the end of the ramp in closed wake conditions is identical to that of the open wake, as are the edge Mach Numbers. Similarly the mass flow profiles from the ramp surface to the envelope shock are identical, resulting in identical displacement thickness at the separation point. In standard wake analyses with uniform external flow, the definition of the edge Mach Number (equal to freestream Mach Number) and displacement thickness prior to separation were sufficient to determine the base pressure. In this case, the wake structure and the resulting base pressure are uncoupled from the initial conditions at the ramp corner and the entire inviscid flow along the wake must be considered.

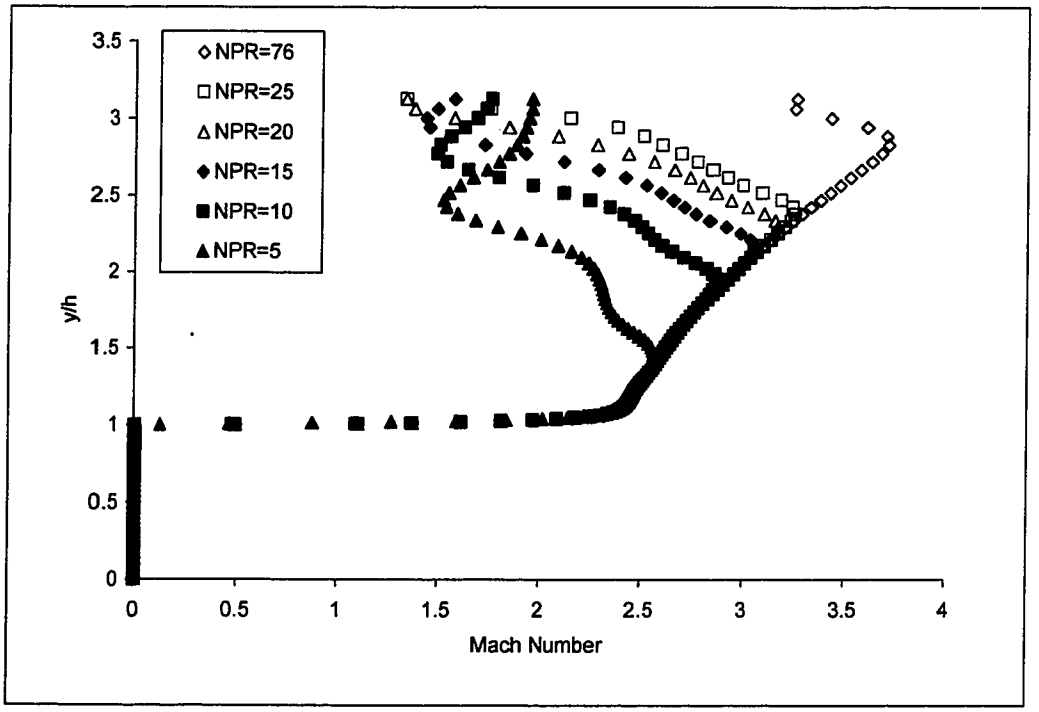

Figure 4.6: Mach Number Profile at Ramp Lip Separation

4.2.4 Centerline Wake Changes

The distributions of properties along the centerline provide an aggregate view of the changes occurring in the wake as NPR decreases. The changes in inviscid flow are reflected in the outer boundary conditions, which are then propagated into viscous wake and to the base pressure. Figure 4.7 depicts the calculated centerline pressure distribution as NPR is varied. These distributions are similar to the experimental data shown in Figure 3.7 and show the divergence of downstream pressure from the closed wake conditions as the envelope shock moves forward. Once the divergence point reaches the closed wake peak pressure, the slope of the curve during recompression decreases and the base pressure increases. At the NPR that the base pressure nears the peak pressure, the entire curve lifts off of the closed wake distribution. This may be indicative of a dramatic change in corner flow characteristics from an expansion process to the compression seen in Figure 4.5.

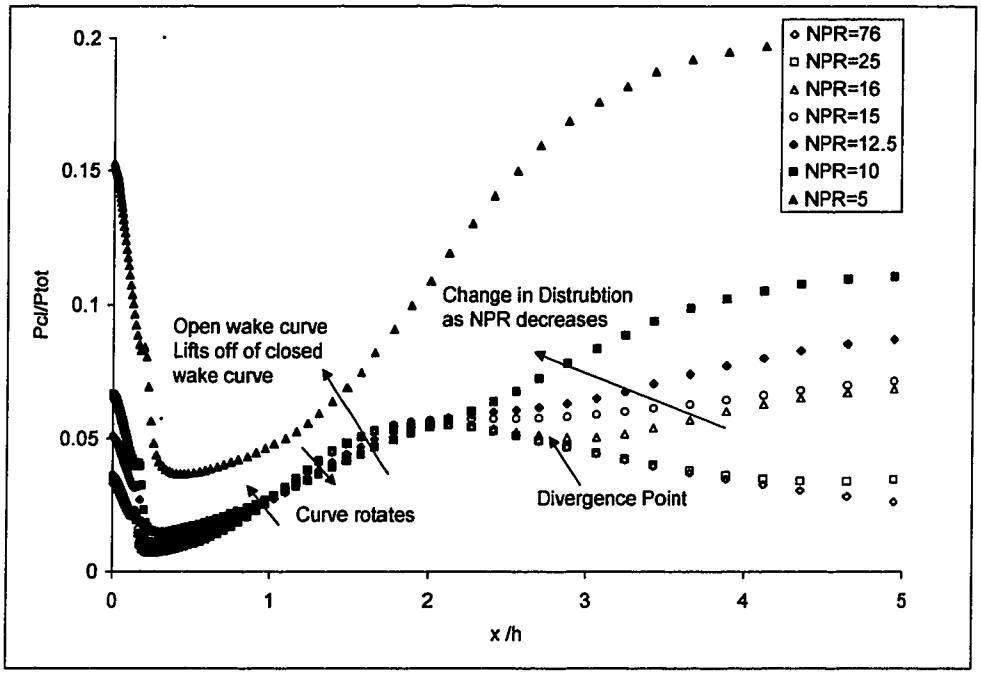

Figure 4.7: CFD Centerline Pressure Changes

From the analysis of the experimentally measured centerline pressures, it was concluded that the wake was changing structurally and that base pressure was not being directly influenced in the open wake conditions by upstream propagation of pressure. The CFD solution refines this picture slightly in that the open wake structural changes should be viewed in two phases. Just after the wake opens, there are moderate adjustments by the wake that affect base pressure, but the wake remains structurally unchanged. As the base pressure reaches the peak closed wake pressure, the entire wake structure shifts and leads to a completely new pressure distribution.

The increasing back pressure raises an additional issue regarding the prediction of wake closure. The link between an increase in back pressure to wake closure is consistent with the wake closure interpretation by Fick and Schmucker (17). They hypothesized that the wake closure behavior resulted from similar mechanisms as the flow separation in an overexpanded bell nozzle. However, up to the point that the second phase of open wake conditions occurs, downstream disturbances are still prevented from propagating forward. Thus, while the bell nozzle analogy is similar, additional mechanisms are involved.

The centerline velocities for the wake provide additional insight to the changes occurring in the wake. Similar to the pressure distributions, the immediate effect of the envelope shock on the closed wake is to cause the velocity distributions to diverge from a common curve as seen in Figure 4.8. Earlier, it was noted that the flow development and transition from a separated jet to the mixing region led to an RSP for the closed wake ahead of the open wake.

The centerline velocity distributions plotted in Figure 4.8 illustrate the details of this RSP shift. It can be seen that the divergence causes a second minimum in the velocity distribution, which has increasing inflection as the envelope shock moves forward. At a certain NPR, this minimum becomes a second RSP. This second RSP becomes the only reattachment point for the open wake flows at

lower NPR. The creation of the new RSP corresponds to the same NPR where wake closure occurs. This two stagnation point flow should be investigated further to determine its physical reasonableness since it implies there is a secondary recirculation bubble. Several of the IVI Method investigators discuss the possibility of multiple stagnation points, particularly in the presence of an adverse back pressure (which exists here). Physically, this may be an unstable condition since it occurs just at the point of wake closure.

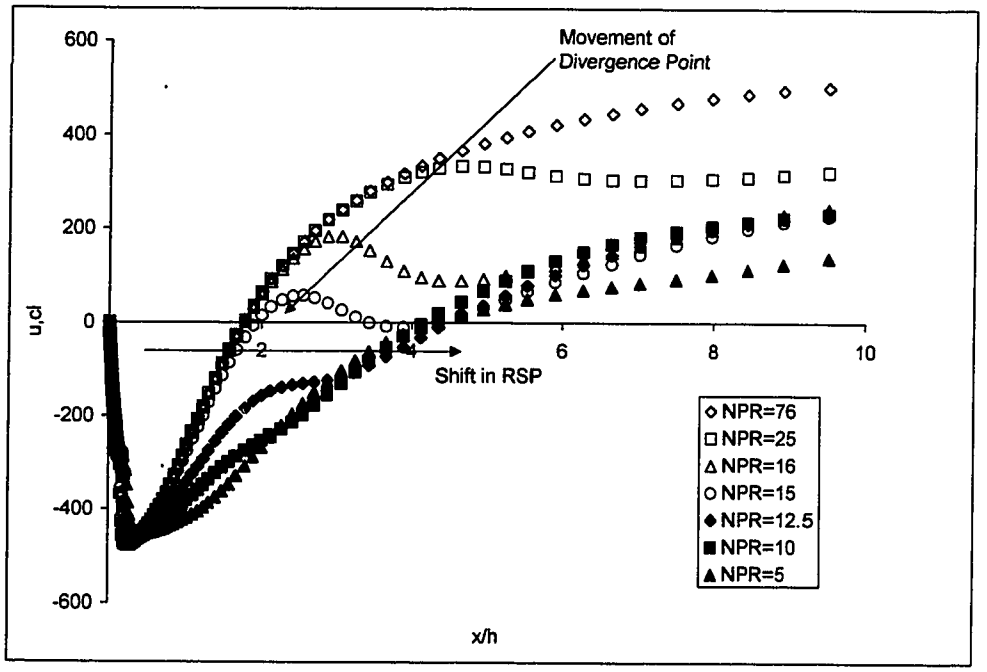

Figure 4.8: CFD Centerline Velocity Changes

The shape parameter H distributions (Figure 4.9) describe the effect of wake closure on the velocity profiles within the viscous wake. The plot of H as a function of the axial distance normalized by the RSP distance illustrates additional changes in the flow besides just an extension of the flow development further downstream. From flat plate incompressible boundary layer theory, decreasing H corresponds to accelerating and expanding flow where the velocity profile becomes "fuller", whereas increasing H correlates to decelerating flow under compression and the velocity profiles are characterized by an inflection

point leading to separated flow profiles. In the near wake, the expansion and recompression processes are thus reflected in the changes to H.

At the RSP, (x-xr)/xr=0, all of the flows have comparable shape factors. Upstream of the RSP, the open wake shape factor distributions are shifted to the left of the closed wake and after reattachment the shape factor fall below the closed wake distribution.

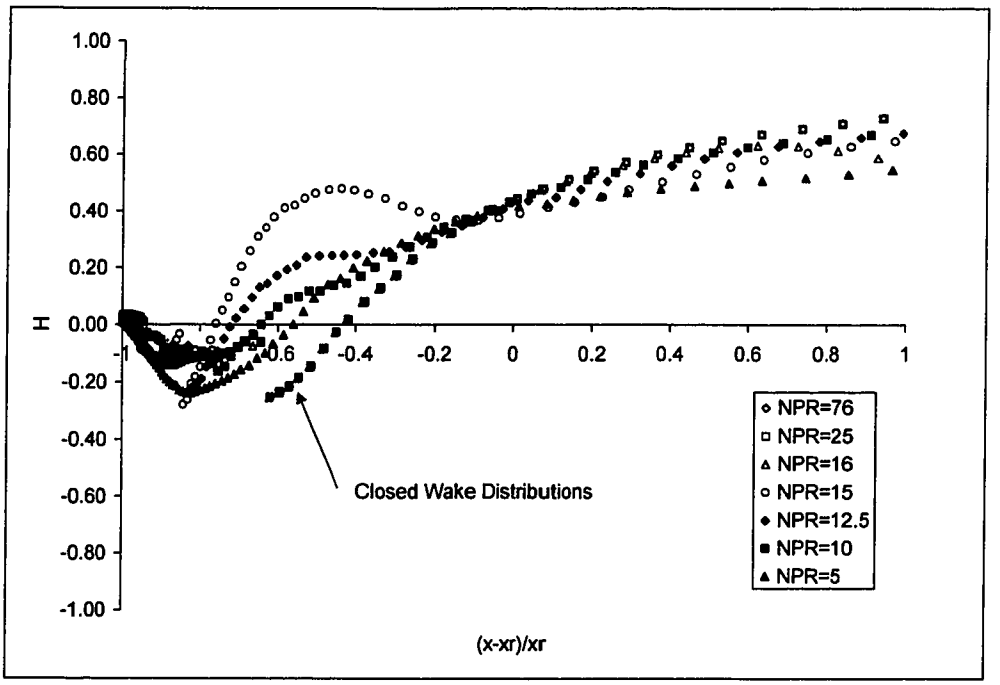

Figure 4.9: Changes in Shape Factor with Wake Closure

From the comparison in Figure D.6 (plug nozzle versus supersonic wake), the upstream shift in shape factor distribution corresponds to a decrease in base pressure. In this case, the shift from closed to open wake shape factor distributions leads to a higher base pressure. Note however that the minimum shape factor value for the open wake is almost the same as the closed wake, whereas the extrema for the supersonic wake and plug nozzle are different. To the extent that velocity profile development alone can be linked to base

pressure, the magnitudes of the shape factors may be more important than the distributions.

4.2.5 Summary

The changes in flow as NPR varied illustrated the interrelationship between expansion and recompression processes. The open wake condition can be divided into two categories: 1) conditions at NPR just below that of wake closure where the wake remains intact, and 2) conditions at much lower NPR where the traditional supersonic wake structure no longer exists. During the transition between closed and open wakes, the wake structure is intact and can be analyzed through traditional wake methods. The separation point conditions and geometry are no longer sufficient for uniqueness as they were for supersonic wakes. The entire inviscid flowfield along the viscous wake boundary becomes important in determining base pressure. The wake closure process is driven by changes in the downstream flow rather than changes to the initial separation conditions.

4.3 Wake Closure Mechanism

Based on the experimental and CFD characterization of wake changes, the wake remains intact during the transition between closed and open conditions. Thus, traditional analytical wake methods should explain how wake closure occurs. The shift in RSP location indicates changes to the wake structure, and that the changes occurring to the wake were driven by changes in downstream conditions moving forward. These changes serve as the basis for the physical interpretation of the wake closure.

4.3.1 Wake Closure Correlation to Critical Point

The data presented thus far discuss the changes in the wake in terms of the RSP position, since this station is easier to identify visually or with global flow properties. To understand the mathematical basis for changes in the wake, the IVI Methods and later refinements to the Multi-Component Method found that the wake critical point discussed in Section 2.3.2 more accurately described the downstream flow criterion governing the supersonic wake flow. Therefore, the wake closure mechanism is analyzed in terms of this wake critical point.

The plot of Lees and Reeves numerators, N1 and N2, and denominator, D, in Figure 4.10 shows that a critical point existed for both closed and open conditions. These critical points are to be expected, since it was found earlier that the supersonic wake structure remained intact. The denominator gives the singularity for the wake solutions, and shows the movement of the critical point as the wake transitioned between the closed and open wake conditions. The open wake critical point generally shifts downstream of the closed wake station.

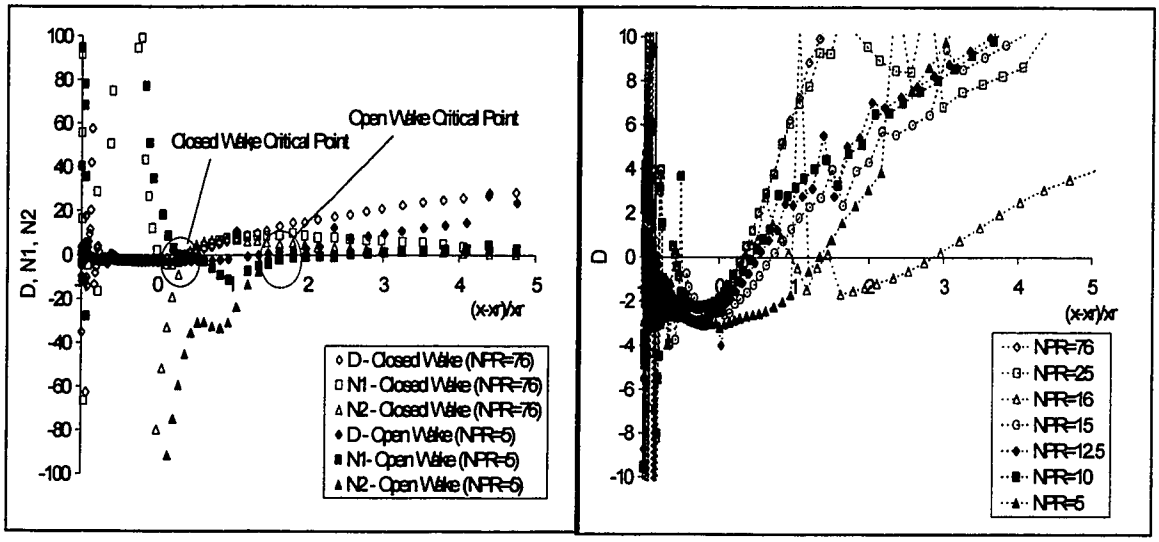

Figure 4.10: Lees-Reeves Critical Points for Plug Nozzle Flow

However, examination of the open wake critical points (i.e., where D=0) indicates that the movement of the critical point locations is not monotonic. At the wake closure NPR, the singularity moves downstream, then subsequent NPR decreases result in critical point movement between the closed wake and NPR=15 critical points. One possible explanation may be related to the centerline pressure distributions in Figure 4.8 where there was a shallower pressure gradient near the critical point, even though the base pressure increased. Although the magnitudes of the open wake edge pressures were significantly greater than the closed wake counterparts, the gradient was also slightly shallower. Eventually, the more dramatic structural change occurs in the wake, causing the critical point to shift downstream again.

From the derivation of Lees and Reeves system of partial differential equations in Section 2.3.2, the three independent variables that defines the wake development are M_e, a(x), and δ^*. The changes in these parameters as the wake transitions between open and closed conditions are shown in Figure 4.11. Similar to the flow property distributions shown in Section 4.3, a(x) and M_e deviate from the closed wake curve until the divergence point reaches a certain location. The entire curve changes once this location is reached. This location coincides with the closed wake critical point shown in Figure 4.10.

The last frame of Figure 4.11 is a plot of the position of the envelope shock impingement on the wake and the critical point. It demonstrates that the critical point shifts just as the envelope shock reaches the closed wake critical point axial location. The δ^* does not contain a similar divergence behavior. All of the closed wake curves have the same δ^* distribution. The open wake thicknesses are smaller in the recirculation region and then larger downstream of reattachment.

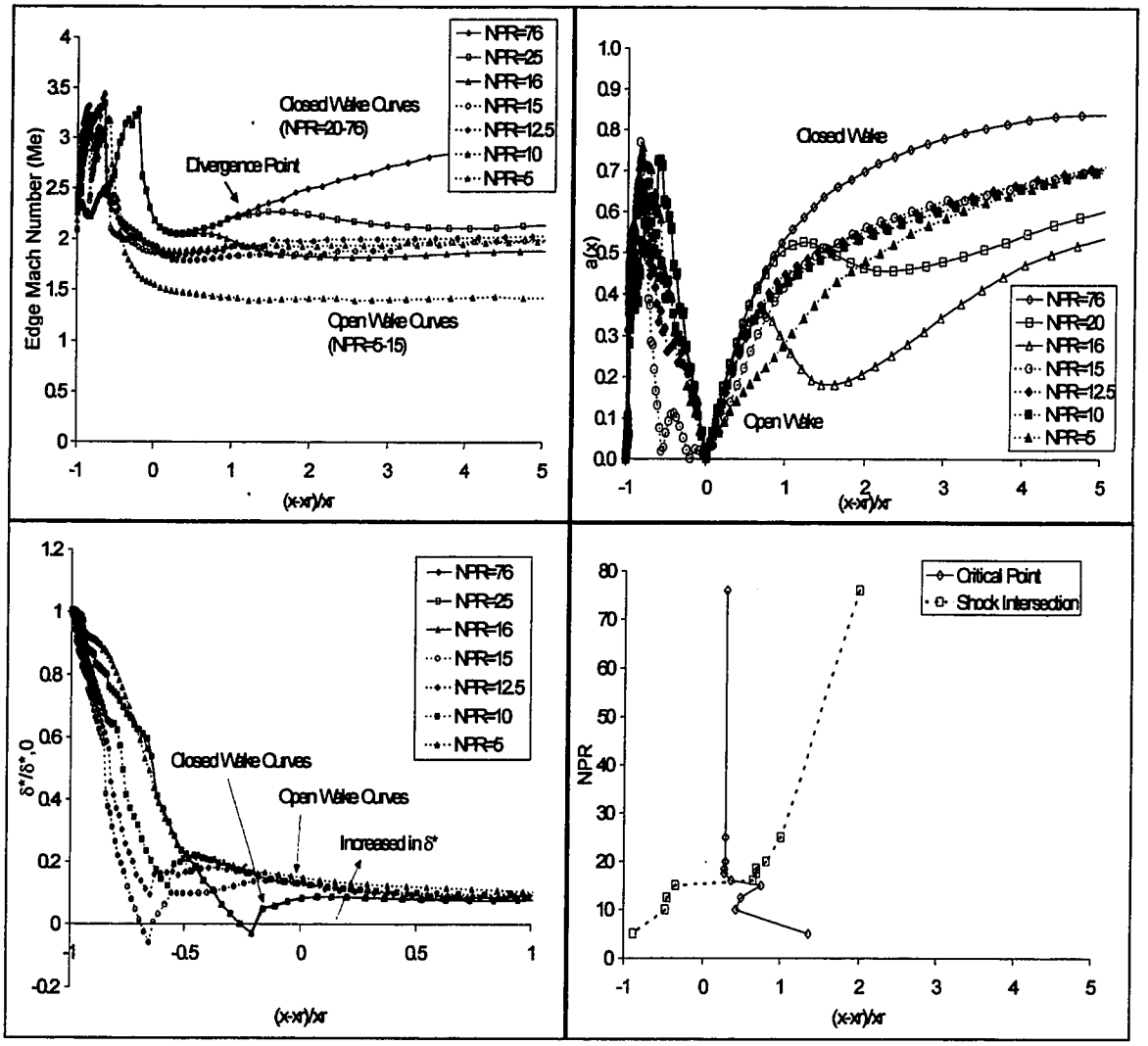

Figure 4.11: Wake Closure Effects on Lees-Reeves Metrics

A plot of edge Mach Number also shows that the entire Mach Number distribution decreases in magnitude once the divergence point reaches the closed wake critical point location. The portion of the curves associated with the flow expansion just after the ramp corner is shortened, and there is little or no recovery after recompression of the jet's Mach Number prior to separation. These changes can be partially explained by visualizing the increase in displacement thickness. The increased displacement thickness results in the increase in outer edge boundary thickness seen in the experimental data

(Figures 3.4, 3.8, and 3.10) and in the CFD Mach isoline pictures (Figure 4.5). The increased wake "core" flow size and downstream shift of the reattachment point geometrically imply that the angles of expansion and recompression are reduced, thereby reducing the range of change in Mach Number. The reduced expansion-recompression process corresponds to an increase in base pressure, which is to be expected since the critical point defines a unique base pressure.

4.3.2 Critical Point Explanation for Wake Closure

Crocco and Lees (36) demonstrated that the properties of the flow at the critical point impose constraints that uniquely define the upstream flow. No such constraint exists downstream of the critical point, and the viscous far wake grows as a function of the laminar or turbulent mixing with inviscid flow. In the plug nozzle case however, the envelope shock imposes a pressure gradient on the wake outer edge, which affects the flow behind it. The effects of the envelope shock cannot be propagated upstream in the inviscid flow because of the hyperbolic nature of the flow, nor can it propagate forward in the viscous wake while it is downstream of the critical point, since the flow is supercritical.

The analytical characterization of the wake behavior at the point the envelope shock reaches the critical point requires a complex mathematical derivation which will not be pursued here. The components that must be addressed include are a bifurcation due to the pressure gradient imposed by the envelope shock, the singularity nature of the critical point, and the system of partial differential equations defining the wake that are elliptic in nature. The derivation would demonstrate that the divergence point cannot move upstream of the critical point, and then link the critical point changes to the upstream flow using Crocco and Lees' (36) uniqueness property. Instead, the physical behavior of the flow at the critical point is examined relative to wake closure using two approaches: 1) its saddle point characteristics and 2) its 2-D viscous throat qualities.

Saddle Point Characteristics. Lees and Reeves (37) describe the wake critical point as a saddle point. Figure 4.12 illustrates a saddle point in the domain of real numbers. Each line (or path) represents a set of solutions to the integration of Equations (12)-(14). The saddle point has a finite number of paths approaching the critical point and a finite number of paths departing the critical point. A logic argument is made that the finite number is either one or more than one. If the finite number is more than one (e.g., 2, 3, 4, etc.), there is no constraint to determine that a given number of paths has preference over another (i.e., 2 versus 3), and so, the number of paths could be infinite. However, the number must be finite from the definition of a saddle point. Therefore, the only way to have a finite number of incoming and outgoing paths is when that number is one. Crocco and Lees (36) found this result numerically by determining that only one set of upstream conditions allows the integrated solution to pass through the critical point and represent a physically real wake.

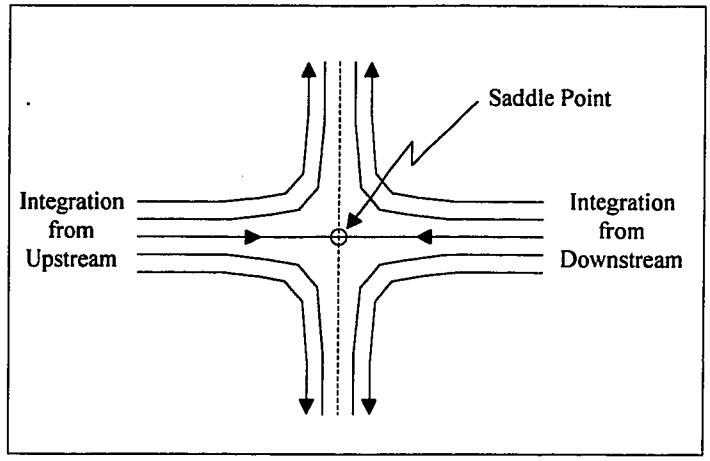

Figure 4.12: Example of Saddle Point Behavior

The integration of equations (12)-(14) determines the distribution of the parameters M_e, a(x), and δ^* that characterize the flow development through the critical point. For adiabatic wake flow, equation (18) is used to locate the critical point singularity by setting D=0. The equation reduces to a function of M_e and a(x) (note: a(x) represents the velocity profile at x, rather than being a

function of x). M_e is directly related to the inviscid flow pressure distribution and determines the angle of inclination of the viscous flow outer edge through the isentropic Prandtl-Meyer relation:

$$\Theta_e = \upsilon(M_\infty) + \Theta_\infty - \upsilon(M_e)$$

where $$\upsilon(M) = \left(\frac{\gamma+1}{\gamma-1}\right)^{1/2} \tan^{-1}\left[\left(\frac{\gamma-1}{\gamma+1}\right)^{1/2}(M^2-1)^{1/2}\right] - \tan^{-1}\left[(M^2-1)^{1/2}\right]$$

Kennedy (60) originally computed the Stewartson similar solutions (Figure 4.13) to the wake problem from Cohen and Reshotko's compressible boundary layer equations. The parameter a(x) formulated by Tani (61) represents a subset of these velocity profiles as a function of the pressure gradient along the wake. The a(x) parameter is a single parameter used in a polynomial function to approximate the velocity profiles. The cubic and quartic polynomial functions used by Ai (45) and Webb, et. al., (39) are also plotted in Figure 4.13 for comparison.

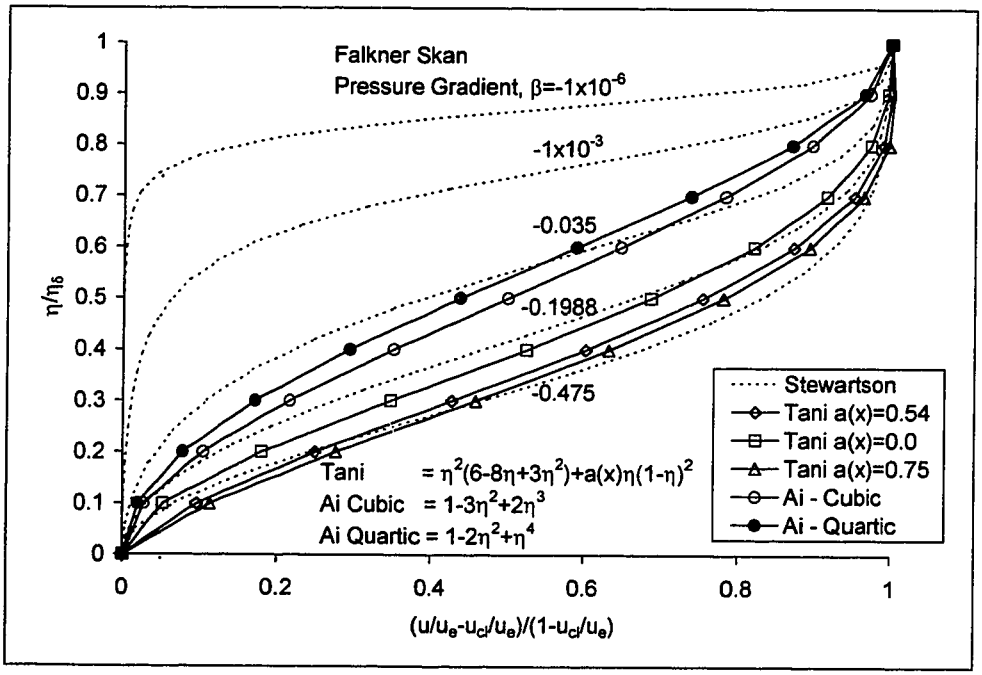

Figure 4.13: Self-Similar Wake Velocity Profiles

The original a(x) parameter represents boundary layer flows under adverse pressure gradients, and is defined with a no-slip wall (i.e., u(x,y=0)=0). When used to approximate the wake solution, these velocity profiles are modified in two respects. First, the left-hand side of equation (19) changes from u/u_e to $(u/u_e-u_{cl}/u_e)/(1-u_{cl}/u_e)$ to change the boundary condition from a no-slip wall to a no-shear condition along the centerline.

$$\frac{u}{u_e} = \eta^2\left(6-8\eta+3\eta^2\right)+a(x)\eta(1-\eta^2) \tag{19}$$

$$\frac{(u/u_e-u_{cl}/u_e)}{\left(1-u_{cl}/u_e\right)} = \eta^2\left(6-8\eta+3\eta^2\right)+a(x)\eta(1-\eta^2) \tag{20}$$

Secondly, a(x) is defined relative to the DSL, centerline velocity, and outer edge velocity in Table 2.3. Therefore, a(x) occurs on both sides of the equation (21).

$$\frac{(u/u_e-a(x))}{\left(1-a(x)\right)} = \eta^2\left(6-8\eta+3\eta^2\right)+a(x)\eta(1-\eta^2) \tag{21}$$

The parameter a(x) varies between a(x)=0 at the RSP to an asymptote value of a(x)=0.75 far downstream of the wake. In the region downstream of the RSP, the pressure gradient, dp_e/dx, is positive and decreases monotonically to zero in the downstream direction. Equation (21) relates the pressure gradient, velocity profile, and centerline velocity for a specified M_e.

The parameter a(x) is plotted versus M_e for a range of plug nozzle NPR in Figure 4.14 from the CFD solution. The a(x) parameter increases monotonically at design conditions (NPR=76) from the RSP where a(x)=0 to some downstream location. Plots of the other closed wake conditions (NPR=25 and 16) follow this curve up to the location where the envelope shock influences the wake. The envelope shock pressure gradient causes a decrease in both a(x) and M_e as indicated by the sharp downward inflection of the closed wake curves.

Downstream of the pressure gradient, a(x) and M_e continue to increase, but not as rapidly as the wake without the envelope shock.

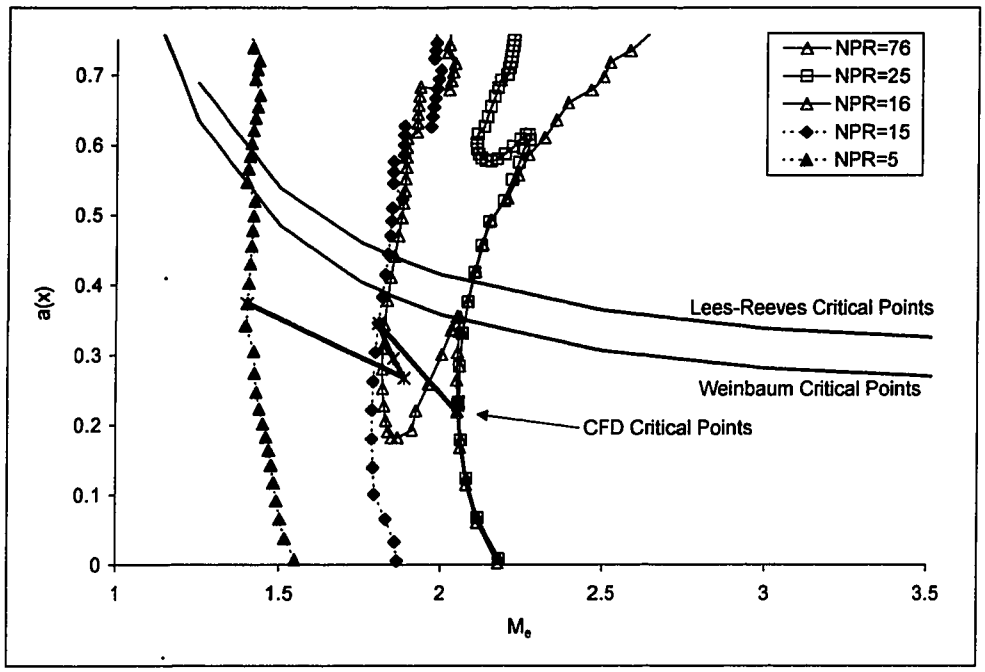

Figure 4.14: Critical Point a(x)-M_e and Plug Nozzle Traces

The pressure gradient of the envelope shock moves upstream along the closed wake curves (NPR=16-76) until it reaches the location of the critical point. The pressure gradient causes a change in the properties at that location, and the critical point itself is changed in its flow properties and location. Once the critical point changes, the saddle point behavior of the critical point dictate a new upstream integration path leading to the critical point (indicated by NPR=15 and 5 curves).

The movement of the critical point follows the bold line that connects the critical points from the CFD solution for each NPR condition. This line represents the locus of possible critical points for the plug nozzle wake. The locus of points is related to the $a(x)_{cr}$ versus $M_{e,cr}$ curve determined by Lees and Reeves (38) in their analytical derivation of the critical point using the boundary

layer equations (where D=0 in equation(18)). A comparable curve is computed from Weinbaum's critical point criterion (43) using a 2-D viscous throat analogy (described later in this section). This form retains the tranverse pressure gradient in the y-momentum equation, and as a result, is offset downward from Lees and Reeves curve. The offset of the CFD solution is due to inaccuracies in the modeling of the wake flow and solution convergence (See Appendix C). The sharp "kink" in CFD locus of critical points (NPR=10-16) may a mathematical artifact of computing gradients in the proximity of the critical point singularity. Ideally, the locus of CFD-based critical points would be identical to one of the analytical curves.

The values of a(x) and M_e at the critical point for the closed wake solutions are limiting values of $a(x)_{cr}$ and $M_{e,cr}$ for the specified nozzle geometry. In other words, changes in NPR due to the jet or ambient conditions will always result in $a(x)_{cr}$ and $M_{e,cr}$ values greater than these closed wake values. As a result, the wake closure NPR should be uniquely dependent on nozzle geometry and the type of gas (which determines γ in equation (11)). Moreover, there is a one-to-one relationship between $a(x)_{cr}$ and $M_{e,cr}$ (depending on the assumptions or method used - i.e., Lees and Reeves, Weinbaum, CFD). So variations in nozzle geometry and gas type will shift the closed wake critical point along the computed locus, but all values of $a(x)_{cr}$ and $M_{e,cr}$ will remain on this locus.

2-D Viscous Throat Qualities. The 2-D viscous throat analogy of the wake developed by Weinbaum offers another means for describing the wake closure-critical point relationship. Weinbaum (43) models the wake region near the critical point as a streamtube (or many streamtubes) in which the boundaries are impressed upon by the external flow through viscous interaction. From 1-D inviscid flow, the area change in nozzle flow is a function of Mach Number and static pressure by the relation

$$\frac{(M^2-1)}{\gamma p M^2}\frac{dp}{dx}=-\frac{1}{A}\frac{dA}{dx}$$

This area rule relation contains a singularity at M=1, which is the minimum area station in nozzle flow, and dP/dx is bounded only if dA/dx=0 simultaneously. The critical point for this flow is defined as the station where a change in pressure gradient has not effect on the area ratio.

To apply this concept to wake flows, Weinbaum begins with the continuity, momentum, and energy equations:

$$\frac{\partial}{\partial x}(\rho u)+\frac{\partial}{\partial y}(\rho v)=0$$

$$\rho u\frac{\partial u}{\partial x}+\rho v\frac{\partial u}{\partial y}=-\frac{1}{\gamma M_\infty^2}\frac{dp}{dx}+\frac{1}{\mathrm{Re}_{\infty,L}}\frac{\partial}{\partial y}\left(\mu\frac{\partial u}{\partial y}\right)$$

$$\rho u\frac{\partial h}{\partial x}+\rho v\frac{\partial h}{\partial y}=\left(\frac{\gamma-1}{\gamma}\right)u\frac{dp}{dx}+\frac{1}{\mathrm{Re}_{\infty,L}\,\mathrm{Pr}}\frac{\partial}{\partial y}\left(\mu\frac{\partial h}{\partial y}\right)+\frac{(\gamma-1)}{\mathrm{Re}_{\infty,L}}M_\infty^2\mu\left(\frac{\partial u}{\partial y}\right)^2$$

But rather than using boundary layer equations assumption that dP/dy=0, y-momentum equation in the form is retained in the form:

$$\rho u\frac{\partial v}{\partial x}=-\left(\frac{1}{\gamma M^2}\right)u\frac{\partial p}{\partial y}-\rho v\frac{\partial v}{\partial y}$$

The equations are then solved in terms of the pressure gradient term, dp_e/dx, leading to:

$$\frac{dp_e}{dx}\int_0^\delta\frac{M^2-1}{\gamma p_e M^2}dy=-\left(\tan\Theta_e+\frac{1}{p_e\,\mathrm{Re}_{\infty,L}}\int_0^\delta\frac{h}{u}\left[\frac{(\mu u_y)_y}{u}-\frac{1}{\mathrm{Pr}}\frac{(\mu h_y)_y}{h}-(\gamma-1)M_\infty^2\frac{\mu u_y^2}{h}\right]dy\right)\quad(22)$$

In this equation, the flow deflection, Θ_e, is determined by an inviscid component associated with dP_e/dx and a viscous contribution related to Reynolds Number. Returning to the nozzle throat analogy, the critical point for a wake is located at the point where the pressure gradient produces no change in the flow inclination of the streamline at the outer edge of the shear layer, or in other words

$$\int_0^{\delta} \frac{M^2 - 1}{M^2} dy = 0 \qquad (23)$$

This criterion for determining the location of the critical point is much simpler in form than the Equation (18) and at the same time avoids many of the questionable mathematical assumptions inherent in the previous IVI Methods. Since the near wake flow along the centerline is subsonic, this form emphasizes that there is some minimum (or conversely maximum) distribution of subsonic and supersonic flow within the velocity profile that allows the integral to attain zero (i.e., the "mean" flow is sonic, in IVI Method terminology). The plot of Equation (23) in Figure 4.15 shows the initially subcritical flow tend toward zero where the critical point is reached. The flow downstream of the critical point is then supercritical. The critical point locations were comparable to the Lees-Reeves derived stations, as were the downstream and then upstream shifts once the wake opened.

Weinbaum (46) also evaluates the pressure gradient in Equation (22) and found that the 2-D viscous throat had a finite length only when the x-derivative of the critical point integral (left-hand side of equation (23) was zero. In the transition between NPR=16 and NPR=15, the critical point integral shown in Figure 4.15 has a downstream inflection so that the x-derivative is no longer zero. This transition represents the effect of the co-location of the envelope shock pressure gradient and the critical point singularity, and suggests a discontinuous mathematical behavior.

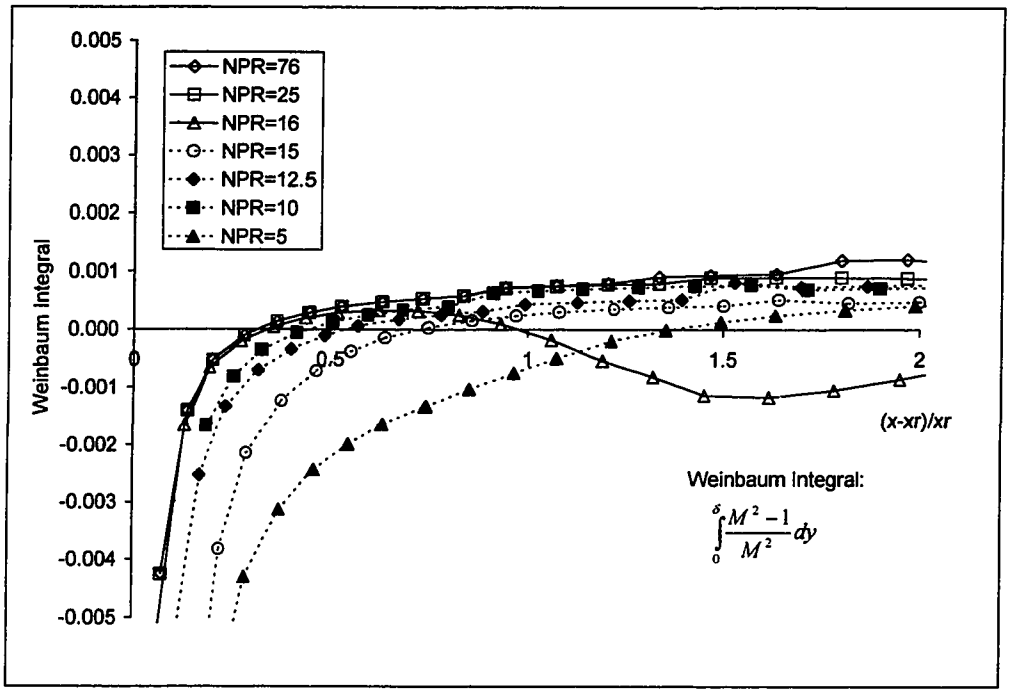

Figure 4.15: Weinbaum's Critical Point for Plug Nozzle Flow Development

Closer examination of Equation (22) explains the changes occurring to the critical point. The envelope shock imposes a positive pressure gradient on the outer edge of the viscous wake and decreases the M_e. As the envelope shock reaches the critical point, the integral term on the left-hand side decreases from zero to a value on some lower M_e curve on Figure 4.16. In doing so, the envelope shock forces the flow from critical to subcritical state, and as a result a continuation of the flow eventually has to pass through a new downstream critical point.

At the closed wake critical point location, the pressure gradient is positive since the flow is still undergoing recompression, so the entire left-hand side of equation (22) is negative once the envelope shock reaches this location. (Note: the critical point appears to move simultaneously as the envelope shock reaches the closed wake critical point location, so the envelope shock and critical point do not occupy the same position – See Figure 4.11).

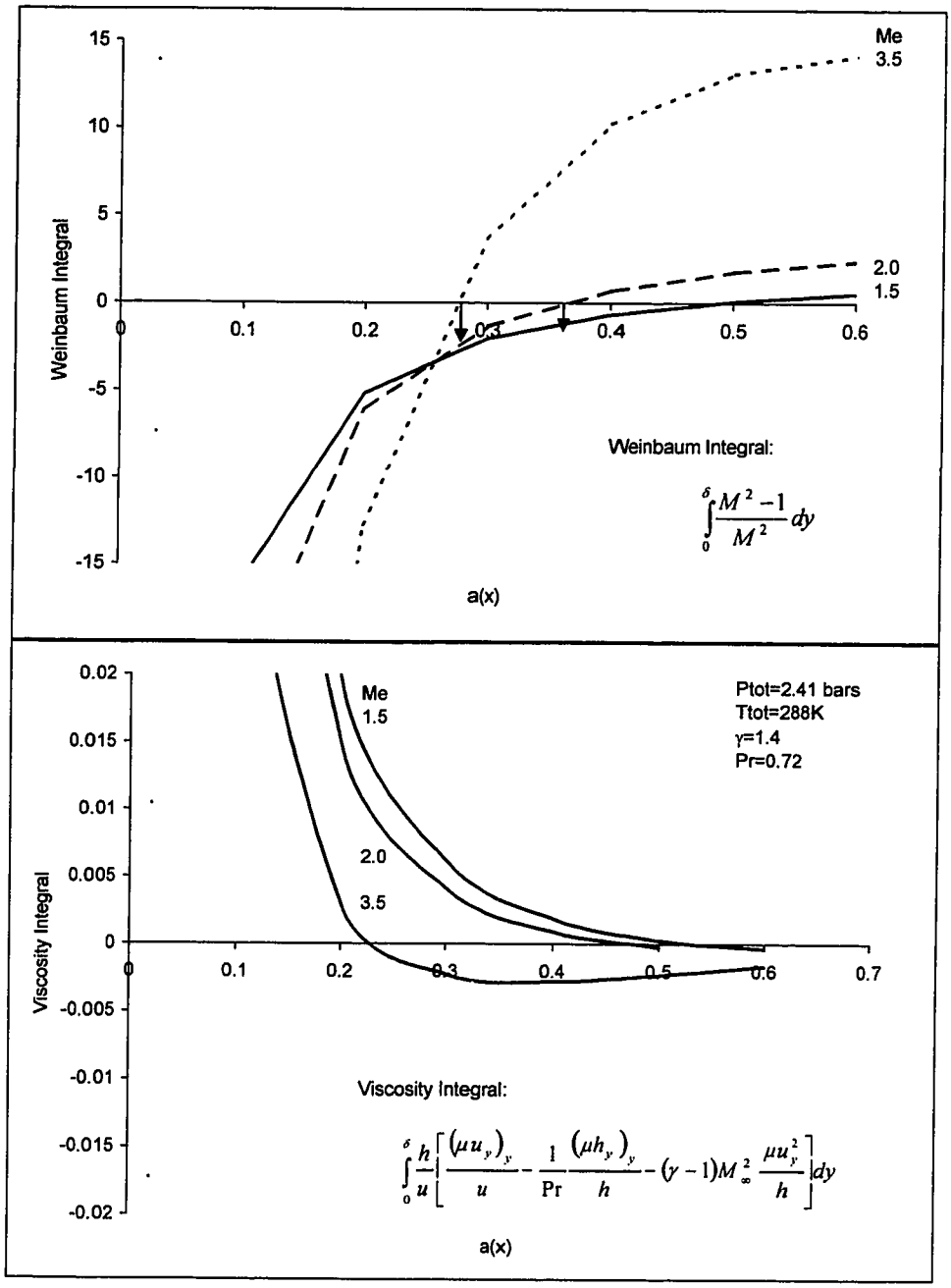

Figure 4.16: Behavior of 2-D Viscous Throat Terms

The right hand side of Equation (22) must also decrease in the negative direction. In order for the right-hand side to increase in the negative direction, the terms inside the parentheses must increase positively. Since the flow is still upstream of the wake neck, the edge flow inclination is negative, so it can only

contribute to the positive increase of the parenthetical term by decreasing toward zero. The edge inclination angle is nearly zero downstream of RSP, so the amount that this term can contribute to the decrease is limited.

In the remaining term, the edge pressure increases due to the shock and Reynolds Number is constant. The viscous integral term is plotted in the second frame of Figure 4.16. A portion of the pressure gradient is negotiated by the increase of the viscous integral inherent in the change in edge Mach Number. But beyond this, the integral term is increased by decreasing a(x). This decrease corresponds to the lower value of a(x) for the open wake curves at the same axial location (Figure 4.11).

For stations downstream of the critical point, several solutions can pass through a given a(x) by adjusting the divergence point location. But once the envelope shock reaches the closed wake critical point location, the pressure gradient forces the flow to be subcritical. Due to the critical point uniqueness property, the entire distribution of a(x) changes to pass through the decreased a(x) value as shown in Figure 4.11. Therefore, the supersonic wake methods completely describe the changes occurring in the wake as a result of wake closure.

4.3.3 Extension to Wall Separation Mode

Limited experimental and CFD data suggest that a similar explanation for wake closure can be applied to the wall separation mode. A common element that was found during the experimental effort for the envelope shock and wall separation modes is the impinging shock passing the reattachment region. In the wall separation mode, this shock is in the form of a normal shock between the wake and the freejet boundary. Such a shock has similar effect in imposing an external pressure gradient on the critical point, thereby causing the critical point to move and change properties. The major difference for the wall

separation mode is the separation of flow from the ramp surface as soon as wake closure occurs.

To understand this flow separation phenomenon, it is necessary to reexamine the shock structures present in each mode. The cross-section of flow properties in Figure 4.17 indicate that the envelope shock is primarily an oblique-type shock that changes Mach Number and static pressure, but there is actually relatively little total pressure loss across the shock. The strength of the shock changes with its curvature and thus the amount of flow turning relative to the ramp contour.

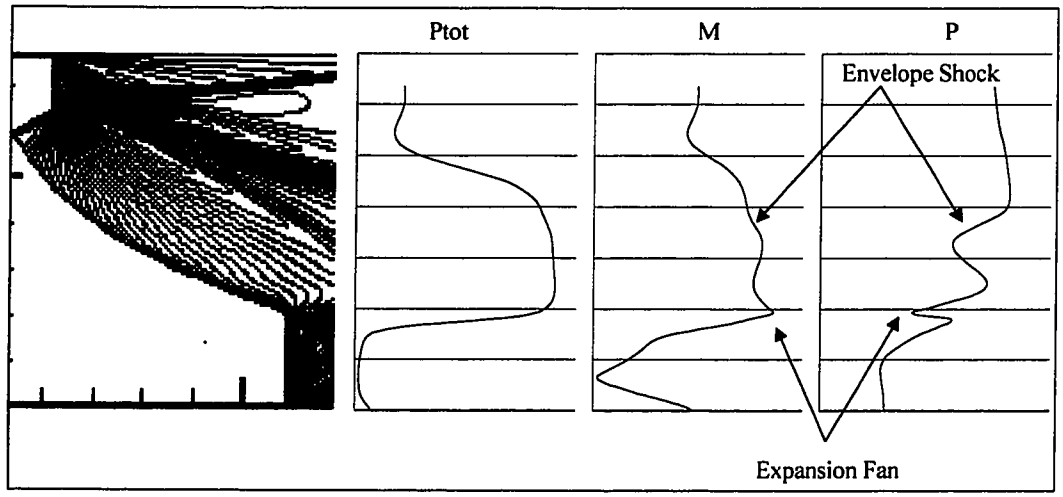

Figure 4.17: Cross-Section of Open Wake Profiles at x/h=0.46

Moving from the flow centerline outward, the first "nose" on the Mach Number profile indicating the expansion around the ramp corner. Just above this, the flow is slightly slower, since it has not reached the expansion fan but increases with transverse distance. Then the presence of the envelope shock reduces the Mach Number and eventually the Mach Number drops dramatically at the outer edge boundary. The static pressure profile accentuates the effect of the envelope shock in bringing the flow to ambient conditions. But the relative change caused by the envelope shock changes the flow depends on the amount

of expansion of gas in the inviscid flow as determined by the ambient environment.

The axial distribution of pressure in Figure 4.18 taken at a station above the ramp corner illustrates the effect of the envelope shock in raising the pressure back to ambient conditions. The x/h=0 station is located at the base plane. The shock becomes stronger as it moves forward in order to accommodate the higher ambient pressures. In general, however, the more significant pressure recovery is accomplished by the recompression shock.

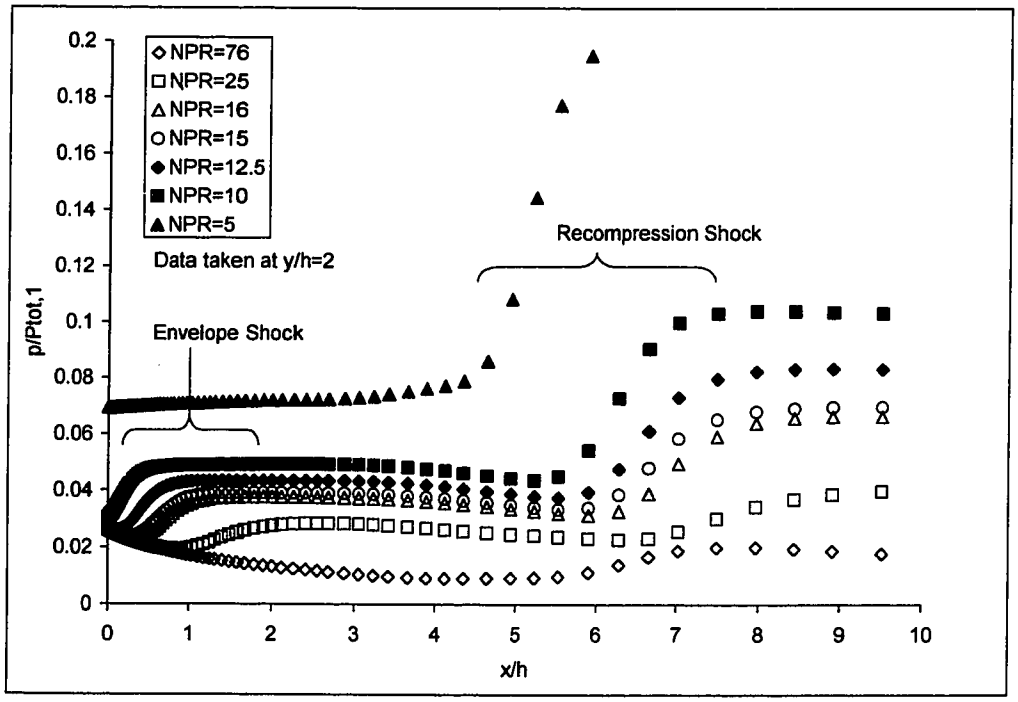

Figure 4.18: Axial Distribution of Static Pressure in Inviscid Flowfield

The NPR=5 curve indicates that there is a compression, or reduced expansion, of the flow prior to reaching the ramp corner under that NPR condition. It can thus be said that the envelope shock is a relatively weak shock that allows the gradual shift of the critical point corresponding to the decrease in NPR.

In contrast, the shock formed between the recompression shock and free jet boundary in the wall separation mode is a normal shock that results in a total pressure loss and a strong pressure gradient. The occurrence of the normal shock is attributed to two factors. First, the planar shape of the ramp creates a much different characteristic line pattern from a contoured ramp. Figure 4.19 shows the Mach isolines (indicative of the characteristic lines) for a planar M=4.0 nozzle of 25% length. The characteristic lines of the planar ramp are relatively normal to the nozzle axis, and therefore more are likely to form a normal shock in the presence of an adverse pressure gradient. (Note that when the planar nozzle was modeled with a slipstream, an envelope shock developed and the mode of wake closure followed the same pattern as the contoured nozzles, so the velocity of the external environment is critical for this mode.)

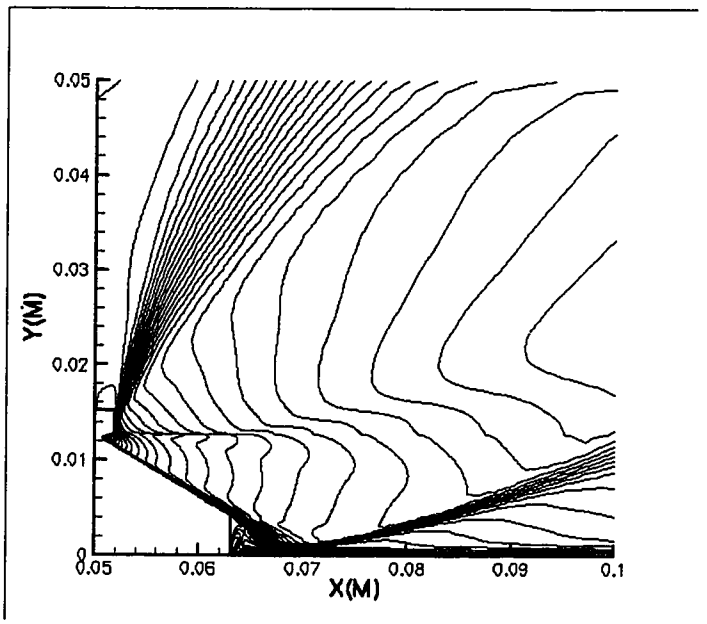

Figure 4.19: Example Planar Ramp Mach Isolines

In general, the magnitude of the pressure gradient is not important for the envelope shock mode. Instead, the imposition of the pressure gradient on the boundary conditions by itself causes the divergence of flow properties from the design or closed wake distributions. At strong enough pressure gradients, the

entire structure of the wake change dramatically, i.e., the NPR=5 case. The pressure gradients associated with the normal shock are clearly stronger than those of the envelope shock. As a result, it is likely that the normal shock causes the critical point to "jump" immediately to a far downstream location and at the same time produce a base pressure which leads to a compression shock at the ramp corner. As the NPR continues to decrease, the base pressure moves the shock up along the ramp and flow separation from the wall.

4.3.4 Comments on the Effects of Turbulence

For most rocket nozzle applications, the near wake mixing region and far wake flow are likely to be turbulent rather than laminar. As discussed in Chapter 2, additional research is required to accurately model the turbulence through CFD.

For the purposes of this research, the effects of turbulence on wake closure are briefly investigated. The C35-10-25 nozzle is simulated with the same grid used for the laminar solutions. (Note that a more complete analysis of turbulence would require reevaluation of the grid itself.) The k-ε model provided by INCA is employed with turbulent flow specified for all zones. The turbulence model constants are left at the INCA default values, i.e., $C_{\varepsilon 1}$=1.44, $C_{\varepsilon 2}$=1.92, C_{μ}=0.09, σ_k=1.0, and σ_{ε}=1.3. The turbulent kinetic energy is set at 1.0 and kinetic energy dissipation rate at 5,000. The simulation is conducted for NPR=15 and 76 to determine qualitatively the effects on the overall flow and wake closure.

The CFD solutions show that the turbulence creates a higher base pressure and pushes the RSP downstream. These results agree with predicted trends usually associated with turbulence. The critical points in Figure 4.20 for both NPR=15 cases are downstream of the NPR=76 solutions. However, while the turbulent

NPR=76 critical point moves significantly downstream of the comparable laminar point, the NPR=15 critical points are in close proximity to each other.

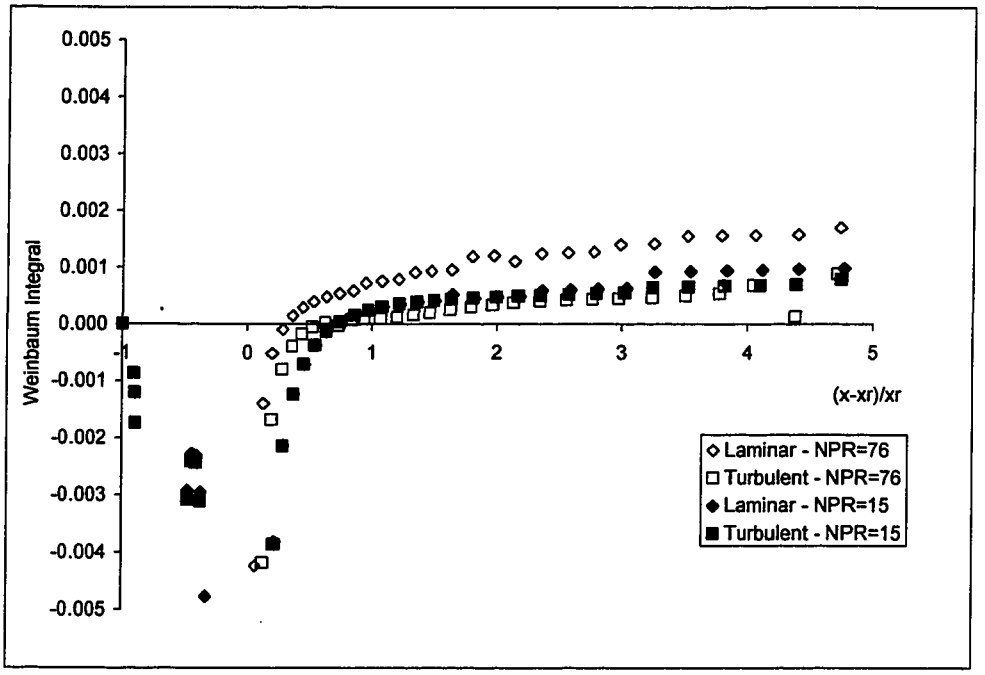

Figure 4.20: Comparison of Laminar and Turbulent Critical Points

Further tests should be conducted to more accurately determine the point of wake closure. These cursory results suggest that wake closure occurs for the turbulent flow at a lower NPR than the laminar flow, which is expected given the changes to base pressure. This brief examination of the critical point demonstrates that the fundamental application of the analytical methods is still valid.

4.3.5 Physical Interpretation

The physical interpretation of the critical point change is most easily described using the 2-D viscous throat analogy. The movement of the divergence point upstream due to envelope shock or downstream conditions is similar to the increase of back pressure in a supersonic nozzle. However, instead of becoming

unchoked and subsonic when the back pressure pushes the shock to the nozzle throat, the wake critical point changes to a new set of conditions to accommodate the downstream distribution of parameters. The difference between the supersonic nozzle and the wake is the outer edge boundary condition. In nozzle flow, there is a rigid boundary condition so that v=0 at the boundary. But in the case of the wake flow, v-velocity is free to self-adjust so that the viscous and inviscid boundaries match. Once the critical point changes, the upstream distribution of analytical wake parameters must also change to allow the solution to pass through the critical point, thereby changing the base pressure.

This physical interpretation is compatible with the existing modes of wake closure. In the envelope shock mode, the compression waves in open wake conditions define the distribution of analytical wake parameters leading to the critical point. Compression waves move beyond the critical point, the upstream distribution of parameters no longer changes and does not affect the critical point. Thus, this physical interpretation provides more detail to the existing characterization of wake closure by making the critical point linkage. The hypothesis by Fick and Schmucker (19) that wake closure is governed by the same mechanism as the back pressure of a supersonic nozzle is partially correct, but is modified by the shift in critical point rather than unchoking of the flow.

4.4 Summary

In summary, wake closure can be physically interpreted in either of two ways. First, it can be considered the limiting case whereby the inviscid flow can affect the wake critical point. Alternatively, the wake closure is here defined as the limiting condition at which external gradients change critical properties and location. Once this limiting condition occurs, the critical point readjusts to accommodate the downstream conditions. These interpretations are essentially

equivalent, but view the problem from opposing perspectives. The former follows the conceptual development of the envelope shock mode explanation. The latter provides a common interpretation that addresses wake closure for both the envelope shock and wall separation modes.

Chapter 5
MISSION DESIGN APPLICATIONS

The final part of the research examines the issue of wake closure in the context of the plug nozzle engine design and performance. Recent system studies by Fick (62) conclude that additional thruster and turbomachinery mass and technical problems associated with the plug nozzle engine potentially outweigh its performance and reduced thrust structure advantages. Some of these trade issues will be resolved during the development and flight testing of the X-33. The investigation of the effect of the design factors on wake closure provides insight to support the evaluation of benefits and limitations of the plug nozzle performance. Some of the key issues addressed included:

- Relative importance of open wake versus closed wake performance,
- Relationship of base pressure and wake closure to performance,
- The effect of design factors on performance, and
- Whether the wake closure can be manipulated to improve performance.

This chapter describes the metrics for assessing plug nozzle performance and the DOE process for analyzing the effect of the design factors on wake closure and base pressure. The investigation results are presented in the context of design decisions that can improve performance.

5.1 Investigation Approach

Although a comprehensive systems trade study is necessary to optimize the design factors for a given mission, some basic performance relationships can be examined to illustrate the contribution of the wake closure design factors to

performance. An example launch ascent trajectory is computed to put into context the range of operations generally corresponding to open and closed wake conditions. Plug nozzle performance is then quantified for its individual components to identify the relative significance of each for improvement efforts. A DOE process is applied to experimental results to isolate the effects of specific design factors to the different aspects of wake closure. Finally, these insights into the relationship between design factors and performance are used to provide examples of potential performance improvements.

5.2 Open and Closed Wake Flight Regimes

One of the key benefits of the plug nozzle is its performance under open wake conditions. From Section 1.1.2, one approach to increasing performance is to maximize the duration of open wake operations. Figure 5.1 shows the trajectory for a typical X-33-class vehicle to low earth orbit.

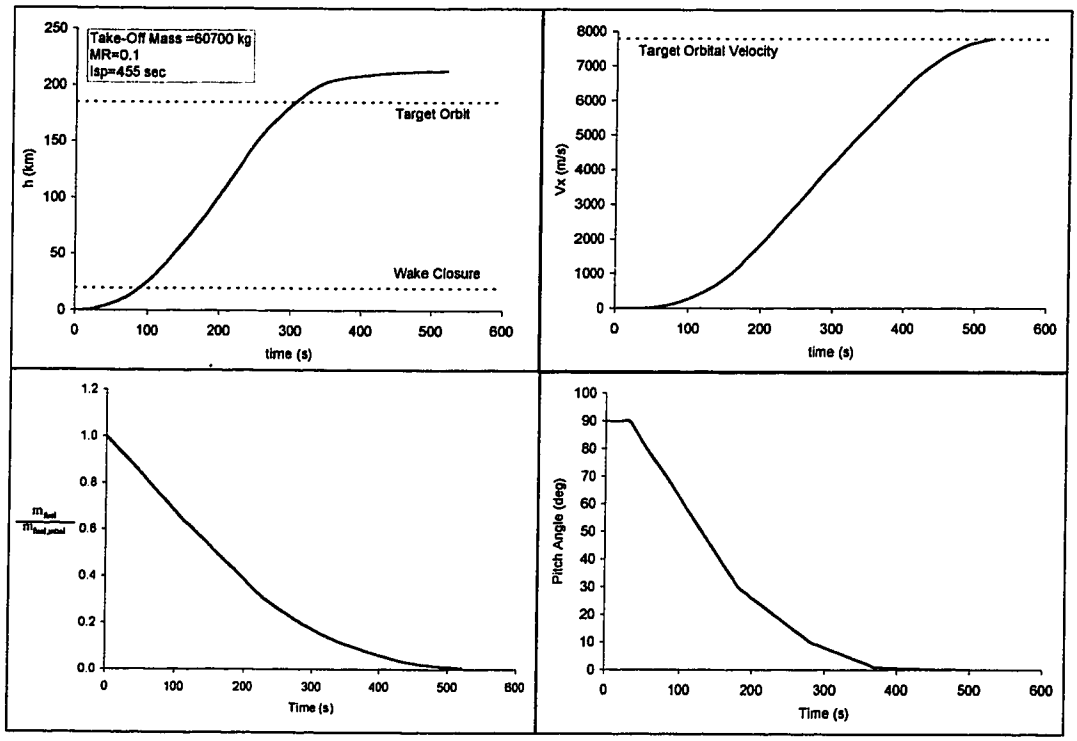

Figure 5.1: Example SSTO Trajectory

The pitch and thrust profiles are selected to achieve the target orbit and limit the vehicle acceleration to less than 3gs. During the first few kilometers of ascent, the vehicle pitch is mostly vertical, i.e., the thrust is lifting the vehicle. Thrust and fuel consumption are at maximum levels during the initial stages of launch. As the vehicle gains speed and altitude, the vehicle pitches toward the horizon to achieve orbital velocity. The thrust is reduced to maintain the acceleration limits and minimize fuel consumption.

A typical rocket engine for orbital launches may have a combustion chamber pressure of 1000 psia. Depending on the nozzle design Mach Number and propellant, wake closure may occur at NPR between 200-2000, which corresponds to altitudes 6-20 km. These altitudes represent a relatively small portion of the flight, and the thrust contributes a small percentage of the eventual orbital velocity. However, 30% of the fuel is expended at this early stage of launch.

As a result, fuel (or thrust) efficiency is a significant concern for all phases of flight. At the low altitudes, thrust efficiency is important for reducing fuel consumption, whereas thrust efficiency is critical to achieving orbital velocities at the higher altitudes.

5.3 Performance Contributions

A preliminary understanding of the impact of plug nozzle design decisions on performance can be developed by examining the thrust equation below. The net thrust, F, for a typical bell nozzle rocket engine is derived from the momentum equation in the x-direction and consists of a momentum component and a pressure component. Expanding the flow to the design conditions so that the exit pressure equals the ambient pressure maximizes the thrust.

$$F = \dot{m}V_{exit} + (p_{exit} - p_{\infty})A_{exit} = C_F A_t p_{exit}$$

From this equation, the nozzle efficiency is the amount of thrust produced for a given set of total (or combustion chamber) gas conditions or thrust coefficient, as given by Equation (21):

$$C_F = \sqrt{\frac{2\gamma^2}{(\gamma-1)}\left(\frac{2}{\gamma+1}\right)^{\gamma+1/\gamma-1}\left[1-\left(\frac{p_{exit}}{p_{tot}}\right)^{\gamma-1/\gamma}\right]} + \left(\frac{p_{exit}-p_{\infty}}{p_{tot}}\right)\left(\frac{A_{exit}}{A_t}\right) \qquad (21)$$

where
- $\dot{m}$ = mass flow rate
- V_{exit} = velocity at nozzle exit
- p_{exit} = static pressure at nozzle exit
- p_{∞} = static pressure of ambient environment
- P_{tot} = chamber or total pressure
- A_{exit} = cross-sectional area at nozzle exit
- A_t = cross-sectional area at nozzle throat
- C_F = thrust coefficient

Equation (21) can be used to compare the thrust coefficients for a vehicle with a bell or full-length aerospike nozzle as it passes through a range of altitudes (or NPR). To compute the thrust coefficient for a bell nozzle, one specifies the thrust chamber total pressure and the exit plane area ratio. For the purposes of simple comparison, the aerospike nozzle thrust coefficient is computed in two parts. First, the momentum component of Equation (21) computed similar to the bell nozzle. Second, the exit and ambient pressures however are set equal to one another once the wake opens.

The resulting thrust coefficients for the bell and aerospike nozzles are plotted in Figure 5.2 as a function of NPR. The variable expansion curve represents the optimum thrust coefficient for all NPR. The bell nozzle (without flow separation)

has an its optimum at the design altitude/pressure conditions, which is corresponds to the selected exit plane area ratio. As seen in the figure, there is a performance trade-off in the area ratio selection. If the area ratio is small, near optimal efficiencies can be achieved at lower altitudes, but the nozzle will have low efficiency at the higher altitudes. On the other hand, a large area ratio will have lower efficiencies at the low altitudes in order to achieve the higher efficiencies later in the flight. The larger area ratios also result in greater weight, so the designer must balance the advantages and disadvantages of these factors.

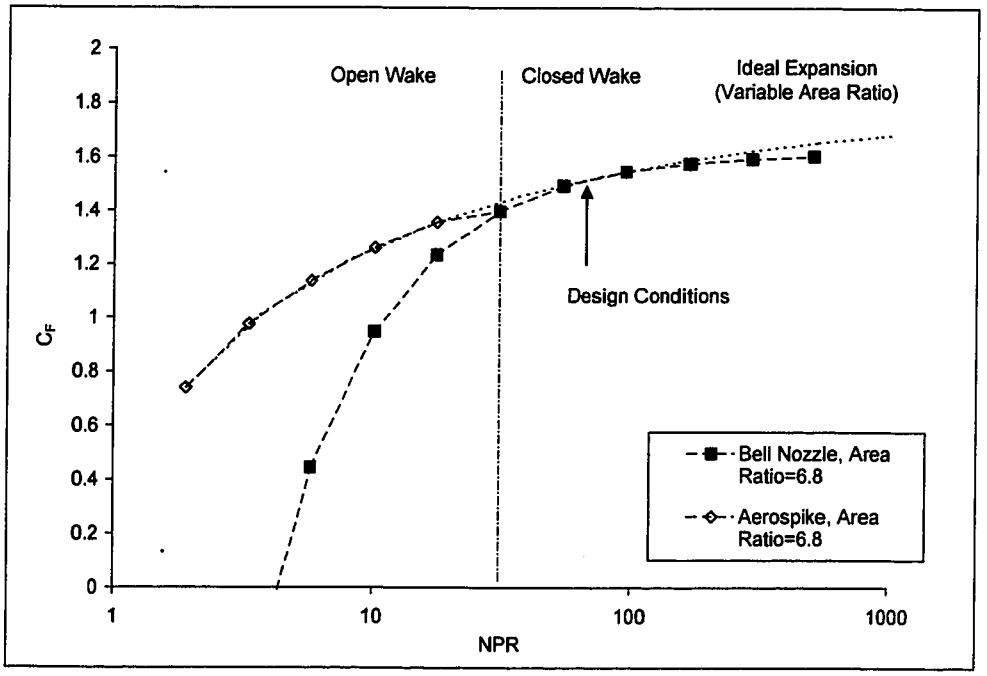

Figure 5.2: Conceptual Example of Open Wake Improvement

For altitudes or NPR above the design conditions, the aerospike nozzle is also constrained by the nozzle expansion limits similar to the bell nozzle. Once the wake opens, the pressures along the ramp and base are nearly equal to ambient pressures and the thrust coefficient follows the ideal expansion curve. Since the aerospike nozzle is not penalized at the lower altitudes and the size can be truncated, a higher design Mach Number and wake closure NPR are desirable.

The optimization of thrust for the plug nozzle is complicated by the different components that contribute to the overall thrust. Since the surfaces over which the propelled gases are different from that of the bell nozzle, the thrust equation must be reformulated in the form:

$$F = F_{thruster} + F_{ramp} + F_{base} \tag{22}$$

where $F_{thruster} = \cos\theta\left(\dot{m}V_{exit} + A_{exit}\left(p_{exit} - p_{\infty}\right)\right)$

$$F_{ramp} = \int_{A_{ramp}} \left(p_{ramp} - p_{\infty}\right) dA$$

$$F_{base} = A_{base}\left(p_{base} - p_{\infty}\right)$$

Nozzle losses must also be incorporated into these computations. Such losses include those due to boundary layer shear/drag along the ramp surface, kinetic losses, inclination of the flow at the thruster exit, and only partial recovery of thrust at the base which could have been produced by extension of the truncated plug. These factors are discussed further by other research efforts and will not be examined here.

To understand the thrust contributors in the context of open versus closed wake performance, the C35-10-25 nozzle are plotted as a function of NPR in Figure 5.3 using the CFD solutions from Chapter 4. The thrusters and ramp surface are typically the primary sources of thrust. The thruster contribution remains relatively constant depending on the amount of gas expansion prior to exiting the thrusters. The base pressure and ramp surface contributions increase with higher NPR, due to the difference between the expanded gas pressure and ambient pressure. Note however, these two contributors drop off rapidly as NPR decreases, and base pressure is shown to have a negative contribution to thrust until nearly design NPR conditions.

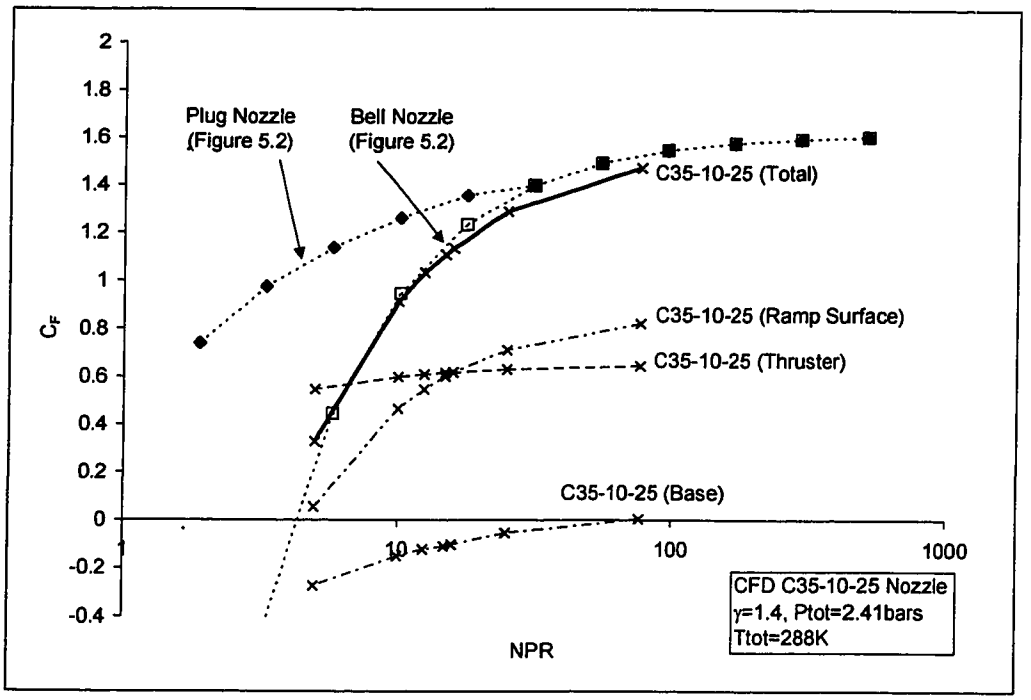

Figure 5.3: Effect of NPR on Thrust Coefficient

The resulting total thrust coefficient from the CFD solutions appears to be inconsistent with plug nozzle curve in Figure 5.2. Specifically, the CFD solution follows a similar trend as the bell nozzle without altitude compensation and does not have the expected open wake performance improvement. The Figure 5.2 thrust coefficients are generally higher than the CFD solutions at the higher NPR due to integration artifacts, but there is an additional consideration at lower NPR.

The surface pressures on the C35-10-25 nozzle ramp are examined more closely. The surface pressures decrease monotonically from the nozzle throat to the ramp corner due to the gas expansion. There was a slight increase in pressure toward end of the ramp, but the process that maintains the surface pressure above ambient pressure is not present. Only at NPR=5 is there a significant pressure increase due to flow separation at the ramp tip. Consequently the sub-ambient surface pressures decrease the ramp surface contribution to thrust coefficient. The experimental data confirms that the

expansion/compression process occurs only at very low NPR for this nozzle length.

A more defined expansion/compression pattern is seen on the longer C35-10-50 nozzle in Figure 3.8. The patterns however appear at the same NPR as the shorter nozzle and begin just downstream of the location where the envelope shock impinges the ramp surface. In other words, the both flows are identical for x/L_{max}=0-25%, and the additional expansion/compression pattern on the C35-10-50 occurs on the added length from x/L_{max}=25-50%. The extended length therefore has three thrust advantages. First, the longer nozzle has a smaller base area subjected to the lower base pressure. Second, the additional length results in greater ramp surface area shifting the thrust contribution from the base to the ramp. Finally, the expansion/compression pattern increases the pressure along the ramp surface.

Further examination is necessary of the mechanism that forces the surface pressures to remain above ambient. Section 2.2 already described the differing views on the role of flow separation on plug nozzle performance. The flow separation from the wall (which corresponds to the "significant" structural change in the wake found in Chapter 4) may be a more effective means for maintaining above ambient surface pressures, but has the same disadvantages as the bell nozzle from an efficiency standpoint.

The base pressure component was also examined further. Although the CFD data had sub-ambient base pressures and consequently negative thrust contributions, the experimental data in Chapter 3 indicate that the open wake base pressure could be above or below ambient pressure depending on the test conditions. In Figure 4.4, the difference between base pressure taken at the axis and ambient pressure decreases with NPR. The increasingly negative thrust coefficient contribution by base pressure in Figure 5.3 suggests that the pressure variations along the base become more critical at low NPR.

Further analyses should be conducted to better understand the detailed intricacies of performance optimization, but the above discussion begins to illustrate some of the considerations for incorporating wake closure into the design process. Specifically, the utilization of wake closure to improve nozzle performance can be approach from the following perspectives:

- Higher wake closure NPR is desirable,
- Thrusters and ramp surface pressure are more critical than base pressure in contributing to thrust,
- Shortened nozzle lengths may not benefit from the self-adapting gas expansion characteristics of plug nozzles except at very low NPR, and
- Base pressure should be increased, but without detracting from thruster and ramp surface thrust contributions.

5.4 Design Factor Analysis

The analysis of design factors apply the DOE process to the experimental data in order to quantify the effect of design Mach Number, nozzle size and shape on wake closure.

5.4.1 Design of Experiment Process

The DOE process is used to analyze the relationship between design factors and wake closure. The DOE process is a disciplined methodology for analyzing complex systems: DOE is typically in the quality control setting, but there is growing application to the design process. In the aerospace environment, DOE has been applied to such designs processes as High Speed Civil Transport, space launch and fighter jet propulsion systems (63, 64, 65). The advantages of DOE are improved performance characterization, reduced resource requirements, and reduced schedule requirements. As discussed earlier, wake closure prediction and the effect on rocket performance involve many

interrelated factors. For the purpose of the type of research conducted here, DOE reduces the number of tests required to characterize a system and provides a methodical approach for analyzing the effect of individual factors as well as combinations of factors simultaneously.

The DOE process begins with the identification of system inputs, the input settings, and the output measurements. Every system has a certain number of inputs (e.g., pressure, temperature, velocity, and gas type/molecular weight) and settings for each input (e.g., pressure=1 bar, 5 bar, 10 bar). Each input, or factor, has its own effect on the output of the system, but it also "interacts" with the other inputs to result in a combined effect. For a system with four inputs of three settings each, a Full Factorial Design represents the largest test matrix in which the number of different permutations of the three different settings taken four (i.e., all the inputs must be set) at a time with repetitions. In other words, all factors and all interactions are tested, leading to a total number of tests given by 3^4 or 81 tests (note: the number of permutations of n different things taken all at a time is n!).

Other designs such as Fractional Factorial, Foldover Designs, Plackett-Burman Designs, Box-Behnken Designs, and Taguchi Designs, design the test matrix such that one can focus on just the primary factors or the primary factors and a selection of interactions. As a result, a Taguchi L_9 Design, for example, requires only 9 tests of the above system to analyze the effect of the four primary inputs, or an L_{18} Design of 18 tests can analyze the four primary inputs and four interactions (e.g., pressure-velocity or pressure-velocity-gas type). Details about the design of test matrices are discussed by Schmidt/Launsby (66).

Once the test matrix is selected, the output measurements must be determined. The DOE process is structured so that several measurements can be taken and analyzed simultaneously, i.e., the same data set is used to analyze all of the

outputs. Several tests of the same conditions can also be conducted to determine the statistical variance of the outputs. The test matrices discussed above are designed such that the inputs and combinations of inputs are orthogonal. In this form, each input or interaction can be analyzed mutually exclusive of the others, i.e., the input or interaction can be linked to an effect on the output, independent of the other inputs that are changing simultaneously. The products of the DOE process include Paretto Charts depicting the relative significance of a factor, graphical trend graphs, prediction equations, and statistical variance and confidence information for multiple test outputs.

5.4.2 Design Factors Analysis Approach

As a part of the wake closure conditions experiments, the test data are incorporated into the analysis of design factor impacts on wake closure. The purpose of this analysis is to determine how changes in the plug nozzle geometry affect the occurrence of wake closure. During this phase of the experimental analysis, the design factors evaluated include design Mach Number, jet height (or cowl lip height), ramp length, and ramp shape. Table 5.1 lists the design factor settings, test configurations, and conditions. Although the link between the factors and the outputs involve complex relationships, a simple linear relation with the two factor settings provides a qualitative trend.

Table 5.1: Design Factor Settings and Test Conditions

Factor	Code	Low Setting (-1)	High Setting (+1)
Design Mach	A	2.5	4.0
Cowl lip height (half height, in)	B	0.5	1
Ramp length (%)	C	25	50
Ramp Shape	D	Contour	Planar

Table 5.1: Design Factor Settings and Test Conditions - continued

Config No.	Design Mach	Cav. Step Height (in)	Length (%)	Ramp Shape
1	2.0	1.0	25	Contour
2	2.0	1.0	50	Planar
3	2.0	2.0	25	Contour
4	2.0	2.0	50	Planar
5	4.0	1.0	25	Planar
6	4.0	1.0	50	Contour
7	4.0	2.0	25	Planar
8	4.0	2.0	50	Contour

The data collected for this analysis include NPR of wake closure and closed wake p_{base}/P_{tot}. These measurements define the base pressure characteristic for the entire span of conditions. The results are then used in the quantitative DOE analysis to compute factor effects and assess the significance of changes in these design factors on wake closure.

5.4.3 Design Factors Analysis Results

Using a subset of the wake closure conditions data, a DOE matrix is developed to assess the design components of the plug nozzle. A Taguchi L_8 matrix is selected to examine the effects of four factors and several interactions. The configurations used for the analysis and the associated responses are presented in Table 5.2.

Table 5.2: Design Factors Analysis Data

Test Set	Design Mach	Jet Height (in)	Plug Length (%)	Ramp Shape	Closure NPR	Closed Wake p_{base}/P_{tot}
1	2.0	1.0	25	Contour	4.7	0.20
2	2.0	1.0	50	Planar	5.9	0.14
3	2.0	2.0	25	Contour	4.3	0.22
4	2.0	2.0	50	Planar	4.2	0.15
5	4.0	1.0	25	Planar	47.6	0.0094
6	4.0	1.0	50	Contour	60.1	0.011
7	4.0	2.0	25	Planar	60.2	0.012
8	4.0	2.0	50	Contour	95.8	0.0093

The average responses indicate the effect of each factor or interaction on the subject measurement. The average response is the average of the output measurements for each test with a factor at the setting in question. For example, the average response for the closure NPR with the design Mach Number at its high setting (i.e., M=4.0) is (47.6+60.1+60.2+95.8)/4=65.93. The average response for the closed wake p_{base}/P_{tot} with the jet height at its low setting (i.e., h=1.0 in) is (0.20+0.14+0.0094+0.011)/4=0.09.

The average responses are computed for each factor and several interactions, and shown in Figure 5.4. An increase in most all of the factor levels result in wake closure occurring at a higher NPR. This result is intuitive for the design Mach Number and plug length since the higher Mach Number flow at the ramp corner prior to separation leads to lower base pressures.

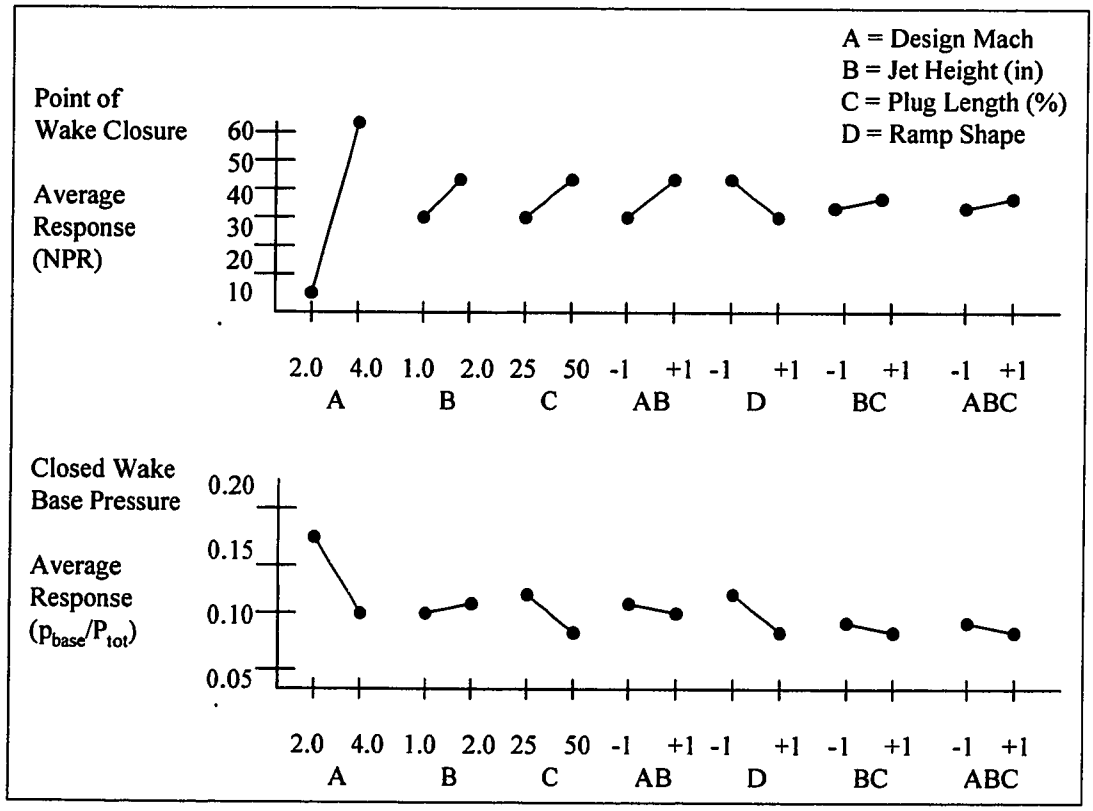

Figure 5.4: Average Effects on Wake Closure

Jet height (which represents the size of the nozzle) moderately increases base pressure, while at the same time increases the point of wake closure to a higher NPR. The size effect on the wake closure NPR may partially account for the significantly higher wake closure points (e.g., NPR=2000) found by Rocketdyne on their full-scale linear aerospike testbed (4). From the analytical wake models, the size of the base affects the base pressure through θ/h, and a higher θ/h increased base pressure. If this is the case, then the Reynolds Number and more specifically, the length of the plug (since the flow conditions were the same), as opposed to the actual height, may be the dominant feature affecting the flow interactions.

The truncation length itself increases the wake closure NPR, but also involves other changes to the flow such as the separation Mach Number. If one considers the ramp surface to be "pushing" the envelope shock away from the axis, then the longer length provides a greater obstacle to the envelope shock than a shorter length which relies on the base pressure to "push" the flow away. Clearly, additional examination of this effect is required.

The thrust components for an M=3.5, contoured nozzle are plotted as a function of plug length in Figure 5.5. The surface pressure data is computed for an isentropic expansion at design conditions and an average base pressure from Equation (3) is used to compute the base contribution. As the plug length is shortened, the base area increases and thus increases the contribution of thrust due to base pressure. However, the amount of thrust provided by the base pressure does not compensate for all of the thrust lost from the ramp surface. A truncation of the plug to 25-30% length does not significantly affect overall thrust coefficient. However, this conclusion must be considered relative to the ability for the nozzle to benefit from the self-adapting expansion discussed in Section 5.3.

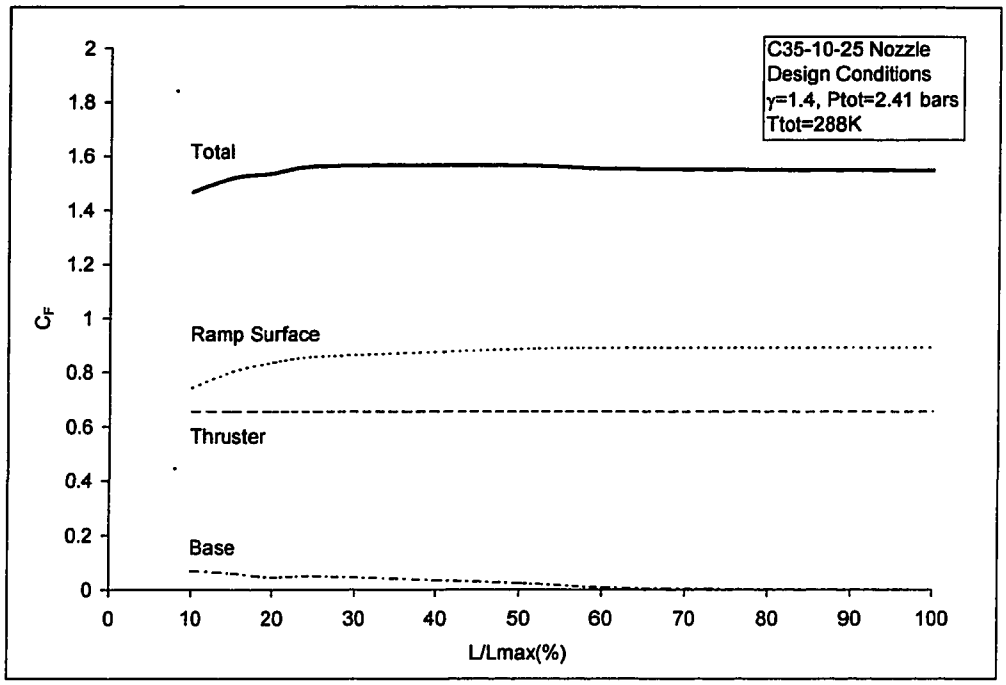

Figure 5.5: Thrust Coefficient Contributors versus Nozzle Length

A contoured ramp has a higher wake closure NPR and higher closed wake base pressure than a planar ramp. From supersonic wake experiences, a boat-tailed afterbody increases base pressure, since the inclined edge of the body reduces the amount of flow expansion. Since the planar ramp has a greater angle of incidence toward the axis at the corner, it was anticipated that it would result in a higher base pressure. However, a greater amount of expansion occurs on the planar ramp than the contoured ramp. The planar ramp separation Mach Number is significantly higher, thereby leading to lower base pressures. Since the expansion outward from the ramp surface also hinders the envelope shock from moving closer to the nozzle axis, requiring higher ambient pressures (or lower NPR) to open the wake. For the wall separation mode of wake closure, higher ambient pressures would be required to push the normal shock toward the reattachment region.

5.4.4 Design Applications

From the examination of performance measures, two key objectives in maximizing performance are to maximize the wake closure NPR and then focus increase closed wake base pressure. The former is achieved through high design Mach Number. In bell nozzles, the increased design Mach Number involves longer exit cones and increased weight. Plug nozzles have the advantage of changing design Mach Number by the ramp shape or inclination without necessarily increasing weight. The amount of truncation must be increased to minimize weight impacts, but a significant amount of truncation can be accommodated without affecting performance.

Once the design Mach Number is specified, the plug length itself increases the wake closure NPR further. However, the added length of the plug requires additional weight. Moreover, both the design Mach Number and plug length reduce the base pressure in closed wake conditions. Alternatively, the jet height or nozzle size can increase wake closure NPR, but have the effect of increasing closed wake base pressure. The increased size of course must be assessed for it increased weight implications.

Generally, the ramp shape should be contoured as opposed to planar since the planar ramp reduced wake closure NPR and closed wake base pressure. However, the relative effect of the ramp shape is relatively small in comparison to the design Mach Number effects, so it may be a desirable design trade if savings can be achieved from the simpler fabrication process.

In supersonic wake problems, one means for increasing closed wake base pressure was to incline the afterbody corner. Simply increasing the inclination of the ramp, as was found from the planar nozzle data had the opposite effect due to the gas expansion along the ramp. Further examination is necessary to

determine whether any inclination (e.g., at the very tip of the plug) can be used to increase closed wake base pressure.

Another means for increasing base pressure in wake flows is to induce transition along the afterbody prior to separation. The turbulent flow increases base pressure in plug nozzle flow. However, the wake closure NPR is decreased, and therefore may not be desirable with respect to controlling open and closed wake conditions. On the other hand, flow transition can be induced actively (e.g., surface bleed), so one potential option is to foster transition after the wake is closed. This means of controlling base pressure may have added weight implications depending on the fluid controls used for base bleed, but it does mean that the overall geometry of the plug can remain constant.

5.5 Summary

In summary, the key driver of increasing design Mach Number to increase performance is common to both bell nozzles and plug nozzles. However, the plug nozzle can have an increase design Mach Number with less impact to the nozzle configuration and weight, since the nozzle length can be truncated. The factors that increase wake closure NPR, also decrease base pressure once the wake is closed. Some modifications to the nozzle design can counter the base pressure effect while minimizing the effect on wake closure NPR.

Chapter 6
CONCLUSIONS

The plug nozzle engine offers potential benefits for the next generation of space launch vehicles. However, the advantages of increased performance and reduced size and weight must be balanced with the overall system impacts. In order to make key design decisions or improve upon existing flight designs, a better understanding of the plug nozzle flowfield, and in particular wake closure, is necessary.

This research characterizes the changes occurring in the flowfield and wake as the wake undergoes transition between open and closed conditions. The primary supersonic wake features are present for closed wake and initial open wake conditions. The flow in the far wake recovers supersonic velocities for these conditions. Therefore it is concluded that the influence of the ambient environment on the base region is not communicated by upstream propagation. The common element between the wake closure modes is the movement of a shock through the reattachment region of the wake.

Because the primary supersonic wake features exist through wake closure, traditional supersonic wake methods are used to analyze the mechanism leading to closure. In particular, the downstream divergence point associated with the envelope shock impingement indicates the gradients imposed at the outer viscous edge that force the critical point to reestablish downstream of the closed wake station. Wake closure is therefore defined as the limiting condition at which external pressure gradients change critical point properties and location. Due to the uniqueness property of the critical point, the change in critical point results in the dependence of the base pressure on open wake ambient pressures. A significant structural change to the wake occurs during

the open wake conditions at very low NPR and is likely associated with the break down of the wake structure found experimentally.

While the open wake condition is a small portion of an overall launch ascent, the performance gains due to the plug nozzle can greatly affect the ability to achieve orbital velocity. Supersonic wake methods and the Design of Experiment provide tools for predicting performance for optimization analysis. Higher design Mach Number is the most significant factor in increasing wake closure NPR. Longer nozzle lengths can increase wake closure NPR without decreasing closed wake base pressure. Shorter nozzle lengths save weight and increase base pressure, but can adversely impact performance. The plug nozzle may afford overall system benefits over bell nozzles, depending on the specific application.

Potential areas for further research include:

- Mathematical derivation of the bifurcation-singularity behavior at wake closure,
- Relation between the critical point changes and base pressure,
- Numerical analysis of the no slipstream condition and wall separation mode, and
- Effect of other factors such as turbulence, γ, and scale effects.

REFERENCES

1. Berman, K. and Crimp, F.W., Jr. "Performance of Plug-Type Rocket Exhaust Nozzles," *ARS Journal*, January 1961, pp. 18-23.

2. Ruf, J.H., and McConnaughey, P.K., "The Plume Physics Behind Aerospike Nozzle Altitude Compensation and Slipstream Effect," AIAA Paper 97-3218, 1997.

3. Bollard, R.O., "The Aerospike/Aeroplug Engine: A Technical Development Summary," NASA Contractor Report NAS8-37814, November 1990.

4. Anonymous, "Advanced Aerodynamic Spike Configuration, Final Report, Vol 1: Analytical and Cold Flow Studies," Rept. AFRPL-TR-67-246, Contract AF04(611)-9948, September 1967.

5. Anonymous, "Advanced Aerodynamic Spike Configuration, Final Report, Vol 2: Hot Fire Investigations," Rept. AFRPL-TR-67-246, Contract AF04(611)-9948, September 1967.

6. Connors, J.F., Cubbison, R.W., and Mitchell, G.A., "Annular Internal-External Expansion Rocket Nozzles for Large Booster Applications," NASA TN D-1049, September 1961.

7. Wasko, R. A., "Performance of Annular Plug and Expansion-Deflection Nozzles Including External Flow Effects at Transonic Mach Numbers," NASA TN D-4462, April 1968.

8. Berrier, Bobby L., "Effect of Plug and Shroud Geometry Variables on Plug Nozzle Performance and Transonic Speeds, NASA TN-D 5098, March 1969.

9. Burge, G.W., and Kendle, D.W., "Base Pressure Effects on the Thrust Performance of Unconventional Rocket Nozzles," Engineering Paper No. 1686, Douglas Missile and Space Systems Division, Santa Monica, California, September 1963.

10. Lee, C.C., and Inman, S.J., "Numerical Analysis of Plug Nozzles by the Method of Characteristics," Technical Note R-101, Brown Engineering Company, Inc., Huntsville, Alabama, May 1964.

11. Schmidt, R.C., "Base Pressure and Heating of a Truncated Plug Rocket Exhaust Nozzle," *Bulletin of the 6th Liquid Propulsion Symposium*, Vol. 1, Los Angeles, California, September 1964.

12. Sergeant, R.J., "An Experimental Hot Rocket Model Investigation of a Plug Cluster Nozzle Propulsion System, Part 1: Base Thermal and Pressure Environment for a Module Chamber Pressure of 300 psia and Simulated Altitudes to 1500,000 Feet," Cornell Aeronautical Lab., Inc., CAL HM-2045-Y-5(I), Cornell University, Buffalo, NY, September 1967. (not reviewed, but referred to by Fick).

13. Hendershot, K.C., and Ellison, R.K., "Cold Flow Thrust and Pressure Investigation of a Plug Cluster Nozzle Using Short-Duration Techniques," Cornell Aeronautical Lab Inc., CAL HM-1510-Y-13, Cornell University, NY, April 1965. (not reviewed, but referred to by Fick).

14. Sule, Wayne P., and Mueller, Thomas J., "Annular Truncated Plug Nozzle Flowfield and Base Pressure Characteristics," AIAA Paper 73-137, 1973.

15. Mueller, T.J., Sule, W.P., Fanning, A.E., Giel, T.V., and Galanga, F.L., "Analytical and Experimental Study of Axisymmetric Truncated Plug Nozzle Flow Fields," Final Report, NAS8-25601, UNDAS, TN-601-FR-10, University of Notre Dame, Notre Dame, Indiana, September 1972.

16. Rommel, T., Hagemann, G., Schley, C.-A., Krulle, G., and Manski, D., "Plug Nozzle Flowfield Analysis," *Journal of Propulsion and Power*, Vol. 13, No. 5, September-October 1997, pp. 629-634.

17. Fick, Michael and Schmucker, Robert H., "Performance Aspects of Plug Cluster Nozzles," *Journal of Spacecraft and Rockets*, Vol. 33, No. 1, July-August 1996, pp. 507-512.

18. Tomita, T., Tamura, H., and Takahashi, M., "An Experimental Evaluation of Plug Nozzle Flow Field," AIAA Paper 96-2632, 1996.

19. Fick, M. and Schmucker, R.H., "Linear Aerospike Engine Performance Evaluation," AIAA Paper 97-3305, 1997.

20. Personal Communication, Lang, D. E., and Fick, M., DASA, June 17, 1998.

21. Personal Communication, Lang, D.E., and Beck, J.E., Boeing North American, June 10, 1998.

22. Schmucker, R.H., "Status of Flow Separation Prediction in Liquid Propellant Rocket Nozzles," NASA TM-X-64890, November 1974.

23. Hama, F.R., "Experimental Studies on the Lip Shock," *AIAA Journal*, Vol. 6, No. 2, February 1968, pp. 212-219.

24. Weinbaum, S. and Garvine, R.W., "An Exact Treatment of the Boundary Layer Equations Describing the Two-Dimensional Viscous Analog of the One-Dimensional Inviscid Throat," AIAA Paper 68-102, January 1968.

25. Dutton, J.C., Herrin, J.L., Molezzi, M.J., Mathur, T., and Smith, K.M, "Recent Progress on High-Speed Separated Base Flows," AIAA Paper 95-0472, January 9-12, 1995.

26. Lamb, J. Parker, and Oberkampf, William L., "Review and Development of Base Pressure and Base Heating Correlations in Supersonic Flow," *Journal of Spacecraft and Rockets*, Vol. 32, No. 1, January-February 1995, pp. 8-23.

27. Berger, Stanley A., Laminar Wakes, American Elsevier Publishing Company, Inc. New York, 1971.

28. Delery, J., and Lacau, R.G., "Prediction of Base-Flows," Special Course on Missile Aerodynamics, AGARD-R-754, April 1988.

29. Ohrenberger, J.T. and Baum, E., "Base Flow Region of Supersonic Bodies," Aerodynamics of Base Combustion, edited by S.N.B. Murthy, Vol. 40, Progress in Astronautics and Aeronautics, AIAA, MIT Press, 1976, pp. 255-305.

30. Korst, H.H., "A Theory for Base Pressures in Transonic and Supersonic Flow," *Journal of Applied Mechanics*, No. 23, December 1956, pp. 593-600.

31. Tanner, M., "Theoretical Base Pressure for Steady Base Flow," *Progress in Aerospace Sciences*, Vol. 14, 1973, pp. 177-225.

32. Chow, W.L., "Recompression of a Two-dimensional Supersonic Turbulent Free Shear Layer," Developments in Mechanics, Vol. 6., *Proceedings of the 12th Midwestern Mechanics Conference*, University of Notre Dame, August 1971, pp. 319-332.

33. McDonald, H., "Turbulent Shear-Layer Reattachment with Special Emphasis on the Base Pressure Problem," *Aeronautical Quarterly*, Vol. 15, 1964, pp. 247-280.

34. Nash, J.F., "An Analysis of Two-Dimensional Turbulent Base Flow Including the Effect of the Approaching Boundary Layer," Aeronautical Research Council R & M No. 3344, 1962.

35. Chow, W.L., and Spring, D.J., "Viscous Interaction of Flow Redevelopment after Flow Reattachment with Supersonic External Streams," *AIAA Journal*, Vol. 13, No. 12, December 1975, pp. 1576-1584.

36. Crocco, L. and Lees, L., "A Mixing-Theory for the Interaction Between Dissipative Flows and Nearly Isentropic Streams," *Journal of Aeronautical Sciences*, Vol. 19, No. 10, pp. 649-676.

37. Lees, L. and Reeves, B.L., "Supersonic Separated and Reattaching Laminar Flow: I. General Theory and Application to Adiabatic Boundary Layer-Shock Wave Interactions," *AIAA Journal*, Vol. 2, No. 11, November 1964, pp. 1907-1920.

38. Reeves, B.L. and Lees, L., "Theory of Laminar Near Wake of Blunt Bodies in Hypersonic Flow," *AIAA Journal*, Vol. 3, No. 11, November 1965, pp. 2061-2074.

39. Webb, W.H., Golik, R.J., Vogenitz, F.W., and Lees, L., "A Multimoment Integral Theory for the Laminar Supersonic Near Wake," *Proceedings of the 1965 Heat Transfer and Fluid Mechanics Institute*, Stanford University Press, Stanford, California, pp. 168-189, 1965.

40. Alber, I.E. and Lees, L., "Integral Theory for Supersonic Turbulent Base Flows," *AIAA Journal*, Vol. 6, No. 7, July 1968, pp. 1343-1351.

41. Peters, P.E., and Phares, W.J., "Analytical Model of Supersonic, Turbulent, Near-Wake Flows," AEDC-TR-76-127, September 1976.

42. Ai, D.K., "On the Hypersonic Laminar Near Wake Critical Point of the Crocco-Lees Mixing Theory," AIAA Paper 67-60, January 1967.

43. Weinbaum, S., "Near Wake Uniqueness and a Re-Examination of the Throat Concept in Laminar Mixing Theory," AIAA Paper 67-65, January 1967.

44. Baum, E., and Dennison, M. R., "Interacting Supersonic Laminar Wake Calculations by a Finite Difference Method," *AIAA Journal*, Vol. 5, No. 7, July 1967, pp. 1224-1230.

45. Ai, D.K., "On the Critical Point of the Crocco-Lees Mixing Theory in the Laminar Wake," *Journal of Engineering Mathematics*, Vol. 4, No. 2, April 1970, pp. 169-183.

46. Weinbaum, S., and Garvine, R.W., "On the Two-Dimensional Viscous Counterpart of the One-Dimensional Sonic Throat," *Journal of Fluid Mechanics*, Vol. 39 Part 1, 1969, pp. 57-85.

47. Putnam, L.E., "Results of AGARD Assessment of Prediction Capabilities for Nozzle Afterbody Flows," AIAA Paper 85-1464, July 1985.

48. Petrie, H.L., and Walker, B.J., "Comparison of Experiment and Computation for a Missile base Region Flowfield with a Centered Propulsive Jet," AIAA Paper 85-1618, July 1985.

49. Tucker, P.K. and Shyy, W., "A Numerical Analysis of Supersonic Flow Over an Axisymmetric Afterbody," AIAA Paper 93-2347, 1993.

50. McLaughlin, D.K., Carter, J.E., Finston, M., and Forney, J.A., "Experimental Investigation of the Mean Flow of the Laminar Supersonic Cone Wake," *AIAA Journal*, Vol. 9, No. 3, March 1972, pp 479-483.

51. Blankson, I., and Finston, M., "Measurements in the Laminar Near Wake of Magnetically Suspended Cones at M=6.3," *AIAA Journal*, Vol. 13, No. 12, December 1975, pp. 1562-1567.

52. Demetraides, A. and Bauer, A.B., "Supersonic Wind Tunnel Experiments with Axisymmetric Wakes, AIAA Paper 66-453, 1966.

53. Tassa, Y., and Conti, R.J., "Numerical Computation of Hypersonic Laminar Near Wake Flow via Navier Stokes Solver," AIAA Paper 85-1672, July 1985.

54. Przirembel, C.F.G., and Page, R.H., "Analysis of Axisymmetric Supersonic Turbulent Base Flow," *Proceedings of the 1968 Heat Transfer and Fluid Mechanics Institute*, Stanford University Press, Stanford, California, pp. 258-272, 1968.

55. Murthy, S.N.B, and Osborn, J.R., "Base Flow Phenomena With and Without Injection: Experimental Results, Theories, and Bibliography," Aerodynamics of Base Combustion, Progress in Astronautics and Aeronautics, Vol. 40, American Institute of Aeronautics and Astronautics, New York, pp. 7-210, 1976.

56. Alber, I.E., "Integral Theory for Turbulent Base Flows at Subsonic and Supersonic Speeds," PhD Dissertation, California Institute of Technology, Pasadena, California, 1967.

57. Angelino, G., "Approximate Method for Plug Nozzle Design," *AIAA Journal*, Vol. 2, No 10, October 1964, pp. 1834-1835.

58. Amtec, Inc., INCA User's Manual, Version 2.0, Bellevue, Washington, 1995.

59. Pallone, A., Erdos, J., and Eckerman, J., "Hypersonic Laminar Wakes and Transition Studies," *AIAA Journal*, Vol. 2, No. 5, May 1964, pp. 855-863.

60. Kennedy, E.D., "Wake-Like Solutions of the Laminar Boundary-Layer Equations," *AIAA Journal*, Vol. 2, No. 2, February 1964, pp. 225-231.

61. Tani, I., "On the Approximate Solution of the Laminar Boundary Layer Equations," *Journal of Aeronautical Sciences*, Vol. 21, 1954, pp. 487-504.

62. Fick, M., "Performance Modeling and Systems Aspects of Plug Cluster Nozzles," AIAA Paper 98-3525, 1998.

63. Chen, W., and Allen, J.K., "Statistical Experimentation Methods for Achieving Affordable Concurrent Systems Design," *AIAA Journal*, Vol. 35, No. 5, May 1977, pp. 893-900.

64. Stanley, D.O., Unal, R., and Joyner, C.R., "Application of Taguchi Methods to Dual Mixture Ratio Propulsion System Optimization for SSTO Vehicles," AIAA Paper 92-0213, January, 1992.

65. Wheless, K., Malak, M.F. and Kiker. K., "JFS190 Turbine Engine Performance Optimized Using Taguchi Methods," AIAA Paper 90-2419, July 1990.

66. Schmidt, S.R., and Launsby, R.G., Understanding Industrial Designed Experiments, 3rd Edition, Air Academy Press, Colorado Springs, Colorado, 1992.

67. Kline, S.J., and McClintock, F.A., "Describing Uncertainties in Single-Sample Experiments," *Mechanical Engineering*, Vol. 75, No. 1, 1953, pp. 3-8.

68. Hall, C.R., Jr., "An Analytical and Experimental Study of Non-Uniform Plug Nozzle Flow Fields," PhD Dissertation, Department of Aerospace/Mechanical Engineering, University of Notre Dame, Notre Dame, Indiana, August 1970.

69. Lang, D.E., "Leading Edge Bluntness Effects on High Speed Flow," Project Report 1995-07, von Karman Institute of Fluid Dynamics, Rhode-St-Genese, Belgium, 1995.

Appendix A
TEST FACILITY DEVELOPMENT AND VALIDATION

As part of this research effort, a test facility was designed and fabricated to test plug nozzle configurations over a range of operating conditions. This section describes the design and operations of the facility, the plug nozzle designs used, measurement instrumentation, and an assessment of measurement uncertainties.

A.1 Test Facility and Model Configurations

Wind Tunnel System. A wind tunnel system was developed specifically for the plug nozzle research. Shown in Figure A.1, the wind tunnel system consists of a ballast tube, flow control system, settling chamber, test section, and dump tank. The components are described below:

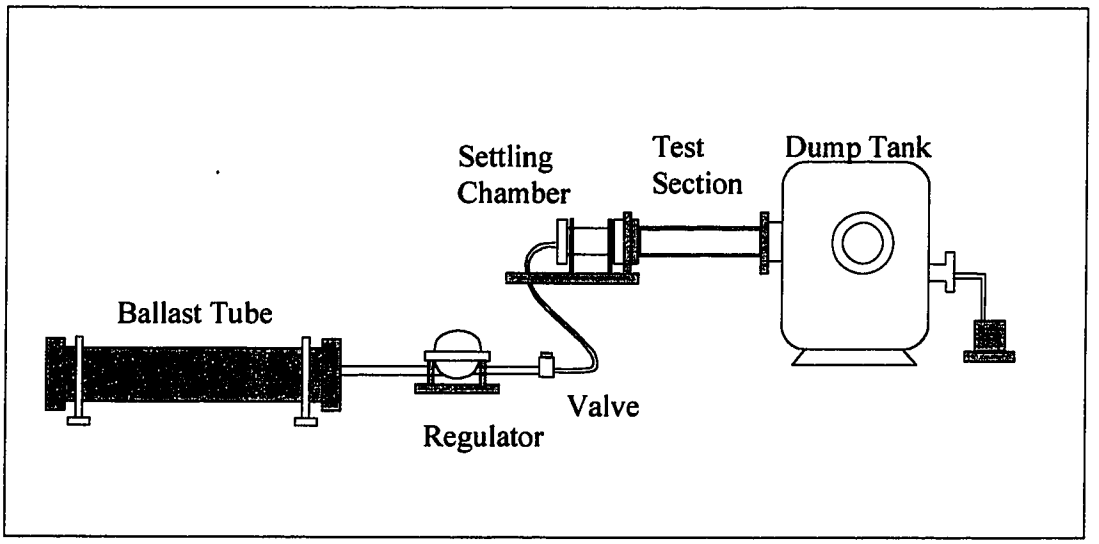

Figure A.1: Plug Nozzle Research Test Facility

Ballast Tube and Flow Control System. The aluminum ballast tube measures 10-foot length x 6-inches ID and holds the supply of gas prior to the test run. The tube can be filled with gas from a compressed gas bottle on the front end or from lab compressed air on the back end. Gas flows from the ballast tube through 1-inch stainless steel tubing to a domed flow regulator and main control valve. Gas from the ballast tube supplies the upstream pressure source to a small gas canister-type regulator to control the domed flow regulator. The gas canister-type regulator can be isolated from the ballast tube once the desired pressure is reached in the line to the domed flow regulator. The main control valve utilizes a 1-inch orifice ball valve that is pneumatically activated by a switch at the operator's desk. The gas is released to a 1-inch flexible rubber hose that connects to the settling chamber.

Settling Chamber. The steel settling chamber measures 9-inch diameter x 6-inches length x ¼ inch wall thickness, and reduces the flow velocity prior to entering the test section. It also provides access ports for the total pressure and base pressure transducers and total temperature thermocouple. A screen can be fitted into the settling chamber to straighten the flow, but at the cost of a slight head loss. Since the length scale of nozzle throat was on the same order of magnitude as the screen openings, the screen had marginal benefit in reducing freestream turbulence and was therefore not used.

Test Section. The test section consists of an aluminum rectangular frame of 2-inch width x 4-inch height x 42-inches length. The sides are replaceable panels. One side is glass, and the other is an aluminum panel with a cutout for schlieren photography or pressure ports. The top is lined with pressure taps and the bottom contains access ports for miscellaneous use.

Dump Tank. The steel dump tank is approximately 8-feet long x 4-feet diameter and is used to control the back pressure in the test section. Two vacuum pumps are used to evacuate the dump tank to the desired pressure in the test

section. A valve on top of the tank can be used to allow gas back into the tank for fine adjustments to pressure.

Nozzle and Nozzle Holder. The aluminum nozzle holder shown in Figure A.2 fits in the test section and holds the plug nozzle and top and bottom cowls. For 2-D flow, the holder spans the width and height of the test section and is held into place by stringers connected to a base plate at the front of the test section. The design allows for interchangeable plug nozzles and cowls. The base and ambient pressure transducer tubing runs through the nozzle holder to the plug nozzle and top cowl. Another pressure transducer line is connected directly to the nozzle holder that has a tap to measure pressure in the channel prior to reaching the nozzle.

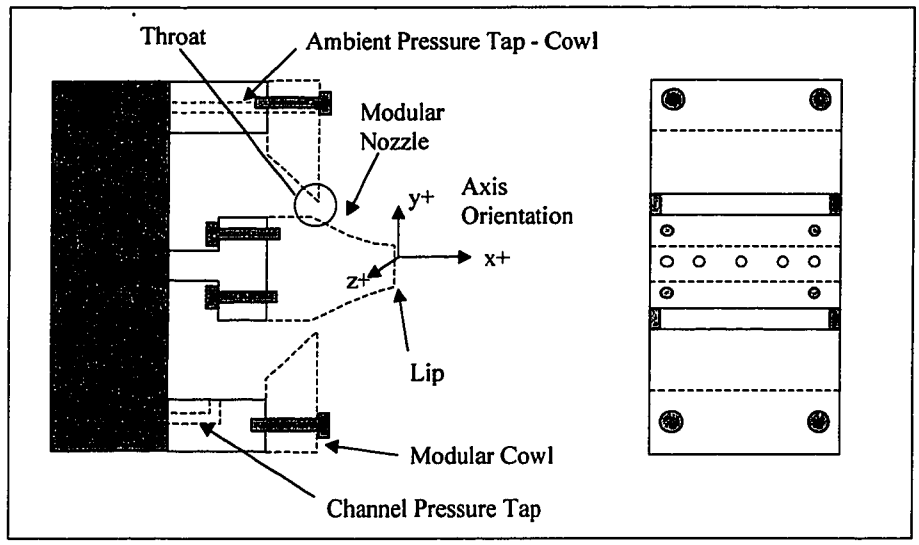

Figure A.2: Nozzle Holder and Plug Nozzle Set Design

The aluminum ramps were fabricated using a numerically controlled mill. Upstream of the throat, the ramp is designed to provide a gradual transition from the channel flow direction to the design inlet angle. The cowl is fabricated within ±0.5 degrees of the design inlet angle using a standard mill and turntable. The actual flow angle into the throat section was thus some average

between the ramp and cowl inlet angle. This angle was not measured, but the C35-10-25 plug nozzle set was fabricated with both a gradual inlet angle and a sharp transition. The measured base pressure-to-total pressure profiles over the duration of a run did not vary significantly between the two geometries.

Table A.1: Plug Nozzle Configurations

Plug Number	Design Mach	Throat Height (inch from axis)	Lip Height (inch from axis)	Ramp Length (inch)	Injection Angle (deg)
C20-10-025	2.0	0.235	0.120	0.249	-26.4
P20-10-050	2.0	0.235	0.047	0.499	-26.4
C20-20-025	2.0	0.469	0.240	0.499	-26.4
P20-20-050	2.0	0.469	0.095	0.998	-26.4
C35-10-025	3.5	0.462	0.160	0.435	-58.5
C35-10-050	3.5	0.462	0.060	0.870	-58.5
P40-10-025	4.0	0.481	0.165	0.495	-65.8
C40-10-050	4.0	0.481	0.062	0.990	-65.8
P40-20-025	4.0	0.962	0.330	0.990	-65.8
C40-20-050	4.0	0.962	0.123	1.979	-65.8
C50-10-050	5.0	0.495	0.063	1.234	-77.0
P50-10-025	5.0	0.495	0.168	0.617	-77.0
P50-15-025	5.0	0.743	0.252	0.926	-77.0
C50-20-050	5.0	0.991	0.125	2.469	-77.0
P50-20-025	5.0	0.991	0.336	1.234	-77.0

Codes:
First Group – C – Contoured; P – Planar
Second Group – Design Mach Number (e.g., 20 represents Mach 2.0)
Third Group – Jet/Cowl lip height (e.g., 10 represents 1.0 inches)
Fourth Group – Nozzle Length (e.g., 025 represents 25%)

A.2 Measurement Techniques

The primary measurement techniques for the experimental investigation were pressure measurements and schlieren photography. Pressure was measured using pressure transducers connected to various pressure taps at the nozzle base, various locations through the test facility, and a modular Pitot rake. These measurements were collected and archived using a PC-based data acquisition system. The schlieren photography system was developed specifically for the plug nozzle test facility.

A.2.1 Data Acquisition System

The data acquisition system consists of an amplifier box, National Instruments data acquisition board Model No. LP-PCM-16, and Intel 486-based personal computer shown in Figure A.3. The data acquisition board can read up to 16 channels of data. Five channels are allocated for base, centerline, or flowfield measurements for any given test, while the remaining channels were allocated to temperature, total pressure, and ambient pressure readings. A Fortran program collects the data as raw voltages during the run. A post-processing Visual Basic program converts the voltages to pressures using user-defined calibration data. A Labview program is used to monitor and record the channels during experiment preparation and pressure transducer calibration. The data acquisition system also sends a signal to initiate a counter for the schlieren system.

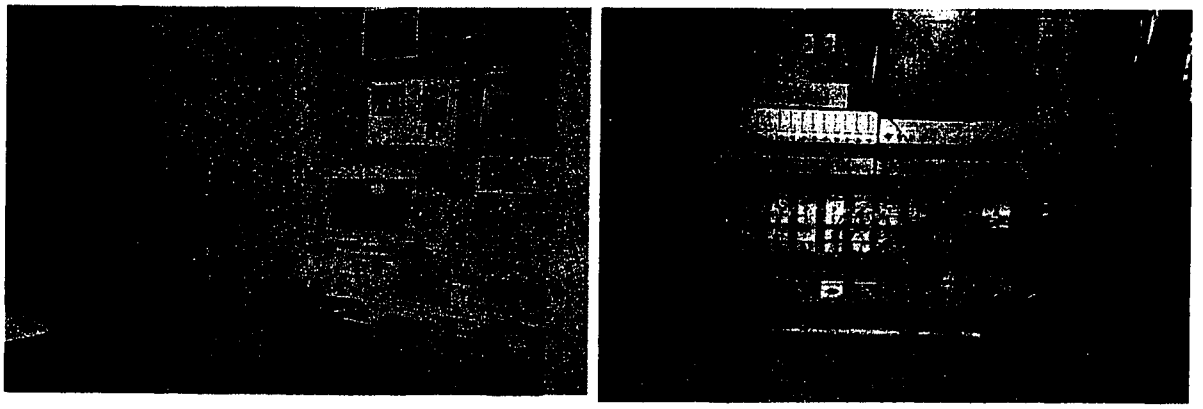

Figure A.3: Data Acquisition System

A.2.2 Pressure Measurements

Eleven pressure readings are taken during a test run. Pressure is read in the ballast tube, the settling chamber, and channel to track the flow total pressure. A Measurement Supply, Inc., MSP 300-500-P-1-N pressure transducer with range of 0-500 psia is used to measure the ballast tube pressure. The

remaining pressure transducers were built by Motorola and are listed with their specifications in Table A.2.

Table A.2: Pressure Transducer Specification

Model	700D	2000A
Range	0-700 kpa	0-200 kpa
Type	differential	absolute
Application	• Settling Chamber pressure • Channel pressure	• Base • Ambient • Centerline Sidewall • Flowfield

Five pressure transducers can be connected to the plug nozzle for measurements along the base or along the plug surface. A transducer is measures ambient pressure through a tap on the top cowl and on the top test section wall just aft of the cowl. The multiple base taps and ambient taps provide redundancy and flow uniformity information.

A cut-out in the side test section panel allows for interchangeable plates to measure centerline and flowfield pressures. Figure A.4 shows the centerline plate, which consists of 10 pressure taps, spaced 0.0079 inches apart to measure centerline pressures along the sidewall of the test section. The flowfield plate holds a position-adjustable Pitot rake for total pressure measurements. One Pitot port is opened on the side for static pressure measurement.

A.2.3 Temperature Measurements

The data acquisition also includes a K-type thermocouple for measuring temperature in the settling chamber to represent total temperature.

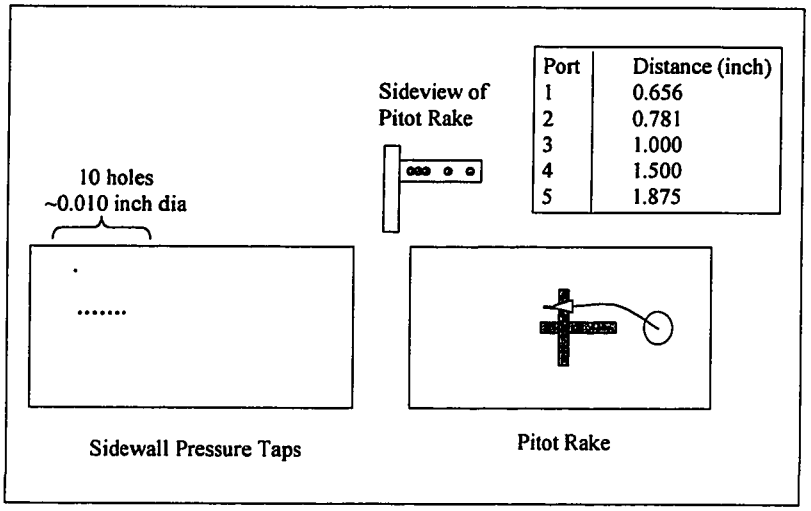

Figure A.4: Sidewall Pressure Taps and Pitot Rake

A.2.4 Schlieren Photographs

A single-pass schlieren Photography system shown in Figure A.5 is used to visualize shock and mixing layer structures in the wake. The system consists of a 500W Halogen lamp with fan cooling, 8-inch primary mirror, 6-inch secondary mirror, adjustable knife-edge, frosted screen, a Light Emitting Diode (LED) counter, black-and-white Panasonic CCD camera, Video Cassette Recorder (VCR), and monitor. The primary mirror has a focal length of 114 inches and the secondary mirror has a 110-inch focal length.

A 1/8-inch diameter hole was cut into the lamp stand to allow a beam of light to pass downward to a planar mirror. The light beam was reflected by the planar mirror to the 8-inch mirror, through the test section, to the 6-inch mirror and onto a frosted glass imaging screen. The sidewalls of the test section were 0.5 inches thick glass panels. In some cases, the sidewall on the 8-inch mirror side was replaced with the aluminum wall/Plexiglas cut-out panel. The Plexiglas measured 0.75 inches and had little effect on the image quality.

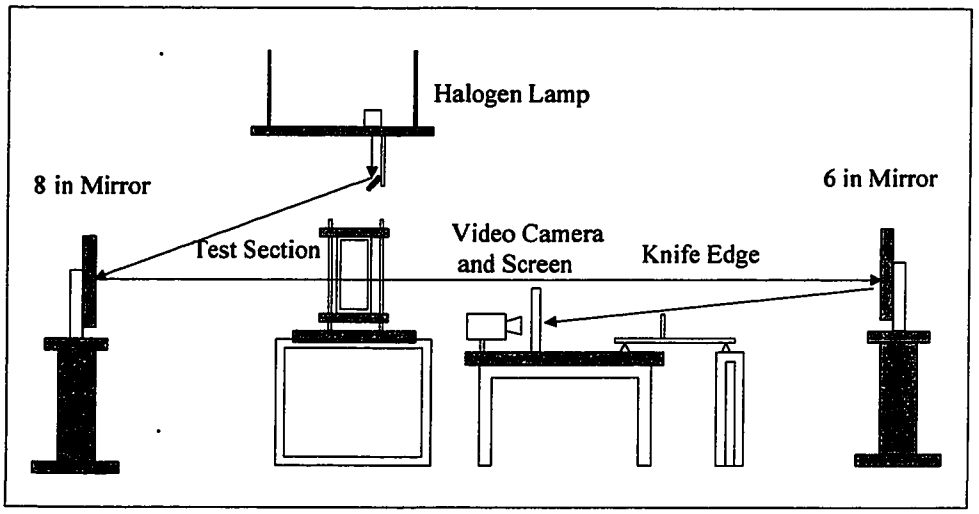

Figure A.5: Schlieren Photography Set-up

In order to correlate the schlieren photographs with the pressure measurements, a LED was attached to the imaging screen and recorded along with the schlieren image. The LED counter was initiated by a command from the data acquisition computer and ran on an internal clock with an accuracy of to 1 millisecond.

A.3 Facility Flow Characterization

Although the ballast tube could be pressurized to at least 300 psia, the pressure differential across the flow regulator limited the line pressure to 120 psia. Significant head loss occurred in the line leading to the settling chamber as a function of mass flow rate. At high Mach Numbers, the mass flow was low and a maximum of 110 psia could be achieved in the settling chamber. At low Mach Numbers and high mass flow, the total pressure in the settling chamber was reduced to as low as 10 psia. The evacuation of gas from the test section using the vacuum pumps allowed supersonic flow at these low total pressures. Generally, the lowest pressure ambient pressure achieved by the vacuum pumps was about 0.75 psia.

The operation of the test facility entailed charging the ballast tube, or setting the regulator, and then evacuating the test section until the combination achieved the desired initial operating total-to-ambient pressure ratio. The tests were run as long as 3 seconds, but a typical run lasted about 1.5 seconds to limit gas usage. Figure A.6 shows the total pressure in the settling chamber and ambient pressure in the test section for each of the Mach Number nozzles. At high ballast pressures, the regulator maintained consistent total pressure; but once the ballast pressure went below 130 psia, the regulator lost control authority. The ambient pressure rise over the run duration was a function of mass flow rate, but did not vary significantly. For a given Mach Number nozzle, an increase in total pressure also increased the rise in ambient pressure, thus limiting the achievable total-to-ambient pressure ratio. But in general, the ability to vary both the total pressure and the ambient pressure provided a degree of flexibility to the system operations.

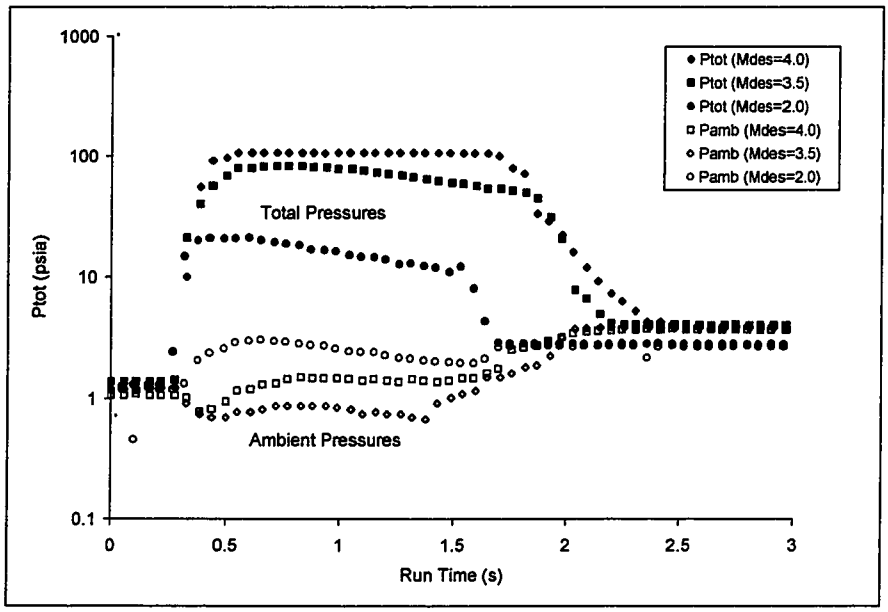

Figure A.6: Test Facility Pressure History for Various Plug Nozzles

The C35-10-25 nozzle was used as a baseline to calibrate the flowfield. It was found that the ability to visualize some of the flow features, e.g., the freejet

boundary, was strongly dependent on the optical system alignment. One of the immediate problems was that the freejet boundary for the baseline and the higher Mach Number nozzles was never straight at the theoretical design conditions. The curvature in the freejet boundary indicated that the closed test section was produced a varying pressure field. The jet flow created a recirculation/base flow on the cowl. This issue was of greater significance for the 2-inch nozzles where the jet was closer to the top and bottom of the test section. As a result, it was difficult to match a specified condition with a design Mach Number. Moreover, the definition of pressure ratio, Ptot/Pamb, was thus relative to the location of the ambient pressure reading. It should be noted that the issue of a cowl base pressure and non-uniform ambient pressure distribution would also exist for flight hardware in a slipstream.

Ambient pressures were measured along the test section for the C35-10-25 nozzle to assess the wall effects on the flow. The x=0.0 inch in Figure A.7 represents the pressure tap on the cowl and the point furthest downstream is measured in the dump tank. Initially, the pressures are fairly uniform. As the run continued, the back pressure in the dump tank moves forward to the nozzle. Based on the schlieren photographs, the first pressure tap on the test section wall after the cowl correlated closest with a NPR to design Mach Number. Therefore, this pressure tap was therefore selected for the experiment NPR references. The relative difference between the pressure ratio based on the cowl pressure tap versus the test section pressure tap was not significant when determining the point of wake closure.

Figure A.8 shows the base pressures for the C35-10-25 nozzle at different times during the run. The pressures along the lateral span of the nozzle base are fairly uniform. Any flow between the nozzle holder and the test section wall does not appear to have significant effect on base pressure. This uniformity degrades as the wake opens, but remains relatively intact. Several other nozzle holder designs were tested, and all had similar uniformity characteristics. For

the purposes of this research, the center pressure tap was used to represent overall base pressure.

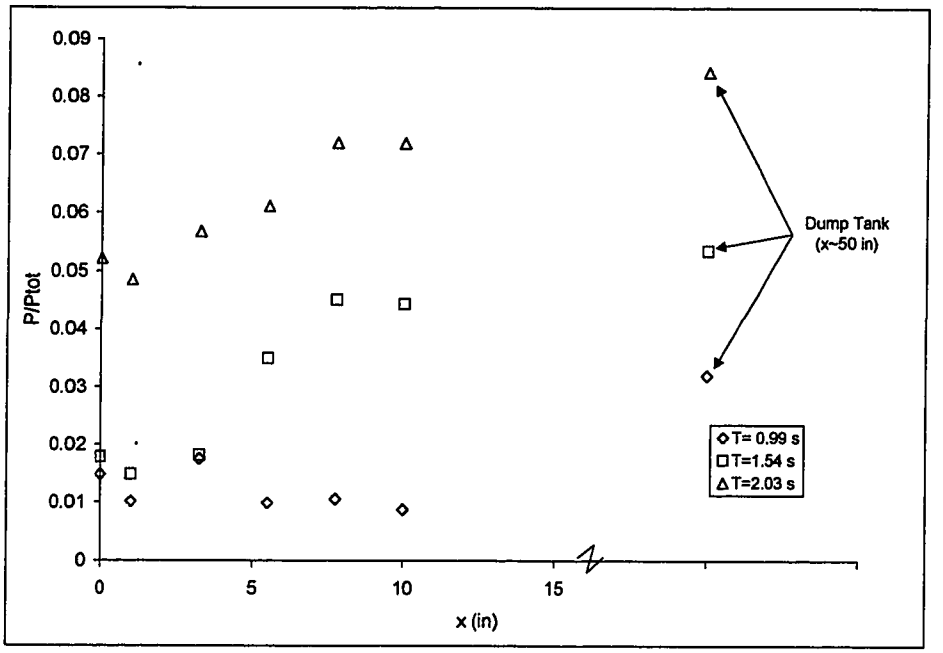

Figure A.7: Pressure Distribution Along Test Section Top Wall

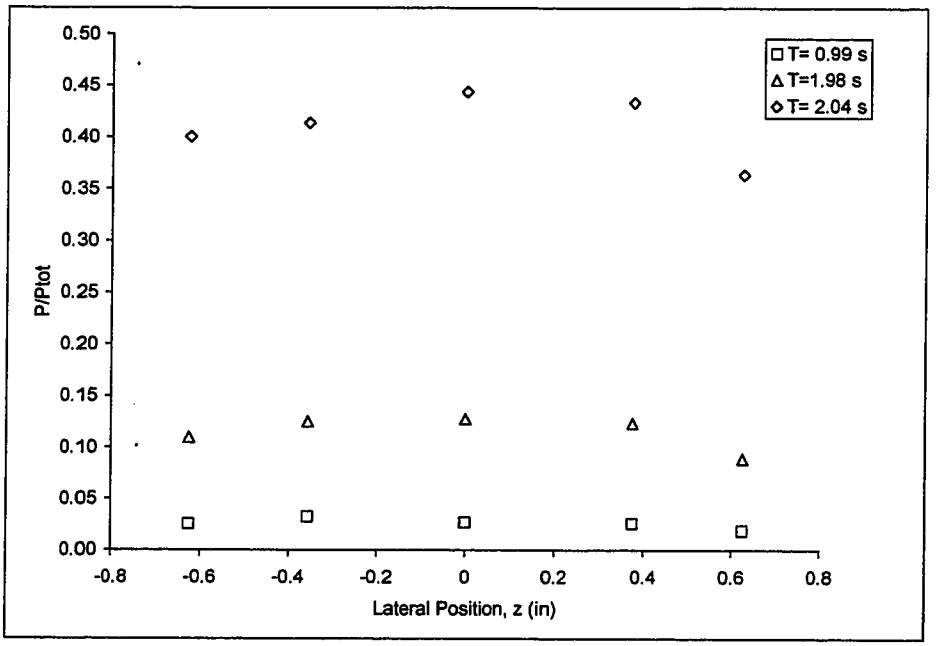

Figure A.8: Pressure Measurement Variations Along Plug Base

A set of Pitot rake tests provided the total pressure distribution in the flowfield for the C35-10-25 plug nozzle to determine flow uniformity. Figure A-9 shows the distribution of Pitot pressure at the location x=0.625 inches from the base of the C35-10-25 nozzle. At NPR=47, there is a spike in the flow just to the upper right of the center. The location of the Pitot port at z=+0.25 inches lies very close to the recompression shock. One possible cause for this deviation is the Pitot port at this location is reading the flow just ahead of the shock, while the others are measuring the flow aft of the shock. However, the NPR=23 shows some additional perturbations at the same lateral location. Inspection of the ramp and cowl did not reveal any nozzle obtrusions, and the base pressure measurements did not suggest any flow deviations. Another potential cause may have been a skewed Pitot port.

The centerline pressure measurements taken from the sidewall panel indicated that there was some flow in the gap between the nozzle and the test section wall. Some filler material was inserted in the gap for the centerline measurements to eliminate this stray flow. There was no significant difference in base pressure between the tests with and without the filler material. The total pressure measurements did not indicate any flow disturbances due to the sidewall in the main flow, but this may also be due to distance of the Pitot ports from the sidewall.

A.4 Uncertainty Analysis

The pressure transducers were calibrated and data acquisition and LED counter timing accuracies were analyzed. The data acquisition system and LED counter timing were also analyzed. The methodology by Kline and Mclintock (67) were used to compute the uncertainty levels for key measurements and their confidence levels. Finally, a qualitative assessment was conducted of potential sources of errors and flow uncertainties.

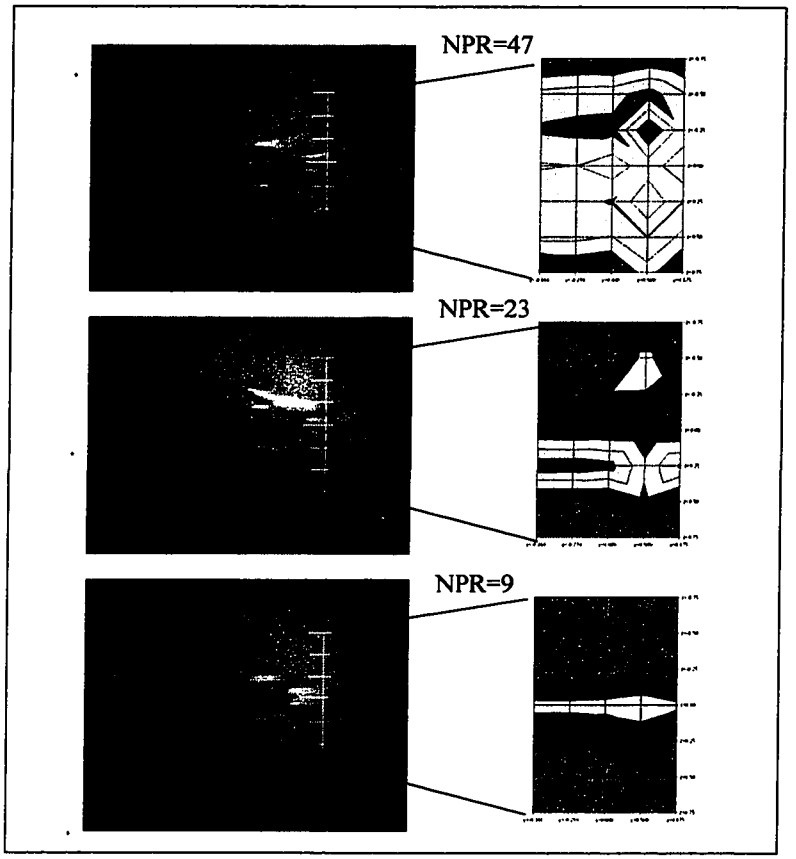

Figure A.9: Pitot Pressure Uniformity

The pressure transducers were calibrated for using a Pennwalt Corporation Series 65-120 Portable Pneumatic Calibrator to maintain a regulated pressure of ±0.1 psia. The Omega and 700D pressure transducers were calibrated in the range of 14.7 to 115 psia. The 2000A pressure transducers were calibrated in the range of 0.5 to 14.7 psia. The uncertainty band and confidence levels for each transducer are listed in Table A.3. The confidence levels for the uncertainty analysis are in the range of 20:1, or a 95% confidence level.

The data acquisition system had a maximum sampling rate of 250 samples/second. The sample rate to collect 13 channels of data was on the order of 50-60 milliseconds. During the normal course of a test run, the tunnel reached maximum pressure within 300 milliseconds and then the maximum

rate of change in total pressure was approximately 60 psia/sec. The maximum rate of change in base pressure was approximately 3 psia/sec, excluding startup and shutdown.

Table A.3: Pressure Transducer Uncertainty and Confidence Levels

Serial Number	Location	Slope (Psia/Volt)	Uncert Band (±Psia)	Confid Level (odds)	Offset (Psia)	Uncert Band (±Psia)	Confid Level (odds)
Omega	Ballast	47.145	0.52	21:1	13.363	0.11	21:1
SN001	Settling Chamber	14.454	0.44	20:1	-0.862	0.05	20:1
SN002	Channel	14.431	0.29	20:1	-0.932	0.05	20:1
SN004	Ambient-Cowl	14.260	0.22	20:1	-0.120	0.05	20:1
SN005	Ambient-Test Section	14.405	0.17	20:1	-0.031	0.05	20:1
SN006	Base/Field	14.394	0.11	20:1	-0.311	0.05	20:1
SN007	Base/Field	14.352	0.14	20:1	-0.267	0.05	20:1
SN008	Base/Field	14.373	0.16	20:1	-0.181	0.04	20:1
SN009	Base/Field	14.404	0.41	20:1	-0.196	0.05	20:1
SN010	Base/Field	14.320	0.31	20:1	-0.303	0.06	20:1
SN011	Dump Tank	14.270	0.08	20:1	-0.067	0.04	20:1

The data acquisition computer initiated and terminated the LED counter, but the timing mechanism for the counter ran on an independent clock. The LED counter had an adjustable clock speed, and was set to run at 1millisecond intervals. Based on the computer clock, it appeared that there was about a ±50 milliseconds difference between the LED counter and data acquisition sample time. This difference was generally associated with the delay in initiation of the LED counter.

The uncertainty in pressure measurement consists of the uncertainty in the calibration slope and an uncertainty in the measurement reading. Since the calibration offset was significantly large compared to the accuracy of the readings, the offset uncertainty was included as an additional component in the uncertainty computation. The overall uncertainty levels in the data

measurements for a typical run are listed in Table A.4. The first set of uncertainty values represent the uncertainty level in pressure reading by itself. The second set of values represent the uncertainty in the pressure reading and associated computed values as a result of correlating the data acquisition with the schlieren photographs.

Table A.4: Overall Uncertainty Levels

	Variable	Typical Value	Uncertainty Band	Uncertainty (%)
Pressure	P – Total (psia)	40	0.139	0.3
	P – Base/Field (psia)	1.4	0.042	3.0
	Pbase (or field)/Ptot	0.035	0.001	3.1
	NPR	28.57	0.870	3.1
Pressure Correlated With Schlieren	P – Total (psia)	40	0.223	0.6
	P – field (psia)	1.4	0.222	15.9
	Pfield/Ptot	0.035	0.006	15.9
	NPR	28.57	4.534	15.9
	Mach	2.93	0.773	26.4

In addition to the uncertainty levels computed above, there are several sources of errors and uncertainties that were identified, but not quantified. These included fabrication issues as well as disturbances in the flowfield that were not resolved.

As described above, the cowl was fabricated to a tolerance of 0.5 degrees. The ramp contour was machined to a tolerance of 0.001 inches. But the inlet curvature was only roughly designed to reduce the turning gradient of the flow as it entered the throat region. No attempt was made to measure the flow inlet angle. Hall and Meuller (68) reported that the flowfield is sensitive to the sonic line at the throat. The base pressures measured for these experiments did not show a significant variation for the different inlet conditions tested on the C35-10-25 nozzle. The pressure taps along the base wall and on the ramp itself are relatively large in comparison to the respective length scales. No attempt was

made to assess the impact of the hole sizes or shapes on the flowfield or measurements.

There were several sources of error and uncertainty within the flow itself. The non-uniformity of the flow to the right of the center was repeatable during the Mach Number measurements, but the source of this disturbance was not found. One possible source was a misalignment of the Pitot port. Three-dimensional and sidewall effects appeared to be minor, but should be examined more carefully. The presence of the upper and lower wall affected the ambient pressure measurements by creating another closed base region at the cowl. As a result, the difference in ambient pressure as measured by the cowl position tap versus the top wall of the test section was about 0.5 psia. This difference was significant in correlating the flow to a design Mach Number, but did not affect the p_{base}/P_{tot} versus NPR profiles. There was no attempt to quantify the effects of impurities in the air. Laboratory-supplied compressed air was used for the low total pressure tests. This source of gas has been reported to contain oil impurities from the compressor. None of the tests appeared to have condensation. A honeycomb screen was placed in the settling chamber during the facility commissioning, but was later removed to reduce total pressure losses. The turbulent length scales were therefore limited by the size of the throat heights.

Appendix B
COMPUTATIONAL ANALYSIS VERIFICATION

The initial step in implementing the CFD analysis began with a "code validation" process. Since the CFD code is commercial-off-the-shelf software, the validation focused on the selection of input parameters rather than the efficacy of the program itself. In this case, the supersonic flat plate and supersonic wake were used to determine the flux function, grid sizes, and node spacing that would provide the best results for eventual application to the plug nozzle configuration. Finally, the baseline plug nozzle is examined to ensure adequate solution convergence.

Supersonic Flat Plate Test Case. The first test case was a supersonic flat plate with a sharp leading edge. This test case provided a benchmark for assessing the code's ability to resolve compressible shear flow - the boundary layer in this case - and shock waves. The objective was to assure adequate grid sizes, initial node spacing from the wall (and eventually the configuration axis), flux function selection, and convergence levels and stability. This test case was then used to verify the computation of shear flow thicknesses, such as boundary layer thickness, displacement thickness, and momentum thickness.

The two-zone grid in Figure B.1 was used to represent represented the oncoming freestream and sharp leading edge flat plate. The inlet plane was defined for as a supersonic flow with M_∞=3.5, P_{tot}=35 psia, and T_{tot}=288K. The top and outlet planes were defined as supersonic outlet boundaries. The lower boundary of Zone 1 (freestream) was defined as a symmetry plane, and the flat plate of Zone 2 was given a no-slip wall boundary condition. Exponential stretching was used to distribute the grid points, with a first spacing of 0.001 inches above the wall surface and node clustering at the leading edge of the

plate. The Mach-isolines for the fine mesh depict the main flow structures along the plate. The leading edge shock is clearly depicted coming off the start of the plate, and the clustering of isolines near the body surface indicates the presence of the viscous boundary layer.

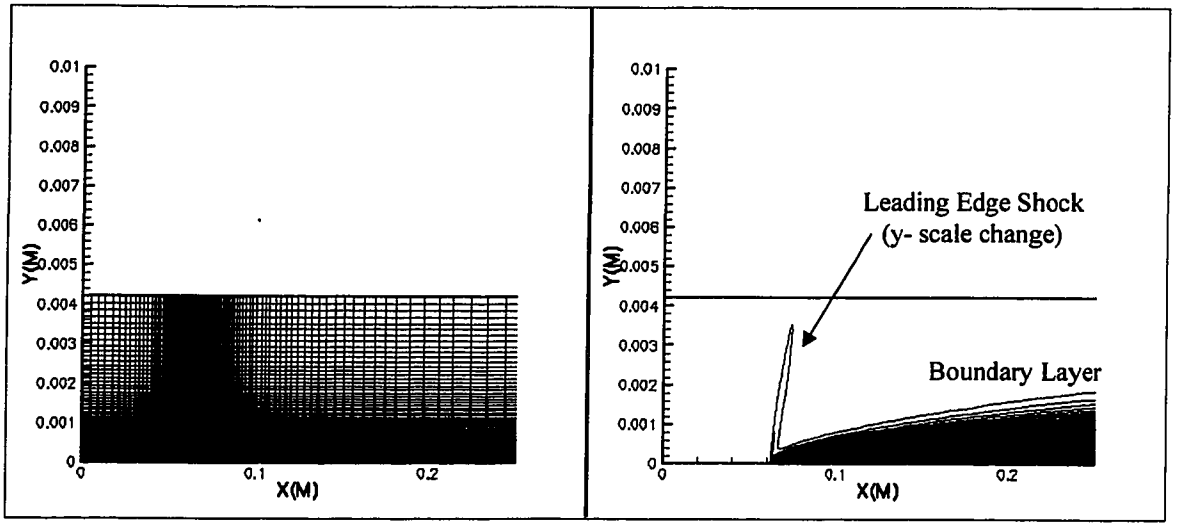

Figure B.1: Flat Plate Grid and Mach Isolines

Three grid sizes listed in Table B.1 were used to determine grid convergence. The fine mesh and velocity, cross-sectional pressure, and surface pressure convergence profiles at x=0.0686158 m are shown in Figure B.2. The velocity profile shows the zero velocity, or no-slip, wall condition and then increases to the freestream value for M_∞=3.5 flow. The cross-sectional pressure profile shows a nearly constant pressure within the boundary layer above the surface and then reaches its freestream value for M_∞=3.5 flow. The spike in surface pressure distribution represents the viscous-inviscid interaction at the leading edge of the plate found in supersonic flows and then settles down to a constant pressure in the boundary layer downstream of the interaction. The convergence history is based on the L-2 norm of the momentum equation residual. Each grid size was run until the residual was reduced by at least 7 orders of magnitude. The graph shows stable convergence for the duration of the run.

Table B.1: M=3.5 Flat Plate Grid Sizes

Grid Size	Zone 1 Size	Zone 2 Size
Coarse	21x21	33x21
Medium	41x41	65x41
Fine	81x81	129x81

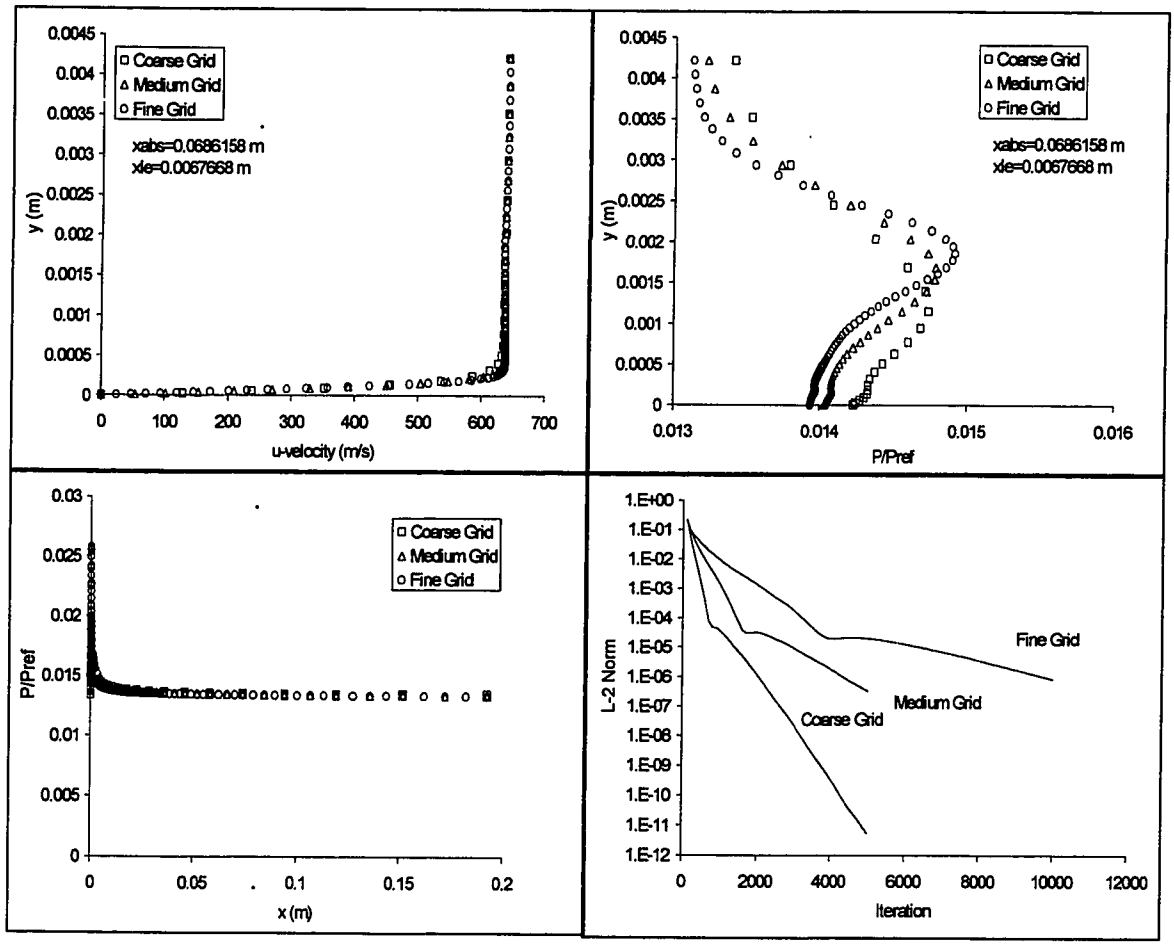

Figure B.2: Flat Plate Grid Convergence

Initially, a Steger-Warming flux function was used because of its robustness. However, consistent overshooting of the velocity profiles at the boundary layer edge suggested that there was too much numerical dissipation. The Harten-Yee flux function was invoked and removed the overshoot. But in order to minimize the numerical dissipation in the viscous region - particularly in the later wake flow studies, the Roe flux function option was eventually selected.

Supersonic Wake Test Case. The supersonic wake test case was the next increment in the validation process after the flat plate, leading toward the plug nozzle configuration. This phase verified the capability to resolve the recirculation regions and key features of wake flow such as trailing edge separation, initial corner expansion, recompression, reattachment, and downstream flow recovery. The results were then used to verify computation of the critical point parameters that would be applied to the plug nozzle flow.

Three zones were used to model the wake flow as shown in Figure B.3. Nodes were clustered along the wake axis (i.e., the lower boundary), and in the vicinity of the wake shear outer layer. Although the solution would have benefited by adapting the meshes to the shear layer and shock locations, a simple orthogonal grid was used in the wake region in order to facilitate post-processing analysis. The Mach isolines indicate the key flow features such as the initial flow expansion, shear layer, recompression shock, and recirculation region.

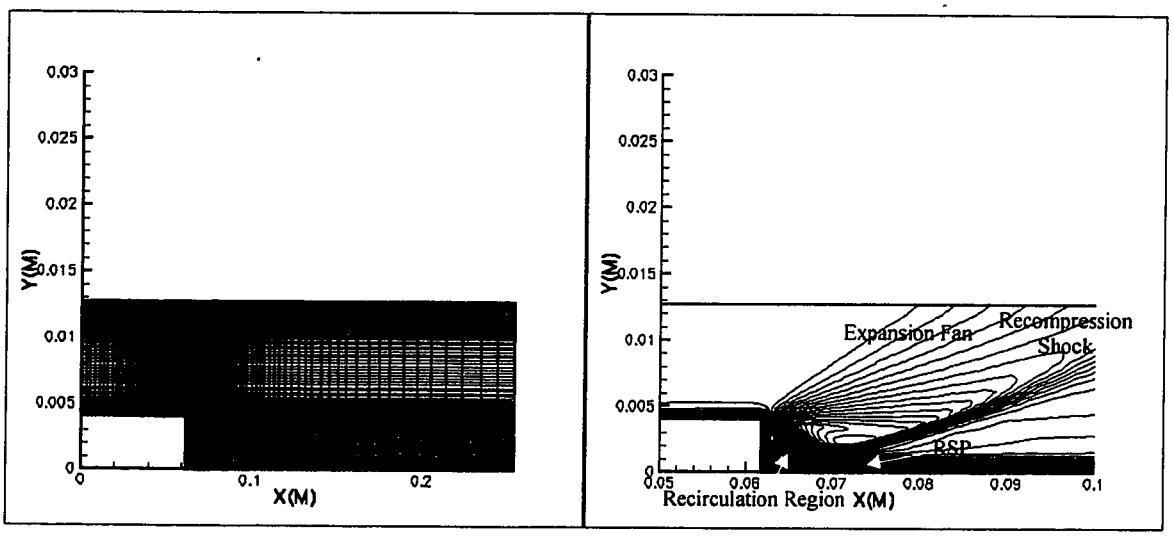

Figure B.3: Supersonic Wake Grid and Mach Isolines

The inlet conditions and afterbody dimensions were selected for later comparison of the results with the plug nozzle results. The inlet freestream conditions were with M_∞=2.5, P_{tot}=35 psia, and T_{tot}=288K. The afterbody was 2.5 inches long and 0.160 inches high. These conditions resulted in a Reynolds Number at separation of $Re_x=1.56x10^6$ and a momentum thickness-to-lip height ratio, θ/h=0.008. The solid surfaces were given no-slip boundaries. The lower boundary aft of the trailing edge was defined as a symmetry plane, and the top and outlet boundaries were defined as supersonic outflows.

The grid sizes for convergence are listed in Table B-2. The wake solutions shown in Figure B-4 were computed using a Roe flux function. The velocity profiles captured the reverse flow in the recirculation region, and then increased until freestream velocity is achieved outside of the shear flow. The velocity profiles for each grid converged as grid size is increased. The cross-sectional pressure showed strong convergence in the inviscid flow region, but had more difficulty converging near the centerline.

Table B-2: Supersonic Wake Test Case Grid Sizes

Grid Size	Zone 1 Size	Zone 2 Size	Zone 3 Size
Coarse	21x21	33x21	33x21
Medium	41x41	65x41	65x41
Fine	81x81	129x81	129x81

The centerline pressure distribution follows similar trends as the laminar CFD results of Tassa and Conti (53). The sharp drop is pressure just aft of the base was noted by Tassa and Conti to correspond with a local velocity minimum located near the center of rotation of the recirculation. The solution converges well near the base and far downstream. The empirical base pressure prediction from Equation (1) by Lamb and Oberkampf is presented with the centerline distributions from the CFD results, and lies closer to the value of the centerline pressure after the expansion process than exactly at the wall. This result should be examined further to determine whether the post-expansion pressure is more appropriate for comparison with experimental data than the base

pressure at the wall. The uncertainty in CFD base pressure is measured in terms of percent difference from an empirically predicted value. The percent difference between the empirical result and the CFD base pressure at the wall is 72% and 48% for the base pressure after the corner expansion. The level of uncertainty is large, but not significantly larger than that found in other CFD solutions described in Section 2.3.3. The CFD solutions are therefore considered sufficient for a qualitative assessment of wake flow trends.

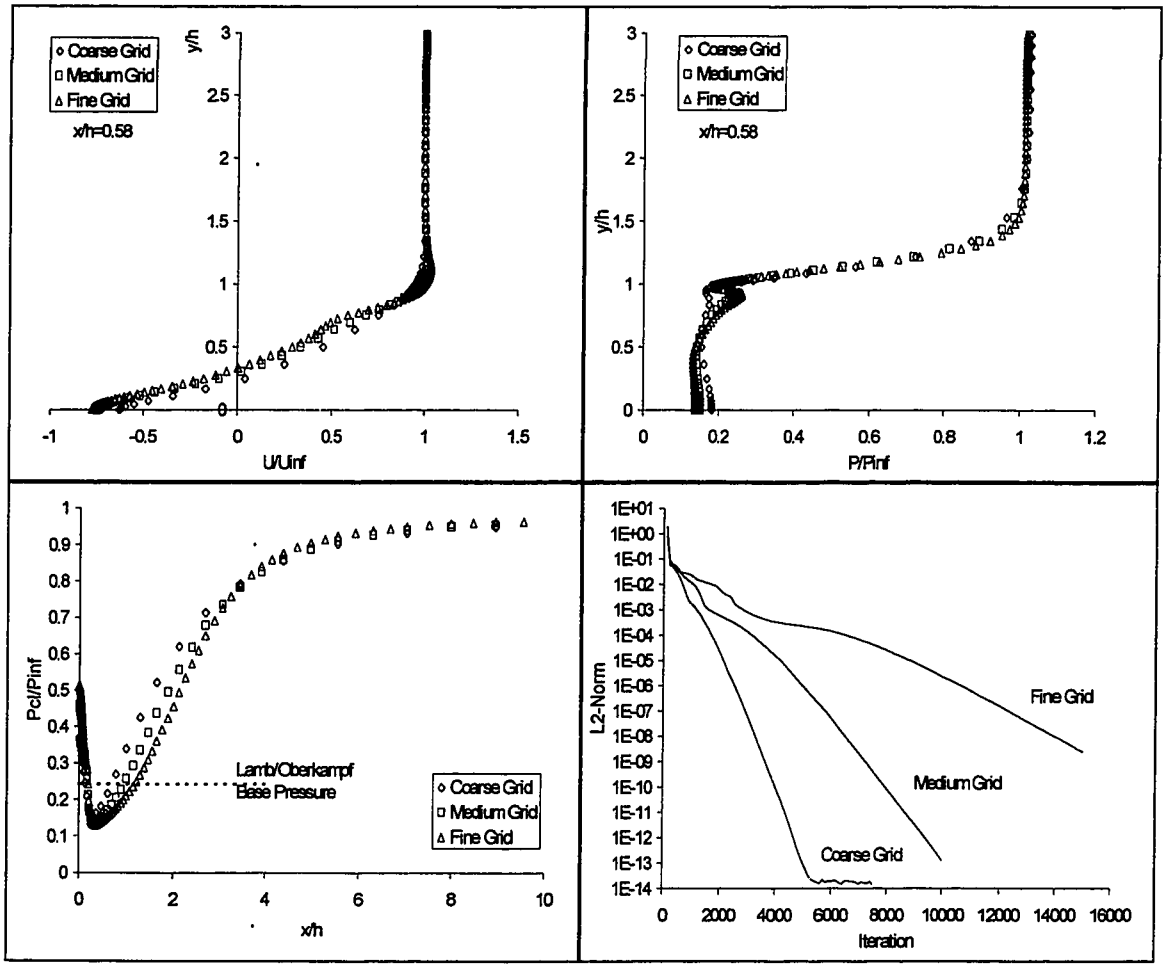

Figure B.4: Supersonic Wake Grid Convergence

The pressures in the recompression region are more dispersed, but appear to be converging with grid size. The accuracy of this solution should be investigated

further, but for these should be sufficient for the purposes of qualitative analyses. Additional confidence in the CFD results can be achieved by comparison of the plug nozzle experimental data to that of the CFD solution.

All of the grids converge to at least six orders of magnitude, though the fine mesh requires significantly higher number of iterations to converge to this level. This difficulty in converging may be indicative of the grid convergence problem found in the pressure profiles near the centerline.

Plug Nozzle Baseline. The 8-zone grid, boundary conditions and Mach Isolines for the plug nozzle flow were discussed in Chapter 4: Wake Closure Mechanisms. Tables B.3 and B.4 list the dimensions and grid sizes used to determine grid convergence.

Table B.3: C35-10-25 Dimensions for CFD Model

	Zone Size							
Size	1	2	3	4	5	6	7	8
Coarse	16x11	21x11	33x11	21x11	33x11	21x21	33x21	33x21
Medium	31x21	41x21	65x21	41x21	65x21	41x41	65x41	65x41
Fine	61x41	81x41	129x41	81x41	129x41	81x81	129x81	129x81

B.4: M=3.5 Plug Nozzle Dimensions

Dimension	Size (in)
Throat Distance from Centerline	0.461
Cowl Lip Distance from Centerline	0.500
Cowl Height	0.100
Ramp Lip Distance from Throat	0.435
Ramp Lip Distance from Centerline	0.160
Freestream Boundary Distance from Cowl Corner	2.400
Outlet Boundary Distance from Ramp Lip	7.565

Figure B-5 shows the cross-sectional velocity and pressure, centerline pressure distributions, and solution convergence for the plug nozzle baseline. All of these curves show that the solution converges well as the grid size is increased from coarse to fine. In fact, cross-sectional pressure profiles converged much

better than their counterparts in the supersonic wake with the same grid size and spacing. As a result, the accuracy of the plug nozzle solution should be greater than that computed for the supersonic wake.

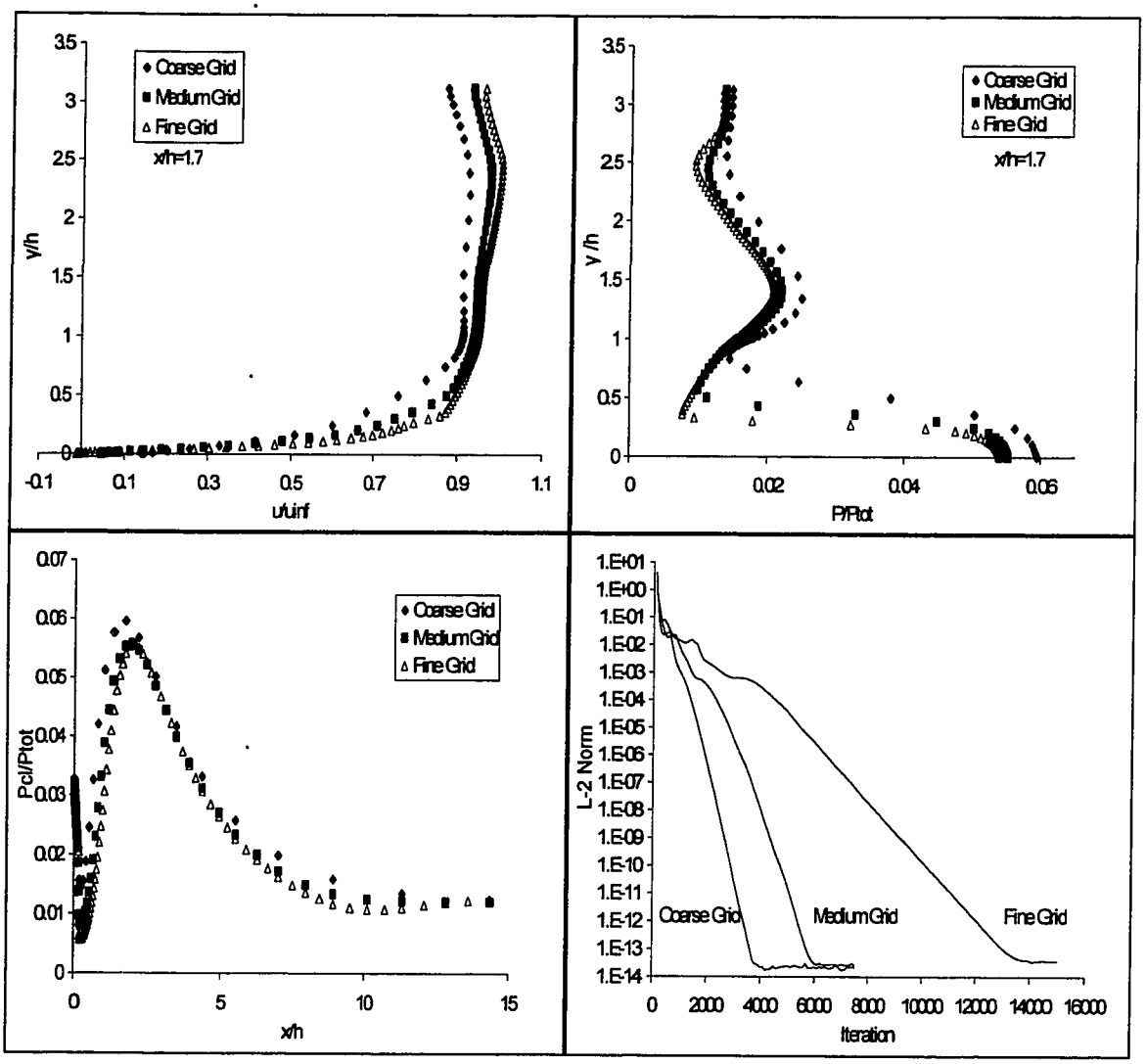

Figure: B.5: Plug Nozzle Grid Convergence

Appendix C
POST PROCESSING ANALYSIS VERIFICATION

Several key wake characteristics, such as initial conditions at separation, centerline velocity, pressure, and Mach Number can be extracted directly from the CFD results. The remaining parameters must be derived from the CFD data. This process involves the determination of key surfaces to locate the necessary data and then conducting the computations. However, the analytical modeling of the wake flows generally include some simplifying assumption and these analytical parameters are based on momentum integral approximations, boundary layer theory simplifications, and integral quantities. In contrast, CFD gives a finite difference solution, and its accuracy is limited to discrete nodal points. Therefore, prior to their application to the plug nozzle analysis, it was necessary to evaluate the capability and limitations of applying these analytical concepts and measures to CFD data.

C.1 Key Wake Surfaces

Several key surfaces within the wake had to be determined in order to select the data used in the computation of the analytical wake parameters. These surfaces included the shear flow outer edge, the DSL, the locus of U=0, and locus of M=1. These surfaces were generally located by marching through the CFD nodal point data in the traverse (j-direction) until a specified criterion was satisfied. Depending on the specific surface being located, the points used to define the surface were either the closest nodal point or an interpolated value.

The shear flow outer edge (or boundary layer thickness) is used to define the edge velocity, Mach Number, and pressure distributions. The boundary layer or shear flow outer edge was located by marching in the minus-j direction until a

specified criterion was satisfied and defined as the closest nodal point to meet this criterion. Figure C.1 shows the boundary layer thickness for the flat plate test case with the u/u_e=0.99 criterion. The boundary layer and the resulting displacement thickness and momentum thickness were compared with the theoretical predictions represented by Chapman and Rubesin's relations for compressible flow. The CFD results show good convergence on the theoretical predictions as grid size is increased.

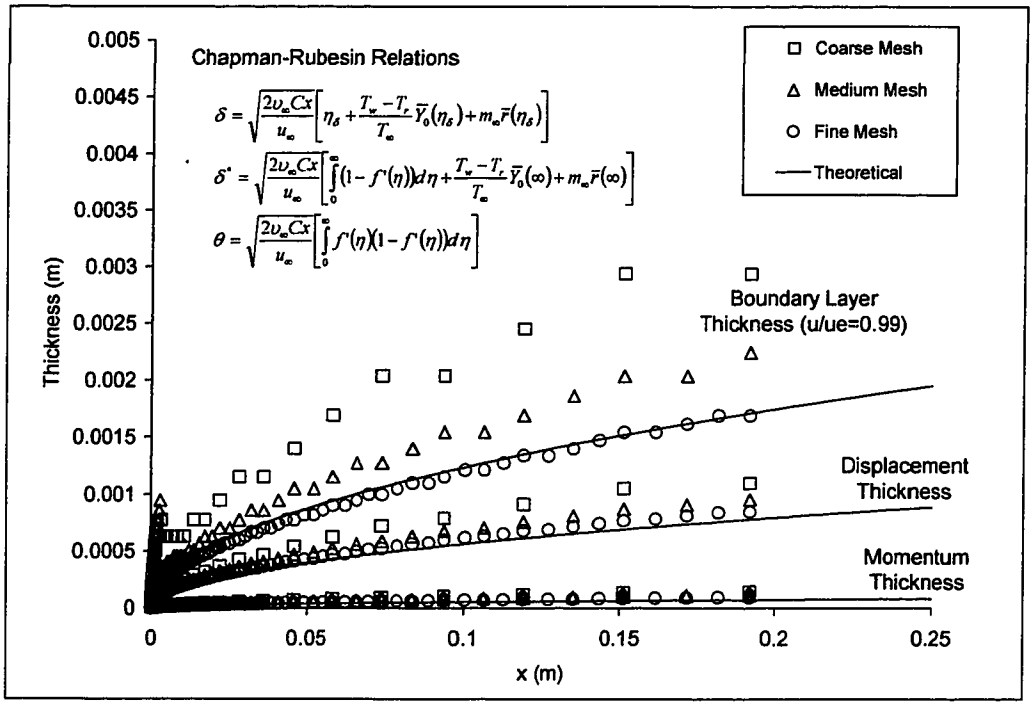

Figure C.1: Flat Plate Boundary Layer Thicknesses

Determination of the shear flow outer edge for the supersonic wake was more difficult. The analytical models of supersonic wakes assumed a monotonically increasing velocity profile toward an asymptotic freestream condition. But the CFD solution shown in Figure C.2 shows a more complex set of velocity profiles, which made the determination of an outer edge problematic. The profile at x/h=0.1 represents the transition from a separated jet to a mixing region with backflow. At x/h=1.0, the velocities greater than freestream are associated with

the corner expansion. The decreased pressure in x/h=4.0 is due to the presence of the recompression shock. And eventually, the flow returns to a more "normal" boundary layer type flow at x/h=9.6. These results are comparable to CFD data and experimental results presented by Delery (28) and McLaughlin (50).

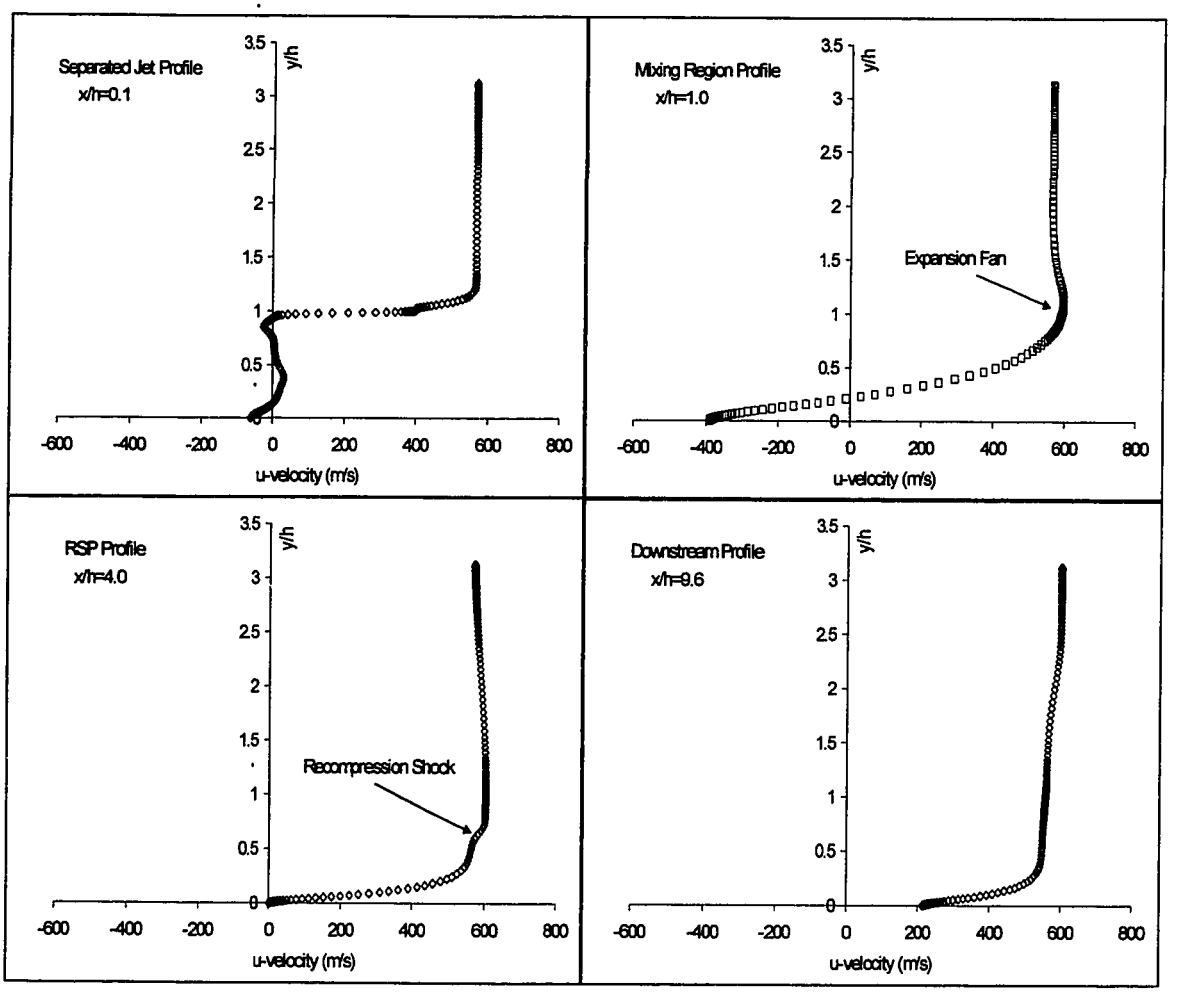

Figure C.2: Supersonic Wake Velocity Profiles

As a result, three alternate criteria were investigated for determining the outer shear flow edge and compared in Figure C.3. The first method based on an enthalpy ratio criteria, $(h-h_{wall})/(h_{\infty}-h_{wall})=0.99$, has been used for boundary layers with entropy gradients and separated flows (69). The ratio criteria

provided smooth surfaces that worked well up to the recompression shock. Thereafter, the criteria generally found a point ahead/above the recompression shock. Note that these criteria also assumed that the freestream condition was constant, which is valid for uniform inviscid flows, but not necessarily the plug nozzle flow. The other two criteria were based on the local slope of the velocity and vorticity profiles. These criteria assume that a change in the profiles to a "steep" slope is comparable to the asymptotic nature of the conventional boundary layer profile. The velocity slope, atan(dy/du)=75 degrees, and vorticity slope, atan(dy/dw)=30 degrees, showed relatively good results ahead and aft of the recompression shock, but had difficulty at the recompression shock root. The discretized nature of the CFD solution also caused the slope-based surfaces to be noisier than those derived from the ratio-based criteria. Since the flow behind the recompression shock was important for locating the wake critical point, the vorticity criteria was used and discontinuities were eliminated manually.

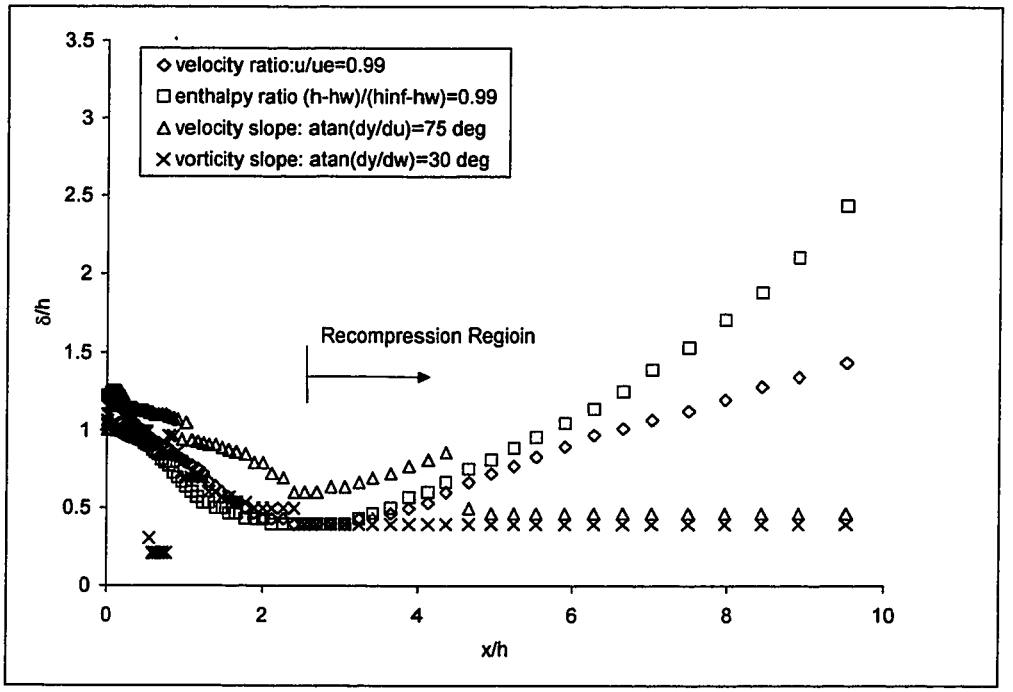

Figure C.3: Comparison of Outer Edge Criteria

The u=0 surface identifies the reattachment point, or rear stagnation point(s), along the wake centerline. The u=0 surfaces found by marching through the u-velocity values at each node in the minus-j direction, and then interpolating between nodes to define the desired surface. The analytical wake model has a single u=0 surface leading from the separation point to the reattachment point. With the presence of a solid wall in the CFD model, several "mini-recirculation" regions developed - each with its own zero u-velocity contours. Moreover, the discretization again seemed to impact the ability to track the u=0 surface upon separation C.4 leaves the afterbody surface, finds the recirculation bubble just below the afterbody corner and then reaches the surface that leads to the reattachment point. Note however, these discontinuities do not pose problems for the intended objective of locating downstream stagnation points.

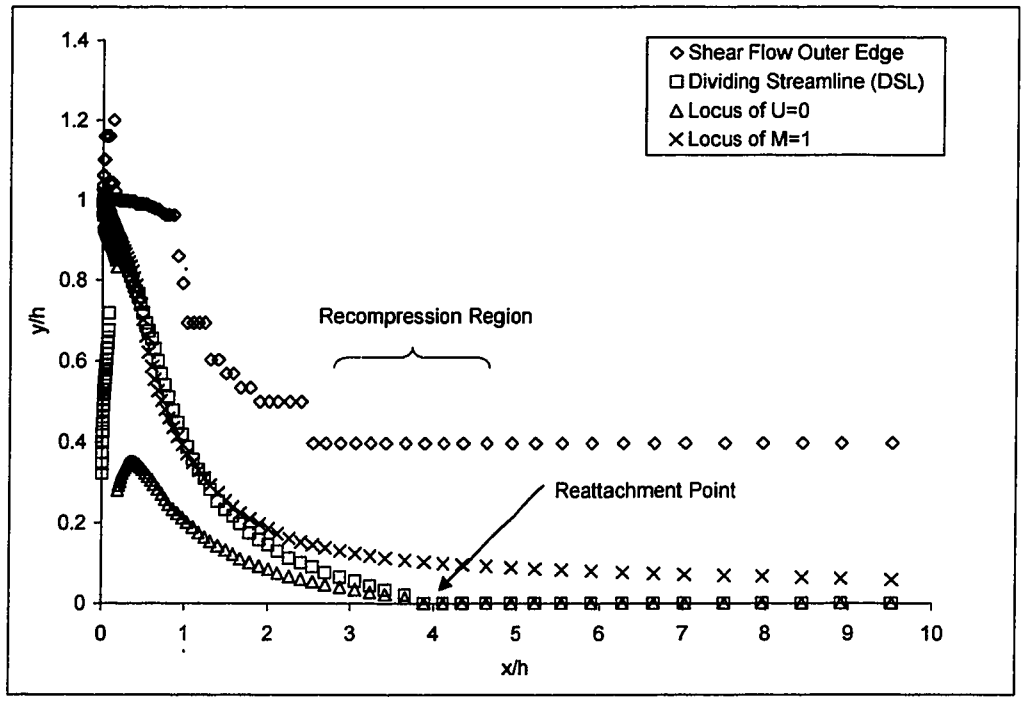

Figure C.4: DSL, U=0, and M=1 Surfaces

The DSL defines the u-velocity component of Tani's a(x) parameter and is found by locating the streamline whose streamfunction, ψ=0, or utilizing the

continuity condition that no mass flow inside the recirculation region crosses the DSL.

$$\text{Method 1:} \quad \frac{\rho}{\rho_0}u = \frac{\partial \psi}{\partial y}, -\frac{\rho}{\rho_0}v = \frac{\partial \psi}{\partial x}$$

$$\text{Method 2:} \quad \int_{wall}^{DSL} \rho u dy = 0$$

The analytical DSL connects the separation point to the reattachment point. The discretized nature of the CFD solution had the greatest impact on Method 1. Using this method, the DSL starting from the separation point was different the DSL originating from the reattachment point. Method 2 avoided this problem by its integral nature, but sometimes picked up streamlines from the "mini-recirculation" regions, thus creating discontinuities in the overall streamline. Overall, the methods compared relatively well to one another. The continuity condition provided a smoother solution from the point of separation at the trailing edge to the reattachment point on the axis, but the streamfunction method is independent of base bleed or open wake conditions.

The M=1 surface was determined by marching in the j-minus direction at each axial location until the Mach Number between two nodes changed from supersonic to subsonic. The surface was then interpolated between the two points. Since the inviscid flow was supersonic and the upper viscous portion of the recirculation region was monotonically decreasing, the M=1 locus was easy to locate.

C.2 Analytical Wake Parameters

The analytical wake parameters identified in Chapter 2 that require additional computation included the a(x) parameter, displacement thickness, and critical point. The reattachment point, a(x), and displacement thickness were generally computed directly from their definitions once the relevant key surface was determined. The evaluation of the wake critical point was conducted using Lees

and Reeves and Weinbaum's relations. Since Lees and Reeves method was heavily dependent on boundary layer approximations and edge conditions (which were difficult to determine from the CFD data), Weinbaum's relations provided additional validation of the results.

Based on the DSL surface found above, Tani's a(x) parameter is given in Table 2.4 as the ratio of the DSL or centerline velocities to the edge velocity. Figure C.5 plots Tani's a(x) parameter through the wake's development based on the CFD solution for the M=2.5 supersonic wake. The initial increase in a(x) is comparable was predicted by Lees, et. al., (37) and is compared to that seen with the initial separation of flow from a surface in the case of the impinging shock case. As the wake approaches reattachment, a(x) tends back toward zero. After reattachment, $da/dx>0$ and correspondingly, $d\delta^*/dx>0$ as the flow continues downstream until it passes through the critical point.

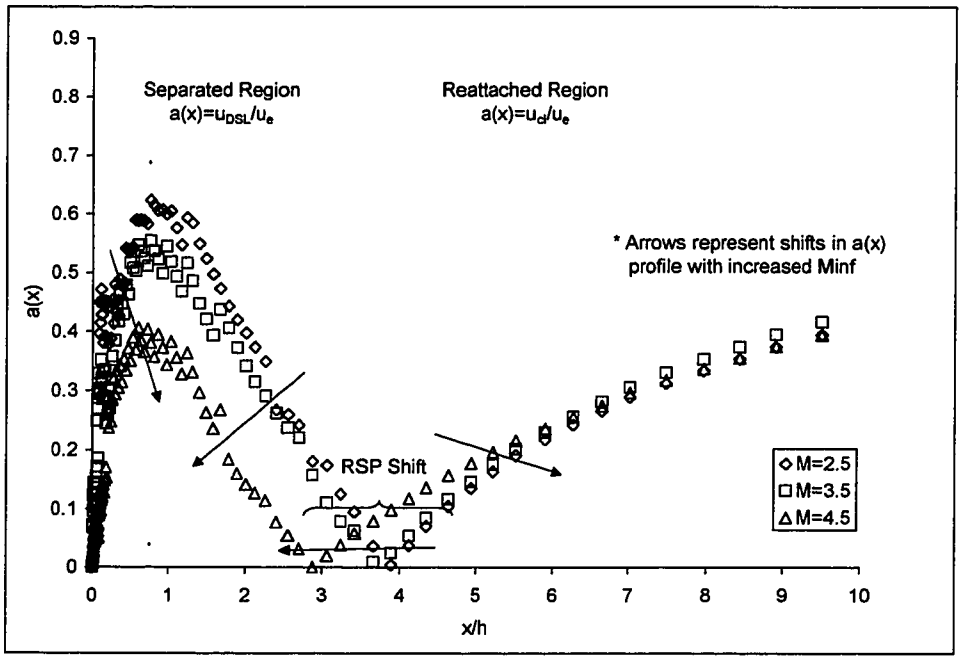

Figure C.5: Trends in Tani's a(x) Parameter for a Supersonic Wake

Using the same geometry and stagnation conditions, the M=3.5 and M=4.5 supersonic wake solutions are shown for comparison. The values of a(x) in the recirculation region decrease in magnitude with increasing freestream Mach Number and indicate the higher pressure gradients associated with the greater expansion and recompression process. The RSP moves upstream with increased freestream Mach Number, and the downstream values of a(x) eventually asymptote to a(x)=0.75 when dp_e/dx goes to zero.

The displacement thickness is computed by integrating the velocity and density profiles through the shear flow according to Equation (8) and the trapezoidal integration technique. The displacement thickness for the supersonic wake test case is plotted in Figure C.6. The graph displays the anticipated decrease in thickness from the afterbody corner to the neck region. The dip in the curve prior to reattachment (near x/h=2) results from the overshoot of the velocity profile associated with the corner expansion. The mass flow rate is being increased, in contrast to the normal displacement effect in shear flows.

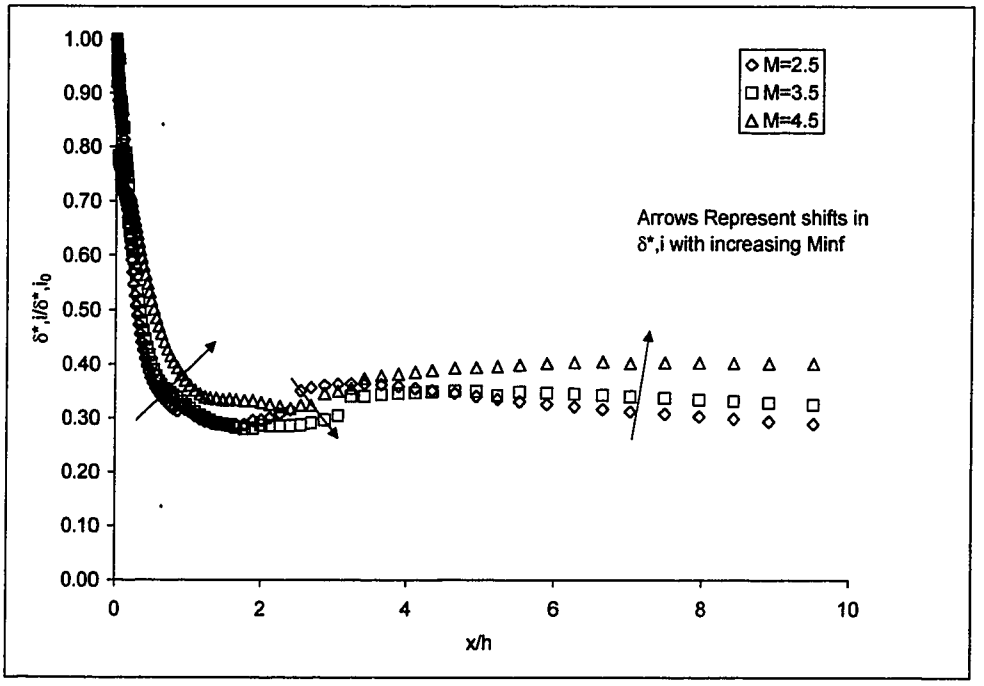

Figure C.6: Supersonic Wake Displacement Thickness

Displacement thickness is commonly used as a measure as opposed to boundary layer thickness since it is more easily quantified. In boundary layer theory, the displacement thickness reaches a limit near the boundary layer edge and is insensitive to the exact edge location. However, the CFD solution to the wake did not always have asymptotic, monotonic freestream quantities, the displacement thickness had some sensitivity to the shear flow outer edge definition.

The M=3.5 and M=4.5 supersonic wake displacement thicknesses are also plotted for comparison. It was expected that the M=2.5 wake would have a larger displacement thickness in the separated region correspond with the higher base pressure and smaller amount of expansion. The larger M=3.5 and M=4.5 recirculation thicknesses may be associated with the transformation coordinate system from compressible to incompressible form. Alternatively, the Reynolds Number prior to separation may also affect the initial boundary layer displacement thickness used to normalize the flow quantities. These trends should be examined in later research.

The Lees and Reeves critical point occurs at the singularity of the governing equations for wake flows where D=N1=N2=N3=0. These variable are function of the shape factors H, J, R, and Z shape factors, which can be computed directly from the CFD results by using the definitions given by Equation (9). The trapezoidal method was used to integrate the desired functions through the shear layer. Figure C.7 shows the distribution of these variables for the supersonic wake test case, compared to their approximated values using Lees and Reeves (38) polynomial curve fits as functions of a(x). While the H, J, and R shape factors are relatively comparable in the separated region, the Z shape factor is significantly different. Definition of the shear flow outer edge was eliminated as a cause. One potential source of error may be associated with the velocities that are integrated for Z, $\int u/u_e dy$ - the slopes of which were also problematic in the computation of skin friction coefficient for the flat plate test

case. The Z shape factor affected the function f, which is used to compute D and N2, but the terms containing f were not driving factors for the magnitude of these parameters.

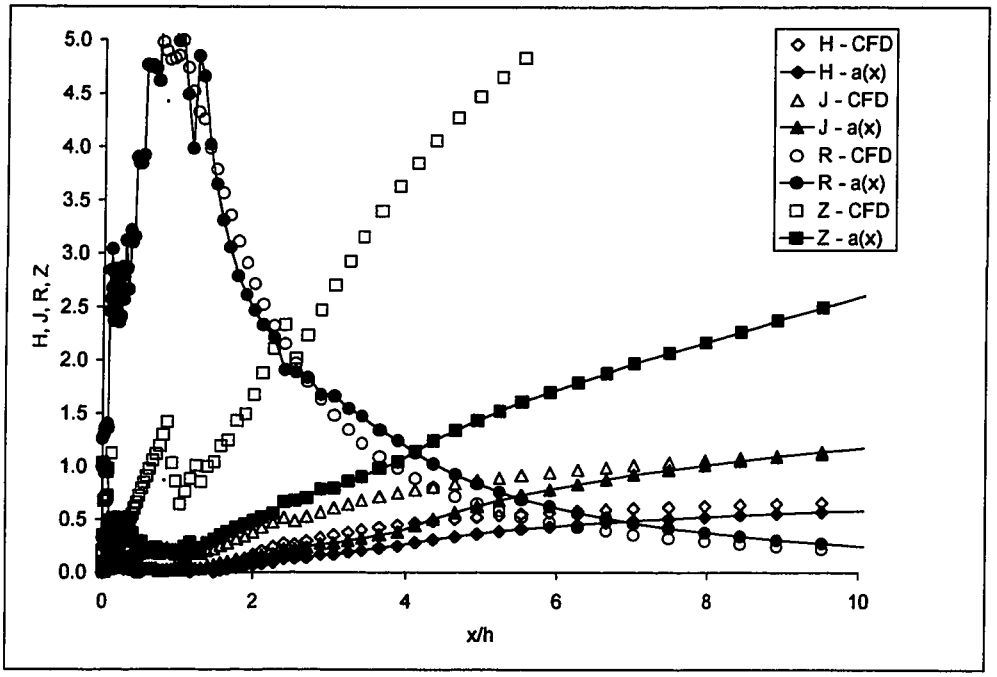

Figure C.7: Comparison of CFD and Curve-Fitted Shape Parameters

Lees and Reeves D, N1, and N2 parameters were computed along the wake using the CFD results and plotted in Figure C.8 (N3 is not plotted since it is just a function of N1 and N2). D, N1, and N2 reach zero almost simultaneously near x/h=5.75, indicating the location of the downstream critical point. The curves qualitatively follow the correct trend with D<0, N1>0, and N2<0 in the separated regions. However, the interpretation of results was strongly dependent on the scale of the graph. At enlarged scales, the curves do not reach zero simultaneously, and cross zero much further downstream, if at all. Because the equations are evaluated near a singularity and the inputs are discretized values, the relations have a tendency to blow up rapidly or have wide variances. Moreover, additional uncertainty in locating the critical point is due to asymptotic nature of the curves at this scale.

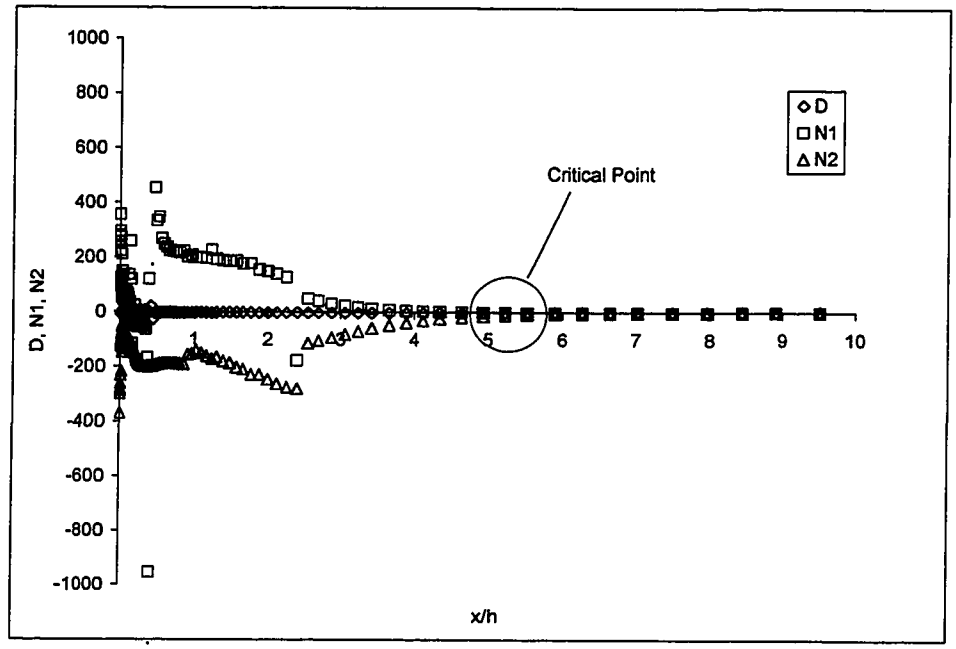

Figure C.8: Lees-Reeves Critical Point - based on CFD Data

Weinbaum's 2-D viscous throat critical point can be derived by two methods. In the first case, the y=Y(x) surface in Figure C.9 is located by integrating the function from Equation (23) through the shear flow in the j+direction until the integral equals zero. Note that the streamtube model used for the 2-D viscous throat approach is assumed valid near the reattachment and critical point regions. The y=Y(x) surface goes to infinite near the afterbody base where the subsonic flows dominate the velocity profiles. Weinbaum relates the 2-D viscous throat model to the Crocco and Lees IVI critical point. From the plot of these key surfaces, the critical point will exist if the M=1 surface is contained by the shear flow outer edge. It can be located at the point where the y=Y(x) surface and the shear flow outer edge. Located near x/h=5.75, this critical point lies in the same location as that found by the Lees and Reeves method. This difference may be due to the determination of the shear flow outer edge.

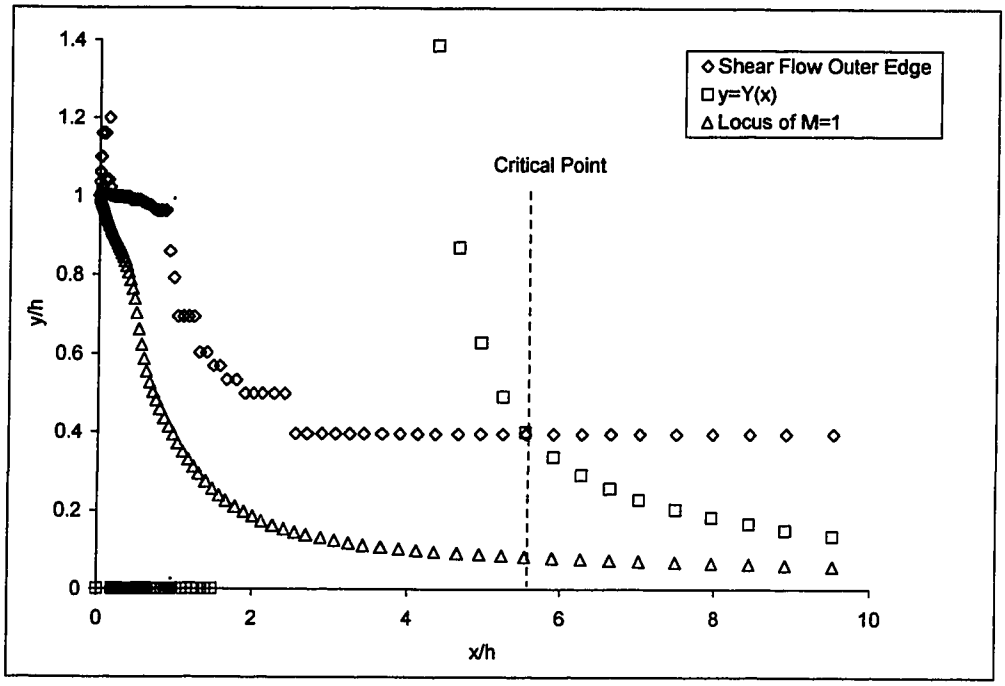

Figure C.9: Weinbaum's y=Y(x) Parameter in the Wake - based on CFD

The integration of Equation (23) in Figure C.10 shows the critical point based on Weinbaum's integral parameter when the curve passes through zero. The integral was also computed for different outer edge heights, and found to shift the curve up or down, but not change its shape. This critical point is closer to the Lees and Reeves result, but the exact location and interpretation is complicated by the asymptotic nature of the curve and dependent on the scale used. Other features include the reattachment point where a singularity occurs at $M_{cl}=0$.

In summary, the discretized nature of the CFD solution posed several difficulties in locating the key surfaces needed for this analysis. The edge conditions would be the most problematic. Those surfaces or parameters that were integral quantities tended to average out some of the data discontinuities, providing smoother data sets. The effects of a no-slip, solid base wall, while more realistic, were generally not considered in analytical models, and therefore, there are likely to be differences between analytical and CFD results.

However, the CFD-computed parameters still provides qualitatively useful insights to the changes occurring in the wake.

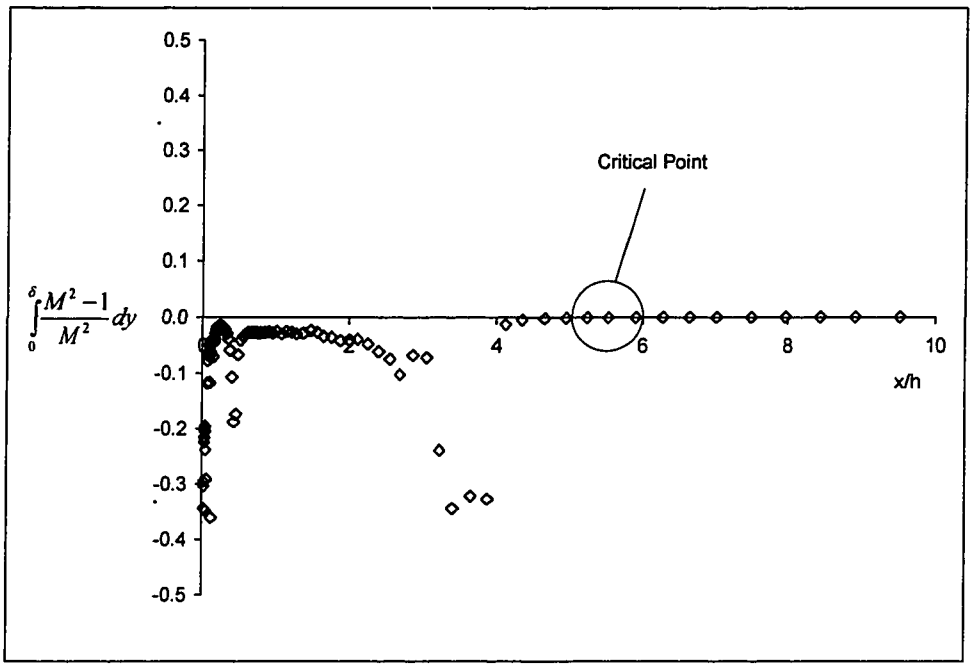

Figure C.10: Weinbaum's Integral Parameter in Wake - based on CFD

Appendix D
SUPERSONIC WAKE-PLUG NOZZLE COMPARISON

With a global understanding of the physical dynamics of the plug nozzle flowfield in open and closed wake conditions, the next analysis examined the internal flow characteristics of the wake region using CFD. Before comparing the open and closed wake flows, the plug nozzle in design conditions is examined in relation to a supersonic wake to identify any unique aspects of plug nozzles that of themselves influence base pressure. The supersonic wake and plug nozzle general flow characteristics are first investigated, and then the analytical wake parameters described in Chapter 2 are computed for each case. Once the plug nozzle flow was benchmarked, the open and closed wake conditions could then be compared and analyzed.

The supersonic wake geometry included the same step height and axial afterbody length as the plug nozzle. The stagnation pressure and temperatures were kept constant. The remaining parameter that was critical to the base pressure prediction was the freestream Mach Number. As shown in Figure D.1, the Mach Number of the C35-10-25 flow varies from zero along the base of the ramp ($y/h<1$) and increases to $M=2.5$ at the outer edge of the ramp boundary layer. In the inviscid flow above the boundary layer, the Mach Number increases with distance above the ramp lip to just above $M=3.5$ at the outer edge freejet boundary. The Mach Number at the outer edge of the ramp boundary layer provided a supersonic wake solution most comparable to the plug nozzle results.

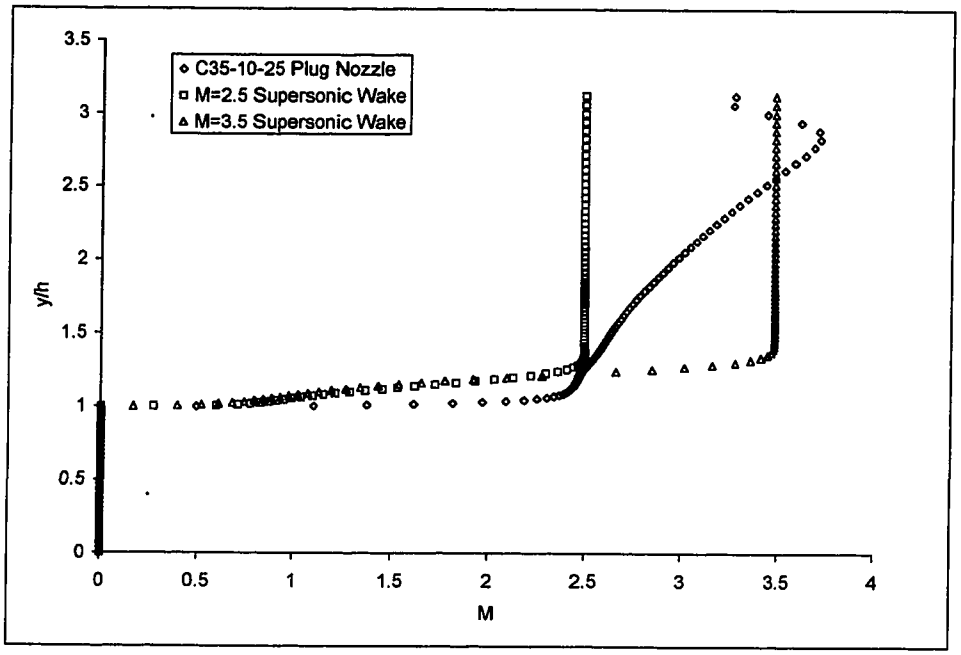

Figure D.1: C35-10-25 Mach Number Profile at Ramp Separation

Figure D.2 compare the plug nozzle and supersonic wake solutions for pressure, velocity, and total pressure at M_∞=2.5 conditions. The supersonic wake is nearly uniform in the freestream until the recompression shock is reached. In contrast, the pressure profile of the plug nozzle in Figure D.2 decreases with height above the lip due to the increase in Mach Number associated with the expanding exhaust jet. The key result however, is that the pressure profiles within the recirculation region relatively similar. Thus, it would appear that differences in the external inviscid jet do not significantly affect base pressure. The lower pressure of the plug nozzle far downstream reflects the recovery of the flow to the M=3.5 design conditions.

Closer examination of the plug nozzle profile reveals that the base pressure is about 13% greater than the supersonic wake. Although the overall Mach field is on average higher than the wake because of this non-uniformity, the base pressure is slightly higher (which is opposite of the general effect of Mach Number on flow). When M_e>2, Lees and Reeves (38) found that the transverse

inertial terms become much more important that the viscous terms. As a result, transverse pressure gradients, dP/dy, in the inviscid flow can have significant impact on the pressure within the wake. In contrast, Baum and Dennison (44) examined the effects of transverse pressure gradient near the critical point and found only negligible effect. While their analysis did not address the upstream separation regions, they concluded that small gradients in this region were likely to have negligible effects on the solution. Though it is possible that the more dramatic pressure gradients in the inviscid plug nozzle flow may be causing this increased base pressure, there are other sources that have analogies from standard wake flows such as the initial angle of the separated flow from the inclined ramp.

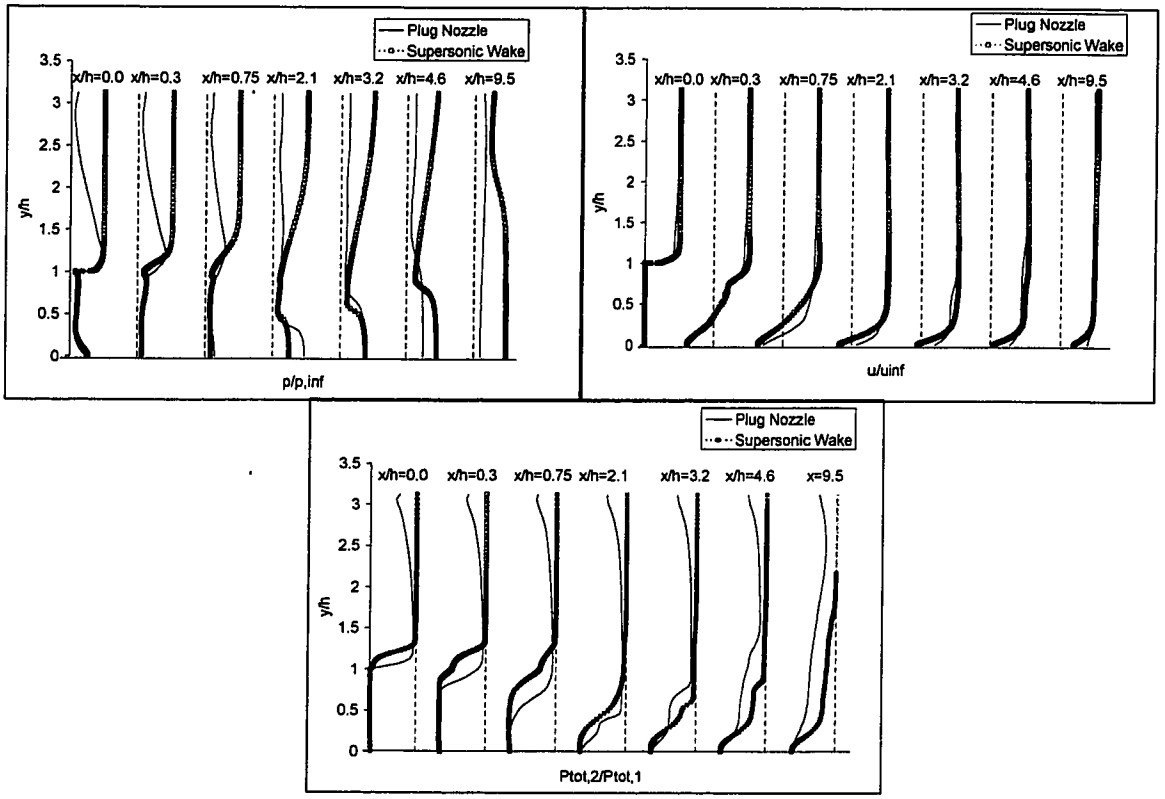

Figure D.2: Plug Nozzle and Supersonic Wake Flow Development

A more important consideration is the effect of transverse pressure gradients within the viscous wake. All of the analytical wake models using integral momentum relations make the assumption from the boundary layer theory that dp/dy=0. Note: Chow (32) and Chow and Spring (35) include the effect of transverse pressure changes through additional relations. Both the plug nozzle and supersonic wake have a significant gradient in the viscous wake close to the base wall. As a result, it is possible that the analytical methods and measures may not be as applicable in this region.

The supersonic wake and plug nozzle velocity profiles are generally similar. The initial boundary layer of the plug nozzle is smaller than the supersonic wake. Even though the plug ramp distance is longer than the supersonic wake afterbody, the smaller edge Mach Number flows early along the ramp and negative pressure gradients suppress boundary layer growth. The distorted velocity profiles at x/h=0.3 represent the transition of the jet from its boundary layer profile to the start of mixing in the recirculation region of the wake. The plug nozzle reaches reattachment earlier than the supersonic wake. Far downstream, both profiles reach nearly freestream velocities. The slight decrease of the velocity profiles near the axis is the velocity defect resulting from the wake. The plug nozzle experiences less of a velocity defect, which suggests that there is less of an energy loss associated with the plug nozzle wake. This difference is similar to that found by boattailed afterbody wakes and explains the higher base pressure of the plug nozzle.

The above data provides a "snapshot" of different characteristic profiles for the plug nozzle and supersonic wake. The determination of key surfaces and analytical wake parameters describes the wake structures in aggregate. Similar to the approach to be used for the wake closure analysis, the first set of parameters examines the overall wake structure. Then those parameters indicating direct changes to base pressure are compared.

Figure D.3 depicts the computation of critical points using Lees-Reeves methodology. From the velocity profiles shown above, it was found that the wake reattachment point occurred downstream of the plug nozzle reattachment point. The axial direction was normalized so that the distances are all relative to the respective reattachment points, yet the wake critical point is still located behind that of the plug nozzle. For general wakes, an increasing Mach Number tends to move the critical points forward. The increasing Mach Numbers in the inviscid plug nozzle flow may have similar effect.

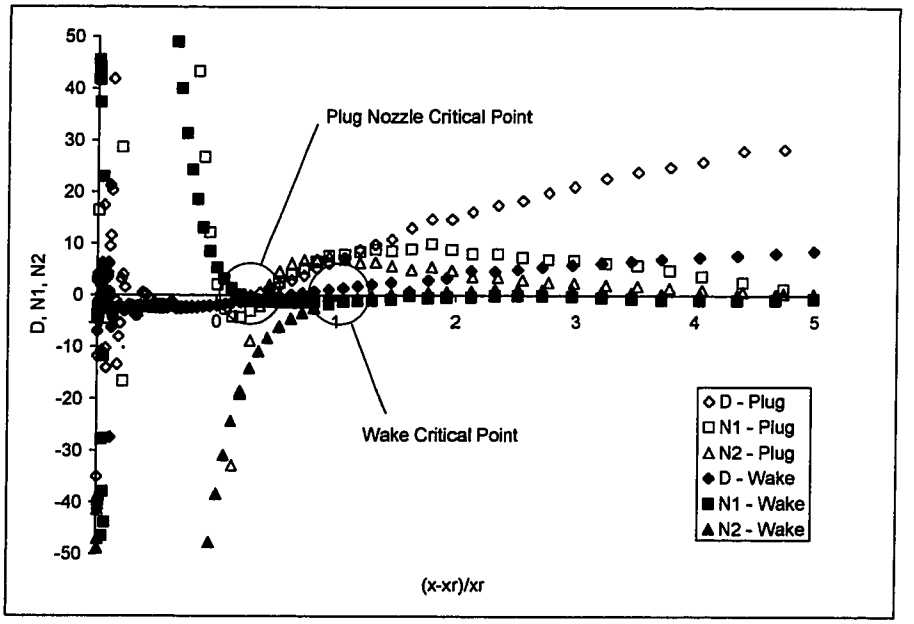

Figure D.3: Lees-Reeves Critical Points for Plug Nozzle and Supersonic Wake

On the other hand, Figure D.4 shows the critical points based on Weinbaum's method to be nearly identical. As found in Chapter 4, the relative locations are strongly dependent on the scales used and the asymptotic curve. In any case, the existence of a critical point for the plug nozzle confirms that the analytical wake methods can be applied at least for closed wake conditions.

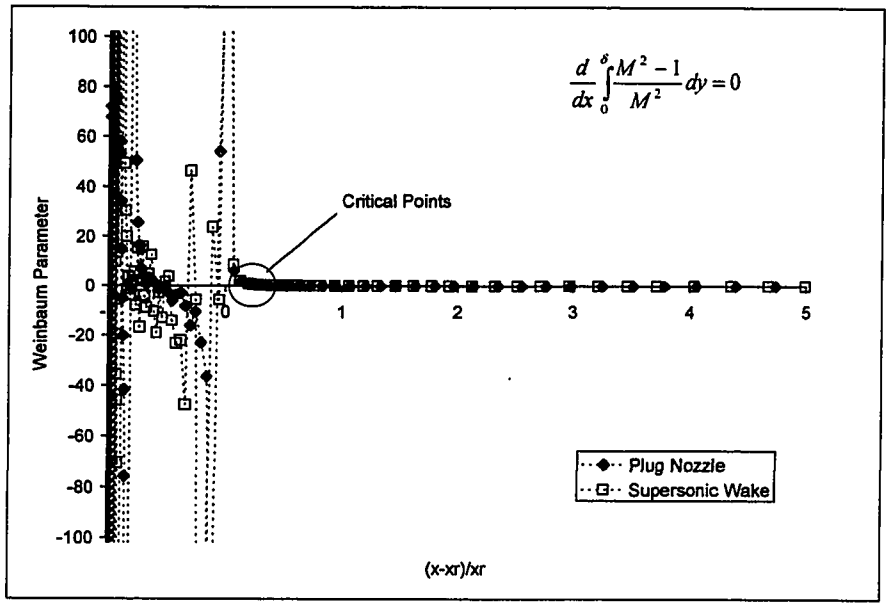

Figure D.4: Weinbaum Critical Points for Plug Nozzle and Supersonic Wake

The differences between structure of the wake for a plug nozzle and supersonic wake pressure characteristics can be gathered from Figure D.5. As explained by Rocketdyne (4), the plug nozzle downstream pressure reaches a maximum and then decreases toward a freestream level, whereas the supersonic wake plateaus at the downstream maximum. In general, the centerline distributions are similar once scaled to their respective reattachment points. The main difference occurs just behind the ramp/afterbody base. This suggests that trends in the downstream centerline pressure distribution do not lead to obvious changes in base pressure.

The static pressure distributions by themselves represent only one component of the mechanical energy that is communicated through the recirculation region. The point at which base pressure is measured is also a stagnation point. Therefore, the kinetic energy of the flow must be represented in the final base pressure. The distribution of kinetic energy may be represented by the velocity profiles within the viscous wake, as measured by various shape factors. The supersonic wake has higher a(x) values near the base in Figure D.6, but

lower values closer to reattachment and then downstream of reattachment. The higher values of a(x) translate into lower $H=\delta^*/\theta$ for separated flows. Alternatively, if a(x) is viewed from the perspective of a shear stress parameter, a larger a(x) translates into greater shear stress. When integrated over the length of the recirculation region, the plug nozzle would appear to have more fluid mixing, and as a consequence, more mass flow in the recirculation region. The net result would be a higher overall pressure level in the recirculation region.

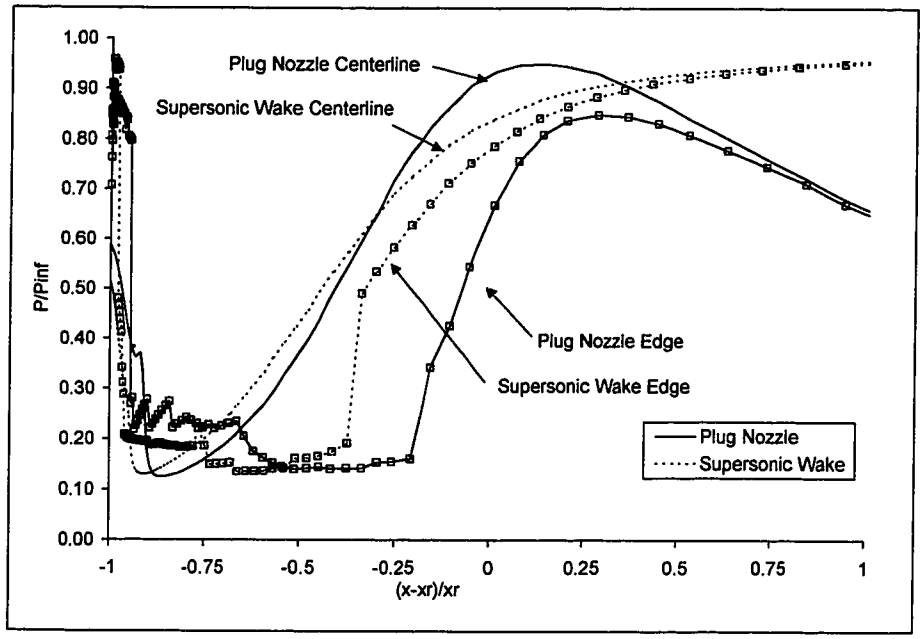

Figure D.5: Plug Nozzle and Supersonic Wake Pressure Distributions

The comparison between displacement thicknesses did not provide any clear trends that would be associated with the differences in base pressure. The sharp drop of both distributions aft of the base is due to the rapid expansion of the flow. The expansion process also increases the mass flow rate in the viscous layer, resulting in the negative displacement thicknesses. Part of the difficulty in interpreting these results is due to the challenges in determining the outer edge of the viscous flow. For boundary layers, the displacement thickness is a more reliable measure than the boundary layer thickness, since

the increments for the integral equation go to zero. But a similar limiting characteristic did not exist for the supersonic wake and plug nozzle flows due to the non-monotonic and non-asymptotic nature of the flow profiles.

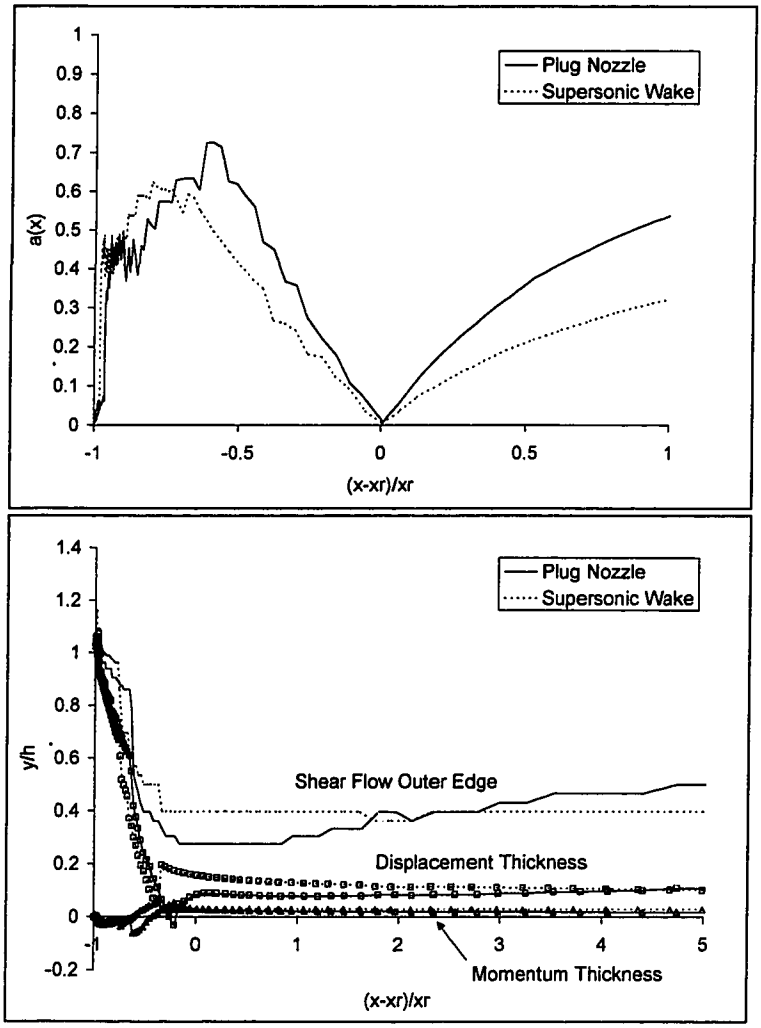

Figure D.6: Plug Nozzle and Supersonic Wake a(x) and Thickness Distributions

Note that the initial displacement thickness is larger for the wake primarily because of a longer afterbody. Normally, the displacement thickness would be larger because of the lower initial Mach Numbers and favorable pressure gradient of the plug nozzle during expansion. Therefore, the comparison between the two configurations was not completely direct.

In summary, the plug nozzle flow characteristics at design conditions are similar to those of the supersonic wake. Pressure field more like the M=2.5 flow that was seen at the edge prior to separation. The inviscid flowfield is definitely non-uniform, varying from M=2.5 to M=3.5. One result of the different external flowfield was the faster flow development and earlier reattachment in the plug nozzle. The recompression occurs later for the plug nozzle, but has a sharper gradient. As a result, the edge pressures were lower and velocities on the DSL were higher. The existence of a critical point and common wake features indicate that the analytical wake parameters identified in Chapter 2 can be applied to the investigation of the plug nozzle wake conditions. Though there are some striking differences in the two flow structures, final impact on base pressure were minor.

DEREK EDWARD LANG

2628 139th Avenue SE #14, Bellevue, Washington 98005 USA
tel: 1-425-644-9294, fax: 1-206-543-4719

QUALIFICATIONS

Engineering and Safety

- Developed conceptual designs for launch vehicles, satellites, and aircraft.
- Evaluated safety and inspected launches of: Delta, Atlas, Conestoga, Pegasus rockets.
- Developed launch operations procedures for range support for Sea Launch program.
- Supported development of Mission Assurance Plan (risk management, quality, reliability) for Sea Launch program.
- Fabricated high-speed test facilities and conducted hypersonic wind tunnel tests.
- Modeled high-speed flows using computational fluid dynamics.
- Analyzed aero-thermochemistry for supersonic reacting flows in Shock Waver Reactor.

Program Development/Management

- Managed multiple contractors for safety evaluation of commercial reentry vehicle.
- Developed strategic plan and prepared budgets for licensing and safety research.
- Team lead for technical and financial evaluation of launch rate improvement study.
- Recruited/supervised personnel for Cal Poly University Space Shuttle experiments.

Industry Policy and Analysis

- Supported national policy development for R&D, infrastructure, and telecom.
- Developed regulatory procedures for licensing of rockets and spaceports.
- Conducted market analysis for reentry vehicles for NASA-Ames Research Center.

Procurement/Acquisition

- Managed $2M research contract and procured $1/2M in contract work annually.
- Developed solicitations; chaired contract award boards.
- Acquired materials for Cal Poly University Space Shuttle experiments.

EXPERIENCE

- U.S. AIR FORCE ACADEMY/AERONAUTICS RESEARCH CENTER, Colorado Springs, Colorado (Summer Graduate Researcher, 1996, 1997)
- BOEING COMMERCIAL SPACE COMPANY, Seattle, Washington (Consultant, 1995-1999)
- UNIVERSITY OF WASHINGTON, Aerospace and Energetics Research Program, Seattle, Washington (Research Assistant, 1995-1997)
- U.S. DEPARTMENT OF TRANSPORTATION. Office of the Secretary of Transportation/Office of Commercial Space Transportation, Washington, D.C. (Aerospace Engineer/GM-14 last grade, 1989-1994).
- CAL POLY SPACE SYSTEMS, California Polytechnic State University, San Luis Obispo, California(Project Administrator, 1987-1988, Materials Supervisor, 1985-1987)
- UNITED TECHNOLOGIES CHEMICAL SYSTEMS DIVISION, Propulsion Systems, Insulation and Nozzle Design Group, San Jose, California (Engineering Clerk, 1986, Consultant, 1987)
- U.S. NAVY/NAVAL FACILITIES ENGINEERING COMMAND, Facilities Planning and Real Estate Department, San Bruno, California (Engineering Aide, 1985)

EDUCATION

- University of Washington, Seattle, Washington, Doctorate of Philosophy: Aernautical/Aerospace Engineering, 1999
- von Karman Institute for Fluid Dynamics, Belgium, Diploma: Aeronautics and Aerospace, 1995
- Stanford University, California, Masters of Science: Aeronautical/ Astronautical Engineering, 1989
- International Space University, held at Massachusetts Institute of Technology, Certificate, 1988
- California Polytechnic State University, San Luis Obispo, Bachelors of Science: Aeronautical Engineering, 1988

PROFESSIONAL AFFILIATIONS AND HONORS

- American Institute of Aeronautics and Astronautics (Senior Member)
- Tau Beta Pi: National Engineering Honor Society
- Sigma Gamma Tau: Aeronautical Engineering Honor Society
- Mercury Scholar (1996-1997, 1997-1998, 1998-1999)
- Boeing Certificate of Achievement (1998, 1999)

PUBLICATIONS

- Lang, Derek E., "Hue Analysis Factors for Liquid Crystal Transient Heat Transfer Measurements," U.S. Air Force Academy/Aeronautics Research Center, Colorado, September 1997.

- Lang, Derek E., "USAFA Trisonic Wind Tunnel Analysis for Heat Transfer Measurements," DFAN Report No. 96-02, U.S. Air Force Academy/Aeronautics Laboratory, Colorado, August 1996.

- Lang, Derek E., Choate, Darrel L., Nance, Marcus L., "Sea Launch: Commercial Launch Competitiveness," Vol. 1, *Proceedings of the Fifth International Conference on Space '96*, Albuquerque, New Mexico, June 1-6, 1996.

- Lang, Derek E., "Leading Edge Bluntness Effects on High Speed Flow", Project No. 1995-07, von Karman Institute for Fluid Dynamics, Rhode-St-Genese, Belgium, June 1995.

- Lang, Derek E., "Paving the Way for a Commercial Space Transportation Industry", IAA-94-IAA.1.1.592, Presented at the 45th Congress of the International Astronautical Federation, Jerusalem, Israel, October 9-14, 1994.

- Lang, Derek E., "Developing a Risk Management Program for Commercial Space Transportation", IAA-94-IAA.6.3.681, Presented at the 45th Congress of the International Astronautical Federation, Jerusalem, Israel, October 9-14, 1994.

- Gress, Ronald K., and Lang, Derek E., "Commercial Space Transportation: Development of a Risk Management Program", *Proceedings of PSAM II: International Conference Developed to the Advancement of Systems-based Methods for Design and Operation of Technological Systems and Processes*, San Diego, California, March 20-25, 1994.

- Bowles, Norman C., and Lang, Derek E., "Commercial Space Tansportation Regulation and its Effects on Space Safety", *Proceedings of OE/Aerospace Sensing 1993 Conference: Space Debris Detection and Mitigation*, April 12-16, 1993.

- Bowles, Norman C., and Lang, Derek E., "Returning Space Back to Earth: Reentry Vehicles - the Newest Space Venture", Ad Astra, June 1991.

- Lang, Derek, and Potter, Michael, "Europe, 1992 and Space Commercialization", Space Commerce, Vol. 1, No. 1, 1990.

- Lang, Derek, and Potter, Michael, "The European Community and Space", Space Commerce, Vol. 1, No. 1, 1990.

- Potter, Michael, and Lang, Derek, "European Integration and Space Commercialization: An American Perspective", Paper No. ST-89-020, Presented at the 40th Congress of the International Astronautics Federation, Malaga, Spain, October 7-12, 1989.

- Lang, Derek, and Prey, Angela, "ISU: A University with an International Future", American Institute of Aeronautics and Astronautics Student Journal, Winter 1989.

- Lee, Burton, Lang, Derek, and Merrihew, Steven, "Overview of Policy, Market and Technology Options for Commercial Reusable Re-entry Satellites", Stanford University Small Satellite Program, School of Engineering, Report to NASA- Research Center, Office of Commercial Programs, Joint Research Interchange Agreement NCA 2-333, June 15, 1989.

- McKenna, David, and Lang, Derek, "Mobile Lunar Probe", Presented at the 1988 American Institute of Aeronautics and Astronautics Regional Student Conference, Irvine, California, April 20-22, 1988.